Neutron Scattering Principal Investigators' Meeting

July 28-30, 2014

Hilton Washington DC North/Gaithersburg

Gaithersburg, Maryland

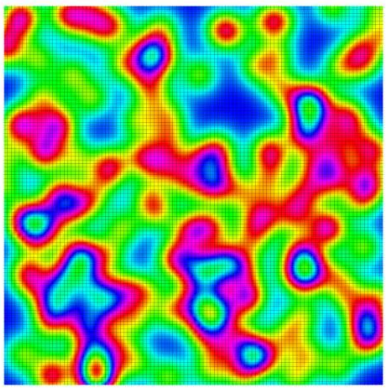

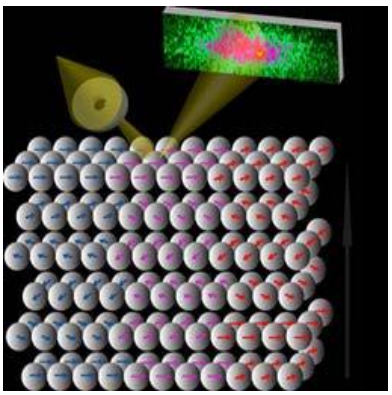

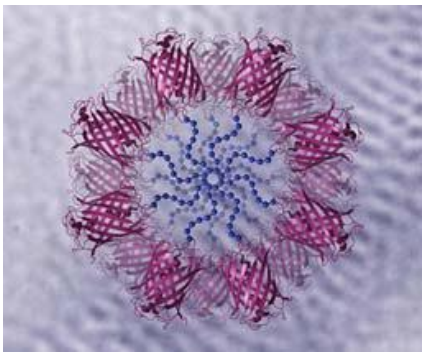

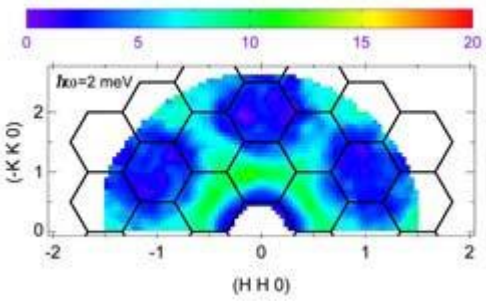

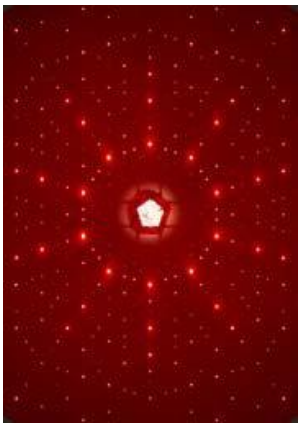

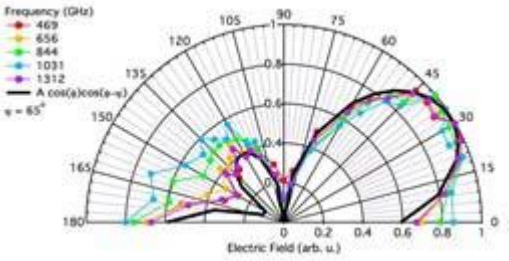

Office of Basic Energy Sciences
Division of Materials Sciences and Engineering

U.S. DEPARTMENT OF ENERGY | Office of Science

On the Cover

Top Left: Numerical simulation of the magnetic inhomogeneity (red = magnetism, blue = superconductivity) caused by replacing 1% of the indium atoms in a superconductor ($CeCoIn_5$) with cadmium atoms. The field of view is approximately 100 nanometers along each edge (Cover Image from Seo et al., *Nature Physics*, 10, 120–125, 2014).

Top Middle: Resonant scattering with coherent x-rays on the size and the dynamics of magnetic domains in a Dysprosium crystal with three different domains (shown in three colors in the schematic). Above 85K, this material exhibits a spiral magnetic state wherein the magnetic moments in a given layer in each domain are parallel, but oriented at a fixed angle with respect to the moments in the adjacent layers (Cover Image from Chen et al., *Physics Review Letters*, 110, 217201, 2013).

Top Right: Schematic illustration of cylinder-forming diblock copolymers, where the first block is a protein at the surface and the second block is the covalently attached synthetic polymer at the interior (Cover Image from Lam and Olsen, *Soft Matter*, 9, 2392–2402, 2013).

Bottom Left: Inelastic neutron scattering of high-quality single-crystal samples of the mineral $ZnCu_3(OD)_6Cl_2$ revealed that the scattered neutrons have a broad spread of energies (light green diffuse regions in figure), a hallmark signature predicted by theory (Han et al., *Nature*, 492, 406–410, 2012).

Bottom Middle: High-energy x-ray diffraction pattern from a single grain of a gadolinium – cadmium alloy (shown in center) displaying the novel five-fold rotational symmetry, characteristic of an icosahedral quasicrystal. Diffraction images were obtained by using the recently developed high-energy x-ray precession camera on a high brilliance superconducting undulator X-ray beam line at the Advanced Photon Source (Cover Image from Goldman et al., *Nature Materials*, 12, 714-718, 2013).

Bottom Right: Electric field amplitude for terahertz light transmitted through bismuth selenide (Bi_2Se_3). The large polarization rotation angle (arced scale) is direct experimental evidence that a highly conductive surface layer has spontaneously appeared on the topological insulator (Aguilar et al., *Physics Review Letters*, 108, 087403, 2012).

This document was produced under contract number DE-AC05-06OR23100 between the U.S. Department of Energy and Oak Ridge Associated Universities.

The research grants and contracts described in this document are supported by the U.S. DOE Office of Science, Office of Basic Energy Sciences, Materials Sciences and Engineering Division.

Foreword

This volume comprises the scientific content of the 2014 Neutron Scattering Principal Investigators' (PI) Meeting sponsored by the Division of Materials Sciences and Engineering (MSED) in the Office of Basic Energy Sciences (BES) of the U.S. Department of Energy (DOE). This meeting on July 28–30, 2014 at the Hilton Washington DC North/Gaithersburg, Maryland, is the fourth in the series, covering the projects funded by the Neutron Scattering Program. BES MSED has a long tradition of supporting a comprehensive neutron scattering program in recognition of the high impact neutron scattering and spectroscopy tools have in discovery and use-inspired research.

The MSED Neutron Scattering Core Research Activity (CRA) supports basic research on the fundamental interactions of neutrons with matter to achieve an understanding of the atomic, electronic, and magnetic structures and excitations of materials and their relationship to materials' properties. Major emphasis is on the application of neutron scattering and spectroscopy for materials research, primarily at BES-supported user facilities. Development of next-generation instrumentation concepts, innovative optics for time-of-flight instruments and application of polarized neutrons are distinct aspects of this activity. The increasing complexity of DOE mission-relevant materials for various energy applications requires sophisticated scattering and computational tools to investigate the structure and dynamics at relevant length and time scales. Additionally, neutrons allow access to the behavior of matter in extreme environment such as high temperature, pressure and magnetic field. A continuing theme of this program is the integration of material synthesis, neutron scattering measurements and computational modeling as this is vital to obtain controlled samples for experiments and modeling for an in-depth understanding of the structure and dynamics of materials and their relationship to macroscopic properties.

The purpose of the BES biennial PI meetings is to bring together all the researchers funded by the Neutron Scattering Program at BES-MSED on a periodic basis to facilitate the discussion of new results and research highlights by PIs, to nucleate new ideas and collaborations among participants, and to identify new research opportunities. The meetings also serve MSED to assess the state of the program, to chart new research directions and to identify programmatic needs.

We thank all the meeting participants for their active contributions in sharing their ideas and research accomplishments. Sincere thanks are also due to the speakers from other BES programs involved with neutron scattering in multidisciplinary research. We wish to thank Teresa Crockett in MSED and Tammy Click at the Oak Ridge Institute for Science and Education (ORISE) for their outstanding work in all aspects of the meeting organization.

Thiyaga P. Thiyagarajan and Helen Kerch
MSED, BES, Office of Science
U.S. Department of Energy

Table of Contents

AGENDA

2014 Neutron Scattering
Principal Investigators' Meeting
Materials Sciences and Engineering Division
Office of Basic Energy Sciences
U. S. Department of Energy

Program Chair: Thiyaga P. Thiyagarajan, Program Manager, Neutron Scattering

SUNDAY, JULY 27, 2014

*****Arrival, Dinner on Your Own *****

MONDAY, JULY 28, 2014

7:00 – 8:00 am	***** **Breakfast** *****
8:00 – 8:45 am	**BES Welcome** Arvind Kini, Team Lead, Materials Discovery Design and Synthesis P. Thiyagarajan, Program Manager for Neutron Scattering
Session I	**Heterostructures** Chair: Sunil Sinha, University of California, San Diego
8:45 – 9:00 am	Sang Cheong, Rutgers University (1) *Improper Ferroelectricity and Frustrated Magnetism in Hexagonal Multiferroics: Neutron and Ellipsometry Studies*
9:00 – 9:15 am	Chris Leighton, University of Minnesota (5) *Neutron Scattering Studies of Cobaltite Crystals and Heterostructures*
9:15 – 9:30 am	Suzanne te Velthuis, Argonne National Laboratory (21) *Neutron and X-ray Scattering Studies of the Structure and Dynamics of Bulk and Heterostructures of Strongly Correlated Materials*
9:30 – 9:45 am	Eric Fullerton, University of California, San Diego (27) *Neutron and X-Ray Studies of Spin and Charge Manipulation in Magnetic Nanostructures*
9:45 – 10:45 am	**Break and Poster session related to the above talks** **(N) is the Poster Board Number Location**

Session II	**Energy Materials** Chair: Sang Cheong, Rutgers University
10:45 – 11:00 am	Olivier Delaire, Oak Ridge National Laboratory (2) *Impact of Dynamic Lattice Instabilities and Microstructure on Functional Materials*
11:00 – 11:15 am	Ravi Chandran, University of Utah (6) *Design and Validation of an In situ Electrochemical Cell for Neutron Diffraction Investigation of Phase Transitions in Mg/Si Electrodes for Li-ion Batteries*
11:15 – 11:30 am	Lilo Pozzo, University of Washington (14) *Neutron Scattering Investigation of the Relationship between Molecular Structure, Morphology and Dynamics in Conjugated Polymers*
11:30 – 11:45 am	Adam Moulé, University of California–Davis (20) *Engineering Doping Profiles in Organic Semiconductor Materials*
11:45 – 12:00 noon	John Budai, Oak Ridge National Laboratory (24) *Impact of Dynamic Lattice Instabilities and Microstructure on Functional Materials*
12:00 – 1:00 pm	***** **Working Lunch** *****
1:00 – 2:15 pm	**Break and Poster session of the above talks for further discussion and Other poster:** Eliot Spect (26)
Session III	**High Tc Superconductivity** Chair: Joe Thompson, Los Alamos National Laboratory
2:15 – 2:30 pm	Pengcheng Dai, Rice University (3) *Using Neutron as a Probe to Study Magnetic Excitations in Strongly Correlated Electron Materials*
2:30 – 2:45 pm	John Tranquada, Brookhaven National Laboratory (7) *Neutron and X-Ray Scattering Studies of High-Temperature Superconductors*
2:45 – 3:00 pm	Martin Greven, University of Minnesota (13) *New Insights into the Cuprate Phase Diagram from Neutron, X-Ray and Transport Measurements of* $HgBa_2CuO_{4+\delta}$

3:00 – 3:15 pm	Alan Goldman, Ames Laboratory (19) *Correlations and Competition between the Lattice, Electrons, and Magnetism*
3:15 – 3:30 pm	Stephan Rosenkranz, Argonne National Laboratory (23) *Neutron and X-ray Scattering Studies of the Structure and Dynamics of Bulk and Heterostructures of Strongly Correlated Materials*
3:30 – 3:45 pm	Bob Cava, Princeton University (29) *Experimental Realization of a Single Crystal Bond-Disordered Pyrochlore Antiferromagnet*
3:45 – 5:00 pm	**Break and Poster session of the above talks for further discussion and Other poster:** Andreas Kreyssig (10)
5:00 – 6:30 pm	**Break for interactive discussion and free time**
6:30 – 7:30 pm	***** **Working Dinner** *****
Session IV	**Quantum Materials (Round Table Panel Discussion)** Discussion Leaders: Alexander Balatsky (Los Alamos National Laboratory), David Singh (Oak Ridge National Laboratory), and Oleg Tchernyshyov (Johns Hopkins University)
7:30 – 9:00 pm	**Key neutron scattering experiments to advance quantum materials?**
9:00 pm	End of the day remarks

TUESDAY, JULY 29, 2014

7:00 – 8:00 am	***** **Breakfast** *****
Session V	**Soft Matter** Chair: Arun Yethiraj, University of Wisconsin–Madison
8:00 – 8:15 am	Brad Olsen, Massachusetts Institute of Technology (1) *Thermodynamics of Self-Assembly in Globular Protein-Polymer Conjugates*
8:15 – 8:30 am	Mahesh Mahanthappa, University of Wisconsin–Madison (5) *Understanding Functional Lyotropic Liquid Crystal Network Phase Self-Assembly and the Properties of Nanoconfined Water*

8:30 – 8:45 am	Wei-Ren Chen, Oak Ridge National Laboratory (10) *Multiphasic Soft Colloids: Fundamentals to Application of Energy Sustainability*
8:45 – 9:00 am	Dvora Perahia, Clemson University (19) *From Interfaces to Bulk: Experimental–Computational Studies across Time and Length Scales of Multi-functional Ionic Polymers*
9:00 – 9:15 am	Alamgir Karim, University of Akron (23) *In Situ Neutron Scattering Determination of 3D Phase-Morphology Correlations in Fullerene Block Copolymer Systems*
9:15 – 9:30 am	Roger Pynn, Indiana University (27) *Development of New Methods to Study Materials Structure using Spin Echo Scattering Angle Measurement (SESAME) of Neutrons*
9:30 – 10:30 am	**Break and Poster session of the above talks for further discussion**
Session VI	**Dynamics** Chair: Collin Broholm, Johns Hopkins University
10:30 – 10:45 am	Brent Fultz, California Institute of Technology (2) *Vibrational Thermodynamics of Materials at High Temperatures*
10:45 – 11:00 am	Henry Glyde, University of Delaware (6) *Neutron Scattering Studies of Classical and Quantum Fluids in Porous Media*
11:00 – 11:15 am	Sow-Hsin Chen, Massachusetts Institute of Technology (14) *Scattering Studies of the Liquid-Liquid Transition in Supercooled MCM41 Confined Water, Protein Hydration Water and Microstructure of New Green Cement*
11:15 – 11:30 am	Dmitry Reznik, University of Colorado–Boulder (20) *Inelastic Neutron and X-ray Scattering Investigation of Electron-Phonon Effects in Quantum Materials*
11:30 – 11:45 am	Morten Eskildsen, University of Notre Dame (24) *Vortex Lattices Studies in Type II Superconductors*
11:45 – 12:00 noon	Michael Manley, Oak Ridge National Laboratory (28) *Impact of Dynamic Lattice Instabilities and Microstructure on Functional Materials*
12:00 – 1:00 pm	***** **Working Lunch** *****
1:00 – 2:30 pm	**Break and Poster session of the above talks for further discussion**

Session VII	**Advanced Capabilities** Chair: Guangyong Xu, Brookhaven National Laboratory
2:30 – 2:45 pm	Thomas Proffen, Oak Ridge National Laboratory (4) *Center for Accelerating Materials Modeling from SNS Data*
2:45 – 3:00 pm	Stephan Rosenkranz, Argonne National Laboratory (16) *Neutron and X-ray Scattering Studies of the Structure and Dynamics of Bulk and Heterostructures of Strongly Correlated Materials*
3:00 – 3:15 pm	Boris Khaykovich, Massachusetts Institute of Technology (18) *Optics for Advanced Neutron Imaging and Scattering*
3:15 – 3:30 pm	Jason Hayward, University of Tennessee–Knoxville (22) *Neutron Scattering Instrumentation Research and Development for High Spatial and Temporal Resolution Imaging at Oak Ridge National Laboratory*
3:30 – 3:40 pm	Suzanne te Velthuis, Argonne National Laboratory (26) *National School on Neutron and X-ray Scattering*
3:40 – 3:50 pm	Takeshi Egami, University of Tennessee–Knoxville (30) *Neutron Scattering Study of Strongly Correlated Systems*
3:50 – 5:00 pm	**Break and Poster session of the above talks for further discussion and Other poster:** John DiTusa (12)
5:00 – 6:30 pm	**Break for interactive discussion and free time**
6:30 – 7:30 pm	***** **Working Dinner** ***** Prepare questions for the Panel Discussion (Session VIII)
Session VIII	**Panel Discussion** Discussion leader: Thomas Proffen, Oak Ridge National Laboratory
7:30 – 8:30 pm	Advanced Capabilities needed for the Neutron Scattering Community
8:30 pm	End of the day remarks

WEDNESDAY, JULY 30, 2014

7:00 – 8:00 am	***** **Breakfast** *****
Session IX	**Correlated Electron Materials** Chair: Takeshi Egami, University of Tennessee–Knoxville
8:00 – 8:15 am	Collin Broholm, Johns Hopkins University (1) *Institute for Quantum Matter*
8:15 – 8:30 am	Joe Thompson, Los Alamos National Laboratory (5) *Complex Electronic Materials*
8:30 – 8:45 am	Despina Louca, University of Virginia (15) *Local Complexity and the Mechanics of Phase Transitions in Novel Materials*
8:45 – 9:00 am	Peter Armitage, Johns Hopkins University (19) *A Hierarchy of "Meson" Bound States in the 1D Ferromagnetic Ising Chain $CoNb_2O_6$ Investigated by High Resolution Time-Domain Terahertz Spectroscopy*
9:00 – 9:15 am	David Vaknin, Ames Laboratory (23) *Correlations and Competition between the Lattice, Electrons, and Magnetism*
9:15 – 9:30 am	Igor Zaliznyak, Brookhaven National Laboratory (29) *Neutron Scattering Studies of Magnetism, Orbital Hybridization and Electron Itinerancy in Fe-based Superconductors*
9:30 – 11:00 am	**Break and Poster session of the above talks for further discussion and Other posters:** Eric Bauer (7), Marc Janoschek (10), Filip Ronning (12), and Oleg Tchernyshyov (26)
11:00 – 11:30 am	**Wrap-up, debriefing, evaluation** Thiyaga P. Thiyagarajan, Program Manager, Neutron Scattering
11:30 am	***** Adjourn*****

Session I

Heterostructures

Improper Ferroelectricity and Frustrated Magnetism in Hexagonal Multiferroics: Neutron and Ellipsometry Studies

Principal Investigator: S-W. Cheong. Co-PIs: V. Kiryukhin and A. Sirenko

Program Scope

Colossal magnetoelectric effects in multiferroics open up an entirely new way of the phase control with potential for device applications in many areas, such as transducers, field sensors, data recording, *etc.* Colossal magnetoelectric properties of multiferroics are closely associated with the collective nature of simultaneous magnetic and ferroelectric phase transitions. This Project aims to reveal the features of the magnetic structure and the corresponding magnetic and lattice excitations underlying the giant effects associated with these transitions. We focus on studies of multiferroic materials in which magnetic frustration and closely related effects of geometrical constraints on ferroelctricity could lead to enhanced functional properties, such as improper hexagonal ferroelectrics REMnO$_3$ (RE=Ho-Lu). A complementary combination of neutron scattering and far IR ellipsometry, together with closely coordinated crystal growth activity, is used.

Recent Progress

Studies of spin waves are "bread and butter" of inelastic neutron scattering. They are of the key importance for physics of magnetism because they provide the direct way of measuring magnetic interaction parameters in crystals. Linear spin wave approximation is generally accepted to hold for large spins at zero temperature, making such measurements possible. However, for some geometrically frustrated magnets, it fails for any spin value. This fact is not well known, and demonstration of the spin-wave picture failure in a well-known magnetic system is clearly of significant importance. We have investigated [1] hexagonal LuMnO$_3$, in which Heisenberg Mn spins (S=2) reside on a 2D triangular lattice, forming a well-known 120° structure. Linear spin-wave approximation fails for this system. We observe all three key features of the predicted nonlinear effects: a rotonlike minimum, a flat mode, and a (zero-T) line-width broadening. This is a direct demonstration that quasiparticles in a system commonly thought of as classical can break down.

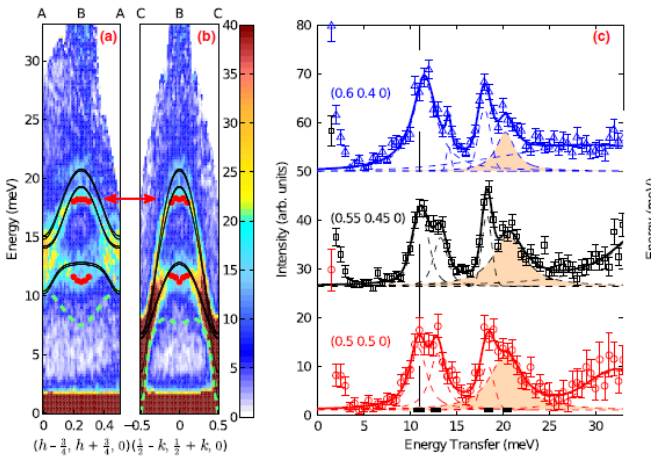

(a,b) Flat mode and rotonlike minimum, and (c) anomalously broad magnetic excitations in LuMnO$_3$.[1]

Inelastic neutron experiments are typically time consuming. To efficiently monitor the relevant excitations in a large number of compounds, we use our Mueller matrix ellipsometry setup. Optical properties of hexagonal multiferroic oxides RMnO$_3$, where R= Ho, Er, Tm, Yb, and Lu were studied in the far-infrared spectral range (100 to 2000 cm^{-1}) and temperatures between 1.5 K and 300 K. Spectra of the optical phonons have been described in terms of the temperature dependencies of their frequency, damping, and oscillator strength. For all studied oxide materials, clear signatures of the spin-phonon interaction have been found below the temperature of the antiferromagnetic phase transition T_N due to magnetic ordering of Mn^{3+} spins. A decrease of the ionic radius for R^{3+} ions between Ho^{3+} and Lu^{3+} in the corresponding RMnO$_3$ compounds resulted in a systematic variation of the frequency for several optical phonons. A magnetic excitation at ~190 cm^{-1} was observed at low temperatures below T_N and interpreted as due to two-magnon absorption.

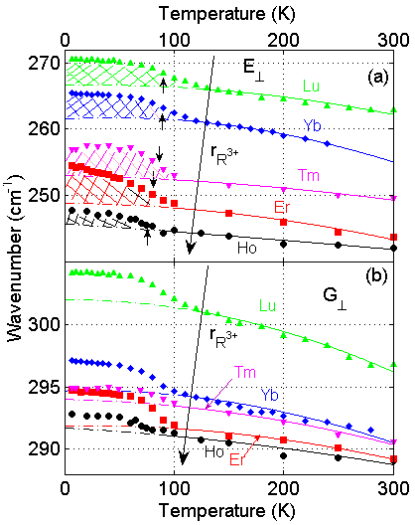

Temperature dependence of the frequency for two *ab*-plane E_1-symmetry optical phonons with the strongest spin-phonon interaction for RMnO$_3$, The AFM ordering temperature for Mn^{3+} spins is shown in (b) with small vertical arrows. The long arrows in both (a) and (b) show schematically an increase of the R^{3+} ionic radius r_{R3+} from Lu to Ho.

The physical nature of magnetoelectric coupling was also investigated in other multiferroics, including a high-importance compound BiFeO$_3$. Using high-resolution single crystal neutron diffraction techniques, we have determined [2] the contributions of each individual element to the electric polarization in BiFeO$_3$, and concluded that magnetostrictive coupling suppresses the electric polarization at the Fe site below T_N. The observed negative sign of the magnetoelectric coupling was surprising, contradicting the regular expectation of the positive sign due to the spin current contributions arising from the cycloid spin structure.

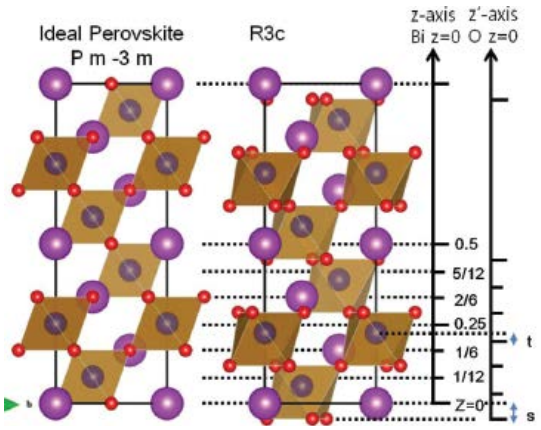

Atomic positions in the paraelectric (left) and ferroelectric (right) phases of BiFeO$_3$ [2].

Future Plans

Continue our efforts to understand the connection between the improper ferroelectricity and magnetic frustration in hexagonal multiferoics using advanced growth, neutron scattering, and Muller matrix spectroscopic ellipsometry. We shall study effects of structural constraints and magnetic geometrical frustration on the ferroelectric, magnetic, and magnetoelectric properties of multiferroics including (*R*,In)(Ga,Mn)O_3, *R*InO_3, and several related systems such as $Ca_3Co_2O_6$. Static and dynamic properties of structural and magnetic transitions will be investigated. The resulting understanding of the mechanism of these phase transitions should help identify the specific systems with a potential for giant static and dynamic response to external fields. In particular, we plan the following: (i) Studies of the low-energy magnetic excitations and search for hybrid modes using polarized inelastic neutron scattering experiments, as well as optical measurements. (ii) Measure the degree of electric- and magnetic hybridization for electromagnons, magnons, and phonons in the compounds described above, as well as in 2H-$BaMnO_3$, and *R*FeO_3 using far-infrared ellipsometry, identify the most interesting materials/experimental regimes, and investigate them in detail using neutron scattering.

Publications

[1] Joosung Oh, Manh Duc Le, Jaehong Jeong, Jung-hyun Lee, HyungjeWoo, Wan-Young Song, T. G. Perring, W. J. L. Buyers, S.-W. Cheong, and Je-Geun Park, *Magnon Breakdown in a Two Dimensional Triangular Lattice Heisenberg Antiferromagnet of Multiferroic $LuMnO_3$,* Phys. Rev. Lett. **111**, 257202 (2013).

[2] Sanghyun Lee, M. T. Fernandez-Diaz, H. Kimura, Y. Noda, D. T. Adroja, Seongsu Lee, Junghwan Park, V. Kiryukhin, S.-W. Cheong, M. Mostovoy, and Je-Geun Park, *Negative magnetostrictive magnetoelectric coupling of $BiFeO_3$,* Phys. Rev. B **88**, 060103(R) (2013).

[3] Shin-ichiro Yano, Despina Louca, Songxue Chi, Masaaki Matsuda, Yiming Qiu, John R. D. Copley, and Sang-Wook Cheong, "*Intertwining of Frustration with Magneto-Elastic Coupling in the Multiferroic $LuMnO_3$*", Journal of the Physical Society of Japan **83**, 024601 (2014).

[4] Jae Wook Kim, Y. Kamiya, Eun Deok Mun, M. Jaime, N. Harrison, J. D. Thompson, V. Kiryukhin, H. T. Yi, Y. S. Oh, S.-W. Cheong, C. D. Batista, and V. S. Zapf, *Multiferroicity with coexisting isotropic and anisotropic spins in $Ca_3Co_{2-x}Mn_xO_6$,* Phys. Rev. B **89**, 060404(R) (2014).

[5] Nara Lee, Young Jai Choi, and Sang-Wook Cheong, "*Magnetic control of ferroelectric polarization in a self-formed single magnetoelectric domain of multiferroic $Ba_3NbFe_3Si_2O_{14}$*", Appl. Phys. Lett. **104**, 072904 (2014).

[6] R. D. Johnson, P. Barone, A. Bombardi, R. J. Bean, S. Picozzi, P. G. Radaelli, Y. S. Oh, S.-W. Cheong, and L. C. Chapon, *X-Ray Imaging and Multiferroic Coupling of Cycloidal Magnetic Domains in Ferroelectric Monodomain $BiFeO_3$,* Phys. Rev. Lett. **110**, 217206 (2013).

[7] U. Nagel, Randy S. Fishman, T. Katuwal, H. Engelkamp, D. Talbayev, Hee Taek Yi, S.-W. Cheong, and T. Room, *Terahertz Spectroscopy of SpinWaves in Multiferroic $BiFeO_3$ in High Magnetic Fields,* Phys. Rev. Lett. **110**, 257201 (2013).

[8] J. Lee, S. A. Trugman, C. D. Batista, C. L. Zhang, D. Talbayev, X. S. Xu, S.-W. Cheong, D. A. Yarotski, A. J. Taylor, and R. P. Prasankumar, *Probing the Interplay between Quantum Charge Fluctuations and Magnetic Ordering in $LuFe_2O_4$,* SCIENTIFIC REPORTS | 3 : 2654 | DOI: 10.1038/srep02654 www.nature.com/scientificreports

[9] R. D. Johnson, K. Cao, L. C. Chapon, F. Fabrizi, N. Perks, P. Manuel, J. J. Yang, Y. S. Oh, S.-W. Cheong, and P. G. Radaelli, *$MnSb_2O_6$: A Polar Magnet with a Chiral Crystal Structure,* Phys. Rev. Lett. **111**, 017202 (2013).

[10] N. Lee, C. Vecchini, Y. J. Choi, L. C. Chapon, A. Bombardi, P. G. Radaelli, and S-W. Cheong, *Giant Tunability of Ferroelectric Polarization in $GdMn_2O_5$,* Phys. Rev. Lett. **110**, 137203 (2013).

[11] Y. J. Choi, N. Lee, P. A. Sharma, S. B. Kim, O. P. Vajk, J.W. Lynn, Y. S. Oh, and S-W. Cheong, *Giant Magnetic Fluctuations at the Critical Endpoint in Insulating HoMnO3,* Phys. Rev. Lett. **110**, 157202 (2013).

[12] T. N. Stanislavchuk, T. D. Kang, P. D. Rogers, E. C. Standard, R. Basistyy, A. M. Kotelyanskii, G. Nita, T. Zhou, G. L. Carr, M. Kotelyanskii, and A. A. Sirenko, "*Synchrotron-radiation based far-infrared spectroscopic ellipsometer with a full Muller matrix capability*", Rev. Sci. Instr. **84**, 023901 (2013).

[13] T. N. Stanislavchuk, A. A. Sirenko, A. P. Litvinchuk, X. Luo, and S.-W. Cheong, "*Electronic band structure and optical phonons of $BaSnO_3$ and $Ba_{0.97}La_{0.03}SnO_3$ single crystals: Theory and experiment*", J. Appl. Phys. **112**, 044108 (2012).

[14] T. D. Kang, E. C. Standard, P. D. Rogers, K. H. Ahn, and A. A. Sirenko, A. Dubroka, C. Bernhard, S. Park, Y. J. Choi and S.-W. Cheong, *"Far-infrared spectra of the magnetic exchange resonances and optical phonons and their connection to magnetic and dielectric properties of $Dy_3Fe_5O_{12}$ garnet"*, Phys. Rev. B **86**, 144112 (2012).

Neutron Scattering Studies of Cobaltite Crystals and Heterostructures

Chris Leighton, Chemical Engineering and Materials Science, University of Minnesota

Program Scope

Complex oxides such as perovskites display extraordinarily diverse physical phenomena and a rich interplay between structure and properties. These properties define grand challenges to our understanding of correlated electrons (such as high temperature superconductivity and electronic inhomogeneity/complexity), at the same time providing application potential in areas as diverse as oxide electronics and spintronics, ferroelectric RAM, solid oxide fuel cells, gas separation, and catalysis. Significantly, highly-controlled growth of epitaxial films and heterostructures of these oxides is now possible with atomic-level precision, opening up a plethora of additional opportunities in fundamental science (*e.g.* discovery of new ground states, strain-stabilization of non-equilibrium structures, *etc.*), in addition to novel device concepts.

This program (Fig. 1) is focused on two central challenges: The need for a comprehensive understanding of electronic behavior in complex oxides, and the need for a full appreciation of what can be achieved with oxide hetero-structures. We are tackling these questions using the doped perovskite cobaltites, due to unique attributes that make them model systems for the phenomena of interest. These phenomena include nanoscale electronic inhomogeneity, spin-state transitions, and the influence of interfaces, defects, and strain on magnetism and transport. In addition to synthesis, and a battery of complementary property measurements, the work relies on neutron scattering methods, including small-angle scattering (SANS), neutron diffraction (ND), and polarized neutron reflectometry (PNR). Recently the project has evolved to apply the concepts developed for cobaltites to other systems where magnetic inhomogeneity is important, such as complex fluorides and alloys.

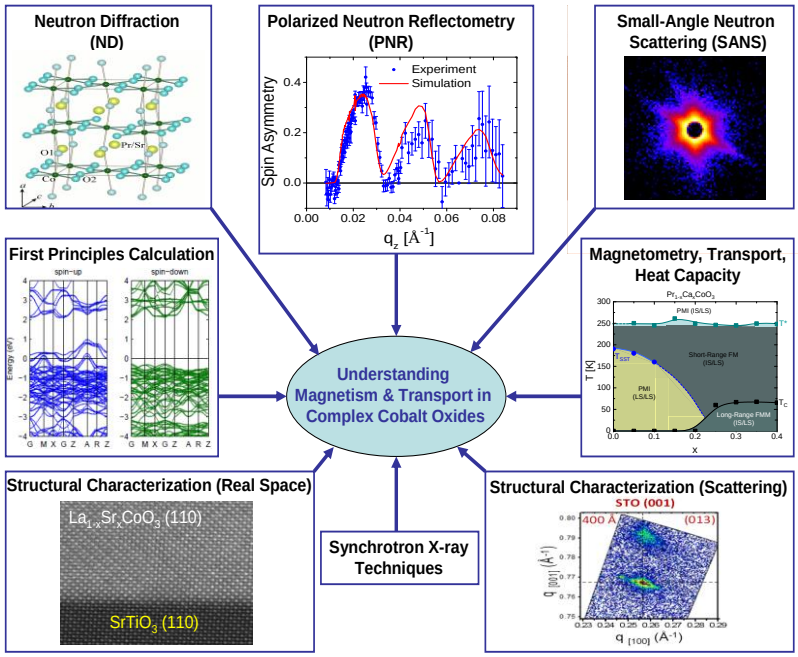

Figure 1: Schematic of the primary experimental and theoretical approaches applied in this project, particularly neutron scattering.

Recent Progress

Nanoscopic inhomogeneity in lightly-doped $La_{1-x}Sr_xCoO_3$ single crystals. Following from the detailed understanding of the phenomenology, consequences and origins of the magnetically phase-separated state of $La_{1-x}Sr_xCoO_3$ developed under prior DOE support, in the last two years we have studied the most important remaining issue with the physics of this system: How the magnetic polarons forming around Sr at light doping evolve into the ferromagnetic clusters that are so dominant at higher *x*. This is an issue of general importance as little is known about how

we connect established ideas regarding magnetic polarons in classic magnetic semiconductors with our understanding of magnetic phase separation in higher carrier density systems such as manganites and cobaltites. By examining carefully-characterized single crystals with AC and DC magnetometry, SANS, magnetotransport and heat capacity, and comparing the results with extensive simulations, we have developed a deep understanding of this doping-driven crossover, emphasizing both it's statistical nature and the key role of spin and charge dynamics.

Narrow bandwidth cobaltites. Narrow electronic bandwidth systems such as $Pr_{1-x}Ca_xCoO_3$ and $Nd_{1-x}Ca_xCoO_3$ represent another important frontier as; (*a*) the narrow conduction bands weaken ferromagnetism, accentuating competition with other phases, (*b*) the accompanying distortions stabilize low spin-states, leading to the anticipated interplay between phase separation and spin-state physics, and (*c*) Pr-based systems have recently been discovered to undergo first-order transitions where the Pr valence abruptly shifts from 3+ to 4+. The latter drives charge transfer from the Co-O hybridized bands, inducing unique first order insulator-metal transitions. Our recent work has contributed to the understanding in this area by making the first detailed comparison between $Pr_{1-x}Ca_xCoO_3$ and $Nd_{1-x}Ca_xCoO_3$ (using ND and SANS), enabling deconvolution of the effects of bandwidth narrowing from the phenomena unique to Pr [5]. Using Y-doping to apply chemical pressure we have also studied (again with SANS) the magnetic inhomogeneity beneath the valence transition, which we find occurs across a broader range of length scales than in simpler systems [4], likely related to the additional disorder.

Cobaltite films and heterostructures. Our first major finding in the area of cobaltite heterostructures was the discovery that not only can magnetic inhomogeneity be *induced* at interfaces, but that this provides the first complete explanation for the "dead layers" that plague such systems. Building on this, our recent work has been the first to directly image the nanoscale inhomogeneity, using scanning tunneling microscopy and spectroscopy [1]. We have also now converged on the concept that the interface-induced magnetic phase separation is due to hole depletion arising from oxygen vacancy accumulation, the driving force being oxygen vacancy *ordering*. In essence the oxygen vacancies in these materials undergo crystallization (Fig. 2) in order to achieve lattice parameters that accommodate lattice mismatch. This creates a direct link between strain and stoichiometry, which we have exploited to demonstrate strain and orientation manipulation of the modulation vector of the defect ordering (Fig. 2) [7]. This in turn controls the oxygen depth profile and thus the transport and magnetism, creating an entirely new means to fine-tune interfacial properties, of broad interest for applications. The magnetization depth profile has been probed with PNR (Fig. 3) directly revealing the suppression in dead layer thickness on appropriately chosen substrates. Finally, we recently discovered a family of phenomena that appear to exist solely due to the presence of oxygen vacancy ordering, the most dramatic example being giant anisotropic magnetoresistance in $LaAlO_3$(001) /$La_{0.5}Sr_{0.5}CoO_{3-\delta}$. These phenomena are being intensively studied.

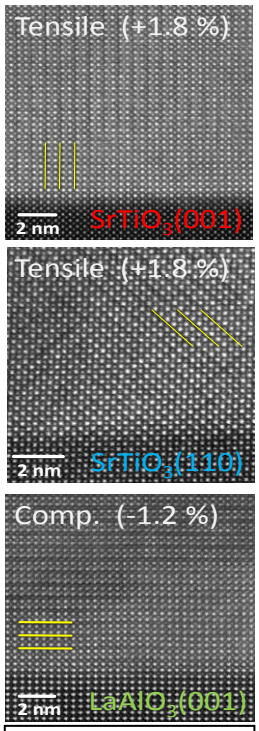

Figure 2: TEM images of oxygen vacancy ordering in $La_{0.5}Sr_{0.5}CoO_{3-\delta}$ on substrates with differing strain and orientation.

Magnetic inhomogeneity in complex metal alloys. Motivated to apply the approaches developed above to other inhomogeneous magnetic systems we performed detailed studies of a fascinating set of recently discovered metal alloys [2,11]. These take the form $Ni_{50-x}Co_xMn_{25+y}Z_{25-y}$ (Z = Sn, In, *etc.*), being

off-stoichiometric versions of the Ni_2MnZ full Heusler alloys. At certain compositions, identified by predictive theory from the U. of Minnesota, these alloys display unusually reversible martensitic transformations, multiferroicity, and acute magnetic phase competition. Our work has shown that this leads to such phenomena as spontaneous nanoscale magnetic inhomogeneity, collective cluster freezing, and intrinsic exchange bias [2,11]. In terms of applications these alloys exhibit field-induced phase transformations, magnetic shape memory, magneto-caloric effects, and low hysteresis, making them attractive for sensors and actuators, magnetic refrigeration, and energy conversion. Our work was the first to directly probe magnetic inhomogeneity (using SANS [11]), the first to build strong evidence for antiferromagnetic order in key regions of the phase diagram (using SANS and ND [2]), and the first to apply transport, heat capacity and NMR. These studies reveal surprisingly high effective mass and remarkable parallels with correlated oxides.

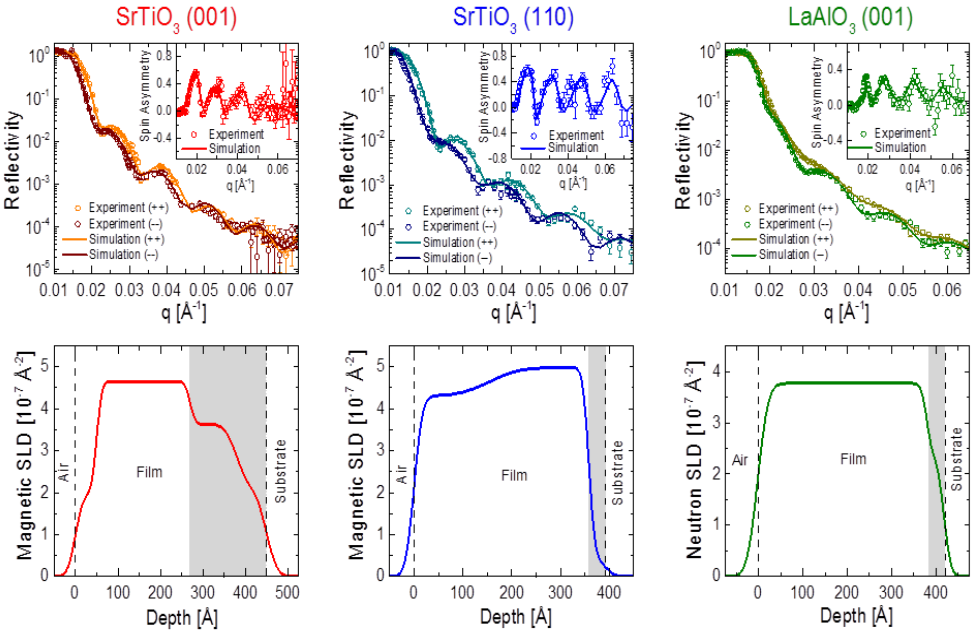

Figure 3: PNR data (10 K, saturating magnetic field) and extracted magnetic depth profiles from $La_{0.5}Sr_{0.5}CoO_{3-\delta}$ films on $SrTiO_3$(001), $SrTiO_3$(110), and $LaAlO_3$(001).

Complex metal fluorides. Working with collaborators in synthesis and theory at the University of Houston and Cornell we are also exploring the magnetic properties of newly-synthesized transition metal oxides [9] and flourides [10]. $RbFe_2F_6$ and $K_4Fe_3F_{12}$ are noteworthy examples, the former being a charge-ordered pyrochlore-related material with strongly frustrated antiferromagnetic interactions [10], the latter being a charge-ordered system with competing ferromagnetic and antiferromagnetic interactions, leading to complex metamagnetism.

Future Plans

In terms of bulk crystals, the Pr systems exhibiting the unique first-order valence transitions are of high interest. We already have underway studies probing this *via* crystal field excitations (which are very different for Pr^{3+} / Pr^{4+}) using inelastic neutrons, as well as the first spatially-resolved measurements using electron microscopy / electron energy loss spectroscopy (with R. Klie, U. of Illinois). Exploration of generality of this phenomenon will also be pursued, using wider bandwidth cobaltites (*e.g.* $Pr_{1-x}Sr_xCoO_3$), as well as manganites. First-principles electronic structure calculations are ongoing with R. Wentzcovitch (U. of Minnesota), seeking to understand the *f*-electron trends across the lanthanide cobaltites. The other major area of new interest is in $La_{1-x}Ba_xCoO_{3-\delta}$, where the possibility of the first true colossal magnetoresistance effect in the perovskite cobaltites has recently been reported. Our initial ND experiments to probe the possibility of field-driven antiferromagnet to ferromagnet conversion are already

complete and large magnetoresistance effects have been confirmed. With regard to the complex alloys discussed above, the two highest priorities are Mn and Co zero-field NMR with the National High Magnetic Field Lab (with the potential to directly verify antiferromagnetic order), and high field transport to probe the possibility of magnetoresistive effects due to nanoscale inhomogeneity. In terms of thin films and heterostructures, the highest priority is to elucidate the fascinating oxygen-vacancy-order-induced anisotropic transport effects we recently discovered, combining this with PNR to fully explore the attractive concept of controlled defect ordering for stabilization of new phenomena. Vertical transport across cobaltite/titanate magnetic *p-n* junctions is also of interest as a novel means to probe the dramatically different dead layer effects on $SrTiO_3$(001) *vs.* $SrTiO_3$(110). Finally, the Pr-based systems discussed above are also exciting prospects for thin film experiments, strain stabilization of the two states, and control/enhancement of the insulator-metal transition being particularly appealing.

Publications (2012 – 2014)

1. "*Direct real space observation of magneto-electronic inhomogeneity in ultra-thin film* $SrTiO_3(001)/La_{0.5}Sr_{0.5}CoO_{3-\delta}$", Kelly, Galli, Aarts, Bose, Sharma and Leighton, submitted, Appl. Phys. Lett. (2014).

2. "*Magnetic phase competition in off-stoichiometric martensitic Heusler alloys: The* $Ni_{50-x}Co_xMn_{40}Sn_{10}$ *system*", Bhatti, Srivastava, Phelan, El-Khatib, James and Leighton, invited chapter, *Handbook of Heusler Alloys*, Eds. A. Hirohata and C. Felser, Taylor and Francis (2014).

3. "*Magnetocaloric effect and critical behavior in* $Pr_{0.5}Sr_{0.5}MnO_3$*: An analysis on the validity of the Maxwell relation and the nature of phase transitions*", Caballero-Flores, Bingham, Phan, Torija, Leighton, Franco, Conde and Srikanth, in press, J. Phys. Cond. Mat. (2014).

4. "*Magnetically inhomogeneous ground-state below the first order valence transition in* $(Pr_{1-y}Y_y)_{0.7}Ca_{0.3}CoO_{3-\delta}$", Phelan, Bhatti, Taylor, Wang and Leighton, Phys. Rev. B. **89**, 184427 (2014).

5. "*Structural, transport, and magnetic properties of* $Nd_{1-x}Ca_xCoO_{3-\delta}$ *and a comparison to* $Pr_{1-x}Ca_xCoO_{3-\delta}$", Phelan, Suzuki, Wang, Huq and Leighton, Phys. Rev. B. **88**, 075119 (2013).

6. "*Thermodynamics of energy conversion via first order phase transformation in low hysteresis magnetic materials*", Song, Bhatti, Srivastava, Leighton and James, Energy Environ. Sci. **6**, 1315 (2013).

7. "*Lattice mismatch accommodation via oxygen vacancy ordering in epitaxial* $La_{0.5}Sr_{0.5}CoO_3$ *thin films*", Gazquez, Bose, Sharma, Torija, Pennycook, Leighton and Varela, APL Materials **1**, 012105 (2013).

8. "*Ferrimagnetism in* $PrCoO_3$ *epitaxial films*", Mehta, Bose, Iwata, Arenholz, Leighton and Suzuki, Phys. Rev. B. Rapid Comm. **87**, 020405 (2012).

9. "*Syntheses, crystal structures, and characterizations of two new* $Tl\text{-}Cu^{2+}\text{-}Te^{6+}$ *oxides:* Tl_4CuTeO_6 *and* $Tl_6CuTe_2O_{10}$", Yeon, Kim, Green, Bhatti, Leighton and Halasyamani, J. Sol. Stat. Chem. **196**, 607 (2012).

10. "$RbFe^{2+}Fe^{3+}F_6$*: Synthesis, structure, and characterization of a new charge-ordered magnetically frustrated pyrochlore-related mixed-metal fluoride*", Kim, Kim, Halasyamani, Green, Bhatti, Leighton, Das and Fennie, Chem. Sci. **3**, 741 (2012).

11. "*Small-angle neutron scattering study of magnetic ordering and inhomogeneity across the martensitic phase transformation in* $Ni_{50-x}Co_xMn_{40}Sn_{10}$ *alloys*", Bhatti, El-Khatib, Srivastava, James and Leighton, Phys. Rev. B. **85**, 134450 (2012).

Neutron and x-ray scattering studies of the structure and dynamics of bulk and heterostructures of strongly correlated materials

S. Rosenkranz (srosenkranz@anl.gov), O. Chmaissem*, R. Osborn, S.G.E. te Velthuis
Materials Science Division, Argonne National Laboratory, Argonne, IL 60439
**Department of Physics, Northern Illinois University, DeKalb, IL 60115*

Research Scope

Many phenomena of recent interest are associated with the presence of complex disorder and short-range correlations that result from the presence of multiple ground-states with incompatible order. Materials, in which long range ordered phases have been suppressed by competing interactions, generally exhibit unusual and often strongly enhanced responses to external stimuli such as magnetic or electric fields and are of considerable technological potential for future applications. We utilize, and when necessary in order to advance the scientific program also develop, the latest advances in neutron and synchrotron x-ray instrumentation to study how bulk and heterostructures of strongly correlated materials respond on a range of length and time scales to competing interactions, in order to obtain an understanding of material functionality. Our programs focus on studies of the influence of different interactions on the formation of charge density wave correlations and their connection to unusual electronic and physical properties, studies of emergent phenomena and competing interactions at interfaces of magnetic heterostructures, and studies of the influence of magnetic and orbital fluctuations in strongly correlated electron systems, particularly in iron-based superconductors.

Recent Progress

Charge density wave (CDW) correlations: Our inelastic x-ray scattering investigations of the soft phonons, combined with *ab-initio* calculations, show that the CDW instability in the prototypical compound *2H*-$NbSe_2$ is primarily driven by strongly momentum-dependent electron-phonon coupling, rather than by the commonly assumed textbook Fermi surface nesting scenario.

In another canonical CDW compound, *1T*-$TiSe_2$, our synchrotron x-ray diffraction investigations combined with transport and specific heat measurements, reveal the transition to a chiral CDW state. These observations confirm theoretical predictions based on orbital ordering of Ti *3d* and Se *4p* electrons and provide the first scattering evidence for chirality in a CDW compound.

Magnetic heterostructures. Polarized neutron reflectivity studies, combined with XMCD and theoretical modeling, reveal a strong effect of an induced interfacial magnetization in cuprates on the transport properties of magnetic junctions consisting of ferromagnetic manganite $La_{0.7}Ca_{0.3}MnO_3$ and insulating, as well as, superconducting cuprates, $PrBa_2Cu_3O_7$ and $YBa_2Cu_3O_{7-\delta}$. The induced magnetization arises from the orbital reconstruction at the interface between interfacial Mn spins and localized states in the CuO_2 planes. Our results, which are of significant interest for both basic research and spintronics applications, provide evidence for a novel emergent spin-filter functionality not previously considered and explain the unusual inverse superconducting spin-switch behavior, respectively. Furthermore, in the case of $PrBa_2Cu_3O_7$, we find a novel form of magnetoelectric coupling arising from the induced magnetization. This results in a ferromagnetic coupling between the manganite layers that can be controlled by a voltage and consequently provides a device can be electrically toggled between two magnetization states in the absence of a magnetic field.

Iron based superconductors: A detailed investigation of the phase diagram of $(Ba,Na)Fe_2As_2$ by high resolution neutron powder diffraction reveals the existence of a novel state, a magnetic phase that restores tetragonal symmetry. Such a tetragonal, magnetic phase is predicted by spin-nematic theories, showing that nematic order in iron-based superconductors is driven by magnetic, rather than orbital, interactions. We also continued to investigate the influence of magnetic and orbital order and correlations in a variety of strongly correlated systems.

Instrument and technique development: We have successfully developed and employed the *Sweep*-mode, a method to measure the full four-dimensional scattering function $S(\mathbf{Q},\omega)$ from single crystals utilizing continuous sample rotation in combination with an event-based data acquisition system [20]. In contrast to the traditional method, whereby data is taken sequentially at a predetermined fixed number of angles and the full data can only be reconstructed *a posteriori*, the sweep method allows the complete result to be monitored immediately, and to adjust the experimental conditions based on scattering features and measurement statistics.

Corelli, the dedicated single-crystal diffuse scattering instrument that was proposed by our group is now under commissioning at the Spallation Neutron Source.

Future Plans

CDW correlations. We will study how various different interactions and their competition lead to short range CDW correlations and how they affect unusual electronic properties in canonical CDW compounds by combining scattering with angle resolved photoemission and scanning tunneling microscopy measurements. Of particular interest is how the suppression of CDW correlations as function of doping, temperature, and pressure leads to the presence of a persistent gap in the electronic spectra over large regions of temperature and doping where long-range order has been suppressed, a phenomenon similar to the pseudogap of relevance to many strongly correlated systems such as the cuprates.

Complex oxide interfaces. We will continue our investigations of superlattices of complex oxide materials. Of particular interest will be to determine the prevalence and influence of induced interfacial magnetization, such as at interfaces between ferromagnetic manganites (LCMO) and cuprates (YBCO and PBCO), as well as titanate and ferrite compounds. The later systems, in which a ferroelectric is sandwiched between two ferromagnetic layers, also provide a pathway to study magneto-electronic coupling. Preliminary work shows that at LSMO/$BaTiO_3$ interfaces there is indeed an induced interfacial Ti-moment. We will explore the impact of this moment on transport properties and how the ferroelectric polarization influences the magnetization in the adjacent ferromagnetic layers (LSMO) and *vice versa*. It is anticipated that since polarization switching is correlated with changes in the lattice, distortions will be induced in the ferromagnetic layers as well, and that the polarization field could modify the charge carrier density close to the interface. Both these effects can strongly modify the magnetization in the vicinity of the interface. Finally, we will investigate the effects of applied electric fields on the magnetization by performing XMCD, optical Kerr, and PNR experiments on heterostructures of strongly correlated materials, which show strong voltage-controlled magnetic anisotropy with in-situ applied electric fields.

Magnetic and orbital fluctuations in Strongly Correlated Electron Systems. We will investigate the extent and universality of the re-entrant magnetic tetragonal C_4 phase that we recently

observed in the Na-doped 122 compounds. To do so, we plan to investigate several series of hole-doped $A_{1-x}A'_xFe_2As_2$ materials (A=Ba, Sr, Ca, A'=K, Na, Cs, Rb). The different electronegativity and ionic size variance of these alkaline earth metals and alkali metals (A and A', respectively) is proven to produce significantly different T_N values, thus providing a systematic investigation of the presence and influence of the C_4 phase over a wide range of transition temperatures. We will also perform high-pressure neutron and x-ray diffraction measurements in order to determine whether this phase can be stabilized by external pressure, as was suggested for the K-doped systems from transport measurements and we plan to determine the magnetic structure and excitations using elastic and inelastic neutrons scattering from single crystals.

A related topic that is currently attracting greatest interest is the nature and role of nematic fluctuations in the magnetism and superconductivity of iron-based superconductors. The presence of anisotropic electronic correlations, through their coupling to the lattice, leads to diffuse scattering signatures, albeit very weak and possibly dynamic in nature. We will measure in detail the diffuse scattering over a large range of temperature and doping on a variety of hole-doped as well as isovalent (P-substituted) compounds in order to determine the presence of nematic correlations and their relation to superconductivity. These experiments are enabled by our ongoing development of both; diffuse scattering measurement techniques and big data analysis tools. The diffuse scattering can be from both static disorder (e.g. Huang scattering from local distortions) as well as dynamic fluctuations (e.g. thermal diffuse scattering), but with data of high accuracy and coverage over large range of temperatures and momentum transfer, it is possible to separate these components with the comprehensive set of analysis tools that we are currently developing. These new experimental tools can also be applied to address similar questions in cuprate superconductors. In particular, this approach could yield important new insight regarding the extent of the short-range CDW correlations recently observed in the pseudogap phase of underdoped compounds as well as the influence of strong electron-phonon coupling. We will therefore perform comprehensive survey of the x-T phase diagram, e.g. of $La_{2-x}Sr_xCuO_4$, to investigate whether a pseudogap line can be associated with either a change in the temperature dependence of CDW correlations, or with anomalies in the thermal diffuse scattering that indicate renormalized electron-phonon coupling.

We will continue to explore other strongly correlated systems in which unusual physical properties are related to magnetic and orbital correlations. Systems of recent interest are the novel class of frustrated cobaltities $RBaCo_4O_{7+x}$, which exhibit very different magnetic and structural properties depending on R and extrinsic conditions, with both long-range and short-range frustrated magnetic order present in R=Y and Lu, respectively. We will perform neutron scattering measurements on powders and single crystal samples to obtain an understanding of the disparate magnetic properties across the series $(Lu_{1-x}Y_x)BaCo_4O_7$.

Publications

1. F. A. Cuellar, Y. H. Liu, J. Salafranca, N. Nemes, E. Iborra, G. Sanchez-Santolino, M. Varela, M. Garcia Hernandez, J.W. Freeland, M. Zhernenkov, M.R. Fitzsimmons, S. Okamoto, S.J. Pennycook, M. Bibes, A. Barthélémy, S.G.E. te Velthuis, Z. Sefrioui, C. Leon, J. Santamaria, Reversible electric-field control of magnetization at oxide interfaces, *Nature Comm.* **5**:4215 (2014).
2. S. Avci, O. Chmaissem, J.M. Allred, S. Rosenkranz, I. Eremin, A.V. Chubukov, D.E. Bugaris, D.Y. Chung, M.G. Kanatzidis, J.P. Castellan, J.A. Schlueter, H. Claus, D.D. Khalyavin, P. Manuel, A. Daoud-Aladin, and R. Osborn, Magnetically-driven suppression of nematic order in an iron-based superconductor *Nature Comm.* **5**:3845 (2014).

3. Sami Vasala, Hassan Saadaoui, Elvezio Morenzoni, Omar Chmaissem, Ting-Shan Chan, Jin-Ming Chen, Ying-Ya Hsu, Hisao Yamauchi, and Maarit Karppinen, Characterization of magnetic properties of Sr_7CuWO_6 and Sr_7CuWO_6, *Phys. Rev. B* **89**, 134419 (2014).
4. S. L. Bud'ko, D. Y. Chung, D. Bugaris, H. Claus, M. G. Kanatzidis, P.C. Canfield, Heat capacity jump at Tc and pressure derivatives of superconducting transition temperature in the $Ba_{1-x}Na_xFeAs_2$ ($0.1 \leq x \leq 0.9$) series *Phys. Rev. B* **89**, 014510 (2014).
5. Yaohua Liu, F. A. Cuellar, Z. Sefrioui, J. W. Freeland, M. R. Fitzsimmons, C. Leon, J. Santamaria and S. G. E. te Velthuis, Emergent Spin-Filter at the interface between Ferromagnetic and Insulating Layered Oxides, *Phys. Rev. Lett*. **111**, 247203 (2013).
6. S. G. E. te Velthuis and C. Pappas, Magnetism and Magnetic Materials probed with Neutron Scattering, *J. Magn. Magn. Mater.* **350**, 86 (2014).
7. J. Zhao, U. Chatterjee, D. Ai, D. G. Hinks, H. Zheng, G. Gu, J.P. Castellan, S. Rosenkranz, H. Claus, M.R. Norman, M. Randeria, J.C. Campuzano, Universal features in the photoemission spectroscopy of high temperature superconductors *Proc. Nat. Acad. Sci.* **110**, 17774 (2013).
8. S. Avci, O. Chmaissem, H. Zheng, A. Huq, P. Manuel, J.F. Mitchell, Oxygen Stoichiometry in the Geometrically Frustrated Kagomé System $YBaCo_4O_{7+\delta}$: Impact on Phase Behavior and Magnetism, *Chem. Mater.* **25**, 4188 (2013).
9. J. C. Lang, S.G.E. te Velthuis, B.C. Chakaoumakos, J.D. Budai, A. Ekkebus, National School on Neutron and X-ray Scattering, Synchrotron Radiation News 26, 9 (2013).
10. Y. Sun, H. Chang, M. Kabatek, Y.-Y. Song, Z. Wang, M. Jantz, W. Schneider, M. Wu, E. Montoya, B. Kardasz, B. Heinrich, S.G.E. te Velthuis, H. Schultheiss, A. Hoffmann, Damping in Yttrium Iron Garnet Nanoscale Films Capped by Platinum, *Phys. Rev. Lett.* **111**, 106601 (2013).
11. S. Avci, J.M. Allred, O. Chmaissem, D.Y. Chung, S. Rosenkranz, J.A. Schlueter, H. Claus, A. Daoud-Aladine, D.D. Khalyavin, P. Manuel, A. Llobet, M.R. Suchomel, M.G. Kanatzidis, R. Osborn, Structural, magnetic, and superconducting properties of $Ba_{1-x}Na_xFe_2As_2$ *Phys. Rev. B***88**, 094510 (2013).
12. M. Zhernenkov, G. Fabbris, O. Chmaissem, J. F. Mitchell, H. Zheng, D. Haskel, Pressure-induced volume collapse and structural phase transitions in $SrRuO_3$ *J. Solid State Chem.* **205**, 177 (2013).
13. M. Marezio, O. Chmaissem, C. Bougerol, M. Karppinen, H. Yamauchi, T. H. Geballe, Overdoped cuprates with high-temperature superconducting transitions *APL Materials* **1**, 021102 (2013).
14. F. Weber, R. Hott, R. Heid, K.-P. Bohnen, S. Rosenkranz, J.P. Castellan, R. Osborn, A.H. Said, B. M. Leu, D. Reznik, Optical phonons and the soft-mode in *2H*-$NbSe_2$ *Phys. Rev. B* **87**, 245111 (2013).
15. J.P. Castellan, S. Rosenkranz, R. Osborn, Q. Li, K.E. Gray, X. Luo, U. Welp, G. Karapetrov, J.P.C. Ruff, J. van Wezel, The chiral phase transition in charge ordered 1*T*-$TiSe_2$ *Phys. Rev. Lett.* **110**, 196404 (2013).
16. L.Y. Zhu, Yaohua Liu, F.S. Begeret, J.E. Pearson, S.G.E. te Velthuis, S.D. Bader, J.S. Jiang, Unanticipated proximity behavior in ferromagnet/superconductor heterostructures with controlled magnetic non-collinearity *Phys. Rev. Lett*. **110**, 177001 (2013).
17. D.P. Shoemaker, D.Y. Chung, H. Claus, M.C. Francisco, S. Avci, A. Llobet, M.G. Kanatzidis, Phase relations in $K_xFe_{2-y}Se_2$ and the structure of superconducting K_xFeSe_2 via high-resolution synchrotron diffraction, *Phys. Rev. B* **86**, 184511 (2012).
18. S.O. Hruszkewycz, M. Sutton, P.H. Fuoss, B. Adams, S. Rosenkranz, K.F. Ludwig Jr., W. Roseker, D. Fritz, M. Cammarata, D. Zhu, S. Lee, H. Lemke, C. Gutt, A. Robert, G. Grüebel, G.B. Stephenson, High Contrast X-ray Speckle from Atomic-Scale Order in Liquids and Glasses *Phys. Rev. Lett.* **109**, 185502 (2012).
19. S. Kolesnik, B. Dabrowski, O. Chmaissem, S. Avci, J.P. Hodges, M. Avdeev, K. Swierczek, Enhancement of the Curie temperature in $NdBaCo_2O_{5.5}$ by A-site Ca substitution *Phys. Rev. B* **86**, 064434 (2012).
20. F. Weber, S. Rosenkranz, L. Pintschovius, J.P. Castellan, R. Osborn, W. Reichardt, R. Heid, K.-P. Bohnen, E.A. Goremychkin, A. Kreyssig, K. Hradil, D.L. Abernathy, Electron-phonon coupling in the conventional superconductor YNi_2B_2C at high phonon energies studied by time-of-flight neutron spectroscopy, *Phys. Rev. Lett.* **109**, 057001 (2012).
21. F. Weber, L. Pintschovius, K. Hradil, D. Petitgrand, Phonon lineshapes in the vortex state of the phonon-mediated superconductor YNi_2B_2C, *Phys. Rev. B* **85**, 224525 (2012).
22. Yaohua Liu, C. Visani, N.M. Nemes, M.R. Fitzsimmons, L.Y. Zhu, J. Tornos, M. Garcia-Hernandez, M. Zhernenkov, A. Hoffmann, C. Leon, J. Santamaria, S.G.E. te Velthuis, Effect of interface induced exchange fields on cuprate-manganite spin switches *Phys. Rev. Lett.* **108**, 207205 (2012).
23. S. Avci, O. Chmaissem, D.Y. Chung, S. Rosenkranz, E.A. Goremychkin, J.P. Castellan, I.S. Todorov, J.A. Schlueter, H. Claus, A. Daoud-Aledine, D.D. Khalyavin, M.G. Kanatzidis, R. Osborn, Phase Diagram of $Ba_{1-x}K_xFe_2As_2$ *Phys. Rev. B* **85**, 184507 (2012).

Neutron and X-Ray Studies of Spin and Charge Manipulation in Magnetic Nanostructures

Eric E. Fullerton[1] and Sunil Sinha[2]
[1] Departments of Electrical and Computer Engineering and NanoEngineering
University of California, San Diego
efullerton@ucsd.edu

[2] Department of Physics
University of California, San Diego
ssinha@physics.ucsd.edu

Program Scope:

Electronic and magnetic materials are some of the most important and highly tunable materials systems with a wide range of new scientific discoveries. Understanding of the dynamics and the fundamental nanoscale physics of these materials is a crucial cornerstone for developing ways in which electronic and magnetic order parameters can be designed, controlled and manipulated. By combining skills in neutron and synchrotron techniques with sample fabrication, magnetic and transport measurements in films, nanostructures and devices we probe fundamental properties of nanoscale magnetic materials. The ongoing research has two research thrusts:

- **Time-dependent studies of magnetic nanostructures**
  This research probes the physics of magnetic nanostructures by studying the underlying excitations of the system with atomic depth resolution and nm lateral resolution. The time scales, physics to be studied and techniques used are divided into three distinct regimes: (i) Microseconds to seconds cover the time-scales of dynamics of slow magnetic fluctuations in materials, such as thermally-induced domain wall motion. (ii) Tens of nanoseconds to tens of picoseconds correspond to magnetic processional frequencies and we will study the dynamic response of nano-magnetic systems to nanosecond current, temperature and field pulses and (iii) pico-seconds to femto-seconds cover the time scales for energy and angular momentum transfer between orbital, spin and lattice degrees of freedom and can be used to probe the fundamental nature of phase transitions and the ultra-fast magnetization dynamics.
- **Interfacial phenomena in oxides**
  We propose to study the fundamental interfacial phenomena in complex oxide interfaces. This includes understanding the role of electric field effects in piezoelectric-ferromagnetic heterostructures and probing electronic reconstruction that occurs at oxide interfaces.

Recent Results:

We have recent results on both time-dependent studies of magnetic nanostructures and interfacial phenomena. Here we focus on recent studies of the latter. In a piezoelectric-ferromagnetic heterostructure or nanoscale device, the applied electric field induces a strain field in the piezoelectric that propagates into the ferromagnetic material and alters its magnetization. Recent theoretical calculations suggest that in ferroelectric insulator/ferromagnetic heterostructures the ferroelectric displacements of the interfacial atoms may be reversed by electric fields, significantly altering the interfacial moment or anisotropy. On the other hand, if the ferromagnetic film is a metallic oxide, the electric field at the surface of the piezoelectric can produce large electric fields at the interface and thus add or remove charges from the

ferromagnetic film, changing the magnetization of the film, as reported recently by Molegraaf et al. [1] for a Lead Zirconium Titanate (PZT)/ Sr-doped Lanthanum Manganese Oxide (LSMO). More generally magneto-electric effects may be a common feature of interfaces between dielectrics and metals [2,3]. Understanding and control of these effects may ultimately lead to new memory and spintronic logic elements.

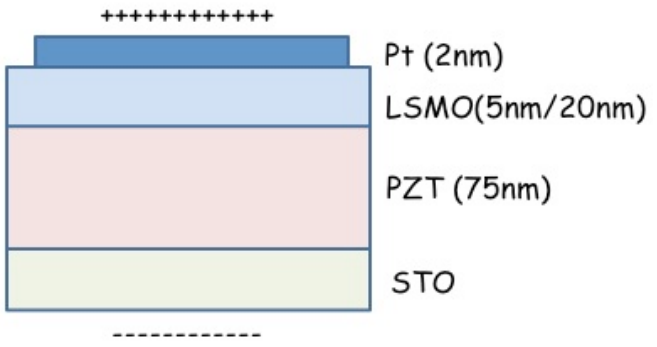

Figure 1: Schematic of samples used for neutron and X-ray reflectivity experiments. The voltage was applied across the top and bottom electrodes.

We have carried out several polarized neutron and resonant X-ray reflectivity studies of LSMO/PZT heterostructure, with and without an external voltage applied to the heterostructure to determine the depth dependence of the change in the magnetization induced in the ferromagnetic LSMO and to attempt to distinguish strain-induced effects from charge carrier injection effects. The samples studied consisted of 75 nm of PZT deposited on a conducting Nb-doped Strontium Titanate substrate (which constituted the bottom electrode), followed by either a 5nm thick or 20 nm thick layer of LSMO on top, finally capped with a 2nm Pt film which constituted the top electrode. (Shown schematically in Fig. 1).

The sample was fabricated by our collaborators at Universite′ Paris Sud. The voltage could be applied in-situ on the sample inside a cryostat during the reflectivity experiments. By applying voltages of up to 4 V of either polarity, electric fields of up to 5 x 10^7 V/m could be applied to the heterostructure. The neutron reflectivity measurements were carried out at the polarized neutron reflectometer at the Spallation Neutron Source with Valeria Lauter and her colleagues and Dr. Edwin Fohtung of the Shpyrko group at UCSD, and the X-ray reflectivity measurements were carried out at the soft X-ray scattering beamline at the NSLS-I synchrotron source with Cecilia Sanchez-Hanke. Most of the measurements were carried out at 105 K on a 6.5-nm-thick LSMO sample.

Both the neutron and X-ray reflectivity studies gave consistent results, which we summarize here: (a) We found that dead layers existed in the magnetization of the LSMO film at both the interfaces: 2-3 unit cells deep at the Pt/LSMO interface, and 4-5 unit cells deep at the PZT/LSMO interface. This is consistent with findings by Hujiben *et al*. [4]. (b) Applying a voltage of 2 V across the heterostructure decreased the magnetization of the central region of the LSMO by about 30 %. (c) Applying a voltage of 4 V of either polarity was sufficient to quench the magnetization in the LSMO film completely. This could be ascribed to either the piezoelectric strain produced by the PZT or due to carrier injection due to the electric field at the PZT/LSMO interface. As we shall see below, we tend to favor the strain effect. The effect of strain on magnetization in thin films has also been seen by the Los Alamos group [5]. (d) The Pt/LSMO interface had a 3 nm thick Mn^{+4} -rich layer in the LSMO film, probably induced by preferential Sr enrichment at the interface, as has been noted by other authors [6].

These results are shown in Figs. 2 and 3.

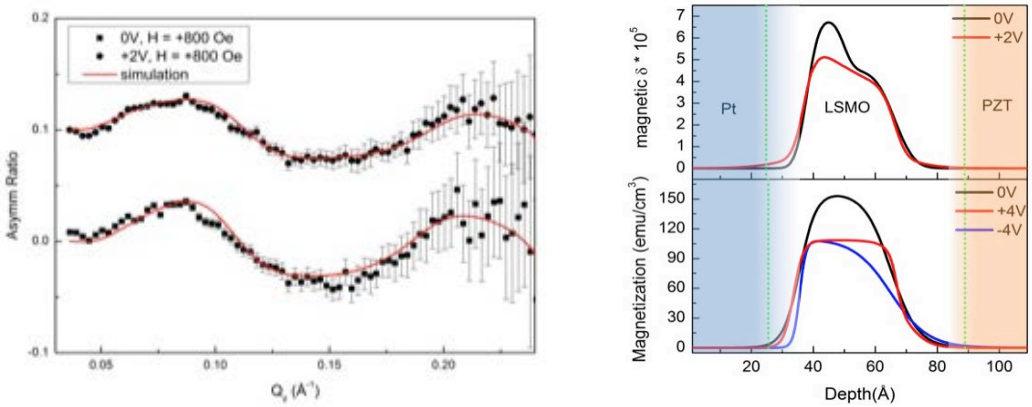

Figure 2: The measured asymmetry ratio from resonant X-ray reflectivity measurements (top) and the fitted magnetization depth profile (bottom) for the PZT/LSMO bilayer with 0 V and 2 V applied voltage respectively from X-ray reflectivity (upper panel) and for 0V , +4V and -4V applied voltage respectively from neutron reflectivity (lower panel) showing the magnetic dead layers at both interfaces of the LSMO film, and the decrease in magnetization induced by the applied voltage.

During the course of these experiments, we had considerable problems with leakage currents in the PZT, which became worse as the voltage was cycled more times. This resulted in some uncertainty as to the validity of the results, since in some cases it was not possible to saturate the electric moment of the PZT for one direction of applied voltage. However, as stated above, the results were repeatable and verified both with polarized neutron and resonant X-ray reflectivity, so we feel they are valid. Nevertheless, we plan to repeat these measurements with fresh samples.

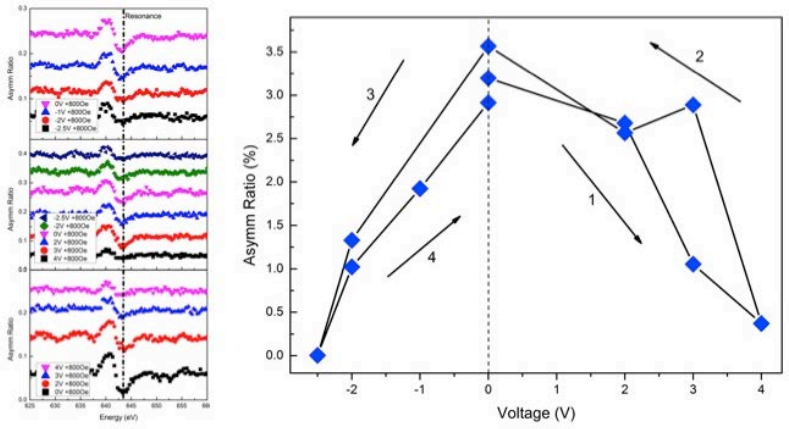

Figure 3: The asymmetry ratio for resonant X-ray reflectivity (a measure of the magnetization) for the LSMO film for different applied voltages.

We have also used neutron scattering techniques to probe arrays of patterned magnetic nanostructures. A recent example is shown in Fig. 4 on a [Co(0.25 nm)/Pd (0.7 nm)]5/Fe(2

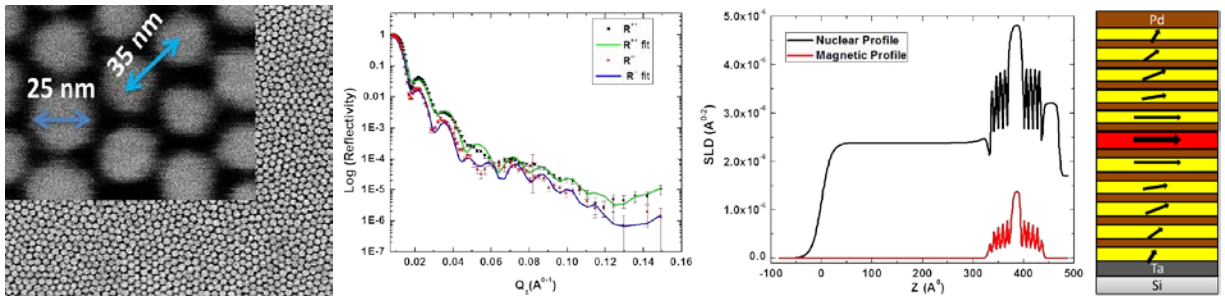

Figure 4: *Polarized neutron reflectometry results for a patterned multilayer structure: Ta(3 nm)/Pd(2 nm)/[Co (0.25 nm) /Pd (0.7 nm)]$_5$/Fe (2 nm) /[Co (0.25 nm) Pd (0.7 nm)]$_5$ patterned to form 25-nm dots on a 35-nm pitch. The left panel shows an SEM image of the patterned structures. The middle-left panel shows the non-spin-flip (R^{++} and R^{--}) scattering with least-squared fit (solid lines). The middle-right panel shows the resulting fit of the nuclear and magnetic profiles. The magnetic profile shows a non-uniform magnetic structure along the depth of the structure shown schematically in the right panel.*

nm)/[Co(0.25 nm)/Pd(0.7 nm)]$_5$ heterostructure of interest for high-density storage patterned into nano-dot arrays using a using self-assembled di-block copolymer as the etch mask. This allows patterning over 1.5 x 1.5 cm^2 areas. Shown in Fig. 4 is the non-spin-flip (R^{++} and R^{--}) scattering giving a depth dependent structural and magnetic profile of the nano islands. The results show a clear incoherent magnetic configuration in an applied field where the Fe responses more strongly to the field and relaxes toward the surface. Research on these structures is expected to continue, including grazing incidence small angle scattering measurements. A manuscript on the neutron scattering is being finalized for publication.

[1] Molegraaf *et al.*, Adv. Matls. 21, 3470 (2009); Vaz et al. Phys. Rev. Lett. 104, 127202 (2010)
[2] M. Zhernenkov *et al*., Phys. Rev. B 82, 024420 (2010).
[3] H. Ohno *et al*., Nature, 408, 944-946, (2000).
[4] M. Hujiben *et al*. Phys. Rev. B 78, 094413 (2008)
[5] S. Singh *et al*. Phys. Rev. B 85, 214440 (2012)
[6] T.T.Fister et al. Appl. Phys. Lett. 93, 151904 (2008)

Future Plans:

We plan to follow up our work on slow magnetic domain wall fluctuations by looking at other antiferromagnetic systems to see to what extent the glassy and jamming behavior we find is universal. We are exploring novel capacitor approaches to apply electric fields to complex heterostructures that avoid the issues of leakage current on large area samples suitable for neutron experiments. We also plan to pursue our pump-probe studies of FeRh, Cr and FePt films which include experiments at the LCLS.

Recent Publications:

"Jamming Behavior of Domains in a Spiral Antiferromagnetic System", S.-W. Chen, H. Guo, K. A. Seu, K. Dumesnil, S. Roy, and S. K. Sinha, Phys. Rev. Lett. **110**, 217201 (2013)

"Non-switchable Magnetic Moments in Polycrystalline and (111)-epitaxial Permalloy/CoO Exchange-biased Bilayers", S. -W. Chen, X. Lu, E. Blackburn, V. Lauter, H. Ambaye, K. T. Chan, E. E. Fullerton, A. E. Berkowitz, and S. K. Sinha, Phys. Rev. **B 89**, 094419 (2014)

"Growth of $GaN_xAs_yP_{1-x-y}$ alloys on GaP(100) by gas-source molecular beam epitaxy",Y.-J. Kuang, S.-W. Chen, H.Li, S.K. Sinha, and C.W.C. Tu, J. Vac. Science and Technology **B 30**, 02B121 (2012).

"Phase transition in iron-rhodium thin films probed by ferromagnetic resonance", E. Mancini, F. Pressacco, M. Hartiger, E. E. Fullerton, T. Suzuki, G. Woltersdorf, and C. H. Back, J. of Physics-Condensed Matter **46**, 245302-1-5 (2013).

"Dynamic switching of the spin circulation in tapered magnetic nanodisks", V. Uhlíř, M. Urbánek, L. Hladík, J. Spousta, M.-Y. Im, P. Fischer, N. Eibagi, J. J. Kan, E. E. Fullerton and T. Šikola, , Nature Nanotechnology **8**, 341-346 (2013).

"Tunable resonant properties of perpendicular anisotropy [Co/Pd]/Fe/[Co/Pd] multilayer" J. Dou, M. J. Pechan, E. Shipton, N. Eibagi and E. E. Fullerton, , J. Appl. Phys. **113**, 17C115-1-3 (2013).

"The influence of structural disorder on magnetic domain formation in perpendicular anisotropy thin films", M. S. Pierce, J. E. Davies, J. J. Turner, K. Chesnel, E. E. Fullerton, J. Nam, R. Hailstone, S. D. Kevan, J. B. Kortright, K. Liu, L. B. Sorensen, B. R. York, O. Hellwig, Phys. Rev. B **87**, 184428-1-17 (2013).

"Field mapping and temperature dependence of magnetic domain memory induced by exchange couplings", K. Chesnel, B. Wilcken, M. Rytting, S. D. Kevan and E. E. Fullerton, New Journal of Physics **15**, 023016-1-19, (2013).

Session II

Energy Materials

Impact of Dynamic Lattice Instabilities and Microstructure on Functional Materials

J. D. Budai, O. Delaire, M. E. Manley, E. D. Specht and G. E. Ice
Materials Science & Technology Division, Oak Ridge National Laboratory, Oak Ridge, TN

Program Scope

Motivated by the central role of dynamic lattice instabilities in controlling the physical properties of functional materials, we are currently investigating how anharmonic vibrations and local microstructure interact to enhance materials properties. Our goal is to understand the underlying origins of energy transport and phase stability in functional materials by integrating neutron and synchrotron x-ray scattering studies with first-principles investigations of lattice structure and dynamical excitations. Our studies are focused on interrelated, representative material systems where issues of anharmonic lattice dynamics and broken static symmetry play key but as yet unresolved roles in their properties, in particular: the impact of dynamic instabilities and microstructure on thermal transport in high-efficiency thermoelectrics; the origin of nanoscale dynamic instabilities in relaxor ferroelectrics; and the role of anharmonic dynamics in driving metal-insulator phase transitions in metal oxides.

Recent Progress

Glass-like thermal transport in $AgSbTe_2$ The origin of the extremely-low glass-like thermal conductivity of $AgSbTe_2$ was elucidated with neutron and x-ray scattering, and electron microscopy. Inelastic neutron scattering measurements on both powders and single-crystals established that anharmonicity is not the dominant phonon scattering mechanism in this compound at low T. From a systematic mapping of linewidths and group velocities, we accounted for the experimentally observed very low lattice thermal conductivity. From our diffraction and diffuse scattering measurements, we showed that cations exhibit short-range ordering on a length scale of a few nanometers, similar to the observed phonon mean-free-paths. Large static atomic displacements were also inferred from elastic scattering measurements, and are independent of temperature. The nanostructure arising from cation short-range ordering is thought to be the main contributor to the large, temperature-independent phonon linewidths observed with INS.

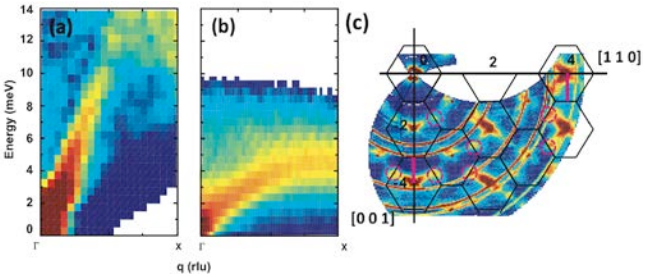

Fig. 1 Inelastic neutron scattering showing phonon dispersions (a,b), and diffuse scattering from nanostructure (c) in $AgSbTe_2$.

Origin of anomalous neutron scattering spectra in SnTe and PbTe. Rocksalt chalcogenides achieve some of the highest known thermoelectric figure-of-merits, favored by an unusually low thermal conductivity for a simple cubic structure. We previously showed that the low thermal conductivity of PbTe arises from strong scattering of heat-carrying acoustic modes by the incipient ferroelectic transverse-optic (TO) branch. In new studies, we have elucidated the differences between the dynamical structure factors, S(**Q**,E), of SnTe and PbTe crystals. The TO

mode exhibits a clear splitting at the zone center in PbTe, but does not in SnTe, although SnTe is closer to the ferroelectric instability. From first-principles simulations including anharmonic effects at finite temperatures, we computed the **Q**-dependent phonon self-energy and dynamical susceptibility, and reproduced experimental observations. The origin of the effect was traced to an amplification of anharmonicity by a larger phase-space for coupling to the TO mode in PbTe.

Phonon localization drives polar nanoregions in a relaxor ferroelectric. Relaxor ferroelectrics are chemically disordered, technologically useful ferroelectrics, with polarization developing in polar nanoregions (PNRs) rather than long-range order. The origin of PNRs is not well understood. Using neutron scattering to characterize the lattice dynamics of relaxor PMN-30%PT, we discovered a new phonon localization mechanism that explains the size and shape of the PNRs as well as the zone-edge antiferroelectric nanoregions in terms of the coherent trapping of the TO phonons by randomly distributed localized resonance modes. Near the Burns temperature (T_d) a dispersionless mode forms in resonance with the TO phonon, indicating a fully localized stationary mode (Fig. 2). On cooling towards the ordering temperature, T_c, however, the localized mode intensity peaks at the crossing with the TO phonon. These localized modes develop a coherence length (size) that equals a single TO wavelength at the crossing, and this size matches the PNRs. Furthermore, near the zone edge high-symmetry M point (antiferroelectric), intensity becomes enhanced at a 2nd crossing. The size of the localized modes are set by the wavelength of the TO phonon where its dispersion surface crosses the resonance local mode. This relationship explains the evolution of the size, shape, and positions in reciprocal space of the PNR and antiferroelectric nanoregion diffuse scattering patterns in PMN-*x*PT. Our results are explained in terms of an Anderson-type localization mechanism, where constructive interference of the TO phonons interacting with randomly distributed localized resonance modes results in the localization of both the ferroelectric and antiferroelectric TO phonons. This mechanism is generic and should apply to other frustrated ferroic-type materials.

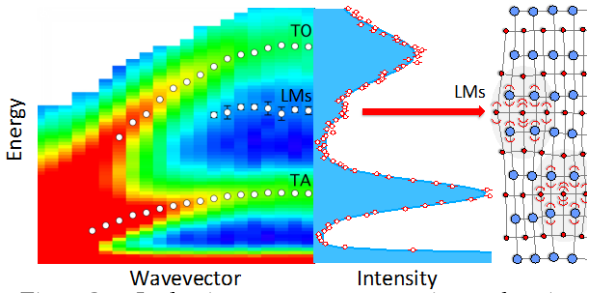

Fig. 2. Inelastic neutron scattering showing localizing modes (LMs) between transverse optic (TO) and transverse acoustic (TA) phonons in relaxor ferroelectric PMN-30%PT.

Impact of lattice dynamics on metal-insulator transition in VO_2 The relatively simple binary oxide, VO_2, challenges our ability to understand how a high-temperature metal emerges from a low-temperature band (Peierls) or strongly-correlated (Mott) insulator. An accurate description of lattice dynamics near the coupled structural (tetragonal-monoclinic) and electronic metal-insulator transition (MIT) in VO_2 is not available due to the

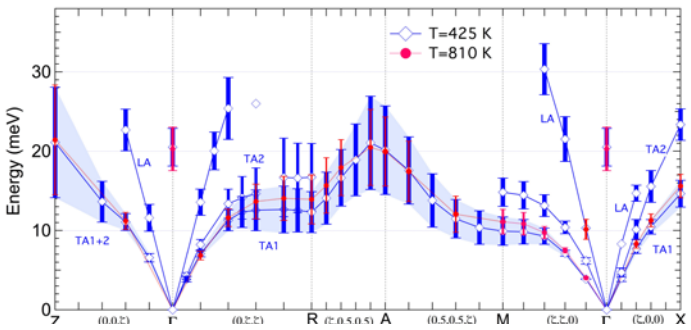

Fig. 3 Phonon dispersions measured using inelastic x-ray scattering at HERIX at 425K and 800K. Vertical bars show very large energy widths due to anharmonicity.

incoherent V cross-section. We have recently determined the changes in lattice dynamics and vibrational entropy associated with the MIT. We used inelastic neutron scattering to obtain the Q-integrated phonon density of states, x-ray scattering to obtain 3-D maps of energy-integrated thermal diffuse scattering, inelastic x-ray scattering to directly measure phonon dispersions, and *ab initio* calculations to interpret the atomic mechanisms. Our results show that the entropy change driving the MIT is dominated by vibrational rather than electronic contributions. Moreover, we show that "soft mode" phase transition models are incorrect, and instead, strongly anharmonic phonons stabilize the metallic phase.

Future Plans

Phonon scattering for low thermal conductivity. We will continue to investigate the influence of strong anharmonicity, lattice instabilities and structural inhomogeneities on thermoelectricity, in which low thermal conductivity is beneficial. We will extend our inelastic neutron scattering and x-ray diffuse scattering studies of $AgSbTe_2$ to the case of $AgBiSe_2$, which undergoes an order-disorder transition of cations at 560K, amenable to in-situ measurements of the effect of ordering in single-crystals. We will also extend our measurements in rock-salt chalcogenides to the case of orthorhombic systems with GeS structure, which have very low thermal conductivities, yet show 1/T behavior indicative of anharmonicity. Large single-crystals have been obtained and preliminary neutron scattering measurements have been performed. Neutron scattering studies will be complemented with first-principles simulations.

Phonon anharmonicity and competition between ferroelectric and antiferroelectric orders. We will continue our on-going studies of $BaTiO_3$, $K(Ta,Nb)O_3$, and $SrTiO_3$ under electric fields. By tuning the ferroelectric instability with an applied electric field, the coupling of optic and acoustic modes can be controlled, providing fundamental insights into the role of anharmonic effects in the lattice instabilities. Preliminary measurements have been obtained.

Phonon localization in frustrated ferroic materials. A new class of disordered shape memory alloys, commonly called "strain glasses", has recently emerged with behavior that in many respects parallels relaxor ferroelectrics. They exhibit precursor nanoregions and frequency dependent relaxation behavior, and the "parent" displacive transitions exhibit soft-phonon precursors. We plan to measure the lattice dynamics and diffuse scattering of these to see if a similar phonon localization mechanism drives the superelastic nanoregions responsible for their properties. We will analyze short-range order to see whether short-range displacements correspond to the long-range displacements in shape-memory alloys or to a novel short-range order. We also plan to investigate phonon localization in additional relaxor ferroelectric materials, including heterovalent PZN-PT and homovalent KTN.

Phonon anharmonicity in metal-insulator transitions Motivated by our finding of strong anharmonicity in VO_2, in the near-term, we will investigate the origins of an elastic "central peak" in VO_2 (reminiscent of $SrTiO_3$) as the transition is initiated. We will then investigate the effect of doping and external strain on lattice dynamics in VO_2. Reducing dopants such as Nb or Mo are known to suppress the MIT temperature, while oxidizing dopants such as Cr or Al or tensile strain stabilize other low-symmetry phases. Understanding how lattice dynamics change

with doping or strain will provide benchmarks guiding predictive theoretical treatments for this prototypical material. In the long term, we will address the broad question of whether or not phonon anharmonicity plays a central role in phase stability for other classes of materials, such as spinel oxides, that exhibit a MIT coupled with displacements caused by dimerization.

Publications

1. M. E. Manley, J. W. Lynn, D. L. Abernathy, E. D. Specht, O. Delaire, A. R. Bishop, R. Sahul, and J. D. Budai, "Phonon localization drives polar nanoregions in a relaxor ferroelectric," *Nature Communications* 5, Article no. 3683 (2014).

2. C. W. Li, O. Hellman, J. Ma, A. F. May, H. B. Cao, X. Chen, A. D. Christianson, G. Ehlers, D. J. Singh, B. C. Sales and O. Delaire, "Phonon Self-Energy and Origin of Anomalous Neutron Scattering Spectra in SnTe and PbTe Thermoelectrics," *Phys. Rev. Lett.* **112**, 175501 (2014).

3. C. E. Carlton, R. De Armas, J. Ma, A. F. May, O. Delaire, and Y. Shao-Horn, "Natural nanostructure and superlattice nanodomains in $AgSbTe_2$," *Jour. Appl. Phys*. **115**, 144903 (2014).

4. M. E. Manley, J. R. Jeffries, H. Lee, N. P. Butch, A. Zabalegui, and D. L. Abernathy, "Multiple high-temperature transitions driven by dynamical structures in NaI," *Phys. Rev. B* **89**, 224106 (2014).

5. E. Lara-Curzio, A. F. May, O. Delaire, M. A. McGuire, X. Lu, C.-Y. Liu, E. D. Case, and D. T. Morelli, "Low-temperature heat capacity and localized vibrational modes in natural and synthetic tetrahedrites," *Jour. Appl. Phys.* **115**, 193515 (2014).

6. W. Siemons, C. Beekman, J. D. Fowlkes, N. Balke, J. Z. Tischler, R. Xu, W. Liu, C. M. Gonzales, J. D. Budai, and H. M. Christen, "Focused-ion-beam induced damage in thin films of complex oxide $BiFeO_3$," *APL Materials* **2**, 022109 (2014).

7. J. D. Budai, A. Tselev, J. Z. Tischler, E. Strelcov, A. Kolmakov, W. J. Liu, A. Gupta and J. Narayan, "In situ x-ray microdiffraction studies inside individual VO_2 microcrystals," *Acta Materialia* **61**, 2751-2762(2013).

8. R. I. Barabash, O. M. Barabash, E. A. Karapetrova, and M. E. Manley, "Structural and Dynamical Fluctuations in Off-Stoichiometric NiMnGa Shape-Memory Alloys," *Appl. Phys. Lett.* **104**, 241905 (2014).

9. J. W. L. Pang, W. Liu, J. D. Budai, and G. E. Ice, "Inhomogeneous deformation behavior in intercrystalline regions in polycrystalline Ni," *Acta Materialia* **65**, 393-399 (2014).

10. N. N. Medvedev, M. D. Starostenkov, and M. E. Manley, "Energy localization on the Al sublattice of Pt_3Al with $L1_2$ order," *J. Appl. Phys.* **114**, 213506 (2013).

11. M. R. Bayati, R. Molaei, F. Wu, J. D. Budai, Y. Liu, R. J. Narayan, and J. Narayan, "Correlation between structure and semiconductor-to-metal transition characteristics of VO_2/TiO_2/sapphire thin film heterostructures," *Acta Materialia* **61**, 7805-7815 (2013).

12. F. Liu, J. D. Budai, X. Li, J. Z. Tischler, J. Y. Howe, C. Sun, R. S. Meltzer and Z. W. Pan, "New Ternary Europium Aluminate Luminescent Nanoribbons for Advanced Photonics," *Advanced Functional Materials* **23**, 1998-2006 (2013).

13. A. Pramanick, S. O. Diallo, O. Delaire, S. Calder, A. D. Christianson, X.-L. Wang, and J. A. Fernandez-Baca, "Origins of large enhancement in electromechanical coupling for nonpolar directions in ferroelectric $BaTiO_3$," *Physical Review B* **88**, 180101(R) (2013).

14. O. Delaire, I. I. Al-Qasir, J. Ma, A. M. dos Santos, B. C. Sales, L. Mauger, M. B. Stone, D. L. Abernathy, Y. Xiao, and M. Somayazulu, "Effects of temperature and pressure on phonons in $FeSi_{1-x}Al_x$", *Phys. Rev. B.* **87**, 184304 (2013).

15. J. Ma, O. Delaire, A. F. May, C. E. Carlton, M. A. McGuire, L. H. VanBebber, D. L. Abernathy, G. Ehlers, T. Hong, A. Huq, W. Tian, V. M. Keppens, Y. Shao-Horn, and B. C. Sales, "Glass-like phonon scattering from spontaneous nanostructure in $AgSbTe_2$", *Nature Nanotechnology* **8**, 445-451 (2013).

16. X. Li, J. D. Budai, F. Liu, J. Y. Howe, J. Zhang, X. J. Wang, Z. Gu, C. Sun, R. S. Meltzer, and Z. W. Pan, "New Yellow $Ba_{0.93}Eu_{0.07}Al_2O_4$ Phosphor for Warm-White Light-Emitting Diodes through Single-Emitting-Center-Conversion" Nature Publishing Group: *Light: Science & Applications* **2**, e50 (2013).

17. C. Beekman, W. Siemons, T. Z. Ward, J. D. Budai, J. Z. Tischler, R. Xu, W. Liu, N. Balke, J. H. Nam, and H. M. Christen, "Unit cell orientation of tetragonal-like $BiFeO_3$ thin films grown on highly miscut $LaAlO_3$ substrates," *Applied Physics Letters* **102**, 221910 (2013).

18. M. R. Bayati, Y. Liu, R. Molaei, J. D. Budai. R. J. Narayan, J. Narayan, "Role of Substrate Crystallographic Characteristics on Structure and Properties of Rutile TiO_2 Epilayers," *Journal of Applied Physics* **114**, 044314 (2013).

19. G. E. Ice, B. C. Larson, J. D. Budai, E. D. Specht, R. I. Barabash, J. W. L. Pang, J. Z. Tischler, and W. Liu. "Emerging capabilities for materials characterization with polychromatic microdiffraction" in *Transactions Symposium: Neutron & Synchrotron Sources: Role in Crystallography*, American Crystallographic Association, Buffalo, NY (2014).

20. R. I. Barabash, G. E. Ice, Editors for book "Strain and Dislocation Gradients from Diffraction", Imperial College Press, London 2014.

21. R. I. Barabash, G. E. Ice, Book chapter "Diffraction Analysis of Defects: State of the Art" in "Strain and dislocation gradients from diffraction", Eds. R.I. Barabash, G.E. Ice, Imperial College Press, London p.1-52 (2014).

22. G. E. Ice, J. D. Budai, E. D. Specht, B. C. Larson, J. Pang, R. Barabash, J.Z. Tischler, W.-J. Liu, "The 3D X-Ray Crystal Microscope: An Unprecedented Tool for ICME," p. 183-188 in 2nd World Congress on Integrated Computational Materials Engineering, Editors M. Li *et al*, John Wiley & Sons, Inc. Hoboken, NJ (2013).

23. G. E. Ice, "X-ray Microprobe for Fluorescence and Diffraction Analysis", *Characterization of Materials 2nd Edition*, Editor P. Booth, John Wiley and Sons, Hoboken, NJ (2013).

24. G. E. Ice, "X-ray and Neutron Diffuse Scattering Measurements", *Characterization of Materials 2nd Edition*, Editor P. Booth, John Wiley and Sons, Hoboken, NJ (2013).

25. G. E. Ice, " Synchrotron diffraction: capabilities, instrumentation and examples", *Modern Diffraction Methods*, Editor E. J. Mittemeijer, Wiley-VCH Verlag, Weinheim, Germany, 439-468 (2013)

26. E. Strelcov, A. Tselev, I. Ivanov, J. D. Budai, J. Zhang, J. Z. Tischler, I. Kravchenko, S. Kalinin and A. Kolmakov, "Doping-Based Stabilization of the M2 Phase in Free-Standing VO_2 Nanostructures at Room Temperature," *Nano Letters* **12**, 6198-6205 (2012).

27. P. F. Tortorelli, E. D. Specht, K. L. More and P. Y. Hou, "Oxide growth stress measurements and relaxation mechanisms for alumina scales grown on FeCrAlY" *Materials and Corrosion* **63**, 857-861 (2012).

28. J. Lang, S. te Vethuis, B.C. Chakoumakos, J. D. Budai, and A. E. Ekkebus, "National School on Neutron and X-ray Scattering," *Synchrotron Radiation News* **26**, 9-12 (2013).

29. G. E. Ice and E. D. Specht, "Microbeam, timing and signal-resolved studies of nuclear materials with synchrotron X-ray sources," *Journal of Nuclear Materials* **425**, 233-237 (2012).

30. C. Liu, R. Conley, J. Qian, C.M. Kewish, W. Liu, L. Assoufid, A.T. Macrander, G.E. Ice, J.Z. Tischler, "Plastic Deformation in Profile-Coated Elliptical KB Mirrors," ISRN Optics, vol. 2012, Article ID 151092, 2012.

31. R. I. Barabash, W. Liu, J. Z. Tischler, H. Bei and J. D. Budai, "Phase-specific elastic/plastic interface interactions in layered NiAl-Cr(Mo) structures," *Acta Materialia* **60**, 3279-3286 (2012).

32. J. W. Elmer and E. D. Specht, "In-Situ X-Ray Diffraction Observations of Low-Temperature Ag-Nanoink Sintering and High-Temperature Eutectic Reaction with Copper," *Metallurgical and Materials Transactions* A **43A**, 1528-1537 (2012).

33. O. A. Delaire and C. Stassis, Book chapter "Phonon Studies", in "Characterization of Materials", Wiley (published Sep. 2012).

Design and Validation of an *in situ* Electrochemical Cell for Neutron Diffraction Investigation of Phase Transitions in Mg/Si Electrodes for Li-ion Batteries

K. S. Ravi Chandran
Department of Metallurgical Engineering, University of Utah, Salt Lake City, UT 84112

Program Scope

The performance of Li-ion battery is determined by the kinetics of the phase transitions occurring in the bulk of electrodes. The nature of these phase transitions governs the battery performance metrics such as maximum charge capacity, reversible number of cycles and capacity fading [1]. The effectiveness of electrochemical techniques in understanding bulk phase transitions is very limited, although they give information about the reactions occurring at the surface [2]. The phase transitions in the bulk electrodes can be more appropriately investigated using neutron diffraction (ND) techniques, but an in situ cell, capable of using small volume electrodes, has been lacking so far. Specific objectives of this research are

- Design of a novel *in situ* electrochemical cell to obtain Rietveld refinable neutron diffraction experiments using small volume electrodes of various laboratory/research-scale Li-ion batteries
- Use this cell to investigate the complexity of phase transitions in Li(Mg) alloy electrodes, which occur under electrochemical lithiation and delithiation, and to determine aspects of phase transition that enable/limit energy storage capacity
- Investigate the phase transitions in electrodes made of nano- and micron-sized Si particles and etched micro-columns and investigate the effect of particle/column size on phase transitions and nonequilibrium structures

Recent Progress

I. Design and validation of novel in situ electrochemical cell for ND experiments

A major objective of the project is to design and validate an in situ electrochemical cell suitable for obtaining Rietveld-refinable neutron diffraction patterns from VULCAN neutron diffractometer at SNS, to study the phase transitions in battery electrode materials. Several cell designs were pursued and revised and the unworkable ones were dropped. Finally, one successful design emerged during 2013-14 project period using which ND experiments in Vulcan, SNS were conducted. Several challenges, including Si windows [3] design and sealing, reliable connections to electrodes, electrolyte retention and making the cell work when compressed between springs etc. were solved after several months of efforts. The final cell design shown in Figure 1 has proved to be very successful in that it yielded very good diffraction patterns even with small volume electrodes of C/$LiCoO_2$ and C/$LiMn_2O_4$ cells. Several validation experiments were successfully run in Vulcan with this cell.

For validation, the designed electrochemical cell (Figure 1) was used to study the phase transitions under *in-situ* ND in both the electrodes (anode/cathode) simultaneously in graphite/$LiCoO_2$ and in graphite/$LiMn_2O_4$ cells each with two cells. The diffraction patterns fully validated the working of the in situ cell. As an example, the indexed diffraction patterns collected from the graphite/$LiCoO_2$ during charging is shown in Figure 2. The formation of various phases such as Li_xC_6, LiC_{12}, LiC_6 during the lithiation of graphite can be clearly seen (Figure 2). The gradual evolution, dissolution of various electrode phases, change in their d-spacing's can also be observed. In $LiCoO_2$, first ordered transition that was observed by others [4] has been observed here using small volume electrodes. The designed cell facilitated the observation even weak Bragg reflections. The diffraction patterns were amenable for Rietveld refinement with goodness of fit $\chi^2<8.2$. The trends expected in the lattice parameters, unit cell volume could be observed using this in situ cell. All of these are described in detail in the publications.

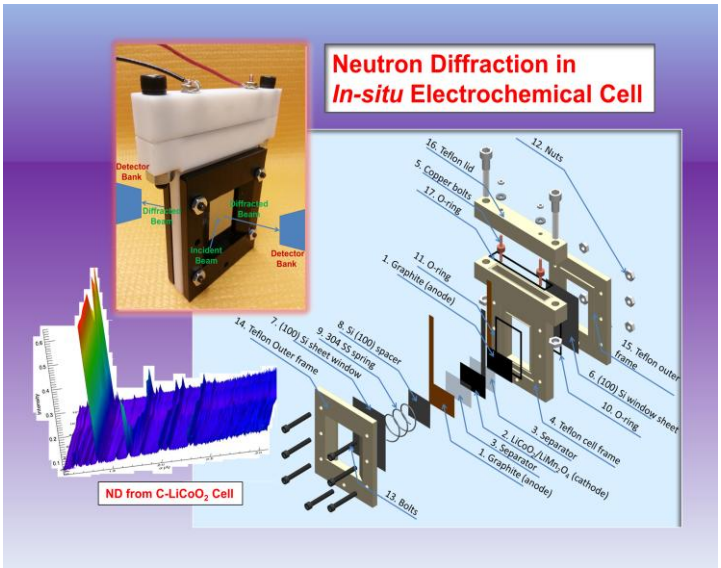

Figure 1. Exploded view of the designed *in-situ* electrochemical for ND studies. The cell consists of single crystal Si (100) sheets for casing and the charging of graphite and $LiCoO_2$ electrodes to study the phase transitions upon lithiation and delithiation. Insets show the photograph of the *in-situ* cell in the assembled form that was used in VULCAN diffractometer in SNS and the ND patterns obtained during the charging of graphite/$LiCoO_2$ cell. The ND experiments were conducted in the VULCAN diffractometer at Spallation Neutron Source beam line 7, ORNL. The work is in collaboration with Dr. K. An, ORNL.

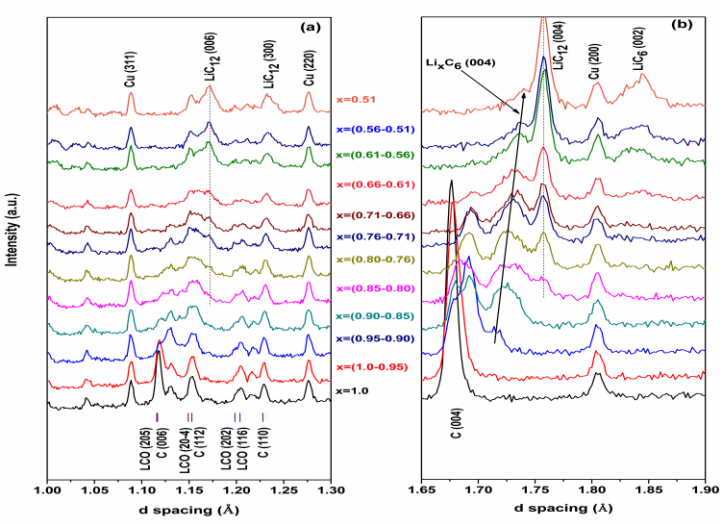

Figure 2. ND patterns obtained in VULCAN using the in situ cell for the electrochemical lithiation/delithiation of graphite/$LiCoO_2$ electrodes. The presence of nearly zero background due to the use of single crystal Si (100) sheet as the casing material can be observed. During the lithiation of graphite, formation of various Li intercalation compounds: graphite solid solution, Li_xC_6, LiC_{12}, LiC_6 can be observed. The validation of the in situ cell has provided the desired pathway for the construction of Mg/$LiCoO_2$ and Si/$LiCoO_2$ cells, which is the second major objective of the proposed research.

Our ND work revealed the transient nature of phase transformation in Li-ion batteries; the key finding is that the multiple lithiated phases, for example, Li_xC_6, LiC_{12}, LiC_6, co-existed/overlapped in the bulk of the electrode during the major period of charging of the Li-ion cell. Such finding has not been made in XRD work. Lithiation proceeded by the consumption of the Li-lean phase by the Li-rich phase. This shows that the phenomenon is akin to equilibrium solid-state phase transformation. This also provided indirect evidence that phase transition occurs by planar front movement, raising questions about the porous electrode theory [5] which is commonly believed.

The ND data was obtained in real time and simultaneously on both anode and cathode, which has not been possible with XRD. This way, our work enabled direct one-to-one correlation of phase transitions in anode and cathode and allowed us to directly identify which electrode is limiting the charge capacity of the cell. In particular, we found out that for the $LiMn_2O_4$ electrode, the electrode thickness needs to be increased to fully transform C to LiC_6. Such simultaneous ND diffraction provides a clear illustration of importance of optimizing electrode thickness, especially keeping mind the full phase transformation path.

The in situ cell ND has simplified lot of conventional XRD experimentation of Li ion cells--ND is one experiment with a real cell as opposed to two separate experiments in XRD with reference electrodes and yet with depth-of-penetration-limitation of XRD. Although the two separate XRD experiments could be

combined to provide results similar to ND, there, one can never be certain about one-to-one correlations of phase transitions in anode versus cathode. So this ND experimentation is a major advancement and is a realistic experiment with respect to Li-ion cells.

To finish up the project, new Mg/Si electrodes of various compositions have been prepared and will be the subject of study in Vulcan at SNS using the validated in situ cell. In the upcoming beam times at SNS in 2014-15, we plan to experiment with these electrodes.

II. Neutron Tomographic Imaging of Lithiation and Delithiation processes in Li-battery Electrodes

In Li(Mg) alloy anodes actual Li distributions in the bulk of the electrode govern the charge/discharge rates and the reversibility of cell performance and/or electrode utilization during the electrochemical insertion/removal of lithium [6,7]. To investigate this, neutron tomographic imaging technique has been used for 3D mapping of Li distribution in bulk Li(Mg) alloy electrodes. Four compositions (in wt.%): Li-70Mg, Li-60Mg, Li-50Mg and Li-40Mg were prepared by melting Mg chips and Li rods under argon. After rolling and annealing, each sample was delithiated to different depth of Li removal under the constant current density of 0.5mA/cm^2. Theoretically, for a given degree of delithiation, the concentration profile can be determined using Fick's second law and appropriate boundary conditions. Our objective is to determine this concentration profiles from neutron attenuation intensity [8] as well and compare with theoretical calculations. The experiments have been performed at CG-1D Neutron Imaging Prototype Station at SNS. The work is in collaboration with Dr. Bilheux.

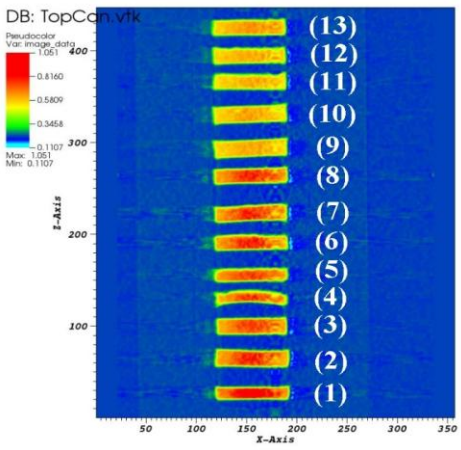

Figure 3

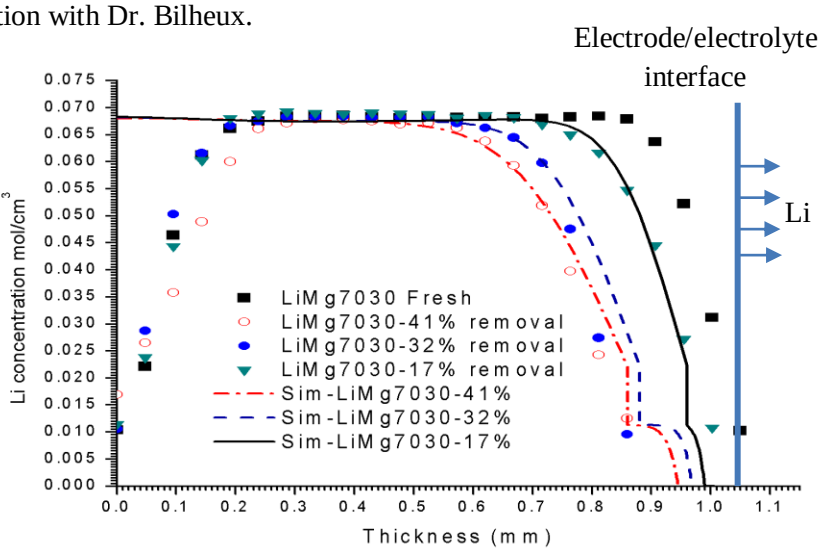

Figure 4

Figure 3. Pseudo-color plot of neutron attenuation intensity in Li(Mg) alloy electrodes. Pure Li (1) is used as a reference to image the distribution of lithium after the electrochemically-induced phase transitions in the following electrodes: One set of high-Li electrodes are of composition (wt.%) Li-70Mg: (2) Fresh II, (3) Fresh I, (4) 42%Li removal, (5) 32%Li removal, (6) 17%Li removal, (7) 14%Li removal and (8) 9%Li removal. The other set of low-Li electrodes are of nominal composition (wt.%) Li-50Mg: (9) Fresh II, (10) Fresh I, (11) 16%Li removal, (12) 12%Li removal and (13) 14% Li removal.
Figure 4. Lithium concentration profiles across the thickness extracted from neutron tomographic data in comparison with the calculated Li concentration profiles

Figure 3 shows the pseudo-color plot of Li distribution across the thickness after reconstruction—the top surface is the active side to which current was applied during cell cycling. The blank space between each sample is created by Aluminum tubing spacer for separation purpose. The green color in this figure represents lower attenuation intensity, which means lower Li concentration in this Li(Mg) system. We

find that even pure Li in this experimental set shows a green shell, which explains the color gradient of the non-active side of Li(Mg) alloy. Also, it is thinner than the green shell from the Li removed one, which is expected. Such edge intensity deviation was also observed by others [9,10]. We suspect that this deviation might be caused by instrument limitation or the reconstruction method. Concentration profiles without the correction and the calculated profiles are shown in Figure 4. This work is in progress and is expected to be completed in 2014-15.

Future Plans

(i) Study of phase transitions in Mg/Li(Mg) electrode: We plan to perform *in-situ* electrochemical experiments on nanostructured Mg/Li(Mg) electrodes using the in situ cell we have developed. The objective will be to determine how phase transitions and Li diffusion is affected in the nanoscale regime.
(ii) Study of phase transitions in Si electrode: Si electrodes of various nanoparticle sizes and a novel electrode architecture—microfabricated Si columnar structure [7] will be investigated using the in situ electrochemical cell. The diffraction volume in the cell will be increased by adding one more electrode layer. This facilitates in obtaining even better quality diffraction data.
(iii) Bulk Li Distribution Study of Delithiated Li(Mg) Alloy Using Neutron Imaging: We have started to explore the fabrication method of porous Li(Mg) alloy which has good electrochemical reversibility. After several cycles, neutron imaging of the Li distribution in the bulk electrode will help us to get further understanding of delithiation/lithiation process and phase transition behavior. Also, the effect of different C-rate to Li spatial distribution will be studied. We are working to developing a correction method for the edge deviation in our neutron imaging data. It is possible to observe the boundary of Li(Mg) alloy which indicating phase transition from Li-rich BCC β-phase to Li-lean α-phase once a reasonable correction has been applied.

References:

1. M. Tang, W. C. Carter and Y.M. Chiang, *Ann. Rev. Mater. Res.*, 40, 501 (2010).
2. H. C. Shin, J. A. Corno, J. L. Gole, M. Liu, *Journal of Power Sources*, 139, 314 (2005).
3. M. Potter, H. Fritzsche, D. H. Ryan and L. M. D. Cranswick, *J. of Appl. Crystallogr.*, 40, 489 (2007).
4. N. Sharma, V. K. Peterson, M. M. Elcombe, M. Avdeev, A. J. Studer, N. Blagojevic, R. Yusoff and N. Kamarulzaman, *J. Power Sources*, 195, 8258 (2010).
5. V. Srinivasan, J. Newman, *J. Electrochem. Soc.*, 151, A1517 (2004).
6. M. Jagannathan and K. S. Ravi Chandran, *J. Electrochem. Soc.*, 160, A1922 (2013).
7. M. Jagannathan, Ph.D. Thesis Research, University of Utah, 2013.
8. J. Nanda, H. Bilheux, S. Voisin, G. M. Veith, R. Archibald, L. Walker, A. Srikanth, J. D. Nancy and P. Sreekanth, *The Journal of Physical Chemistry C*, 116, 8401 (2012).
9. K. Sharma, H. Z. Bilheux, L. M. Walker, S. Voisin, R. T. Mayes, J. O. Kiggans, S. Yiacoumi, D. W. DePaoli, S. Dai and C. Tsouris, *Phys Chem Chem Phys*, 15, 11740 (2013).
10. J.B. Siegel, A. G. Stefanopoulou, P. Hagans, Y. Ding and D. Gorsich in *IEEE American Control Conference, 2011. ACC 2011.*, June 2011, pp. 1362-1367

Publications from this project:

1. B. Vadlamani, K. An, M. Jagannathan and K. S. Ravi Chandran, "A Novel In-situ Electrochemical Cell for Neutron Diffraction Studies of Phase Transitions in Small Volume Electrodes of Li-ion Batteries," J. Electrochemical Society, Revised and Submitted June 2014
2. M. Jagannathan and K. S. Ravi Chandran, "Analytical modeling and simulation of electrochemical charge/discharge behavior of Si electrodes in Li ion cells," J. Power Sources, Vol. 247, 2014, pp. 667-675
3. M. Jagannathan and K. S. Ravi Chandran, "Large increase in electrochemical lithiation of Li-Mg alloy electrodes after anodic polarization at high potentials," Electrochemistry Communications, April 2014

Neutron Scattering Investigation of the Relationship between Molecular Structure, Morphology and Dynamics in Conjugated Polymers

Prof. Lilo D. Pozzo, Dept. of Chemical Engineering, University of Washington Seattle

Program Scope

Our work focuses on developing fundamental relationships between chemical architecture, morphology, dynamics and electronic properties in conjugated polymers. The project is divided into the following objectives: 1) Evaluate effect of polymer molecular structure on conformation and thermodynamics of dissolved conjugated polymers. 2) Determine role of the type and location of substitution moieties on self-assembly of ordered conjugated polymer nanostructures. 3) Measure dynamic fluctuations in conjugated polymer phases and relate this to material properties. 4) Structural investigation of P3AT self-assembly and network formation in emulsions.

Recent Progress

We have completed a systematic study of self-assembly and gelation for a series of poly-3-alkyl-thiophene (P3AT) derivatives. These conductive polymers all had identical backbones but differing side-chains resulting in differences in self-assembly and solubility. The study included rheological and electrochemical characterization of the macroscopic properties. These results were directly correlated to the evolution of the structure as assessed by small angle and ultra small angle neutron scattering.

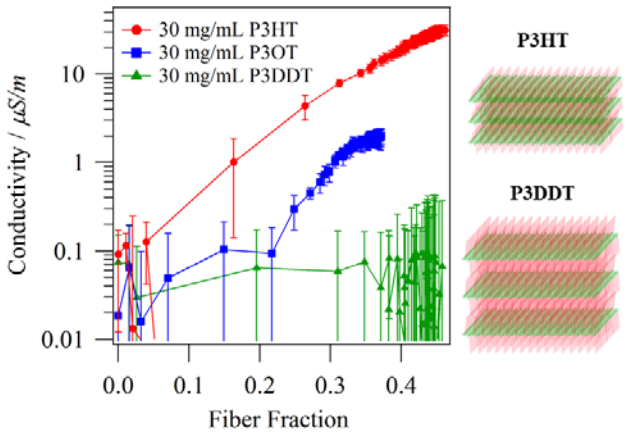

Figure 1: Correlation between conductivity and total fiber fraction.

It was hypothesized that fast gelation (self-assembly) resulted in the formation of a large number of defects and branching. By performing SANS and impedance spectroscopy at the same time we correlated structural parameters, such as the total number of nanofibers, to the sample's conductivity. Figure 1 shows a plot for three different P3AT's of increasing alkyl side-group length. It was determined that the conductivity was primarily affected by the separation of the polymer backbones (modified by the alkyl group) and the structure of the network over micrometer length scales. Figure 2 shows that there is an optimum solvent quality for self-

assembly of each polymer. Each of the polymers showed a distinct maximum in conductivity at an intermediate value of solvent quality (i.e. the fraction of the poor solvent dodecane).

The correlation of polymer structure to solvatochromism (i.e. changing optical properties as a function of solvent) was also studied with SANS, spectroscopy and MD simulations. Conjugated polymers change optical absorption and fluorescence when dissolved in different solvents. This is usually attributed to changes in the stiffness of the polymer. We completed a thorough study of conformation, optical absorption, and solubility for P3AT's with variable side-chains. These experimental results have been augmented by molecular dynamics (MD) and density functional theory (DFT) calculations in collaboration with Prof. J. Pfaendtner (UW). It was found that the major contributions to solvatochromism are from changes to the polarizability of the solvent. MD simulations (Figure 3) also show marked differences in packing density and orientation of solvent molecules as they interact with the conjugated backbone and the alkyl side-chains. Small molecules like chloroform pack closely to the backbone and result in more favorable interactions. Solvents of lower quality result in extended side-chains and in stiffer backbones. This observation, which was confirmed by SANS measurements, suggests that polymers undergo a coil-to-rod transition before self-assembly.

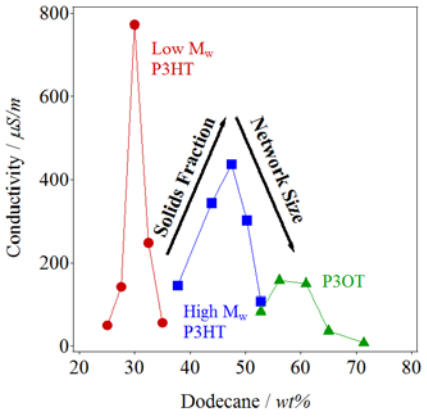

Figure 2: Conductivity for organogels of several P3ATs as a

A neutron scattering and photoconductive scanning probe microscopy investigation has also been completed to correlate the internal structure of conjugated polymer nanoparticles to their photovoltaic properties. Aqueous dispersions of conductive polymer and fullerene nanoparticles have applications in low cost organic photovoltaics, OLEDs and other organic electronic devices. Typically, these particles contain both a conjugated polymer and a fullerene derivative to act as the active layer for PV applications. Just like in thin-film devices, solar cell performance is greatly affected by the material distribution. We have used contrast variation small angle neutron scattering (CV-SANS) for the determination of material distribution within

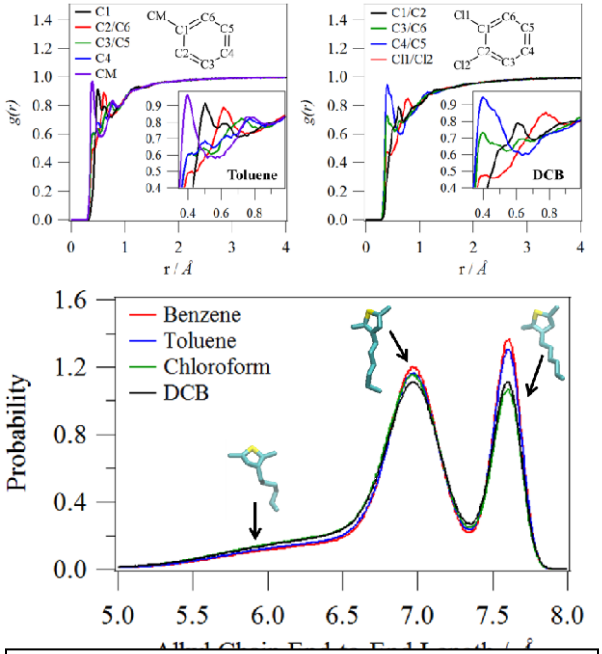

Figure 3: Key results from MD simulations showing the preferred orientation of two aromatic

photoactive nanoparticles. We adopted the classic method of Sturhman to relate the variation in the radius of gyration of particles, dispersed in solvents of variable contrast, to the distribution of the internal phase materials.(1) Figure 4 shows an example of one such experiment for two particles that form either a core-shell structure or a Janus / asymmetric particle. Composite particles tend to form core-shell structures with the polymer enriched in the surface of the particles and the fullerene in the core. Moreover, the particular structure could also be tuned through changes in relative composition or solvent quality. Finally, it was also determined that an even distribution of materials was only possible when the conjugated polymer was gelled before solvent removal.(2)

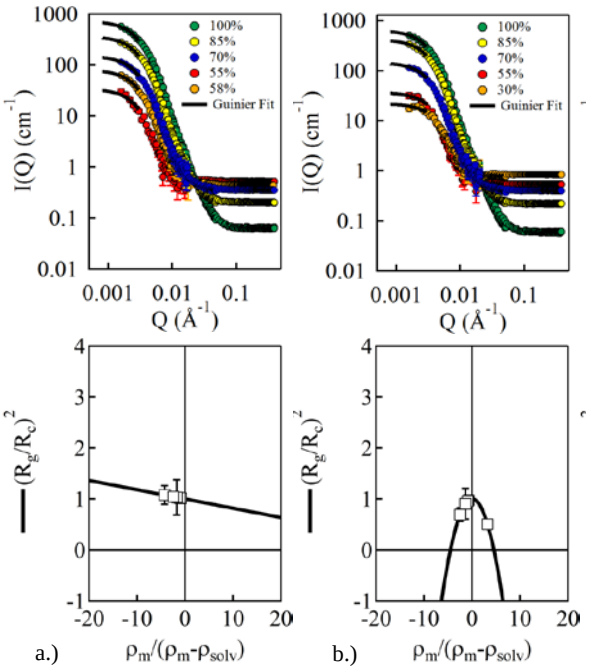

Figure 4: CV-SANS profiles and Sturhman plots for two P3HT/PCBM particles with different

Photoconductive probe microscopy enabled measurement of photovoltaic properties for individual particles. Here, a conductive path is formed between a sharp metallic tip and the underlying substrate and light is used to excite the particles. High photocurrents would occur for samples with even distributions (pre-Gel samples). Figure 5 shows a schematic of the experiment as well as photocurrent histograms for the different particles. Particles with uniform distribution have larger negative currents and larger overall current densities.

Future Plans

We are now performing experiments to probe the dynamic relaxations of conjugated polymers in the solid state. These include (from slow to fast): low amplitude oscillatory rheology, dielectric spectroscopy, neutron spin echo and neutron backscattering spectroscopy. Figure 6 shows preliminary results obtained from neutron backscattering spectroscopy (BASIS-SNS) where probed time-scales and size-scales are most sensitive to monomer fluctuations. We hypothesize that these motions are strongly affected by the type and location of alkyl side-chains and that they will also play a significant effect in modulating charge transport.

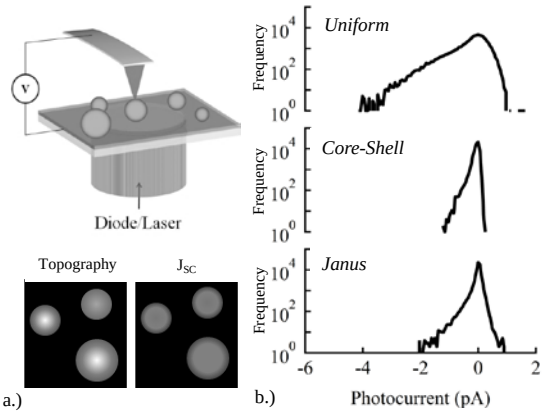

Figure 5: Schematic of photoconductive probe microscopy (Left) and histogram for photocurrent

X-ray diffraction, rheology and impedance spectroscopy are also being used to correlate structure, molecular motions and electronic behavior. In addition we are preparing molecular dynamic simulations that will be used to interpret the quasielastic neutron scattering results with less ambiguity.(3)

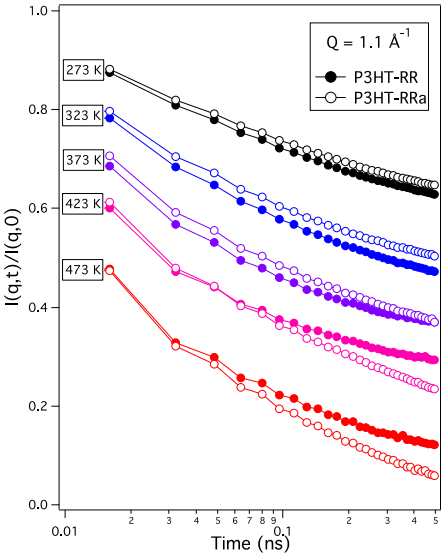

Figure 6: Intermediate scattering functions for regio-regular and regio-random P3HT at variable temperatures (BASIS-SNS).

References

1) “Small-Angle Scattering of Biological Structures”, H. B. Stuhrmann, A. Miller, Journal of Applied Crystallography, 11, 325 (1978)

2) “Aqueous Dispersions of Colloidal Poly(3-hexylthiophene) Gel Particles with High Internal Porosity” J. Richards, K. Weigandt and D.C. Pozzo, J. Colloid and Interface Science, 364, 341 (2011)

3) “Neutron scattering and molecular dynamics simulations: synergetic tools to unravel structure and dynamics in polymers” A. Arbe, F. Alvarez and J.C. Colmenero, Soft Matter, 8, 8257 (2012)

Publications

“Correlating Structure and Photocurrent for Composite Semiconducting Nanoparticles with Contrast Variation Small-Angle Neutron Scattering and Photoconductive Atomic Force Microscopy” J. J. Richards, C. L. Whittle, G. Shao, and L. D. Pozzo, ACS Nano, 8(5), p 4313 (2014)

“Modification of PCBM crystallization via incorporation of C60 in polymer/fullerene solar cells” J. Richards1, A. Rice, R. Nelson, F. Kim, S.A. Jenekhe, C.K. Luscombe, D.C. Pozzo, Advanced Functional Materials, 23(4), 514 (2013)

“Effects of supersaturation on the structure and properties of poly(9,9-dioctyl fluorene) organogels.” P. de la Iglesia, D.C. Pozzo, Soft Matter, 9: 11214 (2013)

“Structure and Property Development of Poly(3-hexyl-thiophene) Organogels Probed with Combined Rheology, Conductivity and Small Angle Neutron Scattering” G. Newbloom, K. Weigandt, D.C. Pozzo, Soft Matter, 8: 8854 (2012)

“Electrical, Mechanical and Structural Characterization of Self-Assembly in Poly(3-hexylthiophene) Organogel Networks.” G. Newbloom, K. Weigandt and D.C. Pozzo, Macromolecules, 45(8): 3452 (2012)

Engineering doping profiles in organic semiconductor materials

Adam J. Moulé (amoule@ucdavis.edu) and Mark Mascal*

Chemical Engineering and Materials Science and Chemistry Department, University of California, Davis, Davis, CA 95616

Research Scope: It would greatly expand the fabrication toolbox for organic electronic materials if a method to produce non-uniform and thermally stable doping profiles existed. We propose here a method to establish p-type doping gradients in organic materials with potential applications towards organic electronic devices. The main goal of the proposal is to develop a method to produce thermally persistent non-uniform doping profiles.

Recently, a large number of doped and self-doped conducting and semiconducting polymers and polymer electrolytes have been developed.[1-3] These materials can mimic most electronic properties of inorganic semiconductors and have several advantages over inorganics including:

(1) high tunability range of properties with small changes in structure or sample processing[4]
(2) low-temperature, low-cost, low-toxicity, and solvent-based deposition[5-8]
(3) material flexibility, light weight, and air stability for device applications

One remaining difference between organic and inorganic semiconductors in the control of materials properties is that non-uniform and complex doping profiles can be established during deposition of inorganic materials, while this is extremely difficult with organic materials. This problem will be addressed by synthesis of multi-functional dopants that are designed for processability. In order to effectively design functional dopants we will need to study the fundamental doping mechanisms. The specific aims of this proposal are:

(1) to determine how neutral and ionic dopants differ in their effectiveness at p-type doping polythiophene polymers
(2) to synthesize a family of p-type dopants for organic films with side groups that can be optimized for solubility, cross-linking to the host film, and doping effectiveness
(3) to use the functionalized dopants to generate non-uniform doping profiles and study the doping effectiveness, thermal persistence of the dopant, and diffusion mechanism.
(4) to develop neutron and x-ray methods to measure the dopant distribution profile, dopant diffusion rate, and doping effectiveness.

Recent Progress: We received funding in August 2013 and have made consistent progress on all four goal areas since then. Progress is listed in the separate areas.

(1) to determine how neutral and ionic dopants differ in their effectiveness at p-type doping polythiophene polymers

We have studied the ionic dopants KI and a polyfluorineated ionomer (PFI) as ionic dopants for the polymers alternating polyfluorine benzodithiazol (APFO-3) and the self-doped thiophene, sulfonated poly(thiophene-3-[2-(2-methoxyethoxy) ethoxy]-2,5-diyl) (S-P3MEET). A paper about the PFI work was recently published.*(J. Mater Chem C (2014), 2(1), 115)*. The main results were that PFI dopes SP3MEET with noted changes in the work function and pre-edge peak in the NEXAFS spectrum. However the PFI does not diffuse into the APFO-3 as did the PSS from PEDOT-PSS. Neutron Reflectometry showed that PFI stays at the interface between the SP3MEET and active OPV layers. We also showed improved device function using PFI for high work function donor polymers. Note that this work was performed before my BES-grant was awarded and was credited to previous DOE-EERE funding

(DEFG3608GO18018) from Moulé, and BES funding (DE-AC52-06NA25396) to the instrument scientists at LANSCE.

For comparison, we also studied the neutral dopants I_2, Br_2, $C_{60}F_{36}$, N,N,N',N'-Tetrakis(4-methoxyphenyl) benzidine (F_4TCNQ), and 2,3 dichloro 5,6 dicyano benzoquinone (DDQ). In the same two polymers. In addition, we studied the $C_{60}F_{36}$ and F_4TCNQ in the small molecule hole transport matrix of methyoxy-tri-phenyl diamine (MeO-TPD) and (BF-DPD). In both of these studies, the F_4TCNQ was an effective dopant that increases the hole mobility of the hole transport material. However, for neutral polymer for polar self-doped polymer and for crystalline small molecules, the dopant was found to diffuse through the material at well below the glass transition temperature of the host material. In both studies we used neutron and x-ray reflectometry to measure the diffusion of the dopants (before and after heating density distributions) and compared the samples using electrical and optical measurements as well.

We found that uncontrolled diffusion of small dopant molecules causes devices failure. But large dopants like $C_{60}F_{36}$ are not effective for polymers or solution coated small molecules because it is insoluble. Mixed layers cannot be created. Therefore, it is necessary to design dopants that have high solubility but can also be immobilized. This work motivated much of the proposal.

The polymer doping paper was submitted to Organic Electronics and is in review. The small molecule doping paper is 95% finished. We are took new XRR data in late May of 2014 to verify several inconclusive results and plan to submit during the summer.

(2) to synthesize a family of p-type dopants for organic films with side groups that can be optimized for solubility, cross-linking to the host film, and doping effectiveness

We proposed to substitute cyano groups for ester groups using an F_4TCNQ base molecule. The Mascal group was successful in synthesizing methyl- and octyl-esters and methyl and octyl- di-esters of F_4TCNQ using the proposed mechanism. As hoped, all of the dopants appear to efficiently dope P3HT and we see increases in conductivity that are nearly identical as a function of concentration as for doping with F_4TCNQ.

Samples	σ (S/cm)	Error
Neat P3HT	2.23E-05	2.40E-06
P3HT with 5 wt% F4TCNQ	8.25E-02	5.19E-03
P3HT with 5 wt% Dimethyl-F4TCNQ	4.51E-03	3.98E-04
P3HT with 5 wt% Dioctyl-F4TCNQ	1.40E-02	1.38E-03
P3HT with 5 wt% Methyl-F4TCNQ	2.95E-02	3.00E-03
P3HT with 5 wt% Octyl-F4TCNQ	1.86E-02	1.11E-03

While working with F_4TCNQ, we came to the conclusion that we need stronger dopants. F_4TCNQ is capable of taking electrons from electron-rich polymers like P3HT and SP3MEET, but is not strong enough to take electrons from APFO-3, MEH-PPV or F8BT, which are all commonly used polymers for OPV, OLEDs, and OFETs, respectively. To address the shortcoming, Prof. Mascal decided to adapt the dopant DDQ (which has a larger electron affinity than F_4TCNQ) to also be tailored with the ester and –R group. The new dopant was successfully synthesized and we are testing it for the first time in June.

(3) to use the functionalized dopants to generate non-uniform doping profiles and study the doping effectiveness, thermal persistence of the dopant, and diffusion mechanism.

We worked mostly with dopants I_2 and F_4TCNQ with the polymer P3HT. While trying to measure the doping effectiveness, we found that deposition was difficult, as the F_4TCNQ tended to make the P3HT crash out of solution. At the same time, our diffusion study showed that F_4TCNQ diffuses readily in P3HT. The made us realize that F_4TCNQ^- is immobile in P3HT and F_4TCNQ – neutral is very mobile. Once we made this realization, we used these principles to design a patterning process that allows us to study most of the basic science principles we would like. We evaporate F_4TCNQ through a shadow mask

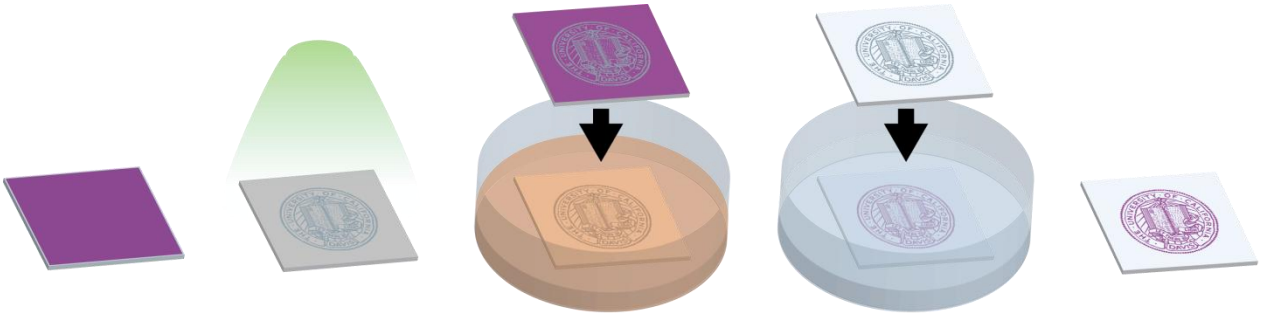

onto a P3HT film. The neutral F_4TCNQ readily penetrates the P3HT film, but quickly the molecules dope the P3HT and become immobile. We then quickly immerse the film into a good solvent for P3HT and the undoped polymer is washed away, while the doped polymer remains insoluble. Finally we can remove the dopants using an orthogonal solvent and a mild base like pyridine. A cartoon of the full process is above. Below are microscope and AFM images of P3HT patterned using a 2000 mesh copper TEM grid as the shadow mask. Please note that this is the finest mesh TEM grid sold with 12.5 μm features on a 20 μm grid.

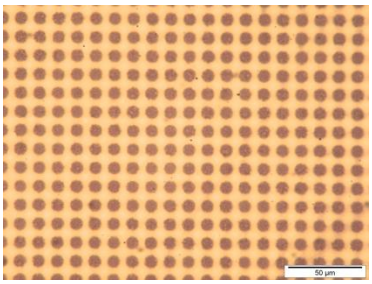

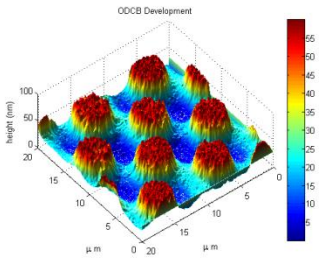

This figure shows an optical microscope image of a P3HT film that was doped through a shodow mask with F_4TCNQ and then developed in Chlorobenzene. We also found that the crystallinity of the polymer prior to doping affects the sharpness of patterned features. The film was deposited with di-cholorbenzene which is a high boiling point solvent that allows P3HT to crystallize into extended domains. We pattern an entire TEM grid, which corresponds to >250000 features created simultaneously.

We have filed a preliminary patent on this process. We plan to submit a paper to a high impact journal in June 2014.

(4) to develop neutron and x-ray methods to measure the dopant distribution profile, dopant diffusion rate, and doping effectiveness.

We applied for and received QENS measurement time at BASIS at SNS (scheduled for late October 2014). We applied for and received vibrational spectroscopy measurement time on VISION and SNS (scheduled for September 2014).

Future Plans: In the immediate future, we are focused on completion of a publication describing the patterning process.

Ian Jacobs is focused on developing the patterning process, demonstrating the patterning capability, and reducing the ideas to their most fundamental scientific principles.

Prof. Moule recruited and trained nine undergraduate researchers over the last year who will stay over the summer 2014 in Davis and volunteer as researchers. This group of students will perform a large number of analytical experiments to (1) determine the electronic mechanism of doping using ultrafast laser experiments (2) better describe the specific material features that affect patterning sharpness (differential solubility of dopants) and (3) to make conductivity, mobility and optical measurements of various polymer films doped with the newly synthesized dopant structures.

Jun Li will take the Neutron summer course and learn to acquire data on BASIS and VISION. He will also take data on SPEAR for the last neutron run from LANSCE.

Mascal Group – will continue to synthesize dopants with various side chains and also new stronger dopant molecules.

List of Papers:

1) Rochester, C. W.; J., L.; Jacobs, I. E.; Friedrich, S.; Stroeve, P.; Moule, A. J., Observing the interlayer diffusion of molecular dopants in organic electronic materials. *submitted* **2014**.
2) Rochester, C. W.; J., L.; Reide, M.; Moule, A. J., Investigating Molecular Dopant Diffusion in MeO-TPD films. *In Preparation* **2014**.
3) Li, J.; Jacobs, I. E.; Bilski, D.; Moule, A. J., Self-assembly of dopant domains controls conductivity anisotropy in doped polymer films. *In Preparation* **2014**.
4) Jacobs, I. E.; Li, J.; Berg, S.; Stroeve, P.; Augustine, M. P.; Moule, A. J., Photopatterning using molecular dopants. *In Preparation* **2014**

Session III

High Tc Superconductivity

Using neutron as a probe to study magnetic excitations in strongly correlated electron materials

Pengcheng Dai (pdai@rice.edu)

Department of Physics and Astronomy, Rice University, Houston, Texas 77005

Program Scope

Understanding the electronic structure and magnetism in correlated electron materials continues to be at the forefront of modern condensed matter physics. Compounds containing quasi-localized *d*-electrons and extended *f*-electrons exhibit a wide range of phenomena, include high-transition temperature and unconventional superconductivity. Elucidating the microscopic spin excitations in these systems is central to understand their exotic macroscopic properties, which continue to defy description of the conventional Fermi-liquid theory. Neutron scattering plays an important role in determining the dynamical spin properties in these materials. The normal operation of the spallation neutron source and upgraded high-flux isotope reactor at Oak Ridge National Laboratory has created a unique opportunity for us to establish a strong materials synthesis and neutron scattering program at Rice University. The scope of our present program is to study spin excitations in iron-based superconductors, with the dual purpose of describing magnetic interactions in these materials and, at the same time, training the next generation of neutron scattering scientists. We also establish a materials growth laboratory capable of producing some of the best Fe-based superconductors for the U.S. condensed matter physics community.

Recent Progress

Effect of Pnictogen Height on Spin Waves in Iron Pnictides

We use inelastic neutron scattering to study spin waves in the antiferromagnetic ordered phase of iron pnictide NaFeAs throughout the Brillouin zone. Comparing with the well-studied AFe_2As_2 (A = Ca, Sr, Ba) family, spin waves in NaFeAs have considerably lower zone boundary energies and more isotropic effective in-plane magnetic exchange couplings. These results are consistent with calculations from a combined density functional theory and dynamical mean field theory and provide strong evidence that pnictogen height controls the strength of electron-electron correlations and

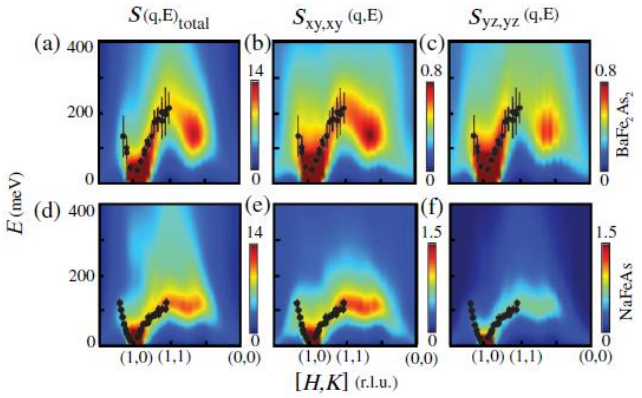

Fig. 1 Comparison of spin waves obtained from ARCS, SNS and dynamic mean field theory calculation of spin waves for NaFeAs, a parent compound of iron pnictides.

consequently the effective bandwidth of magnetic excitations [C. L. Zhang *et al.*, *Phys. Rev. Lett.* **112**, 217202 (2014)].

Measurement of a double neutron-spin resonance and an anisotropic energy gap for underdoped superconducting $NaFe_{0.985}Co_{0.015}As$ using inelastic neutron scattering

We use inelastic neutron scattering to show that superconductivity in electron-underdoped $NaFe_{0.985}Co_{0.015}As$ induces a dispersive sharp resonance near E_{r1}=3.25 meV and a broad dispersionless mode at E_{r2}=6 meV. However, similar measurements on overdoped superconducting $NaFe_{0.935}Co_{0.045}As$ find only a single sharp resonance at E_r=7 meV. We connect these results with the observations of angle resolved photoemission spectroscopy that the superconducting gaps in the electron Fermi pockets are anisotropic in the underdoped material but become isotropic in the overdoped case. Our analysis indicates that both the double neutron spin resonances and gap anisotropy originate from the orbital dependence of the superconducting pairing in the iron pnictides. Our discovery also shows the importance of the inelastic neutron scattering in detecting the multiorbital superconducting gap structures of iron pnictides [C. L. Zhang *et al.*, *Phys. Rev. Lett.* **111**, 207002 (2013)].

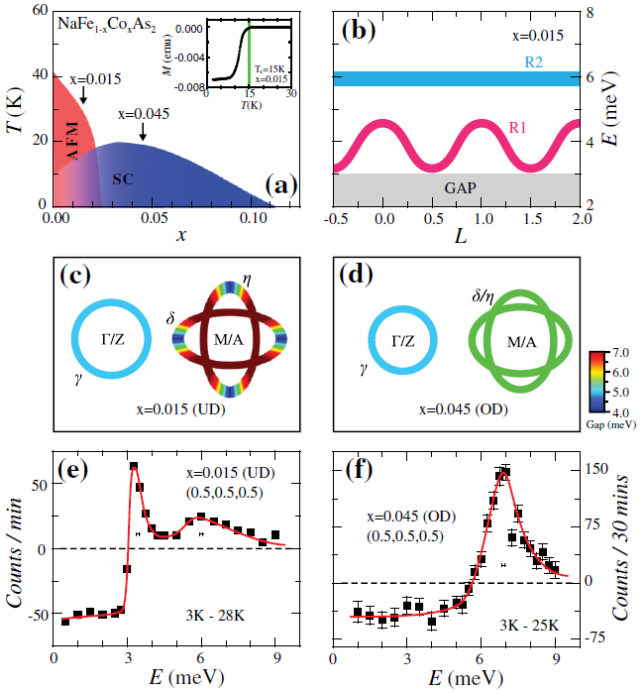

Fig. 2 The phase diagram of Co-doped NaFeAs and the comparison of evolution of the neutron spin resonance as a function of increasing doping and angle resolved photoemission measurements of the superconducting gap anisotropy.

Doping dependence of spin excitations and its correlations with high-temperature superconductivity in iron pnictide

High-temperature superconductivity in iron pnictides occurs when electrons and holes are doped into their antiferromagnetic parent compounds. Since spin excitations may be responsible for electron pairing and superconductivity, it is important to determine their electron/hole-doping evolution and connection with superconductivity. Here we use inelastic neutron scattering to show that while electron doping to the antiferromagnetic $BaFe_2As_2$ parent compound modifies the low-energy spin excitations and their correlation with superconductivity (<50 meV) without affecting the high-energy spin excitations (>100 meV), hole-doping suppresses the high-energy spin excitations and shifts the magnetic spectral weight to low-energies. In addition, our absolute spin susceptibility measurements for the optimally hole-doped iron pnictide reveal that the change in magnetic exchange energy below and above T_c can account for the superconducting

condensation energy. These results suggest that high-T_c superconductivity in iron pnictides is associated with both the presence of high-energy spin excitations and a coupling between low-energy spin excitations and itinerant electrons [M. Wang *et al.*, *Nature Communications* **4**, 2874 (2013)].

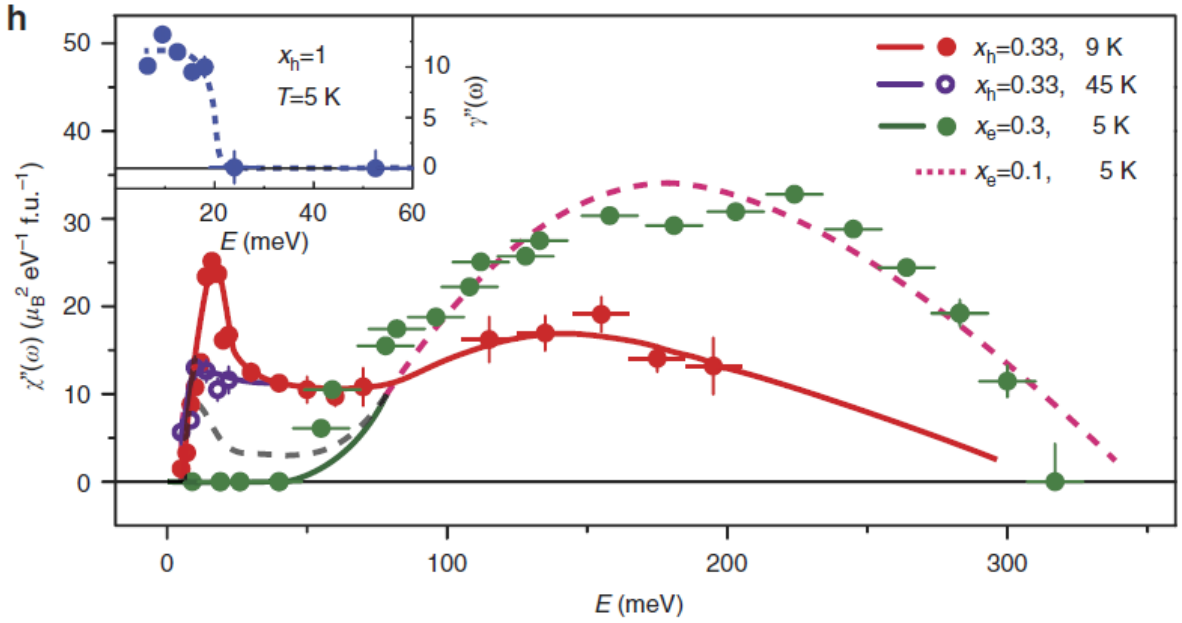

Fig. 3 The electron and hole-doping evolution of the local dynamic susceptibility in $BaFe_2As_2$. The grey dashed line indicate the parent compound $BaFe_2As_2$. Electron-doping to the parent compound suppresses the low-energy spin excitations while leaving high-energy excitations unchanged, while hole-doping pushes the high-energy spin excitation spectral weight to lower energies.

Future Plans

Our ultimate goal in this DOE supported project is to understand the microscopic origin of superconductivity in the high-T_c superconductors. We will continue our successful program to study the interplay between magnetism and superconductivity. In particular, we will focus on spin dynamics in Na(Fe,Co)As family of materials, with the plan of comparing and contrasting the evolution of spin excitations in this family of iron based superconductors with those of the most studies $BaFe_2As_2$ family of materials. Our ability to grow large enough single crystals of Na(Fe,Co)As means that we can now carry out inelastic neutron scattering experiments to determine spin excitations in this system throughout the Brillouin zone. Our recent work (see example 1) on spin waves in NaFeAs has demonstrated that iron pnictogen height can directly control the total spin excitation bandwidth of the system. In the coming years, we will determine the evolution of spin excitations as a function of electron-doping and their relationship to superconductivity. In addition, we will study the evolution of spin excitations in LiFeAs and its Co-doping dependence. By comparing and contrasting the evolution of spin excitations in the sister systems Na(Fe,Co)As and Li(Fe,Co)As and compare the outcome with angle resolved photoemission spectroscopy experiments, we hope to establish if magnetism and superconductivity in these materials arise from quasiparticle excitations between the hole and electron Fermi surfaces. This work complements previous neutron scattering work on electron and hole-doped $BaFe_2As_2$ family of materials (see example 3). By systematically determining the experimental facts concerning the evolution of spin excitations in iron pnictides, one can establish a base for a future comprehensive theory of high-T_c superconductivity.

Publications from DOE support from May 1, 2012 till May 1 2014

1. H. Kim, M. A. Tanatar, Yong Liu, Z. C. Sims, Chenglin Zhang, Pengcheng Dai, T. A. Lograsso, and R. Prozorov, *Phys. Rev. B* **89**, 174519 (2014).

2. Chenglin Zhang, Leland W. Harriger, Zhiping Yin, Weicheng Lv, Miaoyin Wang, Guotai Tan, Yu Song, D. L. Abernathy, Wei Tian, Takeshi Egami, Kristjan Haule, Gabriel Kotliar, and Pengcheng Dai, *Phys. Rev. Lett.* ***112****,* 217202 (2014).

3. Meng Wang, Chenglin Zhang, Xingye Lu, Guotai Tan, Huiqian Luo, Yu Song, Miaoyin Wang, Xiaotian Zhang, E.A. Goremychkin, T.G. Perring, T.A. Maier, Zhiping Yin, Kristjan Haule, Gabriel Kotliar & Pengcheng Dai, *Nature Communications* **4**, 2874 (2013).

4. J. Munevar, H. Micklitz, J. Aguero, Guotai Tan, Chenglin Zhang, Pengcheng Dai, and E. Baggio-Saitovitch, *Phys. Rev. B* **88**, 184514(2013).

5. Chenglin Zhang, Rong Yu, Yixi Su, Yu Song, Miaoyin Wang, Guotai Tan, Takeshi Egami, J. A. Fernandez-Baca, Enrico Faulhaber, Qimiao Si, and Pengcheng Dai, *Phys. Rev. Lett.* **111**, 207002 (2013).

6. Sangwon Oh, A. M. Mounce, Jeongseop A. Lee, W. P. Halperin, C. L. Zhang, S. Carr, Pengcheng Dai, A. P. Reyes, and P. L. Kuhns, *Phys. Rev. B* ***88****,* 134518 (2013).

7. Yu Song, Louis-Pierre Regnault, Chenglin Zhang, Guotai Tan, Scott V. Carr, Songxue Chi, A. D. Christianson, Tao Xiang, and Pengcheng Dai, *Phys. Rev. B* ***88****,* 134512 (2013).

8. L M Wang, Chih-Yi Wang, Un-Cheong Sou, H C Yang, L J Chang, C. Redding, Yu Song, Pengcheng Dai, and Chenglin Zhang, *J. of Phys.: Condensed Matter* ***25****,* 395702 (2013).

9. G. F. Ji, J. S. Zhang, Long Ma, P. Fan, P. S. Wang, J. Dai, G. T. Tan, Y. Song, C. L. Zhang, Pengcheng Dai, B. Normand, and Weiqiang Yu, *Phys. Rev. Lett.* **111**, 107004 (2013).

10. Chenglin Zhang, H.-F. Li, Yu Song, Yixi Su, Guotai Tan, Tucker Netherton, Caleb Redding, Scott V. Carr, Oleg Sobolev, Astrid Schneidewind, Enrico Faulhaber, L. W. Harriger, Shiliang Li, Xingye Lu, Dao-Xin Yao, Tanmoy Das, A. V. Balatsky, Th. Brückel, J. W. Lynn, and Pengcheng Dai, *Phys. Rev. B* **88**, 064504 (2013).

11. Yu Song, Scott V. Carr, Xingye Lu, Chenglin Zhang, Zachary C. Sims, N. F. Luttrell, Songxue Chi, Yang Zhao, Jeffrey W. Lynn, and Pengcheng Dai, *Phys. Rev. B* **87**, 184511 (2013).

12. Sangwon Oh, A. M. Mounce, Jeongseop A. Lee, W. P. Halperin, C. L. Zhang, S. Carr, and Pengcheng Dai, *Phys. Rev. B* **87**, 174517 (2013).

13. Guotai Tan, Ping Zheng, Xiancheng Wang, Yanchao Chen, Xiaotian Zhang, Jianlin Luo, Tucker Netherton, Yu Song, Pengcheng Dai, Chenglin Zhang, and Shiliang Li, *Phys. Rev. B* **87**, 144512 (2013).

14. Q. Q. Ge, Z. R. Ye, M. Xu, Y. Zhang, J. Jiang, B. P. Xie, Y. Song, C. L. Zhang, Pengcheng Dai, and D. L. Feng, *Phys. Rev. X* **3**, 011020 (2013).

15. Lei Shan, Jing Gong, Yong-Lei Wang, Bing Shen, Xingyuan Hou, Cong Ren, Chunhong Li, Huan Yang, Hai-Hu Wen, Shiliang Li, and Pengcheng Dai, *Phys. Rev. Lett.* ***108****,* 227002 (2012).

16. Sangwon Oh, A. M. Mounce, W. P. Halperin, C. L. Zhang, Pengcheng Dai, A. P. Reyes, and P. L. Kuhns, *Phys. Rev. B* ***85***,174508 (2012).

17. Miaoyin Wang, Xingye Lu, R. A. Ewings, Leland W. Harriger, Yu Song, Scott V. Carr, Chunhong Li, Rui Zhang, and Pengcheng Dai, *Phys. Rev. B* **87**, 064409 (2013).

18. Chenglin Zhang, Mengshu Liu, Yixi Su, Louis-Pierre Regnault, Meng Wang, Guotai Tan, Th. Bruckel, Takeshi Egami, and Pengcheng Dai, *Phys. Rev. B* **87**, 081101(R) (2013).

19. Zhenyu Wang, Huan Yang, Delong Fang, Bing Shen, Qiang-Hua Wang, Lei Shan, Chenglin Zhang, Pengcheng Dai& Hai-Hu Wen, *Nature Physics* **9**, 42-48 (2013).

20. N. Spyrison, M. A. Tanatar, Kyuil Cho, Y. Song, Pengcheng Dai, Chenglin Zhang, and R. Prozorov, *Phys. Rev. B* **86**, 144528 (2012).

21. Meng Wang, Miaoyin Wang, Hu Miao, S. V. Carr, D. L. Abernathy, M. B. Stone, X. C. Wang, Lingyi Xing, C. Q. Jin, Xiaotian Zhang, Jiangping Hu, Tao Xiang, Hong Ding, and Pengcheng Dai, *Phys. Rev. B* **86**, 144511 (2012).

22. Pengcheng Dai, Jiangping Hu, & Elbio Dagotto, *Nature Physics* **8**, 709-718 (2012).

23. W. J. Gannon, W. P. Halperin, C. Rastovski, M. R. Eskildsen, Pengcheng Dai, and A. Stunault, *Phys. Rev. B* **86**, 104510 (2012).

24. K. Cho, M. A. Tanatar, N. Spyrison, H. Kim, Y. Song, Pengcheng Dai, C. L. Zhang, and R. Prozorov, *Phys. Rev. B* **86**, 020508(R) (2012).

Neutron and X-Ray Scattering Studies of High-Temperature Superconductors

J. M. Tranquada (jtran@bnl.gov), G. D. Gu, M. Hücker, G. Y. Xu, I. A. Zaliznyak, and D. Fobes
Condensed Matter Physics & Materials Science Department
Brookhaven National Laboratory, Upton, NY 11973-5000

Program Scope

This program is organized around the challenge of understanding the antiferromagnetic spin correlations characteristic of high-temperature superconductors, with particular focus on systems such as copper oxides and the iron-based superconductors. The main experimental tools are neutron scattering and high-energy x-ray diffraction, with experiments performed at the best facilities in the U.S. and abroad. Problems addressed include: doping of correlated insulators, self-organized spin and charge inhomogeneities (such as stripes), electron-phonon coupling, spin dynamics, quantum magnetism in low-dimensional systems, and the impact of disorder. Growth of suitable single-crystal samples is an essential part of the program, with complementary characterizations performed in collaboration with other Brookhaven groups, especially at the National Synchrotron Light Source. There are also close interactions with the Center for Emergent Superconductivity, an Energy Frontier Research Center. This program leads the Instrument Development Team for HYSPEC, an inelastic spectrometer with polarization analysis, now operating at the Spallation Neutron Source; it also participates in the US-Japan Cooperative Program on Neutron Scattering, which has partial access to the cold-neutron triple-axis spectrometer at the High Flux Isotope Reactor.

Recent Progress

Charge-density-wave order in $YBa_2Cu_3O_{6+x}$. There has been considerable excitement over the observation of CDW order in $YBa_2Cu_3O_{6+x}$ (YBCO) and several other cuprate families. Hücker has collaborated with Chang and Zimmermann on hard x-ray diffraction studies of this problem at Petra III and the APS. Recent results [1] confirm that the order parameter is largest for a hole concentration $p \sim 1/8$, falling away at optimal doping and for $p < 0.08$. The ordering wave vector decreases with p, similar to the behavior of the antinodal $2k_F$ measured by photoemission. This doping dependence is opposite to that of the charge-stripe wave vector in $La_{2-x}Ba_xCuO_4$ (LBCO). Application of a c-axis magnetic field causes the CDW order to grow, but only for temperatures less than the superconducting transition temperature, T_c. Hücker has demonstrated a similar magnetic-field response in LBCO.

Incommensurate spin correlations. In LBCO, the incommensurability of the low-energy spin correlations is exactly half of that for charge stripes. Tranquada has collaborated with Fujita (Tohoku) and Yamada (KEK) on a neutron scattering study of low-energy spin correlations in $Bi_{2+x}Sr_{2-x}CuO_{6+y}$. The observed spin incommensurability vs. doping is quantitatively identical to that in LBCO and $La_{2-x}Sr_xCuO_4$ (LSCO). Results for YBCO show qualitatively the same trend. Thus, there appears to be a universal behavior for the spin modulations, even when charge modulations show distinct trends between YBCO and LBCO.

To further test trends, a collaborative study was performed on the magnetic dispersion in LSCO with $x = 0.04$ using a single-domain orthorhombic crystal. This sample has diagonal spin modulations (at low energy) that have a unique orientation with respect to the orthorhombic axes. Inelastic scattering revealed an hour-glass dispersion, with a unidirectional dispersion at

low energy, and isotropic dispersion at high energy. This change in dispersive character with energy is similar to that previously reported in the "nematic" phase of YBCO.

Charge order survives under pressure. Building on previous work, a combined x-ray diffraction and XAFS study was performed on LBCO x=1/8 to test how charge-stripe order is affected by pressure. Even after the charge order superlattice peak becomes negligible, the local atomic arrangement is consistent with the structure that pins stripes, and its evolution is correlated with a very gradual increase in the superconducting T_c.

Charge stripe fluctuations in $La_{2-x}Sr_xNiO_4$. In separate collaborations with the Flucteam (Bozin and Billinge) at BNL and with Reznik (U. Colorado), evidence has been obtained for fluctuating charge stripes above the stripe melting temperature in $La_{2-x}Sr_xNiO_4$ (LSNO). In the former, indirect evidence was obtained from the temperature dependence of the mean-squared displacement for in-plane oxygen sites. In the latter, inelastic scattering provided direct evidence for lattice fluctuations at the charge-stripe wave vector.

Stripes and superconductivity. Inelastic neutron scattering measurements have been performed on LBCO with x = 0.095, a robust superconductor with T_c = 32 K [2]. Contrary to the commonly-expected behavior, no spin gap or resonance develops in the incommensurate magnetic excitations below T_c. To reconcile this result with other experiments, we propose that the superconducting pair wave function must be spatially modulated in order to minimize local coexistence with the gapless spin fluctuations.

Orbital order and phase diagram of $Fe_{1+y}Te$. Recent studies by our group and others have established that electronic properties of the 11 iron chalcogenides are very sensitive to non-stoichiometric iron at interstitial sites. In particular, the antiferromagnetic end member $Fe_{1+y}Te$ has a complex magneto-structural (y, T) phase diagram. At intermediate y, the frustration effects of the interstitial Fe decouple different orders, leading to a sequence of transitions. In our recent work we have established that the development of bicollinear antiferromagnetic order and metallic electronic coherence is uniquely associated with a hysteretic first-order transition to the bond-order wave (BOW) phase, which follows the monoclinic lattice distortion and the incommensurate magnetic order, but at a markedly lower temperature. The BOW state suggests ferro-orbital ordering, where electronic delocalization in ferromagnetic zigzag chains leads to metallic transport. This picture is also corroborated by our earlier study, where it was established that the total amount of magnetic scattering in $Fe_{1.1}Te$ decreases significantly, by about a factor 2, upon cooling from 100 K to 10 K, corresponding to change in the local-spin value from S = 3/2 to S = 1.

Plaquette liquid correlations in $Fe_{1+y}Te_{1-x}(Se,S)_x$. Our analysis of inelastic and quasielastic scattering in poorly-metallic magnetic state of $Fe_{1+y}Te$ reveals short-range spin correlations where four-iron square plaquettes align ferromagnetically, with antiferromagnetic correlations between the neighboring plaquettes. When this material is doped, with Se or S, and begins to develop superconductivity, the structure of magnetic diffuse scattering changes. Here, we observe a different liquid-like magnetic response, which can be described by the newly emergent local structure of slanted four-iron antiferromagnetic plaquettes. These new local correlations break the C_4 symmetry of the underlying square lattice and can therefore be related to "nematicity" observed by other techniques. The competition between the two types of dynamical local magnetic structures is suggestive of liquid-liquid phase transition in the electronic spin system of FeTe when it is doped, with Se or S, to become a superconductor. It is revealed by the change in the relative population of the two phases with temperature, where the C_4 square plaquettes present in $Fe_{1+y}Te$ become dominant at high T. The newly emerging slanted

plaquettes perhaps reflect new electronic hybridization pattern, which is favored by the shift of atomic energy levels that results from doping and which facilitates electron pairing.

Evolution of spin correlations in $Fe_{1+y}(Ni/Cu)_yTe_{1-x}Se_x$. We have studied the change in low-energy magnetic dispersions with temperature and energy in superconducting $FeTe_{1-x}Se_x$ and in samples perturbed by Ni or Cu substitutions, or excess Fe. Even in a good superconductor, we have observed a change in the characteristic wave vector for the magnetic correlations as a function of temperature. Substitutions that reduce the superconducting T_c also inhibit the change in low-energy correlations on cooling. At low temperature, the difference in magnetic excitations between superconducting and nonsuperconducting samples becomes less significant above 10 meV.

Future Plans

LTT character in the LTO phase of LBCO. Together with the Flucteam, we are investigating the thermal evolution of octahedral tilt patterns in LBCO. Measurements indicate that the tilt pattern characteristic of the low-temperature tetragonal phase survives the phase transition into the orthorhombic phase at higher temperature. Such results appear to be compatible with the theoretical proposal that the structural transition is driven by entropy.

Direct determination of longer-range exchange interactions. We plan to directly measure magnetic bond energies in La_2CuO_4 by applying the single-mode approximation to excitation spectra. The goal is to obtain an independent test for magnetic interactions beyond nearest neighbor, such as 4-spin cyclic exchange.

Dynamic charge stripes. Having established the existence of charge stripe fluctuations in LSNO, we intend to obtain more detailed characterizations of such fluctuations. We also intend to look for charge-stripe fluctuations in cuprates. In particular, we intend to collaborate with the X-ray Scattering Group at BNL, using new capabilities at NSLS-II.

Magnetic correlations in superconducting $FeTe_{1-x}Se_x$. We will apply the short-range plaquette correlation model to the analysis of the temperature and energy evolution of the magnetic correlations. Diffraction studies will be used to test for anomalous lattice parameter changes in these samples that might reflect the development of local orbital correlations.

Magneto-structural excitations associated with the BOW in $Fe_{1+y}Te$. We are investigating possible magnetic contributions to phonon excitations near (100) and (010) Bragg peaks, using polarized neutrons. We will also test to see whether the temperature-dependent change in instantaneous magnetic moment is tied uniquely to the BOW transition.

References

1. M. Hücker, N. B. Christensen, A. T. Holmes, E. Blackburn, E. M. Forgan, Ruixing Liang, D. A. Bonn, W. N. Hardy, O. Gutowski, M. v. Zimmermann, S. M. Hayden, and J. Chang, "Competing charge, spin, and superconducting orders in underdoped $YBa_2Cu_3O_y$," arXiv:1405.7001.
2. Zhijun Xu, C. Stock, Songxue Chi, A. I. Kolesnikov, Guangyong Xu, Genda Gu, and J. M. Tranquada, "Indirect Evidence for Periodically-Modulated Superconductivity in Underdoped Cuprates," arXiv:1309.2718v2.
3. Igor A. Zaliznyak, John M. Tranquada. Neutron Scattering and Its Application to Strongly Correlated Systems. arXiv:1304.4214 (2013); in Strongly Correlated Systems: Experimental Techniques. Edited by A. Avella and F. Mancini (2014).

Publications

1. T. J. Reber, N. C. Plumb, Z. Sun, Y. Cao, Q. Wang, K. McElroy, H. Iwasawa, M. Arita, J. S. Wen, Z. J. Xu, G. Gu, Y. Yoshida, H. Eisaki, Y. Aiura, and D. S. Dessau. The origin and non-quasiparticle nature of Fermi arcs in $Bi_2Sr_2CaCu_2O_{8+\delta}$. *Nat. Phys.* **8**, 606–610 (2012).

2. Qing Jie, Rongwei Hu, Emil Bozin, A. Llobet, I. Zaliznyak, C. Petrovic, and Q. Li. Electronic thermoelectric power factor and metal-insulator transition in $FeSb_2$. *Phys. Rev. B* **86**, 115121 (2012).
3. C. Stock, P. M. Gehring, H. Hiraka, I. Swainson, Guangyong Xu, Z.-G. Ye, H. Luo, J.-F. Li, and D. Viehland. Evidence for anisotropic polar nanoregions in relaxor $Pb(Mg_{1/3}Nb_{2/3})O_3$: A neutron study of the elastic constants and anomalous TA phonon damping in PMN. *Phys. Rev. B* **86**, 104108 (2012).
4. John M. Tranquada. Cuprates Get Orders to Charge. *Science* **337**, 811–812 (2012).
5. Jinsheng Wen, Zhijun Xu, Guangyong Xu, M. D. Lumsden, P. N. Valdivia, E. Bourret-Courchesne, Genda Gu, Dung-Hai Lee, J. M. Tranquada, and R. J. Birgeneau. Magnetic order tuned by Cu substitution in $Fe_{1.1-z}Cu_zTe$. *Phys. Rev. B* **86**, 024401 (2012).
6. Ben-Li Young, Zong-Yo Lai, Zhijun Xu, Alina Yang, G. D. Gu, Z.-H. Pan, T. Valla, G. J. Shu, R. Sankar, and F. C. Chou. Probing the bulk electronic states of Bi_2Se_3 using nuclear magnetic resonance. *Phys. Rev. B* **86**, 075137 (2012).
7. Ilija Zeljkovic, Zhijun Xu, Jinsheng Wen, Genda Gu, Robert S. Markiewicz, and Jennifer E. Hoffman. Imaging the Impact of Single Oxygen Atoms on Superconducting $Bi_{2+y}Sr_{2-y}CaCu_2O_{8+x}$. *Science* **337**, 320–323 (2012).
8. A. M. Milinda Abeykoon, Emil S. Bozin, Wei-Guo Yin, Genda Gu, John P. Hill, John M. Tranquada, and Simon J. L. Billinge. Evidence for Short-Range-Ordered Charge Stripes Far above the Charge-Ordering Transition in $La_{1.67}Sr_{0.33}NiO_4$. *Phys. Rev. Lett.* **111**, 096404 (2013).
9. S.-H. Baek, P. C. Hammel, M. Hücker, B. Büchner, U. Ammerahl, A. Revcolevschi, and B. J. Suh. Structural transitions in a doped lanthanum cuprate. *Phys. Rev. B* **87**, 174505 (2013).
10. E. Blackburn, J. Chang, M. Hücker, A. T. Holmes, N. B. Christensen, Ruixing Liang, D. A. Bonn, W. N. Hardy, U. Rütt, O. Gutowski, M. v. Zimmermann, E. M. Forgan, and S. M. Hayden. X-Ray Diffraction Observations of a Charge-Density-Wave Order in Superconducting Ortho-II $YBa_2Cu_3O_{6.54}$ Single Crystals in Zero Magnetic Field. *Phys. Rev. Lett.* **110**, 137004 (2013).
11. Yue Cao, J. A. Waugh, X-W. Zhang, J-W. Luo, Q. Wang, T. J. Reber, S. K. Mo, Z. Xu, A. Yang, J. Schneeloch, G. D. Gu, M. Brahlek, N. Bansal, S. Oh, A. Zunger, and D. S. Dessau. Mapping the orbital wavefunction of the surface states in three-dimensional topological insulators. *Nat. Phys.* **9**, 499–504 (2013).
12. Sungjae Cho, Brian Dellabetta, Alina Yang, John Schneeloch, Zhijun Xu, Tonica Valla, Genda Gu, Matthew J. Gilbert, and Nadya Mason. Symmetry protected Josephson supercurrents in three-dimensional topological insulators. *Nat. Commun.* **4**, 1689 (2013).
13. M. P. M. Dean, G. Dellea, M. Minola, S. B. Wilkins, R. M. Konik, G. D. Gu, M. Le Tacon, N. B. Brookes, F. Yakhou-Harris, K. Kummer, J. P. Hill, L. Braicovich, and G. Ghiringhelli. Magnetic excitations in stripe-ordered $La_{1.875}Ba_{0.125}CuO_4$ studied using resonant inelastic x-ray scattering. *Phys. Rev. B* **88**, 020403 (2013).
14. M. P. M. Dean, A. J. A. James, R. S. Springell, X. Liu, C. Monney, K. J. Zhou, R. M. Konik, J. S. Wen, Z. J. Xu, G. D. Gu, V. N. Strocov, T. Schmitt, and J. P. Hill. High-Energy Magnetic Excitations in the Cuprate Superconductor $Bi_2Sr_2CaCu_2O_{8+\delta}$: Towards a Unified Description of Its Electronic and Magnetic Degrees of Freedom. *Phys. Rev. Lett.* **110**, 147001 (2013).
15. M. Enoki, M. Fujita, T. Nishizaki, S. Iikubo, D. K. Singh, S. Chang, J. M. Tranquada, and K. Yamada. Spin-Stripe Density Varies Linearly With the Hole Content in Single-Layer $Bi_{2+x}Sr_{2-x}CuO_{6+y}$ Cuprate Superconductors. *Phys. Rev. Lett.* **110**, 017004 (2013).
16. G. Fabbris, M. Hücker, G. D. Gu, J. M. Tranquada, and D. Haskel. Local structure, stripe pinning, and superconductivity in $La_{1.875}Ba_{0.125}CuO_4$ at high pressure. *Phys. Rev. B* **88**, 060507 (2013).
17. A. Gyenis, I. K. Drozdov, S. Nadj-Perge, O. B. Jeong, J. Seo, I. Pletikosic, T. Valla, G. D. Gu, and A. Yazdani. Quasiparticle interference on the surface of the topological crystalline insulator $Pb_{1-x}Sn_xSe$. *Phys. Rev. B* **88**, 125414 (2013).
18. Alex Hayat, Parisa Zareapour, Shu Yang F. Zhao, Achint Jain, Igor G. Savelyev, Marina Blumin, Zhijun Xu, Alina Yang, G. D. Gu, Harry E. Ruda, Shuang Jia, R. J. Cava, Aephraim M. Steinberg, and Kenneth S. Burch. Hybrid High-Temperature-Superconductor–Semiconductor Tunnel Diode. *Phys. Rev. X* **2**, 041019 (2012).
19. Junfeng He, Wentao Zhang, Jin Mo Bok, Daixiang Mou, Lin Zhao, Yingying Peng, Shaolong He, Guodong Liu, Xiaoli Dong, Jun Zhang, J. S. Wen, Z. J. Xu, G. D. Gu, Xiaoyang Wang, Qinjun Peng, Zhimin Wang, Shenjin Zhang, Feng Yang, Chuangtian Chen, Zuyan Xu, H.-Y. Choi, C. M. Varma, and X. J. Zhou. Coexistence of Two Sharp-Mode Couplings and their Unusual Momentum Dependence in the Superconducting State of $Bi_2Sr_2CaCu_2O_{8+\delta}$ Revealed by Laser-Based Angle-Resolved Photoemission. *Phys. Rev. Lett.* **111**, 107005 (2013).

20. C. C. Homes, Z. J. Xu, J. S. Wen, and G. D. Gu. Effective medium approximation and the complex optical properties of the inhomogeneous superconductor $K_{0.8}Fe_{2-y}Se_2$. *Phys. Rev. B* **86**, 144530 (2012).
21. M. Hücker, M. v. Zimmermann, Z. J. Xu, J. S. Wen, G. D. Gu, and J. M. Tranquada. Enhanced charge stripe order of superconducting $La_{2-x}Ba_xCuO_4$ in a magnetic field. *Phys. Rev. B* **87**, 014501 (2013).
22. M. Hücker. Structural aspects of materials with static stripe order. *Physica C* **481**, 3–14 (2012).
23. Hovnatan Karapetyan, M. Hücker, G. D. Gu, J. M. Tranquada, M. M. Fejer, Jing Xia, and A. Kapitulnik. Magneto-Optical Measurements of a Cascade of Transitions in Superconducting $La_{1.875}Ba_{0.125}CuO_4$ Single Crystals. *Phys. Rev. Lett.* **109**, 147001 (2012).
24. C. W. Luo, H.-J. Chen, H. J. Wang, S. A. Ku, K. H. Wu, T. M. Uen, J. Y. Juang, J.-Y. Lin, B. L. Young, T. Kobayashi, R. Sankar, F. C. Chou, H. Berger, and G. D. Gu. Ultrafast dynamics in topological insulators. *SPIE Proceedings* **8623**, 86230D (2013).
25. A. Lupascu, Renfei Feng, L. J. Sandilands, Zixin Nie, V. Baydina, Genda Gu, Shimpei Ono, Yoichi Ando, D. C. Kwok, N. Lee, S.-W. Cheong, K. S. Burch, and Young-June Kim. Structural study of $Bi_2Sr_2CaCu_2O_{8+\delta}$ exfoliated nanocrystals. *Appl. Phys. Lett.* **101**, 223106 (2012).
26. M. Matsuda, G. E. Granroth, M. Fujita, K. Yamada, and J. M. Tranquada. Energy-dependent crossover from anisotropic to isotropic magnetic dispersion in lightly doped $La_{1.96}Sr_{0.04}CuO_4$. *Phys. Rev. B* **87**, 054508 (2013).
27. L. K. Narangammana, X. Liu, Y. F. Nie, F. J. Rueckert, J. I. Budnick, W. A. Hines, G. Gu, and B. O. Wells. Low temperature crystal structure and large lattice discontinuity at T_c in superconducting $FeTeO_x$ films. *Appl. Phys. Lett.* **103**, 102604 (2013).
28. Z.-H. Pan, E. Vescovo, A. V. Fedorov, G. D. Gu, and T. Valla. Persistent coherence and spin polarization of topological surface states on topological insulators. *Phys. Rev. B* **88**, 041101 (2013).
29. S. Parham, T. J. Reber, Y. Cao, J. A. Waugh, Z. Xu, J. Schneeloch, R. D. Zhong, G. Gu, G. Arnold, and D. S. Dessau. Pair breaking caused by magnetic impurities in the high-temperature superconductor $Bi_{2.1}Sr_{1.9}Ca(Cu_{1-x}Fe_x)_2O_y$. *Phys. Rev. B* **87**, 104501 (2013).
30. T. J. Reber, N. C. Plumb, Y. Cao, Z. Sun, Q. Wang, K. McElroy, H. Iwasawa, M. Arita, J. S. Wen, Z. J. Xu, G. Gu, Y. Yoshida, H. Eisaki, Y. Aiura, and D. S. Dessau. Prepairing and the ``filling" gap in the cuprates from the tomographic density of states. *Phys. Rev. B* **87**, 060506 (2013).
31. A. Sacuto, S. Benhabib, Y. Gallais, S. Blanc, M. Cazayous, M.-A. Méasson, J. S. Wen, Z. J. Xu, and G. D. Gu. Pseudogap in cuprates by electronic raman scattering. *J. Phys. Conf. Ser.* **449**, 012011 (2013).
32. A. Sacuto, Y. Gallais, M. Cazayous, M.-A. Méasson, G. D. Gu, and D. Colson. New insights into the phase diagram of the copper oxide superconductors from electronic Raman scattering. *Rep. Prog. Phys.* **76**, 022502 (2013).
33. S. Sakai, S. Blanc, M. Civelli, Y. Gallais, M. Cazayous, M.-A. Méasson, J. S. Wen, Z. J. Xu, G. D. Gu, G. Sangiovanni, Y. Motome, K. Held, A. Sacuto, A. Georges, and M. Imada. Raman-Scattering Measurements and Theory of the Energy-Momentum Spectrum for Underdoped $Bi_2Sr_2CaCuO_{8+\delta}$ Superconductors: Evidence of an s-Wave Structure for the Pseudogap. *Phys. Rev. Lett.* **111**, 107001 (2013).
34. G. Simutis, S. Gvasaliya, M. Månsson, A. L. Chernyshev, A. Mohan, S. Singh, C. Hess, A. T. Savici, A. I. Kolesnikov, A. Piovano, T. Perring, I. Zaliznyak, B. Büchner, and A. Zheludev. Spin Pseudogap in Ni-Doped $SrCuO_2$. *Phys. Rev. Lett.* **111**, 067204 (2013).
35. Z. Stegen, Su Jung Han, Jie Wu, A. K. Pramanik, M. Hücker, Genda Gu, Qiang Li, J. H. Park, G. S. Boebinger, and J. M. Tranquada. Evolution of superconducting correlations within magnetic-field-decoupled $La_{2-x}Ba_xCuO_4$ (x=0.095). *Phys. Rev. B* **87**, 064509 (2013).
36. V. Thampy, S. Blanco-Canosa, M. García-Fernández, M. P. M. Dean, G. D. Gu, M. Först, T. Loew, B. Keimer, M. Le Tacon, S. B. Wilkins, and J. P. Hill. Comparison of charge modulations in $La_{1.875}Ba_{0.125}CuO_4$ and $YBa_2Cu_3O_{6.6}$. *Phys. Rev. B* **88**, 024505 (2013).
37. John M. Tranquada. Spins, stripes, and superconductivity in hole-doped cuprates. *AIP Conf. Proc.* **1550**, 114–187 (2013).
38. Fan Wang, Jungho Kim, G. D. Gu, Yongjae Lee, Saebyok Bae, and Young-June Kim. Oxygen stoichiometry and magnetic properties of $LuFe_2O_{4+\delta}$. *J. Appl. Phys.* **113**, 063909 (2013).
39. L. Andrew Wray, J. Li, Z. Q. Qiu, Jinsheng Wen, Zhijun Xu, Genda Gu, Shih-Wen Huang, Elke Arenholz, Wanli Yang, Zahid Hussain, and Yi-De Chuang. Measurement of the spectral line shapes for orbital excitations in the Mott insulator CoO using high-resolution resonant inelastic x-ray scattering. *Phys. Rev. B* **88**, 035105 (2013).

40. Zhijun Xu, Jinsheng Wen, Tom Berlijn, Peter M. Gehring, Christopher Stock, M. B. Stone, Wei Ku, Genda Gu, Stephen M. Shapiro, R. J. Birgeneau, and Guangyong Xu. Thermal evolution of the full three-dimensional magnetic excitations in the multiferroic $BiFeO_3$. *Phys. Rev. B* **86**, 174419 (2012).
41. Zhijun Xu, Jinsheng Wen, E. Mamontov, C. Stock, P. M. Gehring, and Guangyong Xu. Freezing of the local dynamics in the relaxor ferroelectric $[Pb(Zn_{1/3}Nb_{2/3})O_3]_{0.955}[PbTiO_3]_{0.045}$. *Phys. Rev. B* **86**, 144106 (2012).
42. Zhijun Xu, Jinsheng Wen, Yang Zhao, Masaaki Matsuda, Wei Ku, Xuerong Liu, Genda Gu, D.-H. Lee, R. J. Birgeneau, J. M. Tranquada, and Guangyong Xu. Temperature-Dependent Transformation of the Magnetic Excitation Spectrum on Approaching Superconductivity in $Fe_{1+y-x}(Ni/Cu)_xTe_{0.5}Se_{0.5}$. *Phys. Rev. Lett.* **109**, 227002 (2012).
43. Guangyong Xu, Zhijun Xu, and J. M. Tranquada. Absolute cross-section normalization of magnetic neutron scattering data. *Rev. Sci. Instrum.* **84**, 083906 (2013).
44. Jian-Bo Zhang, Ling-Yun Tang, Jiang Zhang, Zhen-Xing Qin, Xiao-Jing Zeng, Jing Liu, Jin-Sheng Wen, Zhi-Jun Xu, Genda Gu, and Xiao-Jia Chen. Pressure-induced isostructural phase transition in $Bi_2Sr_2CaCu_2O_{8+\delta}$. *Chinese Phys. C* **37**, 088003 (2013).
45. Jinggeng Zhao, Haozhe Liu, Lars Ehm, Dawei Dong, Zhiqiang Chen, and Genda Gu. High-pressure phase transitions, amorphization, and crystallization behaviors in Bi_2Se_3. *J. Phys. Condens. Matter* **25**, 125602 (2013).
46. S. Anissimova, D. Parshall, G. D. Gu, K. Marty, M. D. Lumsden, Songxue Chi, J. A. Fernandez-Baca, D. L. Abernathy, D. Lamago, J. M. Tranquada, and D. Reznik. Direct observation of dynamic charge stripes in $La_{1.67}Sr_{0.33}NiO_4$. *Nat. Commun.* **5**, 3467 (2014).
47. Eduardo H. da Silva Neto, Pegor Aynajian, Alex Frano, Riccardo Comin, Enrico Schierle, Eugen Weschke, András Gyenis, Jinsheng Wen, John Schneeloch, Zhijun Xu, Shimpei Ono, Genda Gu, Mathieu Le Tacon, and Ali Yazdani. Ubiquitous interplay between charge ordering and high-temperature superconductivity in cuprates. *Science* **343,** 393–396 (2014).
48. David Fobes, Igor A. Zaliznyak, Zhijun Xu, Ruidan Zhong, Genda Gu, John M. Tranquada, Leland Harriger, Deepak Singh, V. Ovidiu Garlea, Mark Lumsden, and Barry Winn. Ferro-orbital ordering transition in iron telluride $Fe_{1+y}Te$ (y = 0.09(1)). *Phys. Rev. Lett.* **112**, 187202 (2014).
49. C. C. Homes, J. J. Tu, J. Li, G. D. Gu, and A. Akrap. Optical conductivity of nodal metals. *Sci. Rep.* **3,** 3446 (2013).
50. Hovnatan Karapetyan, Jing Xia, M. Hücker, G. D. Gu, J. M. Tranquada, M. M. Fejer, and A. Kapitulnik. Evidence of Chiral Order in the Charge-Ordered Phase of Superconducting $La_{1.875}Ba_{0.125}CuO_4$ Single Crystals Using Polar Kerr-Effect Measurements. *Phys. Rev. Lett.* **112,** 047003 (2014).
51. Takeshi Kondo, Ari D. Palczewski, Yoichiro Hamaya, Tsunehiro Takeuchi, J. S. Wen, Z. J. Xu, Genda Gu, and Adam Kaminski. Formation of Gapless Fermi Arcs and Fingerprints of Order in the Pseudogap State of Cuprate Superconductors. *Phys. Rev. Lett.* **111,** 157003 (2013).
52. Daixiang Mou, R. M. Konik, A. M. Tsvelik, I. Zaliznyak, Xingjiang Zhou. Charge-density wave and one-dimensional electronic spectra in blue Bronze: Incoherent solitons and spin-charge separation. *Phys. Rev. B* **89**, 201116 (2014).
53. Joosung Oh, Manh Duc Le, Jaehong Jeong, Jung-hyun Lee, Hyungje Woo, Wan-Young Song, T. G. Perring, W. J. L. Buyers, S.-W. Cheong, and Je-Geun Park. Magnon Breakdown in a Two Dimensional Triangular Lattice Heisenberg Antiferromagnet of Multiferroic $LuMnO_3$. *Phys. Rev. Lett.* **111,** 257202 (2013).
54. John M. Tranquada, Guangyong Xu, and Igor A. Zaliznyak. Superconductivity, antiferromagnetism, and neutron scattering. *J. Magn. Magn. Mat.* **350,** 148–160 (2014).
55. Eryin Wang, Hao Ding, Alexei V. Fedorov, Wei Yao, Zhi Li, Yan-Feng Lv, Kun Zhao, Li-Guo Zhang, Zhijun Xu, John Schneeloch, Ruidan Zhong, Shuai-Hua Ji, Lili Wang, Ke He, Xucun Ma, Genda Gu, Hong Yao, Qi-Kun Xue, Xi Chen, and Shuyun Zhou. Fully gapped topological surface states in Bi_2Se_3 films induced by a d-wave high-temperature superconductor. *Nat. Phys.* **9,** 621–625 (2013).
56. Jinsheng Wen, Shichao Li, Zhijun Xu, Cheng Zhang, M. Matsuda, O. Sobolev, J. T. Park, A. D. Christianson, E. Bourret-Courchesne, Qiang Li, Genda Gu, Dung-Hai Lee, J. M. Tranquada, Guangyong Xu, and R. J. Birgeneau. Enhanced low-energy magnetic excitations via suppression of the itinerancy in $Fe_{0.98-z}Cu_zTe_{0.5}Se_{0.5}$. *Phys. Rev. B* **88,** 144509 (2013).
57. Zhijun Xu, Jinsheng Wen, J. Schneeloch, A. D. Christianson, R. J. Birgeneau, Genda Gu, J. M. Tranquada, and Guangyong Xu. Low-energy magnetic excitations from the $Fe_{1+y-z}(Ni/Cu)_zTe_{1-x}Se_x$ system. *Phys. Rev. B* 89, 174517
58. Junjing Zhao, Utpal Chatterjee, Dingfei Ai, David G. Hinks, Hong Zheng, G. D. Gu, John-Paul Castellan, Stephan Rosenkranz, Helmut Claus, Michael R. Norman, Mohit Randeria, and Juan Carlos

Campuzano. Universal features in the photoemission spectroscopy of high-temperature superconductors. *Proc. Natl. Acad. Sci.* **110,** 17774–17777 (2013).

New insights into the cuprate phase diagram from neutron, X-ray and transport measurements of $HgBa_2CuO_{4+\delta}$

Martin Greven (greven@physics.umn.edu)
School of Physics and Astronomy, University of Minnesota, Minneapolis, MN 55455

Research Scope

The cuprate superconductors continue to pose one of the most formidable intellectual challenges in condensed matter physics. Among the well over 100 compounds, arguably the most desirable ones for experimental study are the mercury-based materials $HgBa_2Ca_{n-1}Cu_nO_d$, which feature the highest superconducting transition temperatures (T_c) and relatively simple crystal structures. We are uniquely able to grow sizable, high-quality crystals of $HgBa_2CuO_{4+\delta}$ (Hg1201; optimal T_c = 97 K), the first (n=1) and simplest member of this materials family. This is enabling significant new research activities aimed to understand the cuprate phase diagram through our neutron, X-ray, and charge transport experiments, and through an extensive network of collaborations.

Recent Progress

Evidence for Fermi-liquid behavior from transport measurements. As part of our crystal characterization work, we have pursued quantitative transport measurements. Our accomplishments include: (i) the surprising finding of Fermi-liquid-like resistive behavior ($\rho \sim T^2$) deep in the enigmatic pseudogap regime [1]; (ii) the demonstration of universal quantum oscillations in the pseudogap regime, and hence of the fact that the quantum oscillation must be a property of the quintessential Cu-O sheets [2]; (iii) the establishment of the universal resistance of the Cu-O sheets [1]; (iv) the demonstration of the validity (in the pseudogap regime) of Kohler's rule for the magneto-resistance, which had long been thought to be violated in the cuprates, and which provides further evidence for simple Fermi-liquid charge transport [3]. Importantly, these high-quality data serve as benchmarks for future sample quality control and for understanding why the simple properties found for Hg1201 are masked in most other cuprates. An updated temperature-doping phase diagram is shown in Fig. 1.

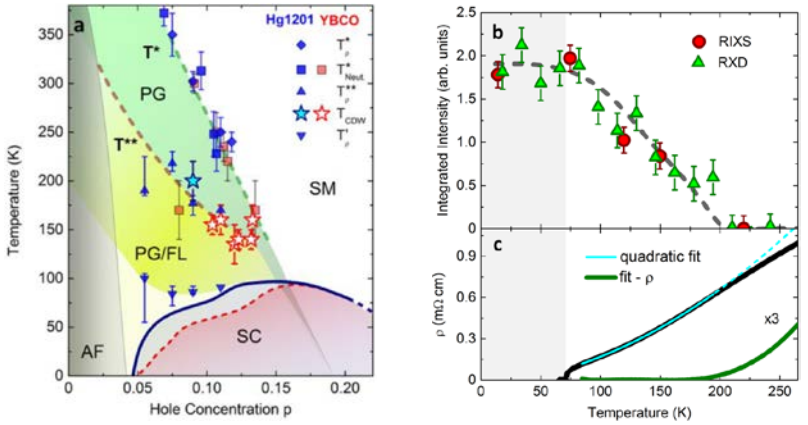

Fig. 1 (a) Updated cuprate phase diagram, with 'strange metal' (SM), pseudogap (PG), and Fermi-liquid (FL/PG) regimes [1,6]. (b) Short-range CDW order, observed via resonant X-ray scattering [6], and (c) Fermi-liquid transport ($\rho \sim T^2$) appear below the same temperature ($T_{CDW} \approx T_\rho^{**} \approx 200$ K) in underdoped samples with T_c = 71 K [1,6].

Signatures of the pseudogap from inelastic neutron scattering. Building on earlier work, our neutron scattering experiments led to the discovery of a second Ising-like mode associated with the pseudogap formation, potentially a collective mode of a q=0 novel charge-current-loop state

[4]. Concerning the antiferromagnetic (AF) response, we made the observation of commensurate, gapped correlations associated with the pseudogap formation (Fig. 2) [5], in contrast to the incommensurate "hourglass" response typically seen and often interpreted in terms of charge-spin stripes in lower-Tc cuprates such as $La_{2-x}Sr_xCuO_4$. Remarkably, these AF correlations grow significantly below the pseudogap temperature, and appear along with the universal quasi-static q=0 order (Fig. 2). There exists a distinct theoretical possibility that AF fluctuations may drive the unconventional q=0 magnetism, and the subsequent CDW order and superconductivity at lower temperatures. Similar to our transport results, the high structural symmetry and minimal disorder effects exhibited by Hg1201 enabled us to reveal the underlying AF response of the quintessential copper-oxygen planes most clearly.

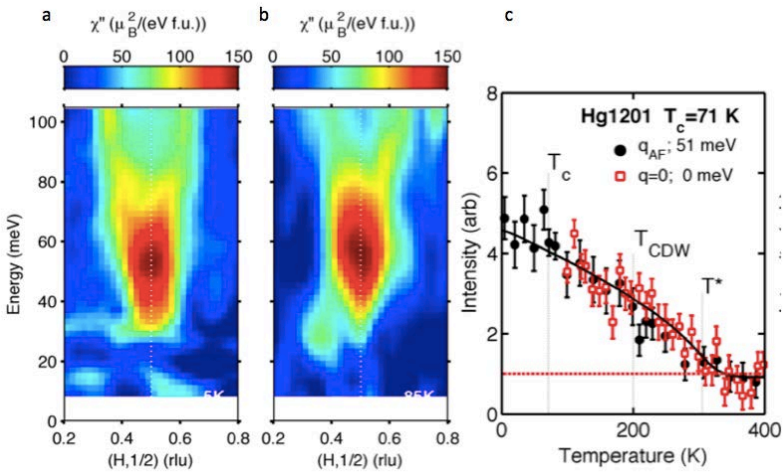

Fig. 2 Gapped inelastic magnetic response centered at the two-dimensional AF wave vector (1/2,1/2) for a large T_c = 71 K sample (a) at 5 K and (b) at 85 K, just above T_c. The data obtained on ARCS at the SNS. (c) Most of the AF response appears below the PG temperature (T^* ≈ 310 K from transport), along with quasi-static q=0 magnetic order [5].

New insights from synchrotron X-ray experiments. After numerous unsuccessful attempts to observed charge-density-wave (CDW) order with hard X-rays, we eventually found relatively weak, short-range CDW correlations in a moderately-doped sample [6]. We furthermore established a simple connection between the reconstructed Fermi surface area and the CDW modulation wave vector. This unifying insight would not have been possible without our new quantum oscillation results for Hg1201 [2]. High-pressure X-ray data allowed the determination of strain derivatives of T_c in Hg1201 and, from comparison with the lower-T_c compound LSCO, this led to the conclusion that the Hg-O charge-reservoir layers of Hg1201 may play a role in the very high T_c of this compound [7]. In yet unpublished work, we carefully mapped out the doping and temperature dependence of oxygen-chain order in the Hg-O reservoir layer and began to investigate the effects of high pressure on this order.

New insights from collaborative work. Our extensive collaborative work [9-16] includes further evidence for Fermi-liquid behavior in the PG regime [10,11] and the important demonstration of the feasibility of quantitative photoemission measurments on the model cuprate Hg1201 [14].

Future Plans

Neutron scattering experiments. The intriguing connection between q=0 magnetism and the AF correlations in Hg1201 warrants full exploration as a function of doping and temperature. Preliminary results obtained at the SNS indicate that the AF gap decreases monotonically with decreasing hole concentration and that it might only close at the hole doping level of p ~ 5% at which superconductivity disappears. It is of high interest to establish the nature of this quantum

critical point from the superconducting to the non-superconducting state. It also will be important to extend the present measurements to higher energy, and to observe the effects of a magnetic field and of intentionally introduced disorder (e.g., Zn doping) on the q=0 order and AF response.

Synchrotron X-ray experiments. We plan to build on our observation for Hg1201 of CDW order and of unusual interstitial oxygen order at moderate and high hole-dopant concentrations, respectively. In order to better assess the role of CDW correlations in the high-T_c phenomenon and in the Fermi-surface reconstruction implied by the observed quantum oscillations, we wish to determine the doping dependence and to investigate the effects of intentionally introduced disorder. We plan to investigate the effects of high pressures on the chain order to establish a possible (anti)correlation with the known pressure enhancement of the optimal T_c from 97 K to 120 K. Using X-ray absorption spectroscopy, we plan to establish the exact hole occupancy of the various O and Cu orbitals.

Transport experiments. Similar to the CDW X-ray work, it will be necessary to extend the quantum oscillation and magneto-resistance experiments to a wide doping range. We also wish to determine the transport properties to very high temperatures in order to better understand how the Fermi-liquid-like state evolves into the strange metal state (Fig. 1a), and complete initial measurements of the Hall and Seebeck effects. The effects of intentionally introduced disorder can be expected to shed light on how the underlying Fermi-liquid behavior becomes masked other cuprates.

Collaborations. Our work will continue to have a far-reaching impact beyond our scattering and transport experiments. We will continue to pursue a comprehensive approach through discussions with theorists as well as collaborations with experimental experts using complementary experimental tools, including photoemission, STM, Raman scattering, optical spectroscopy, Kerr effect, and NMR. At present, we have established more than a dozen such collaborations. A significant number of these collaborators are presently supported by DOE-BES.

Publications

1. N. Barišić, M. K. Chan, Y. Li, G. Yu, X. Zhao, M. Dressel, A. Smontara, and M. Greven. Universal sheet resistance and revised phase diagram of the cuprate hightemperature superconductors. Proc. Nat. Acad. Sci. US **110**, 12235 (2013).
2. N. Barišić, S. Badoux, M. K. Chan, C. Dorow, W. Tabis, B. Vignolle, G. Yu, J. Beard, X. Zhao, C. Proust, and M. Greven. Universal quantum oscillations in the underdoped cuprate superconductors. Nature Phys. **9**, 761 (2013).
3. M. K. Chan, M. J. Veit, C. J. Dorow, W. Tabis, G. Yang, X. Zhao, N. Barišić, and M. Greven. Validity of Kohler's rule in the pseudogap phase of the cuprate high-temperature superconductors. Submitted to Phys. Rev. Lett. (arXiv:1402.4472).
4. Y. Li, G. Yu, M. K. Chan, V. Balédent, Y. Li, N. Barišić, X. Zhao, K. Hradil, R. A.Mole, Y. Sidis, P. Steffens, P. Bourges, and M. Greven. Two Ising-like magnetic excitations in a single-layer cuprate superconductor. Nature Phys. **8**, 404 (2012).
5. M. K. Chan, Y. Tang, C. Dorow, L. Mangin-Thro, Y. Ge, M. Veit, X. Zhao, A. D. Christianson, J. T. Park, Y. Sidis, P. Steffens, D. L. Abernathy, P. Bourges, and M. Greven. Commensurate antiferromagnetic fluctuations as a signature of the pseudogap formation in a model cuprate. Submitted to Nature Physics (arXiv:1402.4517).
6. W. Tabis, Y. Li, M. Le Tacon, E. Weschke, L Braicovich, A. Kreyssig, M. Minola, G.

Dellea, A. Goldman, T. Schmitt, G. Ghiringhelli, N. Barišić, M. K. Chan, C. J. Dorow, M. J. Veit, G. Yu, X. Zhao, B. Keimer and M. Greven. Connection between charge-density-wave order and charge transport in the cuprate superconductors. Submitted to Nature Phys. (arXiv:1404.7658).

7. S. Wang, J. Zhang, J. Yan, X-J. Chen, V. Struzhkin, W. Tabis, N. Barišić, M. K. Chan, C. Dorow, X. Zhao, M. Greven, W. L. Mao, and T. Geballe. The strain derivatives of Tc in HgBa2CuO4+δ: Copper and oxygen are not enough. Phys. Rev. B **89**, 224515 (2014).
8. D. D. Xia, G. Yu, X. Zhao, B. Li, X. Liu, L. Ji, M. K. Chan, and M. Greven. Temperature and field dependence of the anisotropy parameter for the high-temperature superconductor HgBa2CuO4+δ. Super. Sci. Tech. **25**, 115010 (2012).
9. Y. Li, M. Le Tacon, M. Bakr, D. Terrade, D. Manske, R. Hackl, L. Ji, M. K. Chan, N. Barišić, X. Zhao, M. Greven, and B. Keimer. Feedback effect on high-energy magnetic fluctuations in the model high-temperature superconductor HgBa2CuO4+δ observed by electronic Raman scattering. Phys. Rev. Lett. **108**, 227003 (2012).
10. S. I. Mirzaei, D. Stricker, J. N. Hancock, C. Berthod, A. Georges, E. van Heumen, M. K. Chan, X. Zhao, Y. Li, M. Greven, N. Barišić, and D. van der Marel. Spectroscopic evidence for Fermi liquid-like energy and temperature dependence of the relaxation rate in the pseudogap phase of the cuprates. Proc. Nat. Acad. Sci. US **110**, 5774 (2013).
11. N. Doiron-Leyraud, S. Lepault, O. Cyr-Choiniere, B. Vignolle, G. Grissonnanche, F. Laliberte, J. Chang, N. Barišić, M. K. Chan, L. Ji, X. Zhao, Y. Li, M. Greven, C. Proust, and L. Taillefer. Hall, Seebeck, and Nernst coefficients of underdoped HgBa2CuO4+δ: Fermi-surface reconstruction in an archetypal cuprate superconductor. Phys. Rev. X **3**, 021019 (2013).
12. Y. Li, M. Le Tacon, Y. Matiks, A. V. Boris, T. Loew, C. T. Lin, L. Chen, M. K. Chan, C. Dorow, L. Ji, N. Barišić, X. Zhao, M. Greven, and B. Keimer. Doping dependent photon scattering resonance in the model high-temperature superconductor HgBa2CuO4+δ revealed by Raman scattering and optical ellipsometry. Phys. Rev. Lett. **111**, 187001 (2013).
13. A. M. Mounce, S. Oh, J. A. Lee, W. P. Halperin, A. P. Reyes, P. L. Kuhns, M. K. Chan, C. Dorow, L. Ji, D. Xia, X. Zhao, and M. Greven. Absence of static loop current magnetism at the apical oxygen site in HgBa2CuO4+δ from NMR. Phys. Rev. Lett. **111**, 187003 (2013).
14. I. M. Vishik, N. Barišić, M. K. Chan, Y. Li, G. Yu, X. Zhao, D. D. Xia, W. S. Lee, W. Meevasana, T. P. Devereaux, M. Greven, and Z. X. Shen. Angle-resolved photoemission spectroscopy study of HgBa2CuO4+δ. Phys. Rev B **89**, 195141 (2014).
15. F. Cilento, S. Dal Conte, G. Coslovich, S. Peli, N. Nembrini, S. Mor, F. Banfi, G. Ferrini, H. Eisaki, M. K. Chan, C. J. Dorow, M. J. Veit, M. Greven, D. van der Marel, R. Comin, A. Damascelli, L. Rettig, U. Bovensiepen, M. Capone, C. Giannetti, and F. Parmigiani. Photo-enhanced antinodal conductivity in the pseudogap state of the high-Tc cuprates. To appear in Nature Comm. (arXiv:1405.5462).
16. S. Dal Conte, L. Vidmar, D. Golez, M. Mierzejewski, G. Soavi, S. Peli, F. Banfi, G. Ferrini, R. Comin, L. Ludbrook, N. D. Zigaldo, H. Eisaki, M. Greven, S. Lupi, A. Damascelli, D. Brida, M. Capone, J. Bonca, G. Cerullo, and C. Giannetti. Snapshots of the retarded interaction of charge carriers with ultrafast fluctuations in the cuprates. Submitted to Nature Physics.

Correlations and Competition between the Lattice, Electrons, and Magnetism

A. I. Goldman (goldman@ameslab.gov), A. Kreyssig, D. Vaknin, B. N. Harmon, R. J. McQueeney

Ames Laboratory and Iowa State University, Ames, IA 50011

Program Scope

The properties of novel materials, such as high-temperature superconductors, charge/orbital ordering systems, and multiferroics, are all sensitively controlled by correlations and competition among the lattice, electronic, and magnetic degrees-of-freedom. A complete understanding of the interrelations between these systems and the necessary conditions for enhancing or tailoring desirable physical properties have been identified as a Grand Challenge to the scientific community. Neutron and x-ray scattering are powerful techniques that directly probe the structural, electronic, and magnetic aspects of complex ground states, phase transitions, and corresponding excitations. Within this FWP, the varied expertise of the PIs in different scattering methods is employed in a synergistic approach and systems are studied using a wide range of neutron and x-ray techniques. The experimental program is supported by a closely coupled effort in *ab initio* band structure calculations, theoretical modeling, and scattering simulations.

Recent Progress

<u>*Iron Pnictides*</u>: Over the last two years, we have continued our investigations of the iron-based superconductors and our major emphasis has turned to understanding the nature of spin fluctuations and their connection with superconductivity [P2,P6,P7,P13,P19,P25,P31]. In $CaFe_2As_2$, for example, the wide Q and high energy capabilities of ARCS allowed us to conclusively show that the Fe moment is completely quenched in the non-superconducting collapsed tetragonal phase [P25]. We have recently demonstrated that the onset of superconductivity in $Ba(Fe_{1-x}Co_x)_2As_2$ coincides with a crossover from well-defined spin waves to overdamped and diffusive spin excitations. This crossover occurs despite the presence of long-range stripe-like antiferromagnetic (AFM) order for samples in a compositional range from x = 0.04 to 0.055, and is a consequence of the shrinking spin-density wave gap and a corresponding increase in the particle-hole (Landau) damping [P31]. We have also investigated the dispersion of the spin resonance below T_c that appears at $\mathbf{Q}_{AFM}$ = (1/2 1/2 1) in the 122 iron arsenide compounds [P13]. In the cuprates, the dispersion of the resonance is downwards towards the nodes in the *d*-wave superconducting gap forming the characteristic hourglass shape below T_c. For $Ba(Fe_{0.963}Ni_{0.037})_2As_2$, however, we found that the resonance disperses upwards and showed, with the assumption of an $s^{\pm}$ superconducting order parameter, that the details of the resonance's dispersion are determined by the normal state spin fluctuations (e.g. the in-plane anisotropic magnetic correlation length). Finally, our inelastic neutron scattering measurements on a set of co-aligned samples of antiferromagnetic LaFeAsO demonstrated that the magnetic interactions are essentially two-dimensional [P19]. The spin-wave velocities, within the Fe layer, and the magnitude of the spin gap, are similar to the AFe_2As_2 based materials. However, the ratio of interlayer and intralayer exchange is found to be less than ~10^{-4} in LaFeAsO, very similar to the cuprates, and ~100 times smaller than that found in AFe_2As_2 compounds.

<u>*Manganese and cobalt*</u> arsenides: A closely related effort focuses on the manganese and cobalt arsenides [P15, P16, P17, P22, P26]. At the previous PI meeting, we reported that low levels of

K substitutions for Ba induce metallic behavior in $BaMn_2As_2$, however strong AFM ordering (T_N > 500 K) remains, suggesting that charge conductivity and AFM order are independent of one another [1]. In recent work we have shown: (1) that the local-moment AFM ordering is very robust up to at least 40% K substitution [P15]; and (2) using polarized neutron diffraction, we demonstrated that itinerant ferromagnetism coexists with the AFM order below ≈ 100 K [P17]. These results are consistent the weak coupling described above. Turning to the cobalt arsenides, we first note that dilute substitutions of Co for Fe in the AFe_2As_2 compounds (A = Ca, Ba, Sr) destabilizes the stripe-like AFM ordering by shrinking (enlarging) the hole (electron) pockets and detuning the nesting condition. Ultimately, the suppression of stripe AFM ordering upon Co substitutions of a only few percent allows a superconducting ground state to appear in the presence of substantial spin fluctuations at $\mathbf{Q}_{AFM}$. Further Co substitutions (> 12% Co) lead to a complete suppression of both stripe-like spin fluctuations and superconductivity. We have discovered that, at the other end of the compositional range, $SrCo_2As_2$ is close to an instability toward stripe-like AFM order, exhibiting steeply dispersing and quasi-two-dimensional paramagnetic excitations near $\mathbf{Q}_{AFM}$ [P26]. This is quite surprising for several reasons: (1) The sister compound, $CaCo_2As_2$, orders antiferromagnetically in the A-type AFM structure (ferromagnetic planes antiferromagnetically coupled along c) [P22]; (2) Band-structure calculations find a large density of states at the Fermi energy that was proposed to drive a ferromagnetic instability or A-type AFM ordering [2, P16]; and (3) There is no clear nesting feature favoring stripe AFM order in $SrCo_2As_2$, raising the general issue of what drives the stripe-like magnetic ordering in the iron pnictides. The ACo_2As_2 compounds manifest other interesting behaviors as well. For example, both $BaCo_2As_2$ and $SrCo_2As_2$ manifest negative c-axis thermal expansion coefficients [P16], which is unusual for paramagnetic metals.

<u>*Magnetic oxides*</u>: We have grown a high quality single crystal FeV_2O_4 and conducted elastic and inelastic neutron scattering to determine the phase diagram of this unique spinel oxide [P34]. FeV_2O_4 features two transition metal ions that both possess spin and orbital degrees of freedom that are strongly coupled, giving rise to unique properties that are manifested by three structural transitions of which two are accompanied by magnetic transitions. Fe^{2+} occupies the diamond-like A-site in the cubic spinel structure whereas V^{3+} occupies the pyrochlore B-site. FeV_2O_4 is an excellent candidate to investigate the roles of orbital ordering at not only the B site, but also at the A site. The recent discovery of multiferroicity in FeV_2O_4 with a coexistence of ferroelectricity and non-collinear ferrimagnetism, in contrast to the antiferromagnetism in most of the multiferroics, further motivates us to focus on this system. FeV_2O_4 undergoes three transitions from the high temperature cubic phase to Tetragonal-I at T_S = 140 K (due to Fe orbital ordering); Tetragonal-I to Orthorhombic at T_{N1} = 110 K accompanied by ferrimagnetic ordering (iron up-spin – vanadium down-spin); and Orthorhombic to Tetragonal-II accompanied by non-collinear ferrimagnetic order at T_{N2} = 70 K (vanadium spins canted) and the emergence of ferroelectricity. Our neutron scattering studies elucidated the different roles of the two orbital-active Fe^{2+} and V^{3+} species in the magnetic excitations. For example, the strong spin-orbit coupling for Fe^{2+} induces a significant energy gap below T_{N1} with little contribution from the V^{3+}. The absence of a change in the energy gap below T_{N2} is evidence for either a very weak spin-orbit coupling or significantly quenched orbital moment of the V^{3+}.

<u>*Magnetic quasicrystals and related compounds*</u>: We have started a new program to investigate magnetism in quasiperiodic crystals. Our discovery [P10] of a new family of local-moment bearing binary quasicrystals, *i*-*R*-Cd (*R* = Gd through Tm + Y) is particularly exciting because

they represent the compositionally simplest system for the study of the magnetic interactions in aperiodic systems. Furthermore, the existence of a corresponding set of cubic approximants, RCd$_6$, to the icosahedral phase allows for direct comparison between the low-temperature magnetic states of crystalline and quasicrystalline phases with fundamentally similar local structures, since RCd$_6$ may be described as a body-centered cubic packing of the same clusters of atoms as found in the newly discovered *i*-*R*-Cd icosahedral phase. Using x-ray resonant magnetic scattering and neutron diffraction on ^{114}Cd enriched samples, we have demonstrated that the RCd$_6$ approximants manifest long-range magnetic order at low temperatures [3,P14], whereas the related icosahedral phase exhibits only spin-glass-like freezing at low temperatures [P10].

Future Plans

<u>*Iron Pnictides*</u>: Our studies of magnetic fluctuations, and their relation to superconductivity in the iron-based superconductors have led to several new research directions. In particular, we are currently investigating the $Ca(Fe_{1-x}Co_x)_2Fe_2$ system where several "knobs" are available for tweaking the system between AFM order and superconductivity. In contrast to $Ba(Fe_{1-x}Co_x)_2Fe_2$ where there is a continuous crossover between AFM order and superconductivity, the transition from AFM to superconductivity in Co-doped Ca(122) is an abrupt function of Co-doping, applied pressure, or sample annealing [4]. It is then quite interesting to study the modification of the spin excitations as these "parameters" are tuned in comparison to our findings for $Ba(Fe_{1-x}Co_x)_2Fe_2$.

<u>*Manganese and cobalt arsenides*</u>: The reappearance of stripe-like spin fluctuations in $SrCo_2As_2$ raises key questions about how such fluctuations come about in this compound, why this compound is not superconducting, and whether it could be made superconducting by chemical substitution or by the application of pressure. Alternatively, the so induced new ground state of $SrCo_2As_2$ may manifest long-range magnetic order, excluding superconductivity or, perhaps, coexisting with it. If magnetic ordering is induced by "pressuring" $SrCo_2As_2$ into the collapsed tetragonal phase, will that magnetic order be A-type (as found in $CaCo_2As_2$ which is in the collapsed tetragonal phase at ambient pressure) or stripe-like (as suggested by the observed magnetic fluctuations at ambient pressure). Both neutron and x-ray scattering measurements under pressure are in progress.

<u>*Magnetic oxides*</u>: The extended spin wave dispersion curves of FeV_2O_4 will be measured by inelastic neutron scattering and analyzed to determine the various Fe-Fe, V-V, and Fe-V exchange parameters in this system. These exchange parameters are crucial for correlating the magnetic behavior and frustration in this system. Based on our previous results there is strong evidence that magnon-phonon interactions lead to anomalies in the spin waves. We will therefore investigate phonon dispersions in relation to these anomalies in the various phases to further elucidate the extent of coupling between spin and orbital degrees of freedom in this unique system.

<u>*Magnetic quasicrystals and related compounds*</u>: We have grown sizeable samples of both the Tb-Cd icosahedral quasicrystal and the Tb_6Cd periodic approximant phase using the ^{114}Cd isotope for inelastic neutron scattering measurements of the low-energy spin excitations in these systems. Our preliminary measurements on the quasicrystal show that there is significant static diffuse magnetic scattering, with overall icosahedral symmetry, that is likely related to short-range magnetic ordering on the clusters of Tb ions found in the structure. We are also working

towards a refinement of the atomic-scale structure of the icosahedral phase with colleagues from France and Japan to identify the site occupancies for Tb in these clusters.

References (citations starting with "P" are from Publications list)

1. Abhishek Pandey, R.S. Dhaka, J. Lamsal, Y. Lee, V.K. Anand, A. Kreyssig, T.W. Heitmann, R.J. McQueeney, A.I. Goldman, B.N. Harmon, A. Kaminski, D.C. Johnston, Phys. Rev. Lett. **108**, 087005 (2012).
2. A. S. Sefat, D. J. Singh, R. Jin, M. A. McGuire, B. C. Sales, and D. Mandrus, Phys. Rev. B **79**, 024512 (2009).
3. M.G. Kim, G. Beutier, A. Kreyssig, T. Hiroto, T. Yamada, J.W. Kim, M. de Boissieu, R. Tamura, A.I. Goldman, Phys. Rev. B **85**, 134442 (2012).
4. E. Gati, S. Köhler, D. Guterding, B. Wolf, S. Knöner, S. Ran, S. L. Bud'ko, P. C. Canfield, M. Lang, Phys. Rev. B **86**, 220511(R) (2012).

Publications

1. L. Q. Ke, M. van Schilfgaarde, and V. Antropov
   Spin Excitations in $K_2Fe_{4+x}Se_5$: Linear Response Approach
   Phys. Rev. B **86**, 020402 (2012).
2. G. S. Tucker, R. M. Fernandes, H. F. Li, V. Thampy, N. Ni, D. L. Abernathy, S. L. Bud'ko, P. C. Canfield, D. Vaknin, J. Schmalian, and R. J. McQueeney
   Magnetic Excitations in Underdoped $Ba(Fe_{1-x}Co_x)_2As_2$ with x=0.047
   Phys. Rev. B **86**, 024505 (2012).
3. P. E. Stallworth, R. Samueli, P. Sideris, D. Vaknin, and S. G. Greenbaum
   ^{7}Li and ^{31}P Nuclear Magnetic Resonance Studies of Single Crystal $LiMPO_4$ (M = Co, Fe)
   Ceramic Transactions: Advances in Inorganic Phosphate Materials **233,** 117 (2012).
4. R. Toft-Petersen, N. H. Andersen, H. Li, J. Li, W. Tian, S. L. Bud'ko, T.B. S. Jensen, C. Niedermayer, M. Laver, O. Zaharko, J. W. Lynn, and D. Vaknin
   Magnetic Phase Diagram of Magnetoelectric $LiMnPO_4$
   Phys. Rev. B **85**, 224415 (2012).
5. M. G. Kim, A. Kreyssig, Y.B. Lee, R. J. McQueeney; B. N. Harmon and A. I Goldman
   Fe K-edge X-ray resonant magnetic scattering from $Ba(Fe_{1-x}Co_x)_2As_2$ superconductors
   Eur. Phys. J. Special Topics **208**, 157 (2012).
6. G. S. Tucker, D. K. Pratt, M. G. Kim, S. Ran, A. Thaler, G. E. Granroth, K. Marty, W. Tian, J. L. Zarestky, M. D. Lumsden, S. L. Bud'ko, P. C. Canfield, A. Kreyssig, A. I. Goldman, and R. J. McQueeney
   Competition between Stripe and Checkerboard Magnetic Instabilities in Mn-Doped $BaFe_2As_2$
   Phys. Rev. B **86**, 020503 (2012).
7. M. G. Kim, J. Lamsal, T. W. Heitmann, G. S. Tucker, D. K. Pratt, S. N. Khan, Y. B. Lee, A. Alam, A. Thaler, N. Ni, S. Ran, S. L. Bud'ko, K. J. Marty, M. D. Lumsden, P. C. Canfield, B. N. Harmon, D. D. Johnson, A. Kreyssig, R. J. McQueeney, and A. I. Goldman
   Effects of Transition Metal Substitutions on the Incommensurability and Spin Fluctuations in $BaFe_2As_2$ by Elastic and Inelastic Neutron Scattering
   Phys. Rev. Lett. **109**, 167003 (2012).
8. V. Smetana, Q. Lin, D. K. Pratt, A. Kreyssig, M. Ramazanoglu, J. D. Corbett, A. I. Goldman, and G. J. Miller

A Sodium-Containing Quasicrystal: Using Gold to Enhance Sodium's Covalency in Intermetallic Compounds
Angewandte Chemie International Edition **51**, 12699 (2012).

9. S. Medling, Y. Lee, H. Zheng, J. F. Mitchell, J. W. Freeland, B. N. Harmon, and F. Bridges
Evolution of Magnetic Oxygen States in Sr-Doped $LaCoO_3$
Phys. Rev. Lett. **109**, 157204 (2012).
10. A. I. Goldman, T. Kong, A. Kreyssig, A. Jesche, M. Ramazanoglu, K. W. Dennis, S. L. Bud'ko, and P. C. Canfield
A Family of Binary Magnetic Icosahedral Quasicrystals Based on Rare Earths and Cadmium
Nature Materials **12**, 714 (2013).
11. S. E. Hahn, G. S. Tucker, J. Q. Yan, A. H. Said, B. M. Leu, R. W. McCallum, E. E. Alp, T. A. Lograsso, R. J. McQueeney, and B. N. Harmon
Magnetism-Dependent Phonon Anomaly in LaFeAsO Observed Via Inelastic X-Ray Scattering
Phys. Rev. B **87**, 104518 (2013).
12. M. G. Kim, J. Soh, J. Lang, M. P. M. Dean, A. Thaler, S. L. Bud'ko, P. C. Canfield, E. Bourret-Courchesne, A. Kreyssig, A. I. Goldman, and R. J. Birgeneau
Spin Polarization of Ru in Superconducting $Ba(Fe_{0.795}Ru_{0.205})_2As_2$ Studied by X-Ray Resonant Magnetic Scattering
Phys. Rev. B **88**, 014424 (2013).
13. M. G. Kim, G. S. Tucker, D. K. Pratt, S. Ran, A. Thaler, A. D. Christianson, K. Marty, S. Calder, A. Podlesnyak, S. L. Bud'ko, P. C. Canfield, A. Kreyssig, A. I. Goldman, and R. J. McQueeney
Magnonlike Dispersion of Spin Resonance in Ni-Doped $BaFe_2As_2$
Phys. Rev. Lett. **110**, 177002 (2013).
14. A. Kreyssig, G. Beutier, T. Hiroto, M. G. Kim, G. S. Tucker, M. de Boissieu, R. Tamura, and A. I. Goldman
Antiferromagnetic Order and the Structural Order-Disorder Transition in the Cd_6Ho Quasicrystal Approximant
Phil. Mag. Lett. **93**, 512 (2013).
15. J. Lamsal, G. S. Tucker, T. W. Heitmann, A. Kreyssig, A. Jesche, A. Pandey, W. Tian, R. J. McQueeney, D. C. Johnston, and A. I. Goldman
Persistence of Local-Moment Antiferromagnetic Order in $Ba_{1-x}K_xMn_2As_2$
Phys. Rev. B **87**, 144418 (2013).
16. A. Pandey, D. G. Quirinale, W. Jayasekara, A. Sapkota, M. G. Kim, R. S. Dhaka, Y. Lee, T. W. Heitmann, P. W. Stephens, V. Ogloblichev, A. Kreyssig, R. J. McQueeney, A. I. Goldman, A. Kaminski, B. N. Harmon, Y. Furukawa, and D. C. Johnston
Crystallographic, Electronic, Thermal, and Magnetic Properties of Single-Crystal $SrCo_2As_2$
Phys. Rev. B **88**, 014526 (2013).
17. A. Pandey, B. G. Ueland, S. Yeninas, A. Kreyssig, A. Sapkota, Y. Zhao, J. S. Helton, J. W. Lynn, R. J. McQueeney, Y. Furukawa, A. I. Goldman, and D. C. Johnston
Coexistence of Half-Metallic Itinerant Ferromagnetism with Local-Moment Antiferromagnetism in $Ba_{0.60}K_{0.40}Mn_2As_2$
Phys. Rev. Lett. **111**, 047001 (2013).

18. D. K. Pratt, S. Chang, W. Tian, A. A. Taskin, Y. Ando, J. L. Zarestky, A. Kreyssig, A. I. Goldman, and R. J. McQueeney
Checkerboard to Stripe Charge Ordering Transition in $TbBaFe_2O_5$
Phys. Rev. B **87**, 045127 (2013).
19. M. Ramazanoglu, J. Lamsal, G. S. Tucker, J. Q. Yan, S. Calder, T. Guidi, T. Perring, R. W. McCallum, T. A. Lograsso, A. Kreyssig, A. I. Goldman, and R. J. McQueeney
Two-Dimensional Magnetic Interactions in LaFeAsO
Phys. Rev. B **87**, 140509 (2013).
20. Q. Zhang, W. J. Wang, J. W. Kim, B. Hansen, N. Ni, S. L. Bud'ko, P. C. Canfield, R. J. McQueeney, and D. Vaknin
Magnetoelastic Coupling and Charge Correlation Lengths in a Twin Domain of $Ba(Fe_{1-x}Co_x)_2As_2$ (x=0.047): A High-Resolution X-Ray Diffraction Study
Phys. Rev. B **87**, 094510 (2013).
21. A. S. Zimmermann, E. Sondermann, J. Y. Li, D. Vaknin, and M. Fiebig
Antiferromagnetic Order in $Li(Ni_{1-x}Fe_x)PO_4$ (x=0.06, 0.20)
Phys. Rev. B **88**, 014420 (2013).
22. D. G. Quirinale, V. K. Anand, M. G. Kim, A. Pandey, A. Huq, P. W. Stephens, T. W. Heitmann, A. Kreyssig, R. J. McQueeney, D. C. Johnston, and A. I. Goldman
Crystal and Magnetic Structure of $CaCo_{1.86}As_2$ Studied by X-Ray and Neutron Diffraction
Phys. Rev. B **88**, 174420 (2013).
23. B. Roy, A. Pandey, Q. Zhang, T. W. Heitmann, D. Vaknin, D. C. Johnston, and Y. Furukawa
Experimental Evidence of a Collinear Antiferromagnetic Ordering in the Frustrated $CoAl_2O_4$ Spinel
Phys. Rev. B **88**, 174415 (2013).
24. Weiwei Xie, Srinivasa Thimmaiah, Jagat Lamsal, Jing Liu, Thomas W. Heitmann, Dante Quirinale, Alan I. Goldman, Vitalij Pecharsky, and Gordon J. Miller
β-Mn-Type $Co_{8+x}Zn_{12-x}$ as a Defect Cubic Laves Phase: Site Preferences, Magnetism, and Electronic Structure
Inorg. Chem. **52**, 9399 (2013).
25. J. H. Soh, G. S. Tucker, D. K. Pratt, D. L. Abernathy, M. B. Stone, S. Ran, S. L. Bud'ko, P. C. Canfield, A. Kreyssig, R. J. McQueeney, and A. I. Goldman
Inelastic Neutron Scattering Study of a Nonmagnetic Collapsed Tetragonal Phase in Nonsuperconducting $CaFe_2As_2$: Evidence of the Impact of Spin Fluctuations on Superconductivity in the Iron-Arsenide Compounds
Phys. Rev. Lett. **111**, 227002 (2013).
26. W. Jayasekara, Y. Lee, Abhishek Pandey, G. S. Tucker, A. Sapkota, J. Lamsal, S. Calder, D. L. Abernathy, J. L. Niedziela, B. N. Harmon, A. Kreyssig, D. Vaknin, D. C. Johnston, A. I. Goldman, and R. J. McQueeney
Stripe Antiferromagnetic Spin Fluctuations in $SrCo_2As_2$
Phys. Rev. Lett. **111**, 157001 (2013).
27. Q. Zhang, W. Tian, H. F. Li, J. W. Kim, J. Q. Yan, R. W. McCallum, T. A. Lograsso, J. L. Zarestky, S. L. Bud'ko, R. J. McQueeney, and D. Vaknin
Magnetic Structures and Interplay between Rare-Earth Ce and Fe Magnetism in Single-Crystal CeFeAsO
Phys. Rev. B **88**, 174517 (2013).

28. F. Weber, L. Pintschovius, W. Reichardt, R. Heid, K. P. Bohnen, A. Kreyssig, D. Reznik, and K. Hradil
Phonons and Electron-Phonon Coupling in YNi_2B_2C
Phys. Rev. B **89**, 104503 (2014).
29. W. Siemons, C. Beekman, G. J. MacDougall, J. L. Zarestky, S. E. Nagler, and H. M. Christen
A Complete Strain-Temperature Phase Diagram for $BiFeO_3$ Films on $SrTiO_3$ and $LaAlO_3$ (001) Substrates
J. Phys. D - Applied Physics **47**, 034011 (2014).
30. A. Jesche, R. W. McCallum, S. Thimmaiah, J. L. Jacobs, V. Taufour, A. Kreyssig, R. S. Houk, S. L. Bud'ko, and P. C. Canfield
Giant Magnetic Anisotropy and Tunnelling of the Magnetization in $Li_2(Li_{1-x}Fe_x)N$
Nature Communications **5**, 3333 (2014).
31. G. S. Tucker, R. M. Fernandes, D. K. Pratt, A. Thaler, N. Ni, K. Marty, A. D. Christianson, M. D. Lumsden, B. C. Sales, A. S. Sefat, S. L. Bud'ko, P. C. Canfield, A. Kreyssig, A. I. Goldman, and R. J. McQueeney
Crossover from spin waves to diffusive spin excitations in underdoped $Ba(Fe_{1-x}Co_x)_2As_2$
Phys. Rev. B **89** 180503(R) (2014).
32. B. G. Ueland, A. Kreyssig, K. Prokeš, J. W. Lynn, L. W. Harriger, D. K. Pratt, D. K. Singh, T. W. Heitmann, S. Sauerbrei, S. M. Saunders, E. D. Mun, S. L. Bud'ko, R. J. McQueeney, P. C. Canfield, and A. I. Goldman
Fragile antiferromagnetism in the heavy-fermion compound YbBiPt
Phys. Rev. B **89**, 180403(R) (2014).
33. Arjun K. Pathak, D. Paudyal, W. T. Jayasekara, S. Calder, A. Kreyssig, A. I. Goldman, K. A. Gschneidner, Jr., and V. K. Pecharsky
Unexpected magnetism, Griffiths phase, and exchange bias in the mixed lanthanide $Pr_{0.6}Er_{0.4}Al_2$
Phys. Rev. B **89**, 224411 (2014).
34. A. I. Goldman
Magnetism in icosahedral quasicrystals: current status and open questions
Sci. Technol. Adv. Mater. (in press).
35. Qiang Zhang, Mehmet Ramazanoglu, Songxue Chi, Yong Liu, Thomas A. Lograsso and David Vaknin
Magnetic excitations and anomalous spin-wave broadening in multiferroic FeV_2O_4
Phys. Rev. B **89**, 224416 (2014).
36. Tai Kong, Sergey L. Bud'ko, Anton Jesche, John McArthur, Andreas Kreyssig, Alan I. Goldman, and Paul C. Canfield
Magnetic and transport properties of i-R-Cd icosahedral quasicrystals (R = Y, Gd-Tm),
arXiv:1406.4522 (submitted to Phys. Rev. B) (2014).

Experimental realization of a single crystal bond-disordered pyrochlore antiferromagnet*

Jason Krizan[1,2] and R.J. Cava[1,2]

[1]Department of Chemistry, Princeton University
[2]Institute for Quantum Matter, Johns Hopkins University

We describe the crystal growth and magnetic characterization of the frustrated transition metal pyrochlore $NaCaCo_2F_7$. This newly characterized *fluoride* pyrochlore of the $A_2B_2F_7$ type has high spin Co^{2+} in CoF_6 octahedra in a pyrochlore lattice (the B sites), and non-magnetic Na and Ca disordered on the pyrochlore large-atom sites (the A sites). Large single crystals grown by the floating zone method were studied. The magnetic susceptibility is nearly isotropic, and the Co moment is larger than the spin-only value. In spite of the large Curie Weiss theta (-120 K), the freezing of the spin system, characterized by peaks in the ac susceptibility and specific heat, does not occur until ~ 2.3 K. This yields a frustration index of $f = -\theta_{CW}/T_f \approx 50$, an indication that the system is highly frustrated. The observed entropy loss at the freezing transition is low, indicating that magnetic entropy remains in the system at 0.5 K. We propose that this compound is the realization of a pyrochlore antiferromagnet with weak bond disorder. The high magnetic interaction strength in this compound, and the availability of large single crystals, makes it an intriguing alternative to rare earth pyrochlores for the study of geometric magnetic frustration in pyrochlore lattices. Further, fluorides may represent an interesting new materials class for the study of geometric magnetic frustration.

* This research was conducted under the auspices of the Institute for Quantum Matter (IQM) at Johns Hopkins University, and supported by the U. S. Department of Energy, office of Basic Energy Sciences, Division of Materials Sciences and Engineering under grant DE-FG02-08ER46544. Discussions with IQM researchers C. Broholm, O. Tchernyshyov, and K. Ross, and with A. Vishwanath, R. Moessner and L. Balents are greatly acknowledged. The work described here was published as: Phys. Rev. B 214401 (2014).

Session IV

Quantum Materials

(Round Table Panel Discussion)

Discussion Leaders:

Alexander Balatsky
David Singh
Oleg Tchernyshyov

Session V

Soft Matter

Thermodynamics of Self-Assembly in Globular Protein-Polymer Conjugates

Bradley D. Olsen
Department of Chemical Engineering, Massachusetts Institute of Technology
DOE-BES Award ER46824

Program Scope

Engineering enzymes and optically active proteins into bioelectronic devices for the production of H_2,[1,2] the reduction of CO_2,[3,4] or the production of biofuels[5,6] allows the evolutionarily optimized performance of the protein to be exploited to produce high-performance biomolecular variants of catalysts. Engineering biocatalytic materials requires achieving a high protein activity and active site density, controlling substrate/product transport through the material, maintaining protein stability, and developing low-cost processes for material fabrication. Analogous to synthetic catalysts[7,8] or organic electronics,[9,10] this requires the arrangement and orientation of the protein at an interface between two phases that provide for the transport of each reagent or charge carrier.

The self-assembly of block copolymers containing an enzyme or optically active protein block provides a bottom-up method to produce nanostructures that simultaneously achieve control over transport through two phases and yield a high density of oriented protein at an interface. This project investigates the fundamental structure and thermodynamics of block copolymer systems containing a globular protein block, enabling the production of functional nanomaterials (Figure 1). Both the folded protein chain shape and the specific interactions between globular proteins differ significantly from the Gaussian coil block copolymers, adding significant complexity to the phase behavior of these systems. Despite this complexity, we hypothesize that universal rules of self-assembly may be elucidated for these protein-polymer hybrjds, and in the past two years we have addressed three fundamental questions:

(1) How is the phase behavior for a protein-polymer conjugate different than that of traditional block copolymers?
(2) What is the effect of protein shape (steric interactions) on self-assembly?
(3) What is the effect of protein-polymer interactions on self-assembly?

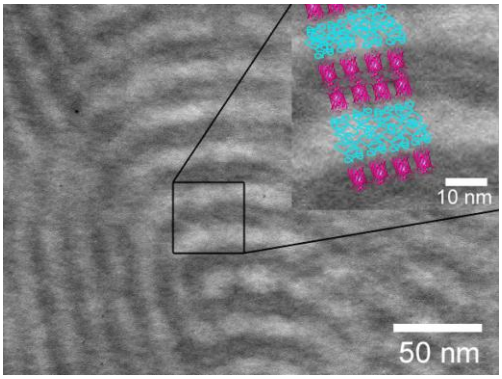

Figure 1. Transmission electron micrograph of mCherry-poly(N-isopropylacrylamide) block copolymer self-assembled into lamellar structures. Protein nanodomains appear dark due to staining.

Recent Accomplishments

In order to maintain the functional secondary and tertiary structure of globular proteins, self-assembly must be performed in aqueous solution, as both thermal and organic solvent annealing methods are incompatible with most proteins. In order to understand the phase behavior of protein-polymer conjugates, the self-assembly of a model conjugate mCherryS131C-poly(N-isopropylacrylamide) (mCherry-PNIPAM) was studied as a function of temperature and concentration for a small set

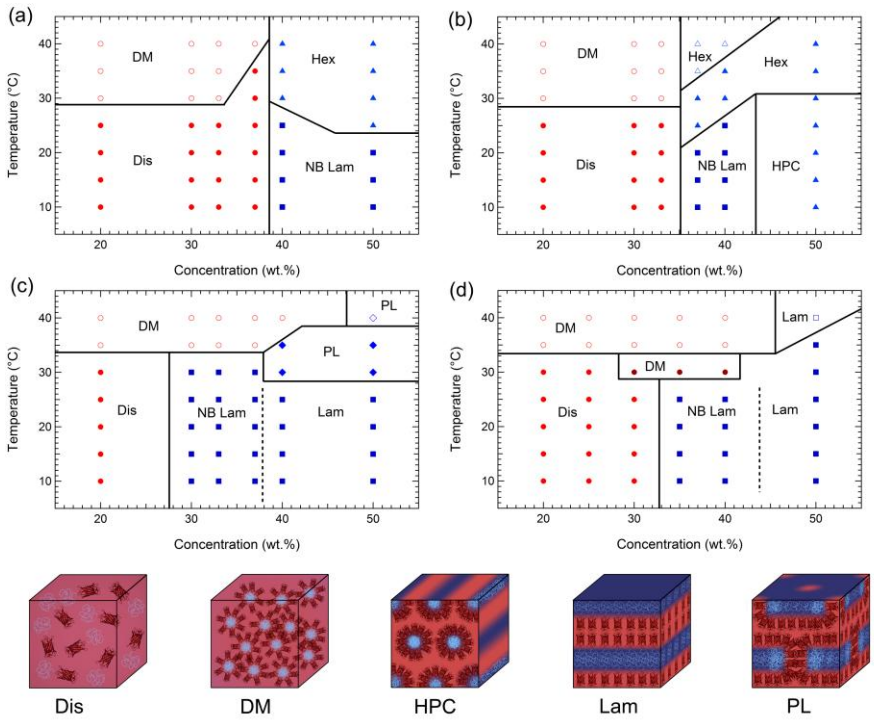

Figure 2. Phase diagram of (a) mCherryS131C-*b*-PNIPAM8k (b) mCherryS131C-*b*-PNIPAM17k (c) mCherryS131C-*b*-PNIPAM30k (d) mCherryS131C-*b*-PNIPAM57k in aqueous solutions.

of conjugates and as a function of concentration and block copolymer composition for a large set of molecules. Phase diagrams as a function of temperature and concentration show that the materials undergo an order-disorder transition with increasing concentration and also exhibit several order-order transitions upon increasing temperature (Figure 2). Small-angle neutron scattering (SANS) was used to demonstrate that changes in hydration drive these thermal OOTs. The phase diagrams change significantly with coil fraction, and notably a number of phases traditionally observed in block copolymer systems are not observed in these conjugate molecules. A more comprehensive study of coil fraction effects reveals that the phase diagram of the conjugates is significantly different than that of traditional diblock copolymers, with hexagonal and lamellar phases being primarily observed and a strong asymmetry with respect to coil fraction. In addition, with increasing conjugate fraction up to 70%, reentrant order-disorder transitions are observed. The same transitions are seen in conjugates with varying polymer blocks and protein types, suggesting that they may be universal for a broad class of similarly shaped molecules.

In order to explore the effect of protein interactions on self-assembly, a carefully controlled experiment was performed to compare the self-assembly of mCherry conjugates with EGFP conjugates. Both the red and green fluorescent proteins have very little primary sequence homology and consequently significantly different electrostatic and hydrophobic surface potential distributions; however, they have similar sizes, shapes, and second virial coefficients. When conjugates with the same molar mass PNIPAM were prepared for both proteins, self-assembly was largely identical. A further experiment was performed to mutate mCherry, systematically altering its electrostatic surface potential. A set of 14 mutants was prepared, and from these five were selected for their high expression and comparative change in surface patchiness for detailed study. Again, only minimal effects on the order-disorder transition concentration, symmetry of nanodomain structure, and domain spacing were observed.

Comparison of self-assembly for conjugates with different polymer types illustrates that protein-polymer interactions are critical to the self-assembly of these systems. Comparing PNIPAM conjugates to those with poly(hydroxypropylacrylate) (PHPA) and poly(oligoethyleneglycolacrylate) (POEGA) illustrates the ability to form previously unobserved phases, including a cubic phase consistent with a gyroid structure (Figure 3), and the ability to tune the ODT based on protein-polymer interactions. To follow up on this observation, two separate methods are currently under development for quantifying these protein-polymer interactions. First, protein-polymer conjugates have been synthesized from a variety of different polymers, and the form factors in dilute solution are being measured using SANS. Fitting these form factors with structural models that have the protein-polymer interaction as a parameter may provide a rapid, single sample method for estimating this interaction. Second, partial structure factor decomposition analysis is being performed on protein-polymer blends with varied H_2O/D_2O solvent systems, enabling quantitative extraction of the protein-polymer structure factor which can then be modeled as a function of interactions.

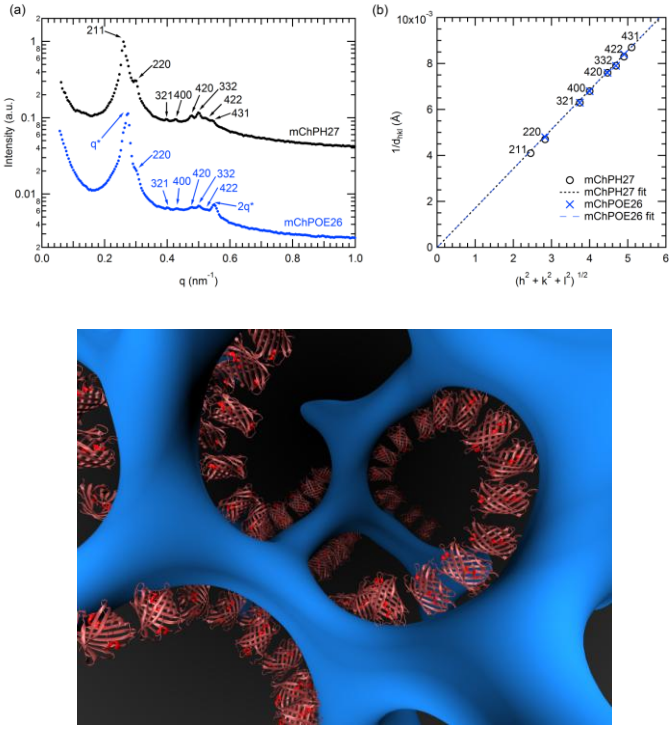

Figure 3. X-ray scattering patterns (top) and schematic illustration (bottom) of the cubic phase (bicontinuous gyroid structure) formed in mCherry-PHPA and mCherry-POEGA block copolymers.

Future Plans

Building upon results from the first performance period of this project, our future work will aim to address critical questions regarding the role of protein interactions in self-assembly and to develop functional catalysts from enzymes such as lipase to perform fundamental studies of structure-property relationships in active biocatalytic systems. To understand protein effects, a variety of proteins with different coarse grained properties of shape and virial coefficient will be systematically studied, and supercharged proteins will be used to understand electrostatic effects in detail. Using proteins with highly anisotropic interactions will also facilitate an understanding of crystallinity and packing in self-assembled systems. Continued development of SANS methods for parameter extraction will be combined with simulations and collaborative interactions with Dr. Chen at ORNL in order to develop robust methods for quantifying relevant parameters, enabling a universal model for self-assembly to be constructed. Finally, DOE-relevant enzymes such as lipase and carbonic anhydrase will be used in conjugates to study the

fundamental science of biocatalysis in these self-assembled nanostructures, identifying the effects of structure and processing on material performance.

References

(1) Hambourger, M.; Gervaldo, M.; Svedruzic, D.; King, P. W.; Gust, D.; Ghirardi, M.; Moore, A. L.; Moore, T. A. *Journal of the American Chemical Society* **2008**, *130*, 2015.

(2) Krassen, H.; Schwarze, A.; Friedrich, B.; Ataka, K.; Lenz, O.; Heberle, J. *Acs Nano* **2009**, *3*, 4055.

(3) Reda, T.; Plugge, C. M.; Abram, N. J.; Hirst, J. *Proceedings of the National Academy of Sciences of the United States of America* **2008**, *105*, 10654.

(4) Parkinson, B. A.; Weaver, P. F. *Nature* **1984**, *309*, 148.

(5) Iso, M.; Chen, B. X.; Eguchi, M.; Kudo, T.; Shrestha, S. *Journal of Molecular Catalysis B-Enzymatic* **2001**, *16*, 53.

(6) Velonia, K.; Rowan, A. E.; Nolte, R. J. M. *Journal of the American Chemical Society* **2002**, *124*, 4224.

(7) Benson, E. E.; Kubiak, C. P.; Sathrum, A. J.; Smieja, J. M. *Chemical Society Reviews* **2009**, *38*, 89.

(8) Mikkelsen, M.; Jorgensen, M.; Krebs, F. C. *Energy & Environmental Science*, *3*, 43.

(9) Yang, X.; Loos, J. *Macromolecules* **2007**, *40*, 1353.

(10) Boudouris, B. W.; Frisbie, C. D.; Hillmyer, M. A. *Macromolecules* **2008**, *41*, 67.

Publications Resulting from Work Supported by DOE-BES Neutron Program

1. "Effect of Polymer Chemistry on Globular Protein-Polymer Block Copolymer Self-Assembly." D. Chang, C.N. Lam, and B.D. Olsen. *Polymer Chemistry* **2014**, *online.*
2. "Phase Behavior of a Model Globular Protein-Polymer Diblock Copolymer." C.S. Thomas and B.D. Olsen. *Soft Matter* **2014**, *10*, 3093-3102.
3. "Nature of Protein Interactions Governing Globular Protein-Polymer Block Copolymer Phase Behavior." C.N. Lam, M. Kim, C.S. Thomas, D. Chang, G. Sanoja, C.U. Okwara, and B.D. Olsen. *Biomacromolecules* **2014**, *15*, 1248-1258.
4. "Self-Assembly of Globular Protein Containing Block Copolymers." B.D. Olsen. *Macromolecular Chemistry and Physics* **2013**, *214*, 1659-1668.
5. "The Effect of Small Molecule Osmolytes on the Self-Assembly and Functionality of Globular Protein Polymer Block Copolymers." C.S. Thomas, L. Xu, and B.D. Olsen. *Biomacromolecules* **2013**, *14*, 3064-3072.
6. "Phase Transitions in Concentrated Solution Self-Assembly of Globular Protein-Polymer Block Copolymers." C.N. Lam and B.D. Olsen. *Soft Matter* **2013**, *9*, 2393-2402.
7. "Processing-Dependent Self-Assembly of Protein-Polymer Diblock Copolymers." C.S. Thomas, L. Xu, and B.D. Olsen. *Biomacromolecules*, **2012**, *13*, 2781-2792.

Understanding Functional Lyotropic Liquid Crystal Network Phase Self-Assembly and the Properties of Nanoconfined Water

Mahesh K. Mahanthappa (mahesh@chem.wisc.edu), Arun Yethiraj (yethiraj@chem.wisc.edu), Grayson L. Jackson, Sriteja Mantha, and Dominic V. Perroni
Department of Chemistry, University of Wisconsin–Madison, Madison, WI 53706

Program Scope

The hydration of small molecule surfactants with water drives their concentration-dependent supramolecular self-assembly into nanostructured lyotropic liquid crystals (LLCs). These soft materials exhibit structurally periodic aqueous and hydrophobic nanodomains, in which the domain interfaces are decorated with the surfactant headgroup functionality. Network phase LLCs (*e.g.*, double gyroid) are potentially useful membrane materials for selective ion transport and molecular separations, as a consequence of their three-dimensionally percolating, functional nanopores with diameters ~0.7–4 nm. However, applications of LLC materials are impeded by the lack of rational molecular design criteria that guide the synthesis of surfactants that form useful network phases. Through the synergistic interplay of chemical synthesis, physical materials characterization, and molecular simulations, we are investigating the aqueous self-assembly behavior of anionic aliphatic gemini ("twin tail") surfactants as a function of the surfactant backbone structure, headgroup, and counterion. We established a new synthetic route to aliphatic bis(sulfonate) gemini surfactants and demonstrated that they form aqueous lyotropic gyroid phases, the breadth of which depends upon the specific headgroup/counterion combination. Concurrent computational studies have focused on understanding the role of gemini surfactant linker length in governing LLC network phase stability, leading to a new molecular design criterion for stabilizing these useful phases to be tested in future experiments.

Recent Progress

Synthesis and Phase Behavior of Bis(sulfonate) Gemini Surfactants

We previously reported that aliphatic dicarboxylate gemini surfactants readily form normal LLC gyroid (G_I) phases over amphiphile concentration windows ~20 wt% wide between T = 22–100 °C.[1] Subsequent molecular simulations of these self-assembling systems suggested that the unusual stability of the G_I-phase arises from a combination of intramolecular and intermolecular interactions set by the gemini architecture, the magnitudes of which depend on the extent of ionic headgroup-counterion dissociation.[2] Our simulations also showed that nanoconfining water in the sub-2 nm pores of these lyotropic phases substantially decreases the water self-diffusion coefficient. These studies suggest the potential utility of these functional LLCs as platforms for studying how pore diameter and pore functionality affect the properties of water in hydrophilic nanoconfinement.

To test the universality of the gemini architecture in stabilizing LLC network phases, we have studied the synthesis and phase behavior of aliphatic bis(sulfonate) gemini surfactants. We developed a modular synthetic route to amphiphiles such as **HSO_3-84** that provides ready access to a wide variety of sulfonated gemini surfactants with variable tail and linker lengths in three steps from commercially available starting materials, which is enabling ongoing studies of the impact of surfactant structure on the observed aqueous LLC phase behavior.

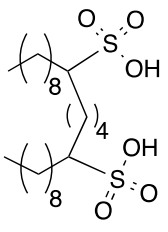

HSO_3-84

Hydration of bis(sulfonate) gemini surfactant **HSO_3-84** with variable amounts of H_2O readily produces ordered LLC phases over the wide concentration range 35-95 wt% amphiphile. Using variable temperature small-angle X-ray scattering (SAXS), we investigated the phase behavior of a series of **HSO_3-84** LLCs with varying H_2O contents. A complete phase diagram for this system is shown in Fig. 1. As the LLC water content increases, we find the progression of phases: $L_\alpha \rightarrow G_I \rightarrow H_I \rightarrow$ micellar. This phase sequence implies that these are normal LLCs, in which the domain interfaces curve toward the hydrophobic domains. Notably, the G_I phase is accessible in the concentration range 62-70 wt% **HSO_3-84** (headgroup hydration numbers w_0 = 8–9). This result supports the notion that the gemini architecture enables access to network phase LLCs, not observed in related single-tail amphiphiles. The wide LLC concentration stability window and the modest G_I-phase window width for **HSO_3-84** are similar to the LLC phase behavior of dicarboxylate gemini surfactants with highly dissociated counterion-headgroup ion pairs. Ongoing studies address the impact of the surfactant counterion (Na^+, K^+, and NMe_4^+) on the width of the LLC G_I-phase window.

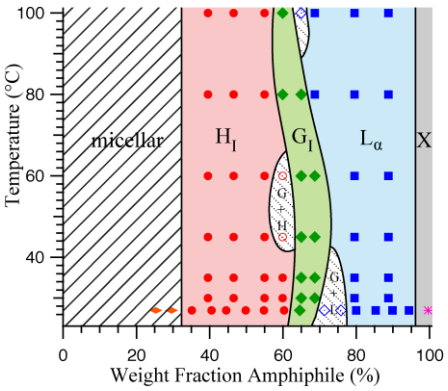

Fig. 1. Aqueous lyotropic temperature *v*. concentration phase diagram for **HSO_3-84**, indicating a substantial G_I network phase window in the range 62-70 wt% amphiphile.

Computational Studies of the Effect of Surfactant Linker Length on Network Phase Stability

Our recent experiments uncovered unexpectedly strong odd-even linker length effects on gemini dicarboxylate LLC network phase stability. While the surfactant derived from decanoic acid with a C_4-linker (**Na-74**) exhibits the expected progression of lyotropic phases with increasing water content $L_\alpha \rightarrow G_I \rightarrow H_I \rightarrow$ micellar, **Na-73** with a C_3-linker exhibits no stable H_I-phase. Additionally, the G_I-phase window spans ~40 wt% in amphiphile concentration at 295 K for **Na-73,** and an unidentified LLC phase forms near 80–85 wt% **Na-73** in H_2O between T = 295–323 K.

Microsecond long MD simulations of **Na-73** aqueous LLCs of varying compositions, employing a GROMOS96 force-field and an explicit SPC water model, have revealed significant differences in the allowed surfactant conformations that govern phase selection in these systems. We have conducted simulations at 55 wt% **Na-73** in H_2O with T = 300–370 K and 80 wt% **Na-73** in H_2O at T = 300 and 350 K. Representative snapshots of these phases shown in Fig. 2a and 2b replicate the experimentally observed L_α and G_I-phases, respectively.

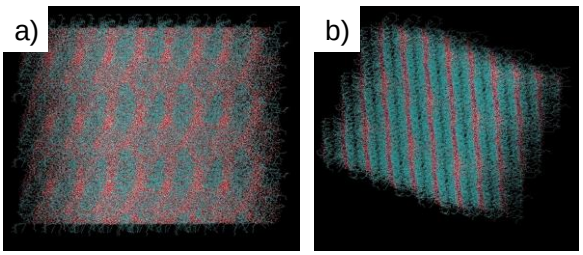

Fig. 2. MD simulation snapshots of: (*a*) a G_I-phase with 55 wt% **Na-73** at 300 K, and (*b*) a L_α phase with 80 wt% **Na-73** at 350 K.

Comparative analyses of the molecular conformations of C_3-linked **Na-73** and C_4-linked **Na-74** surfactants in the G_I-phases have revealed a completely new molecular design rule for stabilizing gemini surfactant LLC network phases. The unusual stability of **Na-74** gyroid phases stems from the anisotropic shape adopted by this hydrated amphiphile, in which the tails splay away from each other to mitigate intramolecular Coulombic repulsions between the ionic headgroups. Changing the tail splay dihedral angle allows the formation of L_α, G_I, and H_I phases.

However, the presence of the C_3-linker in **Na-73** restricts the range of accessible dihedral angles between the tails and seemingly prevents H_I-phase formation. Thus, our simulations demonstrate that gemini surfactants with odd carbon linkers substantially favor the formation of G_I-phase LLCs by destabilizing the adjacent lamellar and hexagonal phases.

Simulation snapshots of the LLC comprising 80 wt% **Na-73** at 300 K suggest that the simulated phase is similar to that of the *Fddd* (space group #70) network phase, which Bates and co-workers have identified in ABC triblock terpolymers. Unlike the gyroid phase, the *Fddd* network is a non-cubic network phase that occurs at intermediate interfacial curvatures between the G and L_α phases. Guided by the symmetry and unit cell parameters of this morphology predicted by MD simulations, we are working to definitively assign this new LLC phase.

Future Plans

Neutron Scattering Studies of Water in Hydrophilic LLC Nanoconfinement

We have started quantitative SAXS studies of the LLC phase behavior of our gemini dicarboxylate surfactants in D_2O, in order to assess the extent to which isotopic substitution affects the observed LLC unit cell dimensions and water channel diameters. These studies will establish a foundation for our wide-angle neutron diffraction (WAND) H_2O/D_2O isotopic substitution studies of the structure of water confined within the hydrophilic nanochannels of a gemini dicarboxylate LLC as a function of surfactant counterion and supramolecular morphology. If strong incoherent background scattering from the hydrogenous surfactant hampers our studies, we will synthesize perdeuterated dicarboxylate gemini surfactants. The results of our studies will be compared to the results from molecular simulations, which predict long-range O-O correlations and a decreased water density within the hydrophilic pores.

Bis(sulfonate) Gemini Surfactant Phase Behavior: Experiments and Simulations

We have already started MD simulations of disodium bis(sulfonate) gemini surfactant aqueous LLC self-assembly, and we will extend these studies to the bis(sulfonates) with Na^+ and $(CH_3)_4N^+$ counterions to enable quantitative comparisons with ongoing experimental studies. Through both experiments and simulations, we will also study whether the odd-even linker effect observed in gemini dicarboxylate LLC phase behavior may be extended to bis(sulfonate) surfactants with a specific emphasis on enlarging the G_I-phase window associated with **HSO_3-84** analogues. On this basis, we will use electrochemical impedance spectroscopy (EIS) to study the proton conductivities of these sulfonated single-ion conductor LLCs in order to gauge how LLC pore diameter affects proton conductivity in the lamellar, hexagonally-packed cylinders, and gyroid phases. These studies aim to establish new molecular and morphological design criteria for the development of ion transporting LLC assemblies.

Synthesis of Gemini Bis(phosphonate) Surfactants

Given the importance of counterion-headgroup correlations in dictating the LLC phase behavior of gemini surfactants, we are working to establish a synthetic route to bis(phosphonate) gemini surfactants that bear dianionic phosphonic acid headgroups. We anticipate that the dianionic phosphonate headgroups will drive surfactant backbone conformations that favor G_I-phase formation.

References

1. G. P. Sorenson, K. L. Coppage, M. K. Mahanthappa. "Unusually Stable Aqueous Lyotropic Gyroid Phases from Gemini Dicarboxylate Surfactants," *J. Amer. Chem. Soc.,* **133**, 14928 (2011).

2. J. Mondal, M. K. Mahanthappa, A. Yethiraj. "Self–Assembly of Gemini Surfactants: A Computer Simulation Study," *J. Phys. Chem. B,* **117**, 4254 (2013).

Multiphasic Soft Colloids: Fundamentals to Application of Energy Sustainability (ERKCSNJ)

Wei-Ren Chen, ***Oak Ridge National Laboratory, Oak Ridge, TN 37831***

Program Scope

The central goal of this research program is to develop a fundamental understanding of the chemical and physical processes occurring on the microscopic length scale that are critical for the molecular-level design of multiphasic soft colloidal systems with desirable macroscopic functionality. This class of structurally heterogenous materials has great promise as a platform for energy related applications including light harvesting, organic light emitting diodes, photonic bandgap devices and supercapacitor. To address the overarching goals, two specific aims form the basis of the proposed research. The first seeks to understand the microscopic interaction mechanisms giving rise to spatial organization on the length scale from that of an individual colloid to collective phase behavior. The second aim focuses on elucidating the relationship between dynamics and structure on both local and collective length scales that give rise to rich equilibrium and non-equilibrium phase behavior. These two specific aims, providing critical link between the bulk material properties in their functional form and the microscopic features of their precursor liquid state, are all underpinned by specific tailored synthesis of targeted systems. designed to optimize the experimental methodology. The knowledge gained from this program will provide insight into fundamental guidelines for sustainable energy-related applications of multiphasic soft colloids that will impact a broad range of DOE's needs in its energy mission.

Recent Progress

1. Structure and Dynamics of Soft Colloids

Previous experimental results show that the size of soft colloids remains invariant below the overlap concentration. In contrast, we carried out neutron spin-echo (NSE) and small angle neutron scattering (SANS) experiments, and discovered the existence of the crossover between the two dynamical degrees of freedom, the inter-molecular translational diffusion and the intra-molecular collective motion, well below the overlap concentration. The concentration, at which the inter-molecular collision time is equal to the intra-molecular relaxation time, is defined as the dynamical crossover point, as shown in Fig. 1 [1]. This is an important discovery, because it discriminates the dilute regime where the inter- and intra-molecular dynamical processes can be fully decoupled, which cannot be described using the existing concept of the overlap density. The two characteristic times are retrieved from the NSE and SANS experimental data through model fitting [1]. Moreover, we developed two new approaches to analyze the contrast variation SANS experimental data, and found the continuous desolvation of soft colloids below and beyond the overlap density due to increasing the concentration, as shown in Fig. 2 [1, 2]. One method is to study the dependence of the total scattering power on the solvent contrast, to obtain the variation of the amount of the associated solvent molecules at different concentrations [1].

The other takes the advantage of the features of the small angle scattering functions of the core-shell spherical colloids with varying the contrast, to obtain the intra-molecular conformation and the distribution of the associated solvent [2]. Furthermore, to understand the effect of the associated solvent molecules on local structure of soft colloids, we developed the small angle scattering function of star polymers with the excluded volume effect [3], and carried out the SANS experiment of polystyrene (PS) star polymers suspended in THF and cyclohexane at different temperature. We plan to reveal the relation between the associated solvent and the local stiffness of polymer chains from the SANS data.

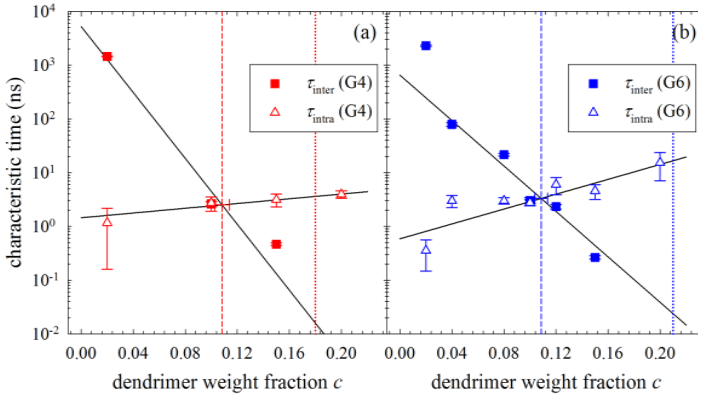

Fig. 1 The average inter-molecular collision time τ_{inter} (filled circles) and intra-molecular relaxation time τ_{intra} (open circles) for (a) G4 and (b) G6 PAMAM dendrimers in water as a function of concentration c. The dotted and dashed lines respectively give the concentrations of the overlap density c^* and the dynamical crossover point c_D^* of G4 and G6 PAMAM dendrimers. Assuming both τ_{inter} and τ_{intra} evolve exponentially with c, c_D^* can be defined by the intersection of two solid lines. [1]

2. Phase Transition and Dynamics of Non-Centrosymmetric Nanoparticles

We developed the small angle scattering function for yolk-shell nanoparticles, a category of functional materials with a mobile core in a hollow shell. [4] It provides the model for the investigation of these novel materials using small angle neutron scattering. Furthermore, we studied the dynamics of yolk-shell nanoparticles using Brownian dynamics simulation and generalized Langevin equation theory. We predicted their dynamical behavior in terms of the diffusion coefficients which can be measured in neutron scattering experiments [5]. Besides, we studied the phase transition of another type of non-centrosymmetric particles, shifted charge colloids, using Monte Carlo simulation. We discovered a liquid-to-crystal transition at a significantly lower concentration than centro-charged colloids. We also found that the system undergoes a continuous disorder-to-order transition with respect to the charge orientation [6].

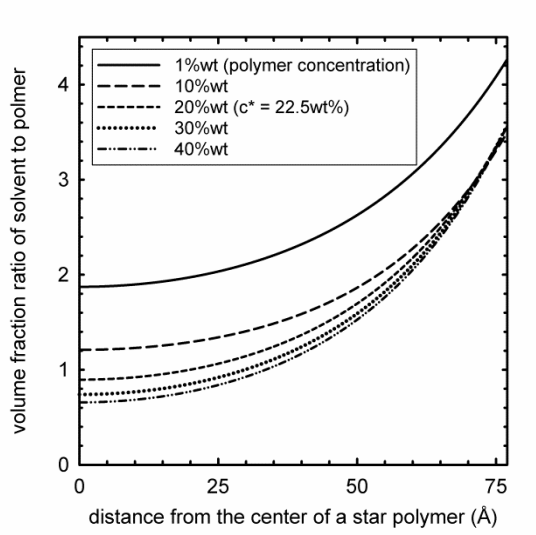

Fig. 2 The ratio of the volume fraction of the associated solvent, THF, to that of the polymer, polystyrene, along the radial direction of a polystyrene star polymer. [2]

These investigations have provided critical information for the practical applications of these novel materials, and we plan to perform scattering experiments to test our predictions.

Future Plans

First, we studied the temperature dependence of the scattering contrast and local structure of star polymers using SANS. The data will be analyzed using our recently developed model and compared to the molecular dynamics simulation result, to understand the influence of the solvent on the microscopic structure of soft colloids. Secondly, we have carried out Rheo-SANS experiments on silica solutions at various concentrations to study the coherency in the response of the inter-molecular structure to the applied shear force. We have developed the methodology to desmear the instrument resolution from the 2D scattering pattern. More data will be accumulated this September at SNS to complete this investigation. Third, we plan to study a tracing amount of fully hydrogenated PS star polymers mixed with fully deuterated PS stars, suspended in cyclohexane at the contrast matching point, at different concentrations using SANS and NSE. The experiments will be carried out this December at SNS, and our goal is to experimentally determine the self-diffusion coefficients, inter-molecular structure factor, and hydrodynamic function, for soft colloids in the whole concentration range. Fourth, we plan to measure the short- and long-time self-diffusion coefficients of generation 4 to 7 PAMAM dendrimers in aqueous solutions in NSE and SANS, to understand the similarity of the dynamical behaviors of the soft colloids with different softness in the scaling plot.

References

1. X. Li, L. E. Sanchez-Diaz, B. Wu, W. A. Hamilton, L. Porcar, P. Falus, Y. Liu, C. Do, G. S. Smith, T. Egami, and W.-R. Chen, "Dynamical Crossover in Soft Colloids below the Overlap Concentration", *Nat. Commun.* (2014). *Under Review* available from arXiv:1403.1812 [physics.chem-ph].
2. X. Li, L. Porcar, L. E. Sanchez-Diaz, C. Do, Y. Liu, T.-H. Kim, G. S. Smith, W. A. Hamilton, K. Hong, and W.-R. Chen, "Influence of Molecular Solvation on the Conformation of Star Polymers", *ACS Macro Lett.* **3**, 458 (2014).
3. X. Li, L. Porcar, L. E. Sanchez-Diaz, C. Do, Y. Liu, T.-H. Kim, G. S. Smith, W. A. Hamilton, K. Hong, and W.-R. Chen, "Scattering from Star Polymers Including Excluded Volume Effects", *J. Appl. Cryst.* (2014). *Under Review* available from arXiv:1404.6269 [physics.chem-ph].
4. X. Li, K.-H. Liu, B. Wu, L. E. Sanchez-Diaz, G. S. Smith, and W.-R. Chen, "Scattering Functions of Yolk–Shell Particles", *J. Appl. Cryst.* **46**, 1551 (2013).
5. L. E. Sánchez Díaz, E. C. Cortes-Morales, X. Li, W.-R. Chen and M. Medina-Noyola, "Dynamic of suspension of interacting yolk-shell particles", *Phys. Rev. Lett.* (2014) *Under Review* available from arXiv 1406.5971 [cond-mat.soft].

6. L. E. Sanchez-Diaz, C.-Y. Shew, X. Li, B. Wu, G. S. Smith, and W.-R. Chen, "Phase behavior under a non- centrosymmetric interaction", *J. Phys. Chem. B* 2014, **118**, 6963−6971.

Publications [FY12(July)-14 (June)]

P1. *Influence of Molecular Solvation on the Conformation of Star Polymers*, X. Li, L. Porcar, L. E. Sanchez-Diaz, C. Do, Y. Liu, T.-H. Kim, G. S. Smith, W. A. Hamilton, K. Hong, and W.-R. Chen, *ACS Macro Lett.* **3**, 458 (2014).

P2. *Scattering from Star Polymers Including Excluded Volume Effects*, X. Li, L. Porcar, L. E. Sanchez-Diaz, C. Do, Y. Liu, T.-H. Kim, G. S. Smith, W. A. Hamilton, K. Hong, and W.-R. Chen, *J. Appl. Cryst.* (2014). *Under Review* available from arXiv:1404.6269 [physics.chem-ph].

P3. *Dynamical Crossover in Soft Colloids below the Overlap Concentration*, X. Li, L. E. Sanchez-Diaz, B. Wu, W. A. Hamilton, L. Porcar, P. Falus, Y. Liu, C. Do, G. S. Smith, T. Egami, and W.-R. Chen, *Nat. Commun.* (2014). *Under Review* available from arXiv:1403.1812 [physics.chem-ph].

P4. *Phase behavior under a non- centrosymmetric interaction*, L. E. Sanchez-Diaz, C.-Y. Shew, X. Li, B. Wu, G. S. Smith, and W.-R. Chen, *J. Phys. Chem. B* 2014, **118**, 6963−6971.

P5. *Dynamic of suspension of interacting yolk-shell particles*, L. E. Sánchez Díaz, E. C. Cortes-Morales, X. Li, W.-R. Chen and M. Medina-Noyola, *Phys. Rev. Lett.* (2014). *Under Review* Manuscript available from arXiv 1406.5971 [cond-mat.soft].

P6. *Scattering Functions of Yolk–Shell Particles*, X. Li, K.-H. Liu, B. Wu, L. E. Sanchez-Diaz, G. S. Smith, and W.-R. Chen, *J. Appl. Cryst.* **46**, 1551 (2013).

P7. *Charge-Dependent Dynamics of a Polyelectrolyte Dendrimer and Its Correlation with Invasive Water*, 5. B. Wu, Y. Liu, X. Li, E. Mamontov, A. I. Kolesnikov, S. O. Diallo, C. Do, L. Porcar, K. Hong, S. C. Smith, L. Liu, G. S. Smith, T. Egami, and W.-R. Chen, *J. Amer. Chem. Soc.* **135,** 5111 (2013).

P8. *Equilibrium structure of a triblock copolymer system revealed by mesoscale simulation and neutron scattering*, C. Do, W.-R. Chen, and G. S. Smith, *Physica B* **430**, 87 (2013).

P9. *Structured Water in Polyelectrolyte Dendrimers: Understanding SANS Results through Atomistic Simulation*, B. Wu, B. Kerkeni, T. Egami, C. Do, Y. Liu, Y. Wang, L. Porcar, E. Liu, G. S. Smith, and W.-R. Chen. *Chem. Phys.* **136,** 144901 (2012).

P10. *MD and Neutron Scattering Study of the Dependence of Polyelectrolyte Dendrimer Conformation on Counterion Behavior*, B. Wu, W.-R. Chen, T. Egami, X. Li, Y. Wang, C.

Do, L. Porcar, K. Hong, L. Liu, G. S. Smith, and S. C. Smith, *J. Chem. Phys.* **137,** 064902 (2012).

P11. *Conformational effect on SANS behavior of interacting polyelectrolyte solutions: A theoretical perspective*, C.-Y. Shew, C. Do, K. Hong, Y. Liu, L. Porcar, and W.-R. Chen, *J. Chem. Phys.* **137**, 024907 (2012).

P12. *Distinguishing the monomer to cluster phase transition in concentrated lysozyme solutions by studying the temperature dependence of the short-time dynamics*, P. Falus, L. Porcar, E. Fratini, W.-R. Chen, A. Faraone, K. Hong, P. Baglioni and Y. Liu, *J. Phys.: Condens. Matter* **24**, 064114 (2012).

P13. *Structural response of polyelectrolyte dendrimer towards molecular protonation*, K. Hong, Y. Liu, L. Porcar, D. Liu, C. Y. Gao, G. S. Smith, K. W. Herwig, S. Cai, X. Li, B. Wu, W.-R. Chen, *et al.*, *J. Phys.: Condens. Matter* **24**, 064116 (2012).

P14. *Contrast variation in spin-echo small angle neutron scattering*, X. Li, B. Wu, Y. Liu, R. Pynn, C.-Y. Shew, G. S. Smith, K. W. Herwig, J. L. Robertson, W.-R. Chen, *J. Phys.: Condens. Matter* **24**, 064115 (2012).

P15. *Elucidation of spin echo small angle neutron scattering correlation functions through model studies*, C.-Y. Shew, and W.-R. Chen, *J. Chem. Phys.* **136**, 064506 (2012).

P16. *Characterizations of Polyamidoamine Dendrimers with Scattering Techniques*, X. Wang, L. Guerrand, B. Wu, X. Li, L. Boldon, W.-R. Chen, and L. Liu, *Polymers* **4**, 600 (2012).

From Interfaces to Bulk: Experimental-Computational Studies Across Time and Length Scales of Multi-Functional Ionic Polymers

Dvora Perahia[1] (dperahi@clemson.edu), Gary S. Grest[2] (gsgrest@sandia.gov)
1-*Chemistry Department Clemson University Clemson SC 29634-0973*
2-Sandia National Laboratories, CINT, Albuquerque, NM 87185-1303

Research Scope

Using a multi-scale approach, we probe the factors that control the behavior of structured ionic polymers with segments tailored to enhance simultaneously transport and mechanical stability. The results will enhance the design of materials for energy generation, capture, and storage. Linking the knowledge obtained from complimentary neutron and x-ray techniques with insight from atomistic and coarse grained molecular dynamics simulations we provide unprecedented new insight into one of the major factors that limits the use of ***ionic polymers***, namely the control over the structure and dynamics at their interfacial regions leading to transformative knowledge that will impact the design of nano-structured materials for energy applications.

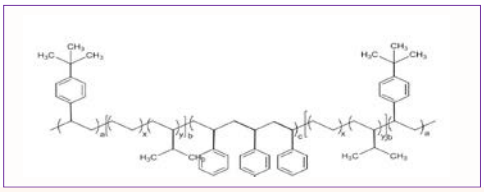

Figure 1 The chemical formula of the pentablock model polymer. The blocks are t-butyl styrene, bound to randomly sulfonated polystyrene by polyethylene propylene (7% random).

The structure and dynamics of tailored multiple functionality co-polymers with a block to enhance transport, one to increase mechanical stability and one to facilitate mobility for the polymer to rearrange into an optimal structure, shown in Figure 1, are probed. Neutron scattering coupled with molecular dynamics (MD) simulations are employed to provide in depth insight into the complex systems formed by this class of polymers. Our studies thus far have demonstrated the power of neutron-computational efforts. We demonstrated that the incompatibility of the ionic segments drive the structure even in dilute solutions, as well as in membranes, where the interfacial regimes are critical for dynamics.

Research Progress

Small angle neutron scattering, [1] neutron reflectometry [2] and inelastic scattering [3] measurements were carried out in conjunction with MD simulations. An important component, developing coarse graining methods to provide means to study large samples while retaining the essential atomistic insight, are underway [4]. Work had been carried out along several pathways including solutions and thin film using scattering, atomistic and coarse grained computational studies, in parallel to development of computational methodology [4-6]. We have resolved for the first time actual solution structure of a complex polymer that serve as precursors for membranes and made significant strides towards understanding membrane structure.

Solution Structure The structure of isolated structured ionic polymers has been resolved by small angle neutron scattering and atomistic MD in solutions [1,5]. We have

demonstrated that internal phase segregation controls solution structure in dilute solutions of cyclohexane-heptane, an industrial used solvent to cast membrane of this pentablock.

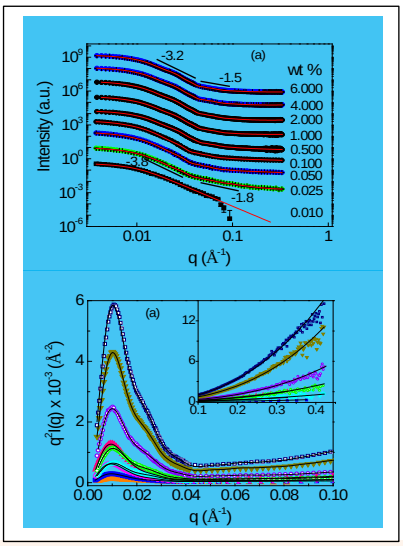

Figure 2: SANS profiles in terms of (a) log I(q) vs. log q, (b) $q^2I(q)$ vs. q for the pentablock copolymer solution at concentration from 0.01 wt% to 6 wt% (orange – 0.01 wt%, blue -0.025 wt%, pink – 0.05wt%, cyan – 0.1 wt%, green – 0.5wt%, red – 1 wt%, violet – 2 wt%, yellow green – 4wt% and navy blue - 6 wt%) at 25 ºC. The symbols represent the experimental data and the solid lines represent the best fits. [ ]

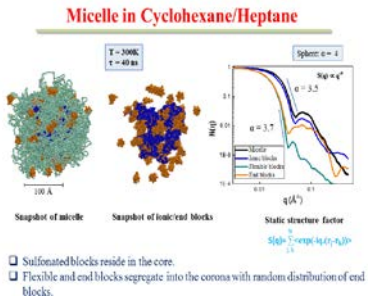

Figure 3. Snapshots of pentablock micelle with sulfonation level f = 0.30. The ionic block is dark blue, the aliphatic segment light blue and the end block brown. Calculated S(q) for entire micelle as well as for the individual blocks The number of molecules included in the simulation is the aggregation number obtained from the experimental SANS studies.

The structure evolution as function of concentration of the polymer in solution from SANS studies is shown in Figure 2. In solution, the pentablock copolymer self-assembles into ellipsoidal micelles with a sulfonated polystyrene center surrounded by solvated rubbery poly-ethylene-r-propylene and poly-t-butyl styrene blocks. The radius of the micelle, the thickness of the corona and the aggregation number increases rapidly and levels off with increasing concentrations, while the solvent fraction in the core decreases with increasing polymer concentration. The increase of micellar size with increasing concentration is attributed to the enhance incompatibilities between the ionic center block and the two outer blocks. These findings provide first insight into the assembly process of a multifunctional polymer that contains an ionic block. In a selective solvent for the non-ionic block, the ionic block dominates the assembly process and the shape of the micelles. This in turn will impact the formation of membranes from solution casting.

Concurrently, MD simulations probed the structure evolution of these micelles from a single molecule [5] to a micelle as shown in Figure 3. The conjunction of neutron measurements with MD simulations provide a detailed insight into the micelle structure than cannot be resolved from modelling the experimental work alone.

Membranes The thermal response of thin layers was studied by neutron reflectometry for ultra-thin films. These films are remarkably stable. The interfacial layers however become rougher with annealing. Computational results showed that the ionic groups form percolating network within the hydrophobic media with limited segregation of the two hydrophobic groups. New studies were initiated to follow the dynamics of water at the interface with the pentablock. The initial results show that the films swell in presence of water. The amount of water uptake depends on degree of sulfonation and film thickness. We attribute film thickness effects to interface induced structures.

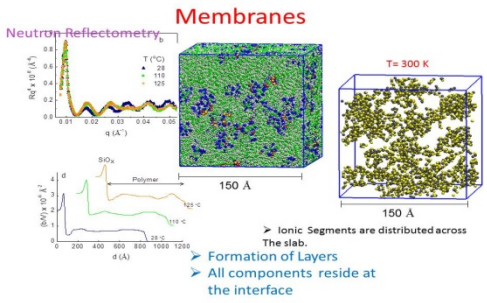

Figure 4 Thermal response of thin pentablock layer as obtained from neutron reflectometry and atomistic simulations.

Computationally several steps were taken to enable these large scale simulations. Maskey et. al [6] have shown that polymers can be collapsed in a cavity and transferred to a real solvent without losing their properties. We then developed pathway to probe the structure and strength of interfaces [7-9]. To couple neutron studies with MD simulations, a hierarchal coarse grained model, shown in Figure 5 was developed and used to model interfacial properties.

Future planes

Experimental Solution: Solvent matching experiments will be carried out in cyclohexane heptane mixtures varying the ratio of the solvents. Polar solvents will be incorporated. Dynamic studies will be carried out to resolve the internal dynamics of the components. The dynamic of the ionic group will be resolved by tuning the ionic strength to allow dynamics within the ionic clusters. The distinction between the regions will be done by tuning the q range and energies.

Membranes: SANS studies will be carried out to resolve the internal structure of the pentablock membranes. The degree of bi-continuity and the internal surfaces as a function of solvent quality and ionic strength will be determined. Neutron reflectometry will be used to study the interfaces between the blocks of the pentablock. Dynamic studies will be carried out in membranes as well as in thin films using inelastic techniques. Beam time requests are currently pending. Macroscopic transport studies will be carried out on selected samples.

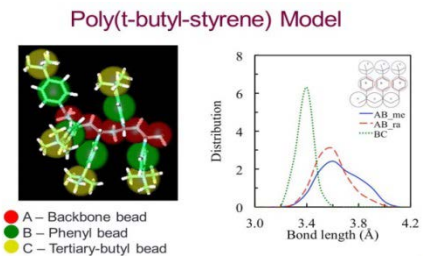

Figure 5 Development of coarse grained models: Schematics of coarse grained t-butyl polystyrene where the A-beads capture the aliphatic part, the B-bead the aromatic group and the C-bead the t-butyl end group. The bond length distribution is shown [4].

Computational Atomistic simulations will be used to follow the aggregation of pentablock co-polymers in solution as they form micelles. Solvent will then be removed to form three dimensional membranes. The static and dynamic structure factors of the resulting membrane will be calculated and compared to experiment, extracting correlations between the segments. The correlation between the motion of water molecules and the ionic group will be followed for varying volume fraction of water. To reach larger time and length scales, flexible blocks will be incorporated into our coarse-grained model of t-butyl and sulfonated polystyrene to model the full pentablock. The coarse grain model will be used to build additional membranes with varying degrees of sulfonation and used both to follow the long time dynamics of the membrane. The coarse grained model of the membrane will be mapped back to a fully atomistic representation from which we can follow the local dynamics of the ionic groups and water.

Publications

1. Thusitha Etampawala, Naresh C. Osti, Dipak Aryal, Lilin He, William T. Heller, Carl L. Willis, Gary S. Grest, and Dvora Perahia
   "Association of a Multifunctional Ionic Block Copolymer in a Selective Solvent"
   Soft Matter (2014), in review.

2. Thusitha Etampawala, Lilin He, Naresh C. Osti, Umesh Shrestha, Dilru Ratnaweera, Jaroslaw Majewski , Christopher J. Cornelius, and Dvora Perahia
   "In Situ Neutron Reflectivity Study of Alcohols at the Interface with Thin Ionomer Films"
   Journal of Chemical Physics (2014), submitted.

3. Naresh C. Osti, Thusitha N. Etampawala, Umesh M. Shrestha, Madhusudan Tyagi, Souleymane O. Diallo, Eugene Mamontov, Chris J. Cornelius, and Dvora Perahia
   "Dynamics of Water in Sulfonated Poly(phenylene) Ionomer Membranes"
   Journal of Chemical Physics (2014), submitted.

4. Anupriya Agrawal, Dipak Aryal, Dvora Perahia, Ting Ge, and Gary S. Grest,
   "Coarse-Graining Atatic Polystyrene and Its Analogues"
   Macromolecules **47**, 3210 (2014).

5. Dipak Aryal, Thusitha Etampawala,Dvora Perahia, and Gary S. Grest,
   "Phase Behavior of a Single Structured Ionomer Chain in Solution"
   Macromolecular Theory and Simulation (2014), in press.

6. Sabina Maskey, Naresh C. Osti, Dvora Perahia, and Gary S. Grest
   "Internal Correlations and Stability of Polydots, Soft Conjugated Polymeric Nanoparticles"
   ACS Macro Lett**ers 2**, 700 (2013).

7. Anupriya Agrawal, Dipak Aryal, Gary S. Grest and Dvora Perahia
   "Interfacial Response of Semi-Fluorinated Multi-block co-Polymers"
   Handbook of Fluropolymer Science and Technology, edited by Dennis W. Smith Jr., Scott T. Iacono, and Suresh Iyer (Wiley, Hoboken, NJ, 2014), p. 43.

8. Ting Ge, Flint Pierce, Dvora Perahia, Gary S. Grest, and Mark O. Robbins
   "Molecular Dynamics Simulations of Polymer Welding: Strength from Interfacial Entanglements"
   Physical Review Letters **110**, 098301 (2013).

9. Ting Ge, Mark O. Robbins, Dvora Perahia, and Gary S. Grest
   "Healing of Polymer Interfaces: Interfacial Dynamics, Entanglements, and Strength"
   Physical Review E (2014), in press.

In-situ Neutron Scattering Determination of 3D Phase-Morphology Correlations in Fullerene Block Copolymer Systems

Alamgir Karim (alamgir@uakron.edu), David Bucknall[+], Dharmaraj Raghavan[++] Xiong Gong
Department of Polymer Engineering, University of Akron, OH 44333
[+]School of Materials Science and Engineering, Georgia Tech, Atlanta, GA 30332
[++]Department of Chemistry, Howard University, Washington D.C. 20059

Research Scope

Nanoscale heterojunction systems consisting of fullerenes dispersed in conjugated polymers are promising materials candidates for achieving high performance organic photovoltaic (OPV) devices. We have two research thrusts focus areas. The first focuses on understanding fundamental phase behavior of model bulk heterojunction thin films, while the second focuses on correlating synthesis, properties and performance of new electron acceptor nanomaterials. In order to understand the phase behavior in these devices, neutron reflection to determine the behavior of model conjugated polymer-fullerene mixtures is used. Specifically, the effect of Polythiophene-fullerene thin film phase behavior on photovoltaic device performance is investigated. Neutron reflection is particularly useful for these types of thin film studies since the fullerene generally have a high scattering contrast with respect to most polymers. We are studying model bulk heterojunction (BHJ) films based on mixtures of poly(3-hexyl thiophene)s (P3HT), a widely used photoconductive polymer, and different fullerenes (C60, PCBM and bis-PCBM). The characterization technique of neutron reflectivity measurements have been used to determine film morphology in a direction normal to the film surfaces. The novelty of the approach over previous studies is that the BHJ layer is sandwiched between a PEDOT/PSS and Al layers in real device configuration. Using this model system, the effect of typical thermal annealing processes on the film development as a function of the polythiophene-fullerene mixtures is measured. On the new materials research and correlation to properties we have synthesized and investigated fullero-pyrillodone as electron acceptors and block copolymers as morphology modifying agents of BHJ's.

Recent Progress

In-Situ Neutron Reflection of Polythiophene-fullerene thin film phase behavior in Devices

J-V characteristics of devices made with bis-PCBM showed larger Voc than its counter parts using PCBM as the electron accpetor. For the devices made with a certain electron acceptor material, P3HT showed the best device peroformance, while P3OT the worst, J_{sc} (P3HT) > J_{sc} (P3BT) > J_{sc} (P3OT). ie. P3HT best facilitates electron transport towards aluminum cathode. Fill factor of the devices reflected the effect from the electron acceptor in fullerene depletion layer. Most devices showed Fill Factors in the range of

~50% except for P3OT-bisPCBM and P3BT-C_{60}. From J-V curve under dark, only P3OT:bis-PCBM and P3BT-C_{60} showed poor diode characteristics. The value for the PCE% was calculated from the Isc, Voc and FF values obtained and subsequently plotted versus the number of C chains in the polyakylthiophene side chain to obtain a trend and subsequently used to correlate with the data on the morphological state of these systems. P3HT-PCBM was seen to give the best device efficiencies among all the devices, as is well known in literature. Interestingly, on annealing, the devices showed negligable improvement in the PCE even in the case of P3HT-PCBM. Number of previous research have cited parameters such as fullerene –polymer segregation, domain sizes of the polymer and fullerene, interfacial interaction energy with the electrodes among others as some of the factors affecting the performance of these devices.

We conducted neutron reflection (NR) measurements on these BHJ systems in full device format for the first time to obtain the morphological profile of the heterojunction area and correlate to the trend in identical device performance. Bulk heterojunctions made with a procedure identical to the ones used for device measurements were used for neutron reflectivity measurements at the SNS facility in DOE's Oak Ridge National Laboratory. The measurements provided us with a plot of the Reflectivity (R) versus momentum vector (Q). Figure 1 a) shows the NR plot variation of the bulk heterojunction of PCBM with different Polyalkylthiophene (P3AT) compounds P3BT, P3HT and P3OT before being annealed. The data was fitted using the software RASCal (developed at ISIS) to determine the corresponding scattering length density distribution of the polymer and fullerene in the heterojunction layer. Figure 1b) shows similar fitted data for the same samples, post annealing. The fitting of the data was obtained by optimizing the three main parameters of the different layers - the scattering length density (SLD), thickness and roughness of the layers. We could thus plot the scattering length density profile for these samples which using the formula given allow us to also predict the composition of the different component in a given layer knowing their standard SLD values. Figure 3c) shows the scattering length density variation for the pre annealed and post annealed sample, as we increase distance from the top Aluminum-air interface.

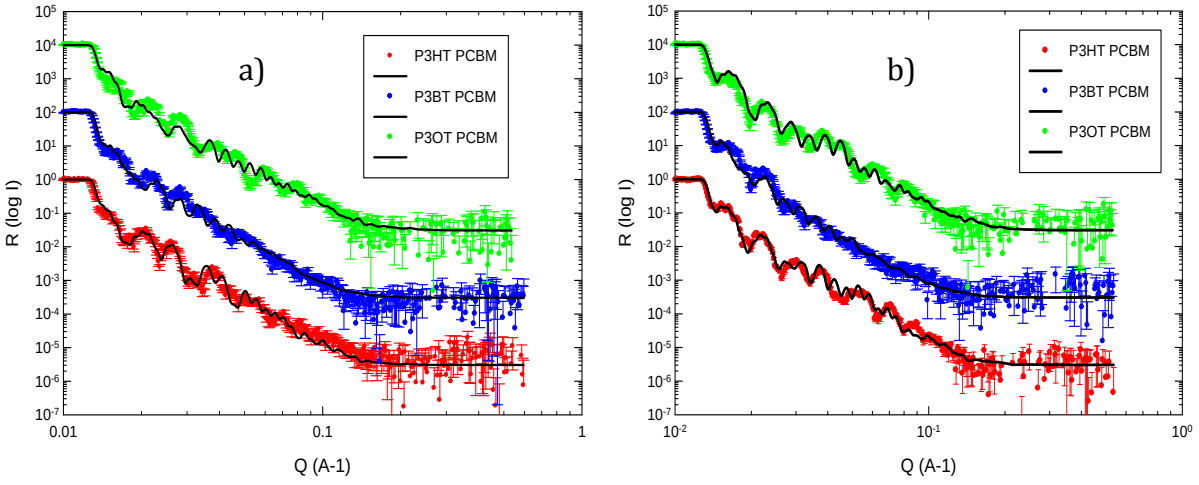

Fig 1 Neutron reflectivity plots (Reflectivity vs momentum transfer) for a) pre and b) post annealed P3AT- PCBM devices

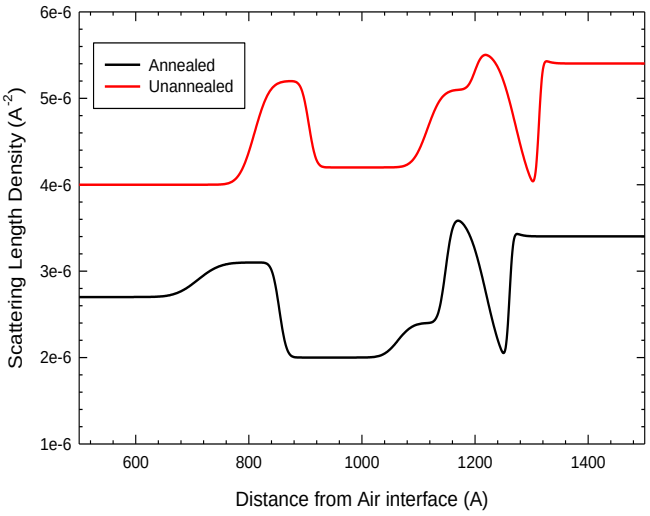

Fig 1 c (left). Scattering length density (SLD) profile through the layers in the bulk heterojunction in full device configuration in-situ under neutron beam, for pre and post annealed P3HT-PCBM

Fig 3 (bottom). Volume fraction of Fullerene variation through the heterojunction layer of P3HT-PCBM. A bimodal distribution is apparent.

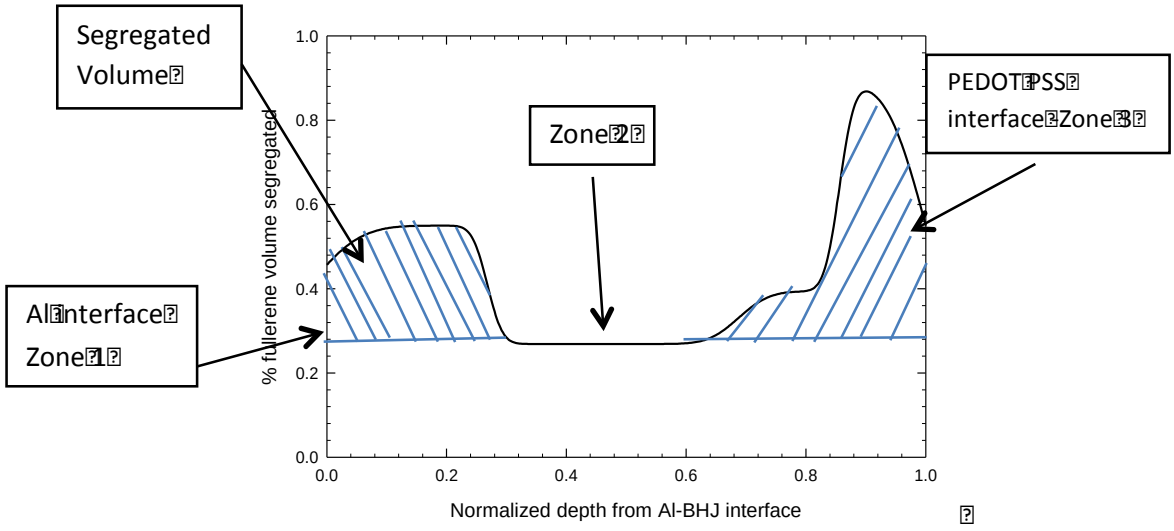

Novel fulleropyrrolidine in P3HT blended bulk heterojunction solar cells

Synthesis of novel fullerene derived electron acceptors and characterization of their organic photovoltaic (OPV) properties is important for next generation organic solar cells. We report the synthesis of a novel fulleropyrrolidine derivative C60-fused N-(3-methoxypropyl)-2-(carboxyethyl)-5-(4-cyanophenyl)fulleropyrrolidine (NCPF) by 1,3-dipolar cycloaddition reaction and characterization of NCPF by 1H NMR, 13C NMR, MALDI-TOFMS, FT-IR, UV-Vis and CV. The synthesized NCPF fullerene derivative showed good solubility in common organic solvents such as chlorobenzene and 1,2 dichlorobenzene important for film formation, with optical absorbance and electronic properties comparable to PCBM. Optical micrographs of P3HT:PCBM thin films reveal formation of sparse, phase segregated needle shape PCBM micro-crystalline aggregates

after 1h of annealing at 150 oC whose length follows nucleation and growth kinetics over 24 h. In contrast, the P3HT:NCPF thin films exhibit homogeneity over 24 h, possibly due to weaker interparticle vanderWaals forces and/or stronger interactions with P3HT. This long term morphological stability of P3HT:NCPF is important for extended use in OPV applications. At an order of magnitude smaller scale, AFM of as cast and 10 min annealed at 150 ^{o}C P3HT:PCBM and P3HT:NCPF films reveal mostly smooth surfaces, with some NCPF cluster formation. Grazing incidence wide angle X-ray scattering (GIWAXS) measurements of P3HT:NCPF films indicate an increase of P3HT crystallinity with thermal annealing, leading to improvement in device performance. Photovoltaic devices fabricated with the active layer of P3HT:NCPF and P3HT:PCBM sandwiched between ITO/PEDOT:PSS and Al layer showed comparable performance upon short term annealing. NR measurements of these BHJ systems is underway at NIST.

Future Studies: NR studies of these BHJ thin film systems at SNS, NIST and ISIS. **PI will have a dedicated post-doc at NIST on NG-7 NR beam line starting Fall 2014.**

Publications (FY12-FY14)

1. F. Fischer, D. Trefz, J. Back, N. Kayunkid, B. Tornow, S. Albrecht, K. Yager, G. Singh, A. Karim, D. Neher, M. Brinkmann, S. Ludwigs, *Highly Crystalline Films of PCPDTBT with Branched Side Chains by Solvent Vapor Annealing: Influence on Opto-Electronic Properties*, **Advanced Materials, Submitted**.
2. S. Samant, S. Hailu, A. Karim, D. Raghavan, *Orientation control in nanoparticle filled block copolymer cold zone annealed films,* **Polymer, Submitted**
2. K. Wang, H. Ren, C. Yi, Y. Sun, A. Karim and X. Gong, *Enhanced efficiency and stability of polymer solar cells by PEDOT:PSS doped with Fe3O4 magnetic nanoparticles as an anode buffer layer,* **Adv. Eng. Mater., 2014, in press.**
3. P. Pitliya, Y. Sun; J. C. Garza; C. Liu, X. Gong, A. Karim, D. Raghavan, *Synthesis and characterization of novel fulleropyrrolidine in P3HT blended bulk heterojunction Solar Cells,* **Polymer, 2014, in press.**
4. Bohao Li, He Ren, Hongyi Yuan, Alamgir Karim and Xiong Gong, *Room-Temperature Solution-Processed MoOx Thin Film as a Hole Extraction Layer to Substitute PEDOT:PSS in Polymer Solar Cells,* **ACS Photonics, 2014, 1, 87-90**.
5. Kai Wang, He Ren, Hangxing Wang, Chao Yi, Li Huang, Haoli Zhang, Alamgir Karim, and Xiong Gong, *Solution-Processed Fe3O4 Magnetic Nanoparticle Thin Film Aligned by an External Magnetostatic Field as a Hole Extraction Layer for Polymer Solar Cells*, **ACS Appl. Mater. & Interface, 2013, 5, 10325-10330.**
6. H. X. Wang, X. F. Yu, C. Yi, H. Ren, C. Liu, Y. Yang, S. Xiao, A. Karim, S. D. Cheng, and X. Gong, *Fine-tuning of fluorinated thieno[3,4-b]thiophene copolymer for efficient polymer solar cells,* **J. Phys. Chem. C. 2013, 117(9), 4358-4363.**
7. K. Wang, C. Yi, Y. Sun, A. Karim and X. Gong, *Enhanced efficiency and stability of polymer solar cells by PEDOT:PSS doped with Fe3O4 magnetic nanoparticles as an anode buffer layer,* **ACS Applied Materials & Interface, 2014, In press.**
8. Praveen Pitliya, Gurpreet Singh, Jose Chapa, Alamgir Karim, Dharmaraj Raghavan, *Dispersion orientation effects of fulleropyrrolidine in zone annealed block-copolymer films toward optimizing OPV interfaces,* **Polymer 54 (2013) 1415 – 1424**

Development of New Methods to Study Materials Structure using Spin Echo Scattering Angle Measurement (SESAME) of Neutrons

Roger Pynn, Indiana University, Bloomington

Program Scope

Neutron scattering is a signal limited technique. Although there have been many incremental advances in neutron measurement technology over the past few decades, the only fundamentally new methods that have been introduced to address this issue involve Larmor encoding. These methods allow one component of the neutron velocity to be encoded in the Larmor phase of a neutron as it propagates through a well-defined magnetic field. The best known of these methods is energy-resolving neutron spin echo (NSE), which is now well established as a method for measuring slow (10 ns to a few 100 ns) dynamics in condensed matter systems such as complex fluids. Our program focuses on the development of Larmor labeling as a technique for measuring static structure. The method, called SESAME or Spin Echo Scattering Angle Measurement, is complementary to conventional SANS in that it provides information as a real space correlation function instead of a structure factor in Q space; it extends the size range that can be accessed by SANS into the range addressed by USANS (up to about 25 microns); and its sensitivity is unaffected by either incoherent or multiple scattering of neutrons. Because it does not require tight monochromatization or collimation of the neutron beam, it offers the possibility of making high-resolution measurements while maintaining strong signal intensity. These potential advantages require sustained development if they are to be realized. The key issues that we have recently addressed include designing suitable magnetic field components; exploring methods to deal with unscattered neutrons, which tend to corrupt the measurement; and exploring science areas where the method can make unique scientific contributions.

Recent Progress

Colloidal Confinement: In a series of experiments using the OFFSPEC instrument at ISIS in the UK, we used SESAME to probe the structure of colloids in confinement[2]. Layering of micron-sized colloidal particles has been observed in wedge shaped confinements using optical microscopy. Our goal was to probe such confinement effects for sub-micron particles in a simpler geometry involving two parallel, planar walls separated by distances slightly greater than the particle size. To this end, periodic arrays of deep (5 to10 microns) microfluidic channels of various widths from 400 nm to 700 nm were etched in silicon wafers by our collaborators at the Center for Nanophase Materials Science (CNMS) at ORNL (cf Fig (B)). The equally spaced channels were separated by either 1 micron or 2 microns and covered an area of ~1 square centimeter. These gratings were placed in contact with a charge-stabilized colloidal suspension of ~185-nm-diameter silica particles and SESAME was used to interrogate the structure. The experiments were done in transmission geometry with the grating tilted with respect to the

neutron beam in order to enhance the scattering contrast. The SESAME signal would be a simple Fourier transform of the Bragg intensities from the periodic grating if constant-wavelength neutrons were used. However, because we used a time-of-flight method at a pulsed neutron source (ISIS), the SESAME pattern is somewhat distorted. Nevertheless, there is a clear difference between the SESAME signal when pure solvent is replaced by colloidal fluid next to the grating. This implies that the average scattering length density (SLD) of the material in the channels changes when solvent is replaced with colloidal suspension. We have previously reported the development of a dynamical theory[1] that accurately accounts for SESAME signals measured with periodic structures and we are using that theory to analyse our data. However, in some cases such a theory is unnecessary as Fig A shows, since we can overlap solvent and colloid data simply by changing the tilt of the sample. It is obvious that the introduction of any colloidal particles into the channel will result in some difference between the SESAME signals obtained with solvent and colloid: we are simply changing the contents of a unit cell in a diffraction experiment so the Bragg intensities will also change. The real issue is whether the volume fraction of the colloid in the channels is the same as that in the bulk or not i.e. whether confinement has an effect on its structure. To make this assessment it is important to know the exact scattering properties of the silica colloidal particles. Both SANS and SESAME have been important in establishing these properties: contrast-matching SANS yielded the SLD and density of the silica; SANS and SESAME both gave the same result for the percentage of each particle occupied by solvent; and SESAME provided an unambiguous volume fraction for the swollen particles. Depending on the width of the channels, we found that the volume fraction of the particles in the grooves could be either greater or less than that of the bulk fluid. The values appear to be consistent with the occurrence of close packed layers in the channels with the number of layers determined by the size of the silica particles and their Debye screening lengths. Data analysis for the most recent experiment is on-going and we will take more data in August 2014.

Although previous experiments using x-rays produced qualitatively similar results we believe that those data should be re-examined because they used incorrect values for the size and shape of dispersed particles (which are only obtained easily using SANS and SESAME). Our experiments show that neutrons can make measurements on very large structures (2 micron period) using SESAME. These measurements complement x-ray diffraction exactly in the cases one would expect, namely where contrast differences between light materials can be exploited.

Structure of Colloids with Depletion Interactions: Using SESAME we have explored the structures of concentrated, prototypical, hard-sphere colloids (PMMA) that are difficult to measure with more traditional neutron methods because of signal contamination by multiple scattering and/or incoherent scattering[3]. Our most important conclusion from this study is that SESAME shows exactly where correlations change in real space when external conditions are changed. The addition of small amounts of depletant caused *only* a small change in the first-neighbor correlations between colloidal particles (panels a, b, c and f of Fig C). Beyond a certain

depletant concentration, long-range, power-law correlations occurred with no further change in short range correlations (panel d of Fig C). Importantly, the power-law correlations do not extend to short distances. Rather they simply cease to exist for inter-particle distances of less than about 3 particle diameters. This type of information is reminiscent of that obtained by pdf analysis at much shorter distance scales and is a powerful adjunct to SANS.

High-Tc Wollaston prisms: Our most important technical development has been the design and manufacture of magnetic fields for SESAME, We use the Meissner effect in high temperature superconducting (HTS) films deposited on thin sapphire substrates to define spatially confined, uniform magnetic fields that mimic the optical device known as a Wollaston prism. Given the performance that we have observed to date, we expect these devices to greatly improve SESAME and to have applications in other areas such as Larmor diffraction, sensitive measurement of line-shapes of phonons using triple axis spectrometers and neutron radiography.

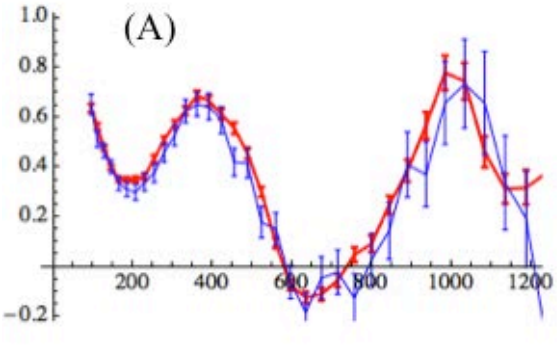

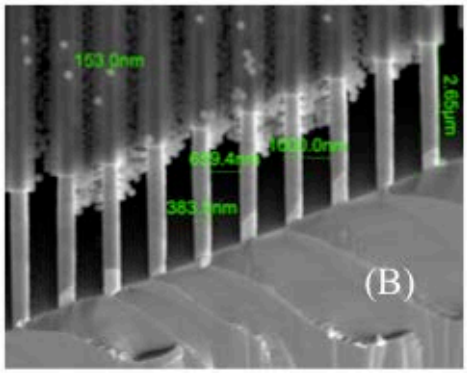

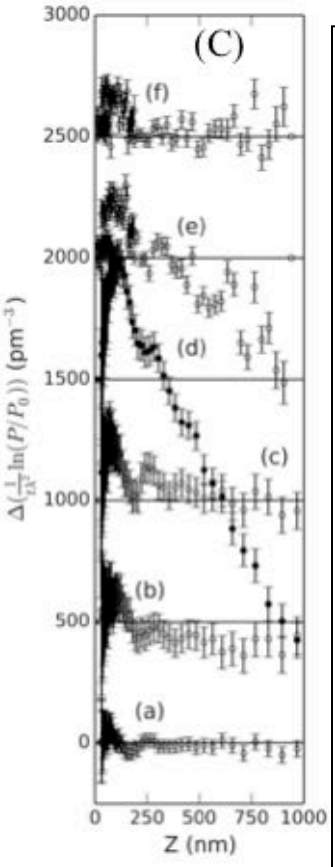

Fig (A): SESAME signal obtained with a grating like that shown in Fig (B) with (red) and without (blue) colloids. The data with colloids are taken with a 1° smaller tilt of the grating than the data without colloids. The overlap of the two curves allows the concentration of the colloids to be determined very accurately. Fig (C): The difference between correlation functions for a 40% sample of spherical 100 nm diameter PMMA particles, with and without polystyrene depletant. Panels (a), (b), (c) and (f) have depletant concentrations below the clustering transition while (e) and (f) have larger concentrations

Future Plans

Our experiments to date have demonstrated several niche areas where we expect SESAME to make unique contributions and we hope to exploit these. Examples include sheared colloids and oil-bearing rocks. In both of these cases, the fact that real systems of interest often scatter strongly makes the use of conventional scattering methods suspect because of multiple scattering

contamination. In some cases this problem can be overcome by appropriate choice of scattering contrast. However, especially in cases where time-dependent information is of interest, such a strategy is obviously self-defeating.

We will continue development of the HTS Wollaston prisms. An LDRD proposal has been submitted at ORNL to build a phonon focusing device for a triple axis spectrometer using this technology.

The one area where progress continues to elude us is in dealing with the unscattered neutrons. At the moment, SESAME measures a signal that includes both scattered and unscattered neutrons making it unsuitable for measurement of weakly scattering systems. We have investigated and rejected various near-field neutron-optical methods of overcoming this problem. In the next month we will try a much simpler method using simple beam blocking.

References

1. R. Ashkar et al, J. Appl. Cryst., **43**, 455 (2010)
2. R. Ashkar et al; J. Appl. Cryst, **47** (2014) (in press)
3. A. L. Washington et al; Soft Matter 10 (17), 3016 (2014)

Publications

1. DCD USANS and Spin-Echo SANS: A comparison of two neutron scattering technqiues applicable for the study of large-scale structures; Christine Rehm, John Barker, Wim Bouwman and Roger Pynn; J. Appl. Cryst., **46**, 354 (2013) DOI: http://dx.doi.org/10.1107/S0021889812050029
2. Neutron Spin Evolution through Broadband Current Sheet Spin Flippers; P.Stonaha, J. Hendrie, W. T. Lee, and Roger Pynn, Rev. Sci. Instrum. **84**, 105113 (2013): DOI: http://dx.doi.org/10.1063/1.4826086
3. Inter-particle Correlations in a Hard-Sphere Colloidal Suspension with Polymer Additives Investigated by Spin Echo Small Angle Neutron Scattering (SESANS); A. L. Washington, X. Li, A. B. Schofield, K. Hong, M. R. Fitzsimmons, R. Dalgliesh and R. Pynn; *Soft Matter*, 10 (17), 3016 (2014) – 3026: DOI: http://dx.doi.org/10.1039/c3sm53027b
4. Superconducting magnetic Wollaston prism for neutron spin encoding; F. Li, S. R. Parnell, W. A. Hamilton, B. B. Maranville, T. Wang, R. Semerad, D. V. Baxter, J. T. Cremer, and R. Pynn; Review of Scientific Instruments **85**, 053303 (2014); http://dx.doi.org/10.1063/1.4875984
5. A new approach for probing matter in periodic nanoconfinements using neutron scattering; Rana Ashkar, Roger Pynn, Robert Dalgliesh, Nickolay V. Lavrik and Ivan I. Kravchenko; to be published in J. Appl. Cryst. **47**, (2014) http://dx.doi.org/10.1107/S1600576714013387
6. Optimization of a solid state polarizing bender for cold neutrons; V. R Shah, A. L. Washington, P. Stonaha, R. Ashkar, H. Kaiser, T. Krist and Roger Pynn; accepted for publication by Nucl. Instr. and Methods (2014)
7. Non-Uniform Transmission of Supermirror Devices for Neutron Polarization; X. Tong, J.L. Robertson, R. Pynn; submitted to Nuclear Instrument and Methods (2014)

Session VI

Dynamics

Vibrational Thermodynamics of Materials at High Temperatures

Brent Fultz (btf@caltech.edu), *Dept. of Applied Physics and Materials Science, Keck Laboratory 138-78, California Institute of Technology, Pasadena, California 91125*

Research Scope

Entropy, *S*, is central to the thermodynamics of materials, especially at high temperatures where the contribution to the free energy, $-TS$, is increasingly important. Most of the entropy of solids comes from phonons, and our program is designed to measure changes in phonons at high temperature. This includes measurements of phonon density-of-states (DOS) from powders, and phonon dispersions from single crystals. Much of materials engineering involves processing materials at high temperatures, where it is well-known that the harmonic model of atom vibrations is not reliable.

The usual next step beyond harmonic models is the quasiharmonic approximation, where phonons are assumed harmonic, but their frequencies are altered by thermal expansion. This contribution is easy to estimate, given the thermal expansion, bulk modulus, heat capacity and density. Unfortunately, it rarely proves adequate by itself. For example, phonons interact through the cubic and quartic parts of their displacement potential. This causes additional frequency shifts and finite phonon lifetimes that give rise to thermal resistivity, for example. Many-body theory has been developed to account for the effects of phonon-phonon interactions, and with modern computing we have found it practical to calculate them. In some cases, such as materials with anomalous (negative) thermal expansion, the anharmonicity is so large that many-body perturbation theory is not reliable. Here ab-initio molecular dynamics methods seem to be successful, but only a few cases have been tested to date. Finally, metals have additional degrees of freedom where phonons can interact with electrons or magnons.

Recent Progress

Oxides and Semiconductors In work with rutile TiO_2 and rutile SnO_2, we were able to use many-body phonon perturbation theory to show how the lifetimes of different phonons varied with temperature. This required summing all three-phonon processes involving the cubic part of the anharmonic potential. For Raman spectra, which are simpler than neutron scattering spectra, we were also able to calculate the many-body contributions from the quartic part of the phonon potential. A thermal phonon anomaly in SnO_2 was attributed to the energy gap between the low-frequency modes dominated by Sn motions, and the high-frequency modes dominated by O motions, in conjunction with thermal phonon softening.

Cubic Ag_2O has a large and negative thermal expansion. This is associated in part with the low coordination around Ag atoms, which are in linear chains with O-Ag-O bonding. The nonlinear restoring forces for transverse displacements of Ag atoms are not easy to interpret, however, since the vibration is not local, and energy is transferred to other Ag atoms through the light O atoms. We were successful in interpreting the highly nonharmonic lattice dynamics in Ag_2O with ab-initio molecular dynamics calculations. These simulations showed that recent prior interpretations with the quasiharmonic model are capable of accounting for only about a third of the negative thermal expansion.

Metals Metals are distinguished by their free electrons, which can screen charge disturbances. When metal ions are displaced from their equilibrium positions, metals with more free electrons are generally able to screen the Coulomb forces more effectively, reducing the energy and the restoring forces. Over the years, we have found a reasonably good correlation between the number of electrons at the Fermi level and the reduced stiffness of the interatomic forces in transition metals and their alloys. Our paper on Fe-Ni alloys showed such trends, but the effects were small.

We recently studied a free electron metal, Au, alloyed with Fe. The electronegativity of Au is greater than Fe, so the Fe atoms tend to donate electrons to the conduction electrons of Au. This increase in electron density causes an increase in stiffness of the alloy, but that is only part of the story. The other piece is a hybridization between the occupied 5d electrons at Au atoms and the unoccupied 3d states at Fe atoms. The combination of these two effects was obtained by density functional theory calculations, which predicted a phonon stiffening when Fe was dissolved in Au. This was in good agreement with the basic trends from inelastic neutron scattering on Au-Fe, and nuclear resonant inelastic scattering from the ^{57}Fe in these alloys.

Alloys of fcc Cu-Fe are unstable, but can be prepared by high energy ball milling. The unmixing of Fe from the fcc Cu matrix is rapid, as shown by atom probe tomography in a collaboration with G. Thompson. The phonon spectra from Fe atoms, however, did not change significantly during the spinodal unmixing in the fcc phase. Only when the bcc phase began to nucleate and grow did the vibrational entropy change significantly.

Finally, in an international collaboration we participated in an assessment of the thermodynamics of aluminum metal. In short, we evaluated the vibrational entropy from phonon measurements by inelastic neutron scattering, and added the electronic entropy (which is small and well-known). We found superb agreement with the entropy of aluminum from historical heat capacity measurements. Although the methods of measurement, heat capacity versus counting phonons, were completely different, the accuracy of both is good enough for thermodynamic predictions. In the course of this work, we made an observation relevant to using many-body theory for predicting thermodynamic properties – the imaginary part of the phonon self energy should be ignored to first approximation.

Future Plans

Methods Part of our work is developing tools for computation and analysis. This summer we will be working to develop better visualization tools for these multidimensional datasets, perhaps including translucent 3D printing of a dataset. In early March 2014 we acquired inelastic neutron scattering data from ARCS on a silicon single crystal at several temperatures. The silicon crystal may be one of the highest quality crystals ever run on the ARCS instrument. A single slice through the data is shown in Fig. 1. Notice the sharpness of the dispersions between 20 and 60 meV, owing to an optimal orientation of the energy resolution of the ARCS instrument. These data may prove important for evaluating the capabilities of ARCS for measuring phonon dispersions. We will be simulating these results to understand how to optimize the use of ARCS for best resolution, and out-of-plane dispersion information.

Silicon In addition to the single crystal dataset, typified by Fig. 1, we acquired full phonon energy spectra from silicon powder at high temperatures, and have extracted the phonon density

of states. There is a significant anharmonicity beyond the quasiharmonic approximation. Our plan is to publish these polycrystal results first, and return to the detailed atomic mechanisms of anharmonicity when we have more thoroughly explored the single crystal data.

Metallic Glass Thanks to the high neutron flux at ARCS we were able, for the first time, to measure the phonon DOS of a metallic glass (CuZr) as it was heated through its glass transition, where it went from a rigid solid to a liquid before it crystallized. The analysis and manuscript are nearly complete. Surprisingly, there is a negligible change in phonon DOS through the glass transition, less than 0.02 k_B/atom. This is an important result for the theory of the glass transition, where vibrational contributions are frequently assumed to be large.

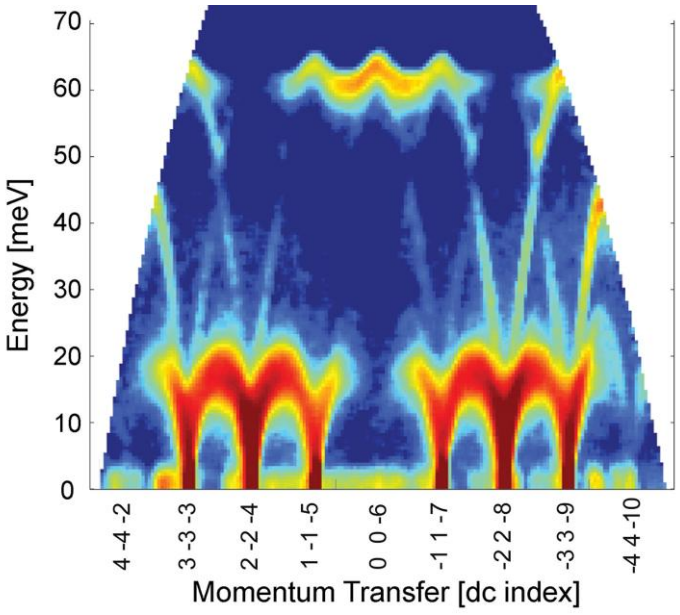

Figure 1. One slice through a large dataset from (110) silicon crystal measured at 100 K. Recall that the diamond cubic structure has systematic absences of the (4 -4 2), (0 0 -6) and (-4 4 -10) diffractions owing to structure factor rules, so this intensity is missing around E=0 meV. On the other hand, the optical modes, which have out-of-phase motions of adjacent Si atoms, show strong intensity at 62 meV for the (0 0 -6) momentum transfer.

Rutile TiO_2 An issue with all previous computational phonon dynamics work on rutile TiO_2 is that the calculations predict the structure is unstable. During thermal expansion, the calculated low transverse acoustic phonons develop imaginary frequencies, leading to structural collapse. We recently found, however, that the unstable modes are in fact highly anharmonic and their low-temperature behavior changes dramatically with temperature. Our ab initio molecular dynamics calculations have shown that these unstable modes are so anharmonic that they actually increase in frequency with increasing temperature, and do not soften as predicted by less complete theoretical treatments. We acquired inelastic neutron scattering data on TiO_2 that have been reduced to phonon DOS curves. These data confirm that a region of the phonon DOS that includes these anomalous modes does increase in energy with increasing temperature. A manuscript is in preparation.

C16 Laves Phase An anomalously large vibrational entropy was calculated by Wolverton and Ozolins for the θ-phase of Al_2Cu (C16 structure) [Phys. Rev. Lett. 86, 5518 (2001)]. In fact they calculated the electronic energy of the θ-phase to be rather high, and concluded that the θ -phase of Al_2Cu is stabilized at finite temperature by vibrational entropy. With the ARCS spectrometer,

we acquired inelastic neutron scattering data from a single crystal of of $FeGe_2$ with this same C16 crystal structure. The data have been reduced, and we see clear phonon softening with temperature. An assessment of the thermal softenings of different phonons is the next step, and this will be undertaken in the next months.

Publications in archival journals

T. Lan, X. Tang and B. Fultz, "Phonon anharmonicity of rutile TiO_2 studied by Raman spectrometry and molecular dynamics simulations," Phys. Rev. B 85, 094305 (2012).

J.A. Muñoz, M.S. Lucas, L. Mauger, J. Horwath, S.I. Semiatin, Y. Xiao, M.B. Stone, D.L. Abernathy, and B. Fultz, "Electronic structure and vibrational entropies of fcc Au-Fe alloys," Phys. Rev. B 87, 014301 (2013).

T. Lan, C.-W. Li, and Brent Fultz, "Phonon anharmonicity of rutile SnO_2 studied by Raman spectrometry and first principles calculations of the kinematics of phonon-phonon interactions," Phys. Rev. B 86, 134302 (2012).

M.S. Lucas, L. Mauger, J.A. Munoz, I. Halevy, J. Horwath, S.L. Semiatin, S.O. Leontsev, M.B. Stone, D.L. Abernathy, Yuming Xiao, Paul Chow, and B. Fultz, "Phonon densities of states of face-centered-cubic Ni-Fe alloys," J. Appl. Phys. 113, 17A308 (2013).

H.L. Smith, W. Hornbuckle, L. Mauger, B. Fu, S. Tracy, G. Thompson, M.S. Lucas, Y. Xiao, M. Hu, J. Zhao, E.E. Alp, and B. Fultz, "Changes in Vibrational Entropy During the Early Stages of Chemical Unmixing in fcc Cu-6%Fe" Acta Materialia 61, 7466 (2013).

M. Palumbo, B. Burton, A. Costa e Silva, B. Fultz, B. Grabowski, G. Grimvall, B. Hallstedt, O. Hellmann, B. Lindahl, A. Schneider, P.E.A. Turchi, and W. Xiong, "Thermodynamic modelling of crystalline unary phases," Physica Status Solidi B 251, 14–32 (2014).

T. Lan, C.-W. Li, J.L. Niedziela, H. Smith, D.L. Abernathy, G.R. Rossman, and B. Fultz, "Anharmonic lattice dynamics of cuprite Ag_2O studied by inelastic neutron scattering and first principles molecular dynamics simulations," Phys. Rev. B 89, 054306 (2014).

C.-W. Li, H. Smith, T. Lan, J.A. Muñoz, J.B. Keith, L. Mauger, D. Abernathy, and B. Fultz, "Phonon anharmonicity of monoclinic zirconia and yttirum-stabilized zirconia at elevated temperatures", Phys. Rev. B, submitted.

Ph.D. theses

Chen W. Li, "Phonon anharmonicity of ionic compounds and metals," Ph.D. in Materials Science, May 4, 2012. presently: postdoctoral fellow, Materials Science Division, Oak Ridge National Lab.

Jorge Alberto Muñoz, Jr., "Electronic Structure and phonon thermodynamics of iron alloys", Ph.D. in Materials Science, May 20, 2013. presently: Intel Corporation, technical staff.

Tian Lan, "Studies of Phonon Anharmonicity in Solids" Ph.D. in Applied Physics, May 6, 2014. soon: postdoctoral fellow, Caltech.

Hillary L. Smith, "Phase Transformations and Entropy of Non-Equilibrium Materials" Ph.D. in Materials Science, May 29, 2014. soon: postdoctoral fellow, Caltech.

Non-Refereed papers and reports

R.I. Barabash, X.-L. Wang, G. Korstorz, B. Fultz, L. Levine, P.K. Liaw, "Neutron and X-Ray

Studies of Advanced Materials V-Diffraction Centennial", Metall. Mater. Trans. A 44, 15-16 (2013).

R.I. Barabash, G. Kostorz, B. Fultz and P.K. Liaw, "Neutron and X-ray Studies of Advanced Materials VI: Diffraction Centennial and Beyond Foreword," Metall. Mater. Trans. A 45, 72-74 (2014).

Neutron Scattering Studies of Classical and Quantum Fluids in Porous Media

Henry R. Glyde
Department of Physics and Astronomy
University of Delaware
Newark, Delaware 19716

Program Scope

The goal of this program is to reveal the interdependence of Bose-Einstein condensation (BEC), well-defined, collective phonon-roton (P-R) modes and superfluidity in liquid ^{4}He confined in porous media. It is particularly to determine how BEC and P-R modes create superfluidity in disorder. Of the three properties, BEC and modes are uniquely observable using neutrons. The superfluid fraction is measured in torsional oscillators [R1, R2].

When liquid ^{4}He is confined to nanoscales in porous media (in disorder), the onset temperature of superfluidity, T_C, is reduced below the bulk liquid value T_λ. The smaller the pore diameter, the further T_C, lies below T_λ. Our measurements show that the onset temperature of BEC, T_{BEC}, and P-R modes, T_{PR}, is little changed by confinement, $T_{PR} = T_{BEC} \approx T_\lambda$. Observable superflow in a porous media (in disorder) sets in at a lower temperature, T_C, when the regions of BEC that support P-R modes overlap and provide phase coherence and an energy gap throughout the whole liquid. In porous media there is a temperature range, $T_C < T < T_{BEC}$ where there is BEC and P-R modes but no superflow, much like the pseudogap phase in cuprate superconductors.

We are measuring the Bose-Einstein condensate fraction of liquid ^{4}He in the porous media MCM-41 (47 Å diameter pores) and in Vycor (70 Å diameter pores) at the Spallation Neutron Source (SNS) in collaboration with S. O. Diallo (SNS), R. T. Azuah (NIST Center for Neutron Research) and D. L. Abernathy (SNS) and at ISIS, Rutherford Appleton Lab, UK. We are also measuring the P-R modes, chiefly at the Institut Laue Langevin, in collaboration with J. Bossy, J. Ollivier and H. Schober. Thirdly, we are making path integral Monte Carlo (PIMC) calculations of the BEC condensate fraction, $n_0(T)$, and the superfluid fraction, $\rho_S(T)$, of liquid ^{4}He in pores as a function of pore diameter and temperature, for direct comparison with and improved interpretation of our experiments. Fourthly, on a quite different topic, we are demonstrating how the intrinsic motional dynamics in proteins can be obtained from neutron scattering experiments, dynamics that is independent of the instrument energy resolution [P6, P10] and the scattering wave vector [P2] used.

Recent Progress

We have recently made the first ever successful measurements of the Bose-Einstein condensate fraction of liquid ^{4}He in any porous media. This was made on the ARCS instrument at SNS on liquid ^{4}He under its saturated vapor pressure ($p \sim 0$) in the porous media MCM-41. This success follows a number of unsuccessful attempts that actually slowed progress in our program

significantly. This success has opened up new science. These measurements of BEC show unequivocally, when combined with our previous measurements of P-R modes in MCM-41, that well-defined P-R modes exist where there is BEC (in the same temperature range). This confirms theory which proposes that well-defined P-R modes exist because there is BEC. The two are common properties of a Bose condensed fluid. When combined with measurements of superfluidity in MCM-41[R2], the measurements also show that there is a temperature range, $T_C < T < T_{BEC}$, where there is BEC but no superfluidity.. The temperature range, $T_C < T < T_{BEC}$, is a range of "localized BEC" as shown in Fig. 2.

The condensate fraction, $n_0(T)$, of liquid helium in MCM-41 is shown in Fig. 1. At low temperature $n_0(T) = 3$ %. Since roughly ½ the ^{4}He in MCM-41 is solid on the MCM-41 walls, the actual n_0 in the liquid in the interior of the pores is 6 %, very close to the bulk value 7.25 %. The onset temperature for BEC, T_{BEC}, (where $n_0(T)$ goes to zero in Fig. 1) in MCM-41 is also the same as the bulk liquid value, T_λ. In bulk liquid ^{4}He, BEC and superfluidity coincide, $T_{BEC} = T_\lambda$. In MCM-41, however, the onset of superfluidity is suppressed to $T_C = 1.6$ K as shown in Fig. 2. In earlier measurements [P8], we have shown that the P-R modes exist up a temperature T_{PR}. The present measurements show that $T_{PR} = T_{BEC}$ within precision. P-R modes exist where there is BEC. Fig.2 shows the superfluid and localized BEC (LBEC) temperature ranges.

There are two competing theories of superfluidity: one based on the existence of well-defined P-R modes proposed by Landau (1941 and 1947) and the other based on BEC and consequent phase coherence in the fluid proposed initially by London (1938). Since the present measurements show that BEC and P-R are common properties of a Bose condensed fluid, the two theories are really complementary rather than competing pictures of superfluidity [P3].

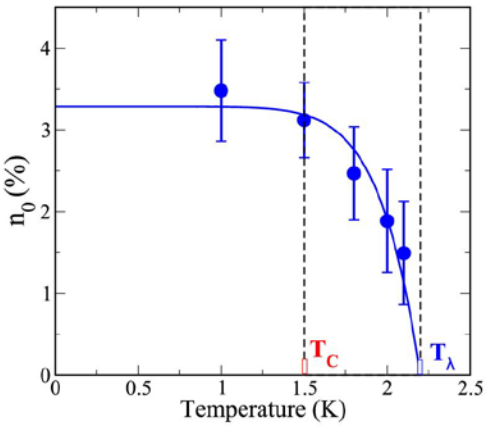

Fig.1. Bose-Einstein condensate fraction $n_0(T)$ of liquid ^{4}He in MCM-41. $n_0(T)$ goes to zero at $T_{BEC} = T_\lambda$.

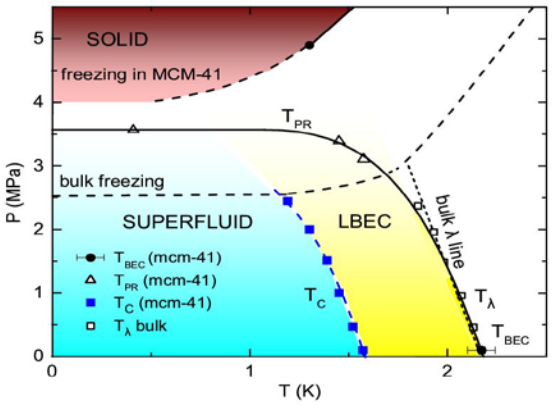

Fig.2. Phase diagram of ^{4}He in MCM-41. T_{BEC}, T_{PR}, and T_C are the highest temperatures at which BEC, P-R modes and superfluidity are observed, respectively.

Future Plans

The immediate future plan is to publish our unique, combined measurements of BEC and P-R modes and superfluidity of liquid 4He in the porous media MCM-41. The BEC and P-R modes are observed by us using neutrons and the superfluid density by our collaborators, J. Taniguchi and M. Susuki, from Chofu, Tokyo, Japan [R2]. The combined measurements show that (1) well-defined P-R modes exist where there is BEC and only where there is BEC (2) and either can be used as a basis for a theory of superfluidity, and (3) superflow in MCM-41 is suppressed to a lower temperature, T_C, leaving a temperature range where there is localized BEC that supports P-R modes but there is no superflow. This has been submitted to Nature [P3].

The successful measurements of BEC and momentum distributions, n(p) in porous media at SNS have opened new science. An immediate goal is to publish a full account of these measurements in MCM-41 and Vycor. We plan to conduct further measurements of BEC and n(p) of liquid 4He under pressure up to solidifcation (35 bar) in Vycor. The superfluid and thermal properties of liquid ^{4}He in Vycor have been extensively investigated, more in Vycor than in any other media. The aim is measurements of BEC to complement those of $\rho_S(T)$, $C_V(T)$ and P-R modes. A specific goal is to reveal how the onset temperatures of BEC, T_{BEC}, of superflow, T_C, and the peak position of $C_V(T)$ and other thermodynamic properties are related in disorder.

We have measured the P-R modes in films of liquid 4He in the porous media (2D bosons in disorder). The aim is to determine whether there is an decaying ordered state (BEC in 2D) at temperatures above the superfluid phase in 2D as in 3D. Our immediate goal is to complete the manuscript [P1].

We plan to complete extensive path integral Monte Carlo (PIMC) calculations of the superfluid fraction, $\rho_S(T)$ and the condensate fraction, $n_0(T)$ of liquid 4He in pores as a function of pore diameter and the degree of disorder. These calculations were begun in September 2013 in collaboration with Dr. L. Vranjes, University of Split, Croatia. She was a Fulbright Scholar with HRG at the University of Delaware (Sept. 2013-June 2014) at no cost this program. The calculations use the current state of the art “Worm”, PIMC algorithm. The goal is to evaluate how $\rho_S(T)$ and $n_0(T)$ are modified from their bulk liquid behavior as a function of pore diameter. Generally, the smaller the pore diameter, the lower is T_c. However, 2D behavior appears to enter. Finite size scaling analysis suggests that $\rho_S(T)$ is more 2D like than 3D like in small pores. The $n_0(T)$ is less affected by confinement but it also shows 2D behavior in small pores. These calculations will greatly enhance interpretation of our measurements in this program.

Motional mean square displacements of nuclei, particularly of H, in proteins are extensively measured in proteins using quasielastic neutron scattering. We plan to explore how the dynamical diversity of hydrogen (H) in proteins might be extracted from neutron scattering data.

In the future, we plan further measurements of the momentum distribution of liquid and solid helium confined in porous media on the ARCS instrument at SNS. Essentially, the helium in porous media is an interfacial quantum system, the quantum analog of interfacial water which has properties quite different from that of bulk water. The variation of properties as a function of filling to reveal how n(p) depends on how far the ^{4}He is from a surface is of special interest.

References

R1 Superfluidity of liquid 4He confined to one-dimensional straight nanochannel structures, J. Taniguchi, Y. Aoki, and M. Suzuki," Phys. Rev. B82, 104509 (2010).

R2 Torsional Oscillator measurements of superfluidity of liquid 4He in MCM-41
J. Taniguchi and M. Suzuki, private communication (2014)

Publications

P1. Phonon-roton modes and local order in disordered liquid ^{4}He films.
J. Bossy, H. Schober, and H. R. Glyde. Phys. Rev. B (to be submitted).

P2. Motional displacements in proteins, the origin of Q dependent values.
D. Vural, L. Hong, J. C. Smith, and H. R. Glyde. Phys. Rev. E (to be submitted).

P3. The origin of superfluidity shows new unity
S. O. Diallo, R. T. Azuah, D. L. Abernathy, J. Taniguchi, Susuki, J. Bossy, N. Mulders and H. R Glyde. Nature (submitted)

P4. Phonon-roton modes of liquid 4He beyond the roton in the porous media MCM-41
R. T. Azuah, S. O. Diallo, M. A. Adams, O. Kirichek, and H. R. Glyde.
Phys. Rev. B88, 024510 (2013).

P5. Bose-Einstein condensation measurements and superflow in condensed helium.
H. R. Glyde. J. Low Temp. Phys. 172, 364 (2013)

P6. Long-time mean-square displacements in proteins.
D. Vural, L. Hong, J. C. Smith, and H. R. Glyde. Phys. Rev. E88, 052706 (2013).

P7. Bose-Einstein condensation in liquid 4He near the liquid-solid line.
S. O. Diallo, R. T. Azuah, D. L. Abernathy, R. Rota, J. Boronat, and H. R Glyde.
Phys. Rev. B85, 140505 (2012)

P8. Excitations of amorphous solid helium.
J. Bossy, J. Ollivier, H. Schober, and H. R. Glyde. Phys. Rev. B86, 224503 (2012).

P9. Phonon-Roton modes in liquid 4He coincide with Bose-Einstein condensation.
J. Bossy, J. Ollivier, H. Schober, and H. R. Glyde. Euro. Phys. Lett. 98, 56008 (2012).

P10. Intrinsic mean-square displacements in proteins.
D. Vural and H. R. Glyde. Phys. Rev. E86, 011926 (2012).

Scattering Studies of the Liquid-Liquid Transition in Supercooled MCM41 Confined Water, Protein Hydration Water and Microstructure of New Green Cement

Sow-Hsin Chen
Department of Nuclear Science and Engineering, Massachusetts Institute of Technology

Program Scope: Neutron and X-Ray Scattering Studies of the Liquid-Liquid Transition in Supercooled Confined Water and the Phonon-Like Collective Excitation in Globular Proteins

Recent Progress

A. Evidence of the existence of both high- & low-density phases in deeply-cooled confined heavy water under high pressures, and the phase diagram of the deeply-cooled confined heavy water

We study the density of D_2O confined in a nanoporous silica matrix (MCM-41) with neutron scattering. We determine the phase diagram of the deeply-cooled confined heavy water by detecting the density hysteresis phenomenon under different pressures. The phase diagram obtained here is shown in Fig. 1.

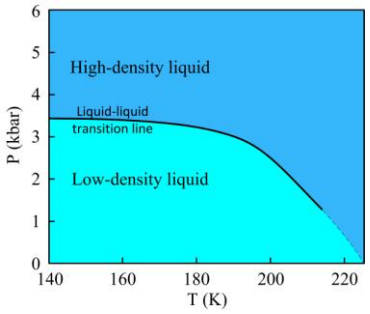

Fig. 1. The phase diagram of the deeply- cooled heavy water confined in MCM-41 [1].

In order to confirm the above phase diagram, we measure the average density of the confined heavy water ρ_{D2O} in both sides of the liquid-liquid transition line (LLTL). The result shows that ρ_{D2O} in the high-density liquid (HDL) region is higher than that in the low-density liquid (LDL) region by ~16%. In addition, the isothermal compressibility in the LDL region is smaller than that in the HDL region. This phenomenon shows that the LDL phase is more rigid than the HDL phase, and is consistent with the structure difference between LDL and HDL.

B. The Boson Peak in deeply-cooled confined water: A possible way to explore the existence of the liquid-liquid transition in water

The Boson peak is a broad peak observed at low frequencies (2 - 10 meV) in the inelastic neutron, X-ray and Raman scattering spectra of many amorphous materials and supercooled liquids. It is widely believed that the Boson peak originates from the collective vibrations of the condensed matter. We systematically investigated the Boson peak in the supercooled water confined in the MCM-41 at different pressures and temperatures. We find that the Boson peak is a possible way to explore the existence of the liquid-liquid transition in water [2].

We study the Boson peak in deeply-cooled water confined in nanopores with inelastic neutron scattering. The quantitative analysis suggests that the frequency of Boson peak and the density of the deeply-cooled water are positively correlated. The width of the Boson peak also exhibits such a behavior. This result is of particular importance to water. In the LLCP hypothesis, the order parameter to distinguish the low-density liquid (LDL) phase and the high-density liquid (HDL) phase is just the density. With this in mind, one may distinguish the hypothetical LDL and HDL phases in deeply-cooled water by looking at the shape of the Boson peak. In other words, the frequency or the width of the Boson peak may exhibit abrupt change as the water transforms

between LDL and HDL, due to significant differences in density and local structure of the different sides of the hypothetical first order transition line between LDL and HDL.

C. Hydration water in proteins: key to the "softening" of the short time intraprotein collective vibrations of a specific length scale [3,4]

Protein exhibits phonon-like excitations based on collective vibrations in the sub-picosecond time scale. In our previous works, we observed that as the temperature increases from 200 K to the physiological temperature, the energies of the intraprotein phonon-like excitations significantly decrease. We call this phenomenon "phonon energy softening". At the same time, the phonon population also increases. Such "phonon energy softening" phenomenon can also be observed by increasing the hydration level of protein sample in a certain range. Understanding of these phenomena is important for clarifying the essence of the intraprotein short time collective vibration and its relation to the protein enzymatic function. By using the inelastic X-ray scattering (IXS) method, here we investigated the effect of the protein native structure and the hydration water on the intraprotein short time collective vibrations. The result shows that the protein hydration water, rather than the protein native structure, plays a central role in intraprotein short time collective vibrations.

Fig. 2 (a) and (c) show the dispersion relations of the native lysozyme and denatured lysozyme. Fig. 2 (b) and (d) show the area of the Brillouin peaks, which is propotional to the phonon population, of the above mentioned two samples. Both samples are with the hydration level of 0.3. For the denatured sample, nearly all the tertiary structures are removed, and a large amount of the secondary structures are destroyed.

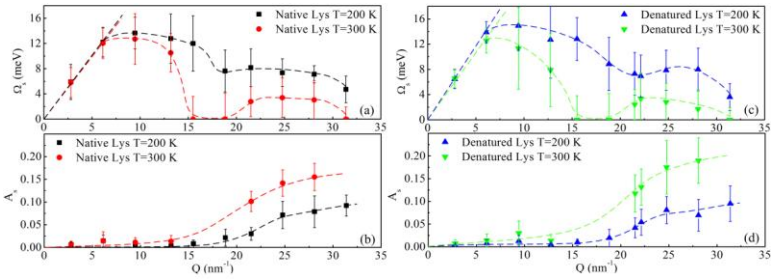

Fig, 2. (a) Dispersion relations of the phonon-like excitations and (b) fractional area of the Brillouin peaks A_s at T = 200 K and 300 K for hydrated native lysozyme. (c) Dispersion relations of the phonon-like excitations and (d) fractional area of the Brillouin peaks A_s at T = 200 K and 300 K for hydrated denatured lysozyme.

From Fig. 2 one can find that the dispersion relations of these two samples are very similar: for both of them, as temperature increases from 200 K to 300 K, the energies of the phonon-like excitations decreases significantly in the Q range from 14 to 30 nm^{-1}. This phenomenon shows that the "phonon energy softening" phenomenon is not directly related to the protein native structure. The weak dependence of the "Phonon energy softening" on the tertiary and secondary structures indicates that this intriguing phenomenon may be closely related to the protein environment, i.e., the hydration water. Therefore a dry lysozyme sample was measured. Its dispersion relation and the fractional area of the Brillouin peaks are shown in Fig. 3(a) and (b) respectively. From Fig. 3(a) one can find that for the lysozyme without water, the "phonon energy softening" is considerably suppressed within Q < 24 nm^{-1}. This indicates that the hydration water plays a key role in the onset of the "phonon energy softening".

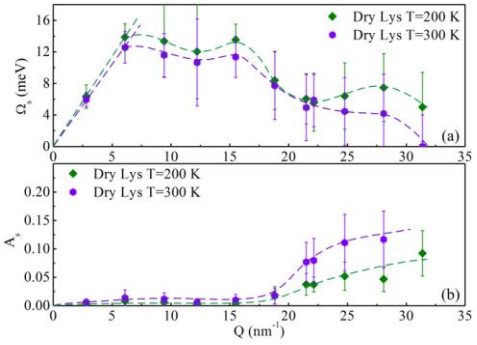

Fig. 3. (a) Dispersion relations of the phonon-likeexcitations and (b) fractional area of the Brillouin peaks A_s at T = 200 K and 300 K for the dry lysozyme. The dashed lines are drawn as a guide to the eye.

D. SAXS study on the microstructure of M-S-H gels show that the "globule" is composed of poly-dispersed spheres, which pack into a smaller and more compact fractal structure having weak mutual interactions due to the point contact of the spheres

Although the ordinary concrete based on CaO is the world's most widely used building material, its production generates large amounts of anthropogenic emitted CO_2. Therefore, one of the main challenges in the cement industry is to develop alternative binders that have similar mechanical robustness but generate less CO_2. Recently, a strong attention has been focused on hydraulic binders based on highly reactive periclase (MgO). This oxide reacts with water and a silica source, forming an amorphous solid phase magnesium-silicate-hydrate ($(MgO)_x$-SiO_2-$(H_2O)_y$ abbreviated as M-S-H) responsible for the structural arrest of the hydrated matrix ("setting" of cement). The newly developed MgO-based cements, though currently still suffering from inferior mechanical properties, can be generated with far less CO_2 emissions. We identify differences in the multiscale structure of the two hydrates: C-S-H gel for CaO-based cements and M-S-H gel for MgO-based cements. By combining wide-angle X-ray scattering (WAXS), SAXS, and SEM, we found the primary unit at the nanoscale level of C-S-H to be a multilayer disk-like globule, whereas for M-S-H it is a spherical globule [5]. These primary units organize themselves to form fractal structures below the micrometer length-scale. The globules pack more compactly in the fractal of the M-S-H case even though the fractal domain is much smaller. The difference in the microstructure of the C-S-H and M-S-H gels can be illustrated as Fig. 4. Structure at nanometer to submicrom length-scale and morphology at micrometer length-scale of C-S-H all suggest a stronger binding force and better mechanical properties because both of the multilayer disk-like globules and foil-like objects in C-S-H have contact rather than point contact between the spherical particles found in M-S-H gel. Finally, results from WAXS, SAXS, and SEM all suggest that the interaction between the fractal structures of C-S-H and M-S-H is negligible in the blend sample although the domains of both fractals become much smaller as indicated by SAXS analysis. Therefore, increasing the interaction between the C-S-H and M-S-H particles can be a potential way to solve the compatibility issue.

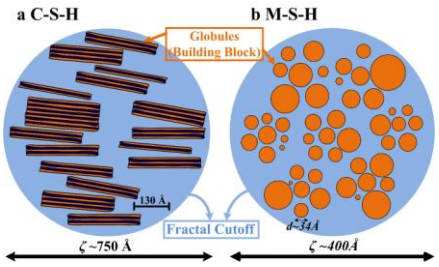

Fig. 4. The illustration of the microstructure of (**a**) C-S-H (Ca/Si=1) and (**b**) M-S-H (Mg/Si=1) both synthesized by double-decomposition of solutions. The big light-blue circles show the cutoff of the fractal structures within which there are globules with different shapes and size distributions. The orange part represents the Ca or Mg silicate hydrate and the dark-blue part, only shown in panel (**a**), denotes the interlayer water [5].

Future Plans

The future plan is to carry out further research developments of the activities described in Plans A-D as described above. More attention is expected to be given to the research development of "Green Cement" described in Plan D.

References

[1] Z. Wang, K.-H. Liu, L. Harriger, J. B. Leão and S.-H. Chen, "Evidence of the existence of the high-density and low-density phases in deeply-cooled confined heavy water under high pressures", *J. Chem. Phys.* (accepted, June 2014).

[2] Z. Wang, K.-H. Liu, P. Le, M. Li, W.-S. Chiang, J. B. Leão, J. R. D. Copley, M. Tyagi, A. Podlesnyak, A. I. Kolesnikov, C.-Y. Mou and S.-H. Chen, "Boson Peak in Deeply Cooled Confined Water: A Possible Way to Explore the Existence of the Liquid-to-Liquid Transition in Water", *Phys. Rev. Lett.*, **112** 237802 (2014).

[3] Z. Wang, C. E. Bertrand, W.-S. Chiang, E. Fratini, P. Baglioni, A. Alatas, E. E. Alp and S.-H. Chen, "Inelastic X-ray Scattering Studies of the Short-Time Collective Vibrational Motions in Hydrated Lysozyme Powders and Their Possible Relation to Enzymatic Function", *J. Phys. Chem. B*, **117** 1186 (2013).

[4] Z. Wang, W.-S. Chiang, P. Le, E. Fratini, M. Li, A. Alatas, P. Baglioni and S.-H. Chen, "One Role of Hydration Water in Proteins: Key to the 'Softening' of Short Time Intraprotein Collective Vibrations of a Specific Length Scale", *Soft Matter*, **10** 4298 (2014).

[5] W. S. Chiang, G. Ferraro, E. Fratini, F. Ridi, Y. Q. Yeh, U S. Jeng, P. Baglioni and S. H. Chen, "Multiscale structure of calcium- and magnesium-silicate-hydrate gels", *J. Mater. Chem. A.*, (accepted June, 2014).

Publications

1. Li, H., W.-S. Chiang, E. Fratini, F. Ridi, F. Bausi, P. Baglioni, M. Tyagi and S.-H. Chen, "Dynamic Crossover in Hydration Water of Curing Cement Paste: The Effect of Superplasticizer" *J. Phys.: Condens. Matter*, **24** 064108 (2012).
2. P. Gallo, M. Rovere and S.-H. Chen, "Water Confined in MCM-41: A Mode Coupling Theory Analysis" *J. Phys.: Condens. Matter*, **24**, 064109 (2012).
3. Y. Zhang, M. Tyagi, E. Mamontov and S.-H. Chen, "Quasi-Elastic Neutron Scattering Studies of the Slow Dynamics of Supercooled and Glassy Aspirin" *J. Phys.: Condens. Matter*, **24** 064112 (2012).
4. F. Mallamace, C. Corsaro, P. Baglioni, E. Fratini and S.-H. Chen, "The Dynamical Crossover Phenomenon in Bulk Water, Confined Water and Protein Hydration Water" *J. Phys.: Condens. Matter*, **24** 064103 (2012).
5. W.-S. Chiang, E. Fratini, P. Baglioni, D. Liu and S.-H. Chen, "Microstructure Determination of Calcium-Silicate-Hydrate Globules by Small-Angle Neutron Scattering" *J. Phys. Chem. C.*, **116** 5055 (2012).
6. H. Li, E. Fratini, W.-S. Chiang, P. Baglioni, E. Mamontov and S.-H. Chen, "Dynamic Behavior of Hydration Water in Calcium-Silicate-Hydrate Gel: A Quasielastic Neutron Scattering Spectroscopy Investigation" *Phys. Rev., E* **86** 061505 (2012).
7. E. Fratini, A. Faraone, F. Ridi, S.-H. Chen and P. Baglioni, "Hydration Water Dynamics in Tricalcium Silicate Pastes by Time-Resolved Incoherent Elastic Neutron Scattering" *J. Phys. Chem.*, **C117** 7358 (2013).
8. S.-H. Chen, Z. Wang, A. I. Kolesnikov, Y. Zhang and K.-H. Liu, "Search for the First-Order Liquid-to-Liquid Phase Transition in Low-Temperature Confined Water by Neutron Scattering", *AIP Conf. Proc.*, **1518** 77 (2013).
9. C. E. Bertrand, Y. Zhang and S.-H. Chen, "Deeply-cooled Water Under Strong Confinement: Neutron Scattering Investigations and the Liquid-liquid Critical Point Hypothesis", *Phys. Chem. Chem. Phys.*, **15** 721 (2013).

10. Z. Wang, C. E. Bertrand, W.-S. Chiang, E. Fratini, P. Baglioni, A. Alatas, E. E. Alp and S.-H. Chen, "Inelastic X-ray Scattering Studies of the Short-Time Collective Vibrational Motions in Hydrated Lysozyme Powders and Their Possible Relation to Enzymatic Function", *J. Phys. Chem. B*, **117** 1186 (2013).
11. W.-S. Chiang, E. Fratini, F. Ridi, S.-H. Lim, Y.-Q. Yeh, P. Baglioni, S.-M. Choi, U-S. Jeng and S.-H. Chen, "Microstructural Changes of Globules in Calcium", *J. Colloid Interface Sci.*, **398** 67 (2013).
12. C. E. Bertrand, K.-H. Liu, E. Mamontov and S.-H. Chen, "Hydration-dependent dynamics of deeply cooled water under strong confinement", *Phys. Rev. E*, **87** 042312 (2013).
13. C. E. Bertrand, W.-S. Chiang, M. Tyagi and S.-H. Chen, "Low-temperature water dynamics in an aqueous methanol solution", *J. Chem. Phys.*, **139** 014505 (2013).
14. K.-H. Liu, Y. Zhang, J.-J. Lee, C.-C. Chen, Y.-Q. Yeh, S.-H. Chen and C.-Y. Mou, "Density and anomalous thermal expansion of deeply cooled water confined in mesoporous silica investigated by synchrotron X-ray diffraction", *J. Chem. Phys.*, **139** 064503 (2013).
15. F. Mallamace, C. Corsaro, H. E. Stanley, D. Mallamace and S.-H. Chen, "The dynamical crossover in attractive colloidal systems", *J. Chem. Phys.*, **139** 214502 (2013).
16. F. Mallamace, C. Corsaro, N. Micali, V. Villari, N. Leone and S.-H. Chen, "The fragile to strong dynamical crossover in supercooled liquids. The o-terphenyl case and its ergodicity at the dynamical arrest", *AIP Conf. Proc.*, **1518** 67 (2013).
17. F. Mallamace, C. Corsaro, N. Leone, V. Villari, N. Miicali and S.-H. Chen, "On the ergodicity of supercooled molecular glass-forming liquids at the dynamical arrest: the o-terphenyl case", *Nature: Sci. Reports*, **4** 3747 (2014).
18. W.-S. Chiang, G. Ferraro, E. Fratini, F. Ridi, Y.-Q. Yeh, U. S. Jeng, P. Baglioni and S. H. Chen, "Multiscale structure of calcium- and magnesium-silicate-hydrate gels", *J. Mater. Chem. A., accepted* (June 2014)
19. Z. Wang, W.-S. Chiang, P. Le, E. Fratini, P. Baglioni, A. Alatas, M. Li and S.-H. Chen, "One Role of Hydration Water in Protein: Key to the 'Softening' of Short Time Intraprotein Collective Vibrations of Specific Length Scale", *Soft Matter*, **10** 4298 (2014).
20. Z. Wang, K.-H. Liu, P. Le, M. Li, W.-S. Chiang, J. B. Leão, J. R. D. Copley, M. Tyagi, A. Podlesnyak, A. I. Kolesnikov, C.-Y. Mou and S.-H. Chen, "Boson Peak in Deeply Cooled Confined Water: A Possible Way to Explore the Existence of the Liquid-to-Liquid Transition in Water", *Phys. Rev. Lett.*, **112** 237802 (2014).
21. Z. Wang, K.-H. Liu, L. Harriger, J. B. Leão and S.-H. Chen, "Evidence of the existence of the high-density and low-density phases in deeply-cooled confined heavy water under high pressures", *J. Chem. Phys.*, accepted (June 2014).
22. Z. Wang, E. Fratini, M. Li, P. Le, E. Mamontov, P. Baglioni and S.-H. Chen, "Hydration-Dependent Dynamic Crossover Phenomenon of Protein Hydration Water", *submitted for publication* (2014).
23. F. Mallamace, P. Baglioni, C. Corsaro, S.-H. Chen, D. Mallamace, C. Vasi, and H. E. Stanley, "The Influence of Water on Protein Activity", *submitted for publication* (2014).

Inelastic Neutron and X-ray Scattering Investigation of Electron-Phonon Effects in Quantum Materials

Dmitry Reznik (dmitry.reznik@colorado.edu), S. Anisimova, D. Parshall, S.-R. Park, J-Y. Yang.
Department of Physics, University of Colorado-Boulder, Boulder, CO 80309.

Research Scope

Many quantum materials, i.e. materials where quantum effects are crucial for key properties, undergo phase transitions driven by electronic charge and/or spin fluctuations. These fluctuations influence electrical and thermal conductivity, specific heat, thermal expansion, etc. Coulomb/magnetoelastic coupling of charge/spin fluctuations to the atomic lattice can induce competing or mutually reinforcing phenomena such as real or incipient structural phase transitions and superconductivity.

My group focuses on inelastic scattering of neutrons (INS) or x-rays (IXS) from atomic lattice fluctuations coupled to *charge/spin fluctuations associated with real and/or incipient phase transitions in quantum materials*. These lattice fluctuations are either phonons or incoherent fluctuations. During the last two years we 1) directly measured the spectrum of dynamic charge stripes for the first time; 2) found evidence of a novel charge collective mode that correlates with the superconducting T_c in a family of copper oxides; 3) clarified the origin of the kink in electronic dispersions in cuprates, 4) Developed a new *Multizone Phonon Refinement (MPR)* time-of-flight data analysis technique that clearly resolves phonon branches separated by as little as 10% of the energy resolution by using data from all measured Brillouin zones. Thanks to MPR an efficient and systematic search for electron-phonon effects in a wide variety of materials is now possible.

Recent Progress

Detection of dynamic charge stripes. In layered compounds, such as $La_{2-x}Sr_xNiO_4$ and $La_{2-x}Ba_xCuO_4$, doped charge carriers can segregate into periodically-spaced charge stripes separating narrow domains of antiferromagnetic order. Although the phase transition to the static stripe phase takes place only in a few special compounds, the role of incipient stripe formation characterized by dynamic (fluctuating) stripes is still not understood. There have been theoretical proposals of dynamically fluctuating stripes, but direct spectroscopic evidence of their charge component has been lacking.

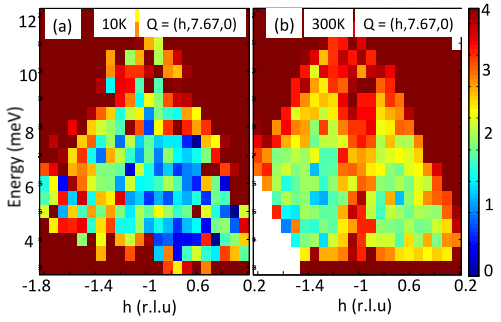

Figure 1. A momentum-energy cut through the stripe-ordering wavevector in $La_{1.67}Sr_{0.33}NiO_4$: Q=(-1,7.67,0). High intensity in the corners in both panels is due to acoustic phonons that are not interesting. At 10K (a) there is no signal near h=1, whereas at 300K (b) a column of scattering intensity from dynamic stripes is clearly visible. Data are from ARCS.

We directly observed and carefully characterized the dynamic charge stripe spectrum in $La_{2-x}Sr_xNiO_4$. [1] The spectrum of these lattice fluctuations is narrow in **q** and broad in energy and appears only above the temperature where *magnetic* stripes melt. For example, Figure 1 shows that there is no signal at 10K, but a column of scattering at the stripe-ordering wavevector **Q**=(-1,7.67,0) is clearly seen at 300K. Our results opened the way towards the quantitative theory of dynamic stripes and for directly detecting them in other systems, including copper oxide superconductors. This work showcased the effectiveness of using pulsed and reactor

sources in tandem by combining surveys of reciprocal space on the ARCS spectrometer with detailed temperature-dependent studies on triple-axis spectrometers at HFIR and at Saclay.

Electron-phonon and related effects in cuprates. Discovery of the giant electron-phonon anomaly in the Cu-O bond-stretching branch in $La_{2-x}Sr_xCuO_4$ and $La_{1.875}Ba_{0.125}CuO_4$ implied that strong low-energy charge fluctuations are present in cuprates. My group showed that this anomaly was strongest near optimal doping and disappeared in nonsuperconducting compositions. Our quantitative measurements correlated the phonon anomaly with other experiments. [2,3] The phonon branch of interest is the Cu-O longitudinal bond-stretching branch (Cu and O vibrating against each other) dispersing in the [100]-direction from the zone center energy of 85meV. The zone boundary for this dispersion is at **q**=(.5,0,0). The giant phonon anomaly is characterized by a large linewidth enhancement and softening near **q**=(0.25,0,0). [3]

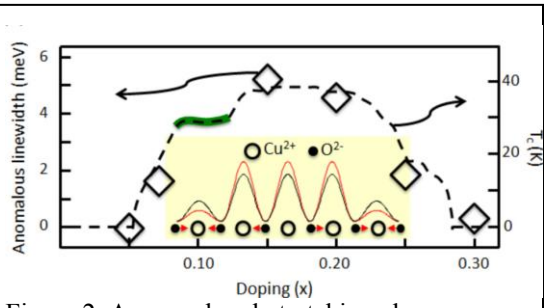

Figure 2. Average bond-stretching phonon "anomalous" linewidths near half-way to the zone boundary as a function of doping. Dashed line represents T_c of LSCO. Green solid line indicates a plateau of T_c that may originate from competition with another order parameter such as stripes. Inset illustrates coupling between the Cu-O bond stretching mode and electronic density fluctuations at h = 0.25. Black and red lines indicate charge densities with and without atomic displacements (red arrows), respectively.

In superconducting copper oxides electronic dispersion kinks are near 70 meV, which is close to the energy of the phonon showing the giant electron-phonon anomaly. These observations suggest that phonon broadening may originate from quasiparticle excitations across the Fermi surface and the electronic dispersion kinks may originate from coupling to anomalous phonons. We compared the doping dependence of the strength of the phonon anomaly with the doping dependence of the strength of the ARPES kink, which we also measured. [2] These doping-dependences turned out to be very different, i.e. the two phenomena are not connected. We showed that the phonon anomaly likely originates from novel collective charge excitations (somehow analogous to plasmons) as opposed to interactions with electron-hole pairs. Their amplitude follows the superconducting dome (Fig. 2), so these charge modes may be important for superconductivity. It is intriguing that the wavevector of the giant phonon anomaly is the same as the wavevector of charge stripes discussed above. At the moment the connection with stripes is possible, but it has not been proven.

Development of a new, better, method to measure phonons in materials with large unit cell at the SNS: Multizone phonon refinement. Fe-based superconductors exhibit a sensitive interplay between the lattice and magnetic degrees of freedom (e.g., the crystal structure is better reproduced by magnetic than nonmagnetic DFT calculations). However, it is not known what effect, if any the long-range magnetic order has on phonons above 28 meV where several branches are very close in energy and it is extremely difficult to isolate them from each other. So we developed a new method to measure phonons in such materials. In order to be able to search for phonon anomalies in these closely-spaced branches, we developed multizone phonon refinement (MPR). [8] It works well for extracting phonon frequencies and linewidths from chopper spectrometer data even when phonon frequencies are an order of magnitude closer than the experimental resolution. It is based on a global fit to the data in many Brillouin zones. (See Fig. 3) We successfully applied this method to measure high energy phonons in $SrFe_2As_2$.

After measuring these phonons on ARCS in ≈ 40 Brillouin zones, we used MPR to determine phonon frequencies and eigenvectors. Although some raw data scans showed hints of nontrivial temperature dependence, we found that these phonons are conventional and soften with the thermal expansion of the atomic lattice. Experimental dispersions agreed with DFT calculations of our collaborators. Magnetic transition had no effect on phonons.

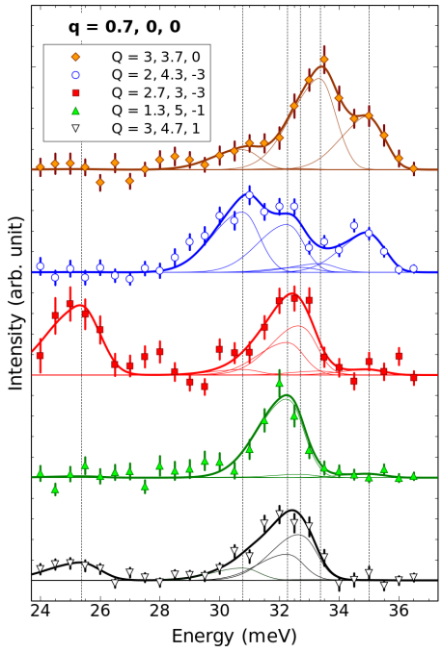

Figure 3. Phonon spectra of $SrFe_2As_2$ at **q**= [0.7, 0, 0] in 5 Brillouin zones (out of 154 symmetry points used for the fitting). The data are vertically offset for clarity. There are 6 phonons in this energy range. The refined values of the centers obtained with MPR are shown by the vertical dashed lines. The individual phonons are shown with thin lines, and the overall fit obtained with solid lines.

Future Plans

The new generation of neutron scattering user facilities brings qualitatively new experimental capabilities. For inelastic scattering, it is producing complete maps of reciprocal space of single crystal samples. The idea behind MPR (see above) of routinely measuring phonons in many different Brillouin zones is new compared with the way phonons are measured by the triple-axis technique: one wavevector at a time. This capability makes the complex art of knowing in advance, which Brillouin zone is the best for which phonon, unnecessary. Thus one can envision a future, when measurements of the complete phonon spectrum become as routine as the measurements of the electrical conductivity once a big enough single crystal sample of a new material is made. So far we demonstrated that MPR works well in conjunction with DFT calculations of phonons and on high quality datasets. In the future we would like to extend the MPR method to cases when no DFT results are available and to cases where statistics are insufficient to extract phonon peak positions and linewidths from a single Brillouin zone.

The long-term goal of our research is to learn how to use observed features of lattice dynamics spectra as markers of microscopic physics of quantum materials responsible for their macroscopic properties of fundamental and practical interest. In this context one benefit of the new capability of MPR to generate complete experimental phonon spectra in a straightforward way is to use these spectra to calculate physical properties that directly derive from phonons such as the lattice specific heat, thermal conductivity, thermal expansion, etc. In fact we will attempt to calculate phonon thermal conductivity of a thermoelectric compound in this way.

The second benefit is that *such datasets can be mined for signatures of hidden inner workings of quantum materials* such as charge fluctuations, Fermi surface nesting, electron-phonon coupling incipient phase transitions etc. While extending capabilities of MPR, we would like to uncover new microscopic mechanisms behind electron-lattice effects in carefully selected specific compounds, so that ultimately it will be possible to go in the opposite direction: Observation of similar effects in new materials will point at the underlying physics.

Publications

1. S. Anissimova, D. Parshall, G. D. Gu, K. Marty, M. D. Lumsden, Songxue Chi, J. A. Fernandez-Baca, D. L. Abernathy, D. Lamago, J. M. Tranquada, D. Reznik, " Direct observation of dynamic charge stripes in $La_{1.67}Sr_{0.33}NiO_4$," Nature Communications, **5**, 3467 (2014).
2. S. R. Park, Y. Cao, Q. Wang, M. Fujita, K. Yamada, S.-K. Mo, D. S. Dessau, and D. Reznik, "Broken relationship between superconducting pairing interaction and electronic dispersion kinks in $La_{2-x}Sr_xCuO_4$ measured by angle-resolved photoemission," Phys. Rev. B Rapid Comm. **88**, 220503 (2013))
3. S. R. Park, T. Fukuda, A. Hamann, D. Lamago, L. Pintschovius, M. Fujita, K. Yamada, and D. Reznik, "Evidence for a charge collective mode associated with superconductivity in copper oxides from neutron and x-ray scattering measurements of $La_{2-x}Sr_xCuO_4$," Phys. Rev. B Rapid Comms. **89**, 020506 (2014).
4. F. Weber, R. Hott, R. Heid, K.-P. Bohnen, S. Rosenkranz, J.-P. Castellan, R. Osborn, A. H. Said, B. M. Leu, and D. Reznik, "Optical phonons and the soft mode in 2H-$NbSe_2$," Phys. Rev. B **87**, 245111 (2013)
5. F. Weber, D. N. Argyriou, O. Prokhnenko, and D. Reznik,"Large lattice distortions associated with the magnetic transition in $La_{0.7}Sr_{0.3}MnO_3$," Phys. Rev. B Rapid Communications **88**, 241106 (2013))
6. F. Weber, L. Pintschovius, W. Reichardt, R. Heid, K.-P. Bohnen, A. Kreyssig, D. Reznik, K. Hradil, " Phonons and electron-phonon coupling in the phonon-mediated superconductor YNi_2B_2C," Phys. Rev. B **89**, 104503 (2014).
7. D. Parshall, G. Chen, L. Pintschovius, D. Lamago, Th. Wolf, L. Radzihovsky, and D. Reznik," Competition between commensurate and incommensurate magnetic ordering in $Fe_{1+y}Te$," Phys. Rev. B Rapid Communications **85**, 140515 (2012).
8. D. Parshall, R. Heid, J. L. Niedziela, Th. Wolf, M. B. Stone, D. L. Abernathy, and D. Reznik, "Phonon spectrum of $SrFe_2As_2$ determined using multizone phonon refinement," Phys. Rev. B **89**, 064310 (2014).
9. D. Reznik, "Phonon anomalies and dynamic stripes," Physica C **481**, 75 (2012).
10. Lothar Pintschovius, Dmitry Reznik, Frank Weber, Philippe Bourges, Dan Parshall, Ranjal Mittal, Samrath LaI Chaplot, Rolf Heid, Thomas Wolf, Daniel Lamago, and Jeffrey W. Lynn, "Spurious Peaks Arising from Multiple Scattering Events the Sample Environment in Inelastic Neutron Scattering" J. Appl. Cryst. **47**, (2014, in press).

Vortex Lattices Studies in Type II Superconductors

M. R. Eskildsen (eskildsen@nd.edu)
Department of Physics, University of Notre Dame, Notre Dame, IN 46556

Program Scope

The program centers on the study of vortices and the vortex lattice (VL) in type-II superconductors and has two main themes.

The first is fundamental studies of superconductivity. The formation and condensation of Cooper pairs varies for different materials, and in many cases the exact microscopic mechanism remains elusive. An important step towards a microscopic understanding is detailed knowledge of the order parameter. This is especially important in materials such as UPt_3 and Sr_2RuO_4 where the carriers in the Cooper pairs are believed to form a triplet, but where the detailed order parameter is not well established. We use the vortices to probes the intrinsic nature of the superconducting state in unconventional and/or new materials.

The second theme is the study of vortex matter dynamics and in particular the recently discovered metastable VL phases in MgB_2. Vortex motion will lead to dissipation and is responsible for limitations in the critical electrical current density and of direct importance to the practical use of superconductors. However, the VL metastability is not due to traditional vortex pinning and instead it appears to be due to VL domain effects. This has opened up a new direction in the study of vortex dynamics with analogues to jamming in granular materials.

Recent Progress

Vortex lattice studies in Sr_2RuO_4

Despite intense studies the exact nature of the order parameter in Sr_2RuO_4 (SRO) has remained elusive. Multiple experimental and theoretical studies provide compelling support for triplet pairing and an odd-parity, *p*-wave order parameter symmetry [1,2]. At the same time, seemingly contradictory experimental results leaves important open questions concerning the detailed structure and coupling of the orbital and spin parts of the order parameter [3].

The Fermi surface in SRO consists of three sheets with Fermi velocity anisotropies ranging from 57 to 174 [1], and one would expect an upper critical field (H_{c2}) anisotropy within this range. Experiments, however, find a much smaller $\Gamma_{Hc2} = 20$ at low temperature and a near constant H_{c2} when the applied field is within $\pm 2°$ of the basal plane [2]. Within the same angular range the transition at H_{c2} becomes

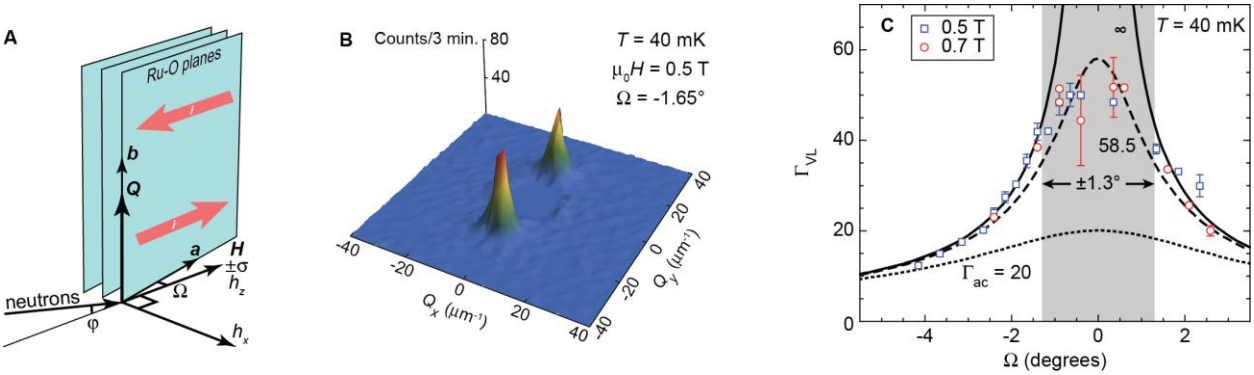

Fig. 1 SANS VL measurements in Sr_2RuO_4. (A) Experimental geometry, showing the "misalignment" angle (Ω) and the currents (red arrows) giving rise to the transverse magnetization. (B) Spin flip scattering due to the transverse VL magnetization. (C) VL anisotropy vs. Ω. The fit to the data is for a superconducting anisotropy $\Gamma_{ac} = 58.5 \pm 2.3$.

first order, suggesting a subtle coupling between the magnetic field and the triplet order parameter [4], or Pauli limiting, which is inconsistent with triplet pairing with the Cooper pair zero spin projection along the *c*-axis [5].

We have performed extensive small-angle neutron scattering (SANS) studies of the VL in Sr_2RuO_4 with the field applied close to the *ab*-plane in order to measure the intrinsic anisotropy of the superconducting state. Taking advantage of the transverse magnetization in this highly anisotropic superconductor, we were able to measure the VL anisotropy as a function of the field angle and determine the intrinsic superconducting anisotropy (Γ_{ac}) between the *c*-axis and the Ru-O basal planes, see Fig. 1. The value of $\Gamma_{ac} \approx 60$ is much larger than Γ_{Hc2} , and is found to be largely independent of field and temperature. Our result imposes significant constraints on possible models of triplet pairing in SRO and raises questions concerning the direction of the zero spin projection axis.

Vortex lattice studies in UPt_3

One of the most striking properties of UPt_3 is the fact that the *H-T* superconducting phase diagram has three distinct mixed (vortex) phases that can only be explained by an unconventional superconducting order parameter [6]. Like the case of SRO a complete theoretical description of the superconducting state of UPt_3 has not been settled.

The order parameter structure that is consistent with a number of experiments is an odd-parity, *f*-wave (*L*=3) orbital state of E_{2u} symmetry [7,8]. However, with some success, comparisons with experiment have also been made for an even-parity, *d*-wave (*L*=2) orbital state of E_{1g} symmetry [9]. Both order parameters are chiral and break time reversal symmetry in the low temperature B-phase. In contrast, a recent proposal for an odd-parity, *f*-wave (*L*=3) model with E_{1u} orbital symmetry is non-chiral and time reversal symmetric in the B-phase [10]. All of these order parameters have nodes in the superconducting energy gap, each with different nodal structure in the three vortex phases.

Using SANS from the VL, we have measured the temperature dependence of the components of the London penetration depth, $\lambda_i(T)$, that probe the gap nodal structure along the principal directions of the crystal finding a linear behavior in the low temperature limit. Our measurements, shown in Fig. 2 (left panel), are consistent with calculations based on an order parameter with E_{2u} symmetry.

To investigate possible effects of a chiral phase on the VL, SANS measurements were performed ***H*** || ***c*** following different *H-T* histories, see Fig. 2 (right panel). These showed a field-dependent azimuthal splitting of the vortex lattice Bragg reflections, indicating a rotation of the vortex lattice away from the

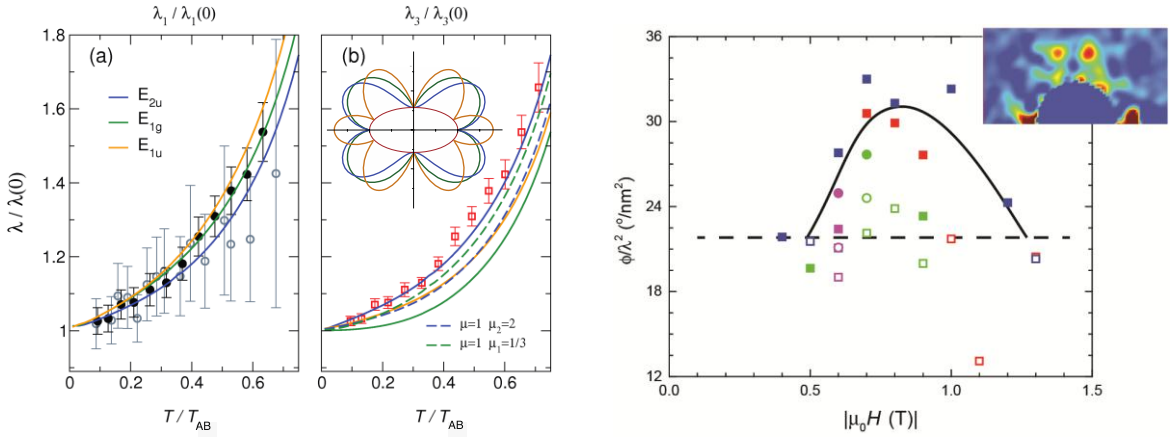

Fig. 2 SANS VL measurements in the B-phase of UPt_3. Left: Temperature dependence of the measured penetration depth along (a) the *a*-axis (λ_1) and (b) the *c*-axis (λ_3). The data is best described by calculations using on a E_{2u} symmetry. Right: Scaled VL splitting (ϕ) for ***H*** || ***c***. Solid (open) symbols correspond to measurements performed without (following) a field reversal.

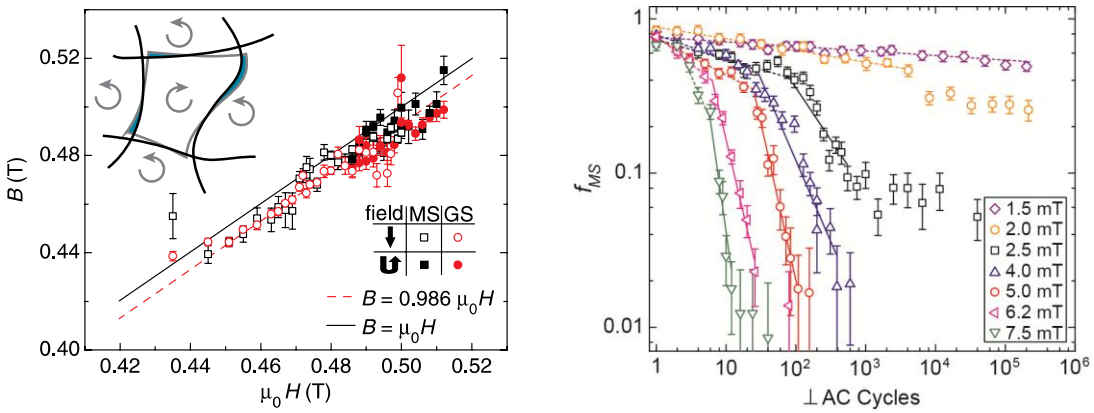

Fig. 3 SANS VL measurements in MgB_2. Left: Magnetic induction determined from the magnitude of the VL scattering vector and showing that both metastable (open symbols) and ground state (solid symbols) VL domains expand/compress as a function of applied field. Right: Metastable VL volume fraction as a function of applied AC magnetic field cycles.

high-symmetry crystalline directions. Most notably a difference in the splitting was observed between measurements following a reduction of the fields from above H_{c2} to respectively a positive and negative field. However, the splitting was found to scale with the neutron wavelength, complicating the interpretation of the results and necessitating further measurements. Still, the measurements strongly suggesting a coupling between the vortex lattice and a chiral superconducting state in UPt_3.

Vortex lattice metastability in MgB_2

The VL configuration is known to depend sensitively on the anisotropy of the screening current plane in the host superconductor. As a result, field- and/or temperature-driven symmetry and reorientation transition are common. In MgB_2 the hexagonal VL undergoes a 30°, second-order rotation transition that is most likely due to a suppression of the superconducting π-band [11]. Surprisingly, the VL exhibits extensive metastability in connection with this transition as discovered by our group a few years ago.

Using SANS we recently observed that a fraction of the VL remain in the metastable configuration even in the presence of significant vortex motion, as shown in Fig. 3 (left panel). This demonstrates conclusively that the metastability is not due to vortex pinning, but rather must be understood in terms of interacting VL domains. This opens up an entirely new direction in studies of collective vortex behavior.

To further investigate the VL metastability and specifically the dynamics governing the transition to the ground state, we have performed extensive measurements subjecting the VL to an increasing number of small-amplitude AC magnetic field oscillations. Fig. 3 (right panel) shows the metastable VL volume fraction as a function of applied AC cycles for a range of amplitudes. In all cases we observe a cross-over from a slow to a fast power law, and with a transitioning that decrease with increasing AC amplitude. This indicates a two-step process, possibly beginning with a nucleation of ground state VL domains followed by their rapid growth once the VL domain walls reach a critical density. This behavior is reminiscent of behavior seen in jamming of granular materials, and the VL metastabilty may then be due to a jamming of VL domains. Further, spatially resolved, measurements are necessary to verify the jamming scenario.

Future Plans

Pauli paramagnetic effects in Sr_2RuO_4 and KFe_2As_2

Measurements in SRO very close to H_{c2} will be attempted to explore a possible second superconducting phase or to directly observe evidence for Pauli paramagnetic effects. In addition, we will take advantage

of the special scattering geometry to perform direction resolved temperature dependence of the penetration depth will be continued. We will use a similar SANS geometry to investigate the VL in KFe_2As_2 where there are presently open questions concerning possible Pauli limiting for fields close to the basal plane. The objective is to provide a measure of the intrinsic superconducting anisotropy as a function of *H* and *T*.

Chiral superconductivity in UPt_3 and Sr_2RuO_4

Measurements to clarify possible effects of chirality on the UPt_3 VL will be carried out, using a varying neutron wavelength and a polarized beam to test whether the direction of the splitting is associated with neutron spin state. Similar measurements will performed on SRO with $\boldsymbol{H} \parallel \boldsymbol{c}$ to search for possible effects of chiral superconducting state.

Vortex lattice metastability

Measurements will be extended to regions of phase space closer to the ground state phase transition, with the objective to look for glassy dynamics and critical slowing-down. Spatially resolved ("scanning-SANS") measurements will be developed using a multi-beam configuration.

References

1. A. P. Mackenzie and Y. Maeno Y, Rev. Mod. Phys. **75**, 657 (2003).
2. Y. Maeno, S. Kittaka, T. Nomura, S. Yonezawa, and K. Ishida, J. Phys. Soc. Japan **81**, 011009 (2012).
3. J.A. Sauls and M. Eschrig, New J. Phys. **11**, 075008 (2009); C. Kallin, Rep. Prog. Phys. **75**, 042501 (2012).
4. S. Yonezawa, T. Kajikawa, and Y. Maeno, Phys. Rev. Lett. **110**, 077003 (2013).
5. K. Machida and M. Ichioka, Phys. Rev. B **77**, 184515 (2008).
6. R. Joynt and L. Taillefer, Rev. Mod. Phys. **74**, 235 (2002).
7. M. J. Graf, S. K. Yip, and J. A. Sauls, Phys. Rev. B **62**, 14393 (2000).
8. J. A. Sauls, Adv. Phys. **43**, 113 (1994).
9. K. A. Park and R. Joynt, Phys. Rev. B **53**, 12346 (1996).
10. Y. Tsutsumi, K. Machida, T. Ohmi, and M. A. Ozaki, J. Phys. Soc. Japan **81**, 074717 (2012).
11. P. Das *et al*., Phys. Rev. Lett. **108**, 167001 (2012).

Publications

1. P. Das, C. Rastovski, T. R. O'Brien, K. J. Schlesinger, C. D. Dewhurst, L. DeBeer-Schmitt, N. D. Zhigadlo, J. Karpinski, and M. R. Eskildsen, *Observation of Well-Ordered Metastable Vortex Lattice Phases in Superconducting MgB_2 Using Small-Angle Neutron Scattering*, Phys. Rev. Lett. **108**, 167001 (2012).
2. W. J. Gannon, W. P. Halperin, C. Rastovski, M. R. Eskildsen, P. Dai, and A. Stunault, *Magnetization in the Superconducting State of UPt_3 from Polarized Neutron Diffraction*, Phys. Rev. B **86**, 104510 (2012).
3. C. Rastovski, C. D. Dewhurst, W. J. Gannon, D. Peets, H. Takatsu, Y. Maeno, M. Ichioka, K. Machida and M. R. Eskildsen, *Anisotropy of the Superconducting State in Sr_2RuO_4*, Phys. Rev. Lett. **111**, 087003 (2013).
4. C. Rastovski, K. J. Schlesinger, W. J. Gannon, C. D. Dewhurst, L. DeBeer-Schmitt, N. D. Zhigadlo, J. Karpinski and M. R. Eskildsen, *Persistence of Metastable Vortex Lattice Domains in MgB_2 in the Presence of Vortex Motion*, Phys. Rev. Lett. **111**, 107002 (2013).
5. W. J. Gannon, W. P. Halperin, C. Rastovski, K. J. Schlesinger, J. Hlevyack, C. Steiner, M. R. Eskildsen, A.B. Vorontsov, J. Gavilano, U. Gasser, and G. Nagy, *Nodal Gap Structure and Order Parameter Symmetry of the Unconventional Superconductor UPt_3*, arXiv:1302.4144.

Session VII

Advanced Capabilities

Center for Accelerating Materials Modeling from SNS Data

Th. Proffen, Neutron Sciences Directorate, Oak Ridge National Laboratory, Oak Ridge, TN 37831

Program Scope

Neutron scattering enables simultaneous measurement of structural and dynamic properties of materials from the atomic scale (0.1 nm, 0.1ps) to the meso scale (1um, 1us). These ranges are remarkable complementary to current capabilities of computational modeling and the simplicity of the scattering cross section allows the prediction of neutron scattering data straight forwardly from atomic trajectories in a computer model. The Center for Accelerating Materials Modeling from SNS Data (FWP-ERKCSNL) is accelerating the rate of scientific discovery by integrating modeling into all aspects of the experimental chain, enabling refinement of model parameters such as force fields and allowing researchers to compare model and experimental results in near real time.

Recent Progress

1. Phonon anharmonicity and ferroelectric instability in SnTe and PbTe

Inelastic neutron scattering (INS) of rock-salt thermoelectric compounds SnTe and PbTe show that, surprisingly, although SnTe is closer to the ferroelectric instability, phonon spectra in PbTe exhibit a more anharmonic character. This behavior is reproduced in first-principles calculations (supported by CAMM) of the temperature-dependent phonon self-energy. The simulations reveal how the nesting of phonon dispersions induces prominent features in the self-energy, which account for the measured INS spectra and their temperature dependence. We establish that the phase-space for three-phonon scattering processes, rather than just the proximity to the lattice instability, is the mechanism determining the complex spectrum of the transverse-optical ferroelectric mode.

Figure 1 shows a comparison of the dynamic susceptibility, $\chi''(Q,E)$, for SnTe and PbTe, measured with the CNCS at SNS (T=50K and 300K), and computed with *SimPhonies* at 300K. The simulation included a rigorous description of the anharmonicity in terms of the full wavevector-dependent phonon self-energy. In particular, our simulations were able to reproduce the anomalous splitting of the transverse optic mode at the zone center in the case of PbTe, and revealed the detailed anharmonic mechanism that gives rise to this effect. This first-in-kind calculation paves the way for systematic simulations of the full shape of phonon spectra, instead of the usual Lorentzian or damped-harmonic-oscillator approximations. Results are published in [1].

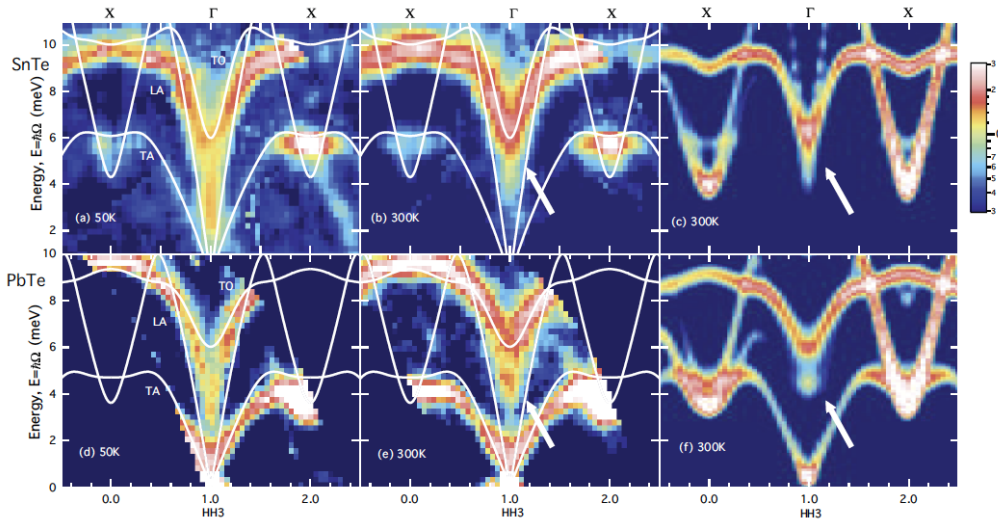

Figure 1: Comparison of INS measurements of phonon dynamic susceptibility in SnTe and PbTe, and comparison with anharmonic first-principles calculations. The white arrows point to the peak splitting of the transverse-optic mode at the zone center in PbTe (on a broadening without splitting is seen in the case of SnTe).

2. "Live CAMM" simulations of anharmonic phonons in $SrTiO_3$ measured on HYSPEC

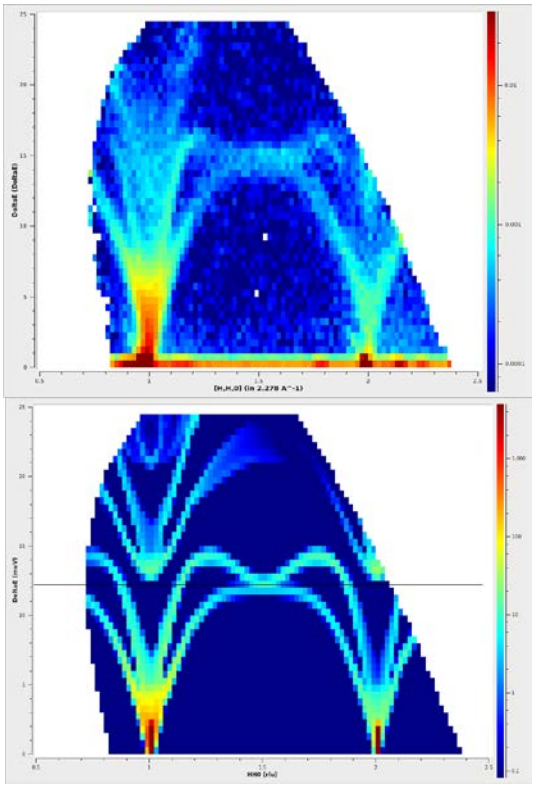

Figure 2: Comparison of plan of S(Q,E) along [HH1] direction. Top shows the experimental data from HYSSPEC and the bottom shows calculated intensities.

The ultimate goal to truly integrate modeling into the experimental chain is the ability of a researcher to interact even with complex simulations 'live' before and during an experiment. In a recent experiment on $SrTiO_3$ on the HYSPEC instrument at the SNS, we ran ab-initio molecular dynamics (AIMD) simulations on the OLCF EOS cluster concurrently with the experiment. The CAMM developed *SimPhonies* software was used to compute the neutron scattering intensity that was simultaneously being measured on the HYSPEC instrument. The AIMD simulations used 23,000 computing cores on EOS (a Cray XC30 cluster), and were executed at the same time as the neutrons scattered by the sample were accumulated by the HYSPEC detector system, thanks to the OLCF mechanism for scheduling jobs synchronized with the SNS experiment. The calculations ran for 5 hours, in order to compute 100,000 configurations of ions in the simulation box, using density-functional theory, from which anharmonic interatomic force-constants were extracted to compute the 4D phonon dynamical structure factor S(**Q**,E). Concurrently, the experimental 4D S(Q,E) was mapped on HYSPEC by rotating a large, high-quality single-crystal (grown at ORNL) over a large range of orientations.

Because the paraelectric cubic phase of $SrTiO_3$ is stabilized by anharmonicity (it distorts into a lower symmetry antiferroelectric phase at low temperatures), it is crucial to perform these large AIMD calculations in order to capture the anharmonic renormalization (stabilization) of phonon dispersions, and achieve good agreement with the experiments (in the sample, thermal agitation at room temperature naturally performs the renormalization). Simpler harmonic calculations would otherwise predict unphysical results. By slightly adjusting the volume in the AIMD simulations, based on the observed scattering intensity, we were able to achieve pretty good agreement between theory and experiment, as illustrated in the plots below. The simulations also helped us refine the range of crystal orientations that were collected on HYSPEC. The results are currently being analyzed in more detail.

3. Coarse grained simulations of polymer electrolyte Polyethylene Oxide-Acrylic Acid

Organic electrolyte batteries are widely used for practical energy storage, however due to fast discharge and thermal problems among others, polymer electrolyte-based batteries are currently being considered as possible next generation power sources for portable electronics. In this project we have focused on the fundamental physics of charge and counterion transport in model polymer electrolyte systems. The material that was used for this purpose is also known as an ionomer electrolyte because of the very low charge density on the backbone of the polymer chain. As a first step, we have already performed coarse-grained Molecular Dynamics (CG-MD) simulations to develop understanding of the effects of the dielectric constant on the microphase separation and counterion transport of this class of ionomer electrolytes The CG-MD results allow us to connect the “dots” between structural inhomogeneity and counterion hopping in ionomer electrolytes at a molecular level thereby providing guidelines for the design of better materials for future technologies. Using the program SASENA, we also calculated the dynamic structure factors (I(q,t)) for counterions showing a slowdown of counterion relaxation with decreasing dielectric constant. We also began working on a fully atomistic MD study (this enables capturing dynamic processes with shorter time and length scales) for ionomer electrolytes using LAMMPS (Large Scale Atomic/Molecular Massively Parallel Simulator) which will be compared with neutron experiments. We have constructed polyethylene (PE) oxide polymers in a highly concentrated solution and then replaced the -oxygen- with acrylic acid (AA) monomer. This allows a fully atomistic model of PE-AA to be generated which can be used as an input to LAMMPS.

We used different force fields (FF) between different bonded and non-bonded atomic interactions and equilibrated the structures to a melt state. Those studies show morphological details, however, the dynamics require more careful observation. There are certain numerical/physics issues in the fully atomistic model that needs to be addressed before a conclusive result can be obtained. A test simulation of a polyethylene melt using the Dreiding force field equilibrates well and the statistical quantities were calculated that match well with previous results. It should be noted the Dreiding force field is united atom not a fully atomistic FF, therefore additional work needed towards a fully atomistic simulation is currently under way.

Future Plans

In the hard matter science thread future work will extend modeling and simulation to the case of anharmonic phonons at finite temperatures and simulations of thermal diffuse scattering. Work on improvements to the calculation of the resolution function into the 4D dynamical structure factor will enable a more quantitative comparison to inelastic neutron scattering data collected on SNS neutron spectrometers.

The soft matter science thread will continue work on poly(3-hexylthiophene) (P3HT) blended with [6,6]-phenyl-C61-butyric acid methyl ester (PCBM). Samples have been obtained from A. Moule (UC-Davis) and neutron scattering experiments will be carried out on BASIS and VISION. In addition to extending the MD capabilities of CAMM, this work will also extend the accessible experimental data to inelastic scattering using *aClimax*.

As part of CAMM we have developed a refinement loop using classical molecular dynamics (MD) as modeling technique in combination with quasielastic neutron scattering data from the BASIS instrument, demonstrating the successful refinement of MD force field parameters for LiCl. The developed tools have been successfully used in several projects initiated by SNS users. We have also recently demonstrated the feasibility of live simulations performed concurrently with a neutron scattering experiment. We will continue to work on tool development relevant to the science drivers within CAMM and make tools available to the wider user community.

Beyond the immediate future plans discussed above, we have started developing a longer term vision for CAMM both being at the cutting edge of science and spinning off tools critical to the materials and neutron scattering community in the future.

Publications

1. C.W. Li, O. Hellman, J. Ma, A.F. May, H. Cao, X. Chen, A.D. Christianson, G. Ehlers, D.J. Singh, B.C. Sales, and O. Delaire, “Phonon self-energy and origin of anomalous neutron scattering spectra in SnTe and PbTe thermoelectrics”, *Phys. Rev. Lett.*, **112**, 175501, 2014 [Neutron modeling supported by CAMM]

Optics for advanced neutron imaging and scattering

B. Khaykovich[1,a], M. V. Gubarev[2], and D. E. Moncton[1,b]

[1]Nuclear Reactor Laboratory, Massachusetts Institute of Technology, 77 Massachusetts Ave., Cambridge, MA 02139
[2]Marshall Space Flight Center, NASA, VP62, Huntsville, AL 35812

Program scope

New techniques and tools for manipulating neutron beams offer significant, even transformative, improvements of neutron instrumentation, enabling new science. We are nearing completion of a program, which has successfully developed such a new tool: an achromatic lens based on axisymmetric grazing-incidence mirrors, often referred to as Wolter mirrors [1]. This project has been a close collaboration between the MIT and NASA groups, synergistically combining our expertise in neutron methods and glancing-incidence focusing optics. Making use of x-ray technologies, which were developed with significant NASA investments, is a substantial benefit for the neutron community.

As a result of our program, NIST has funded a construction of a new instrument (begun in the Fall 2013), a neutron microscope, which will be equipped with Wolter mirrors. This instrument will use the mirrors as a focusing lens for both cutting-edge neutron imaging and SANS. The neutron-imaging instrument VENUS, which is proposed at SNS, could immediately benefit from these developments. We believe that other planned and existing instruments at SNS and other DOE facilities could take advantage of our developments, including SANS, grazing-incidence SANS, and inelastic spectrometers. In addition, the technology used for fabricating Wolter mirrors could be used to make neutron guides.

The current objective of our program is to design the optics for neutron imaging, in collaboration with the imaging group at NIST. The design will optimize the neutron flux on the sample while minimizing aberrations. Another objective is to demonstrate and characterize axisymmetric supermirrors.

Recent progress

We have demonstrated experimental prototypes of focusing SANS and imaging instruments using Wolter optics and demonstrated axisymmetric neutron supermirrors.

SANS is a very important neutron technique, exploited by a large and diverse community of users. The basic instrument design remains the same since original SANS instruments were built: a very small aperture, relative to the source size, is used to collimate the beam illuminating the sample. Such a design is not only very inefficient in terms of the neutron flux, it also requires complex and costly detectors, which move inside large vacuum tanks, reaching 10 meters in length and two meters in diameter. This design is still in use after decades of developments, demonstrating the enormous challenge of building efficient optics for thermal and cold neutrons. To address this challenge, we pioneered the use of Wolter mirrors, which play the role of achromatic lenses with a short focal length and high throughput. We demonstrated the prototype SANS instrument at the instrument development beamline at HFIR [2]. The schematic layout

[a] bkh@mit.edu
[b] dem@mit.edu

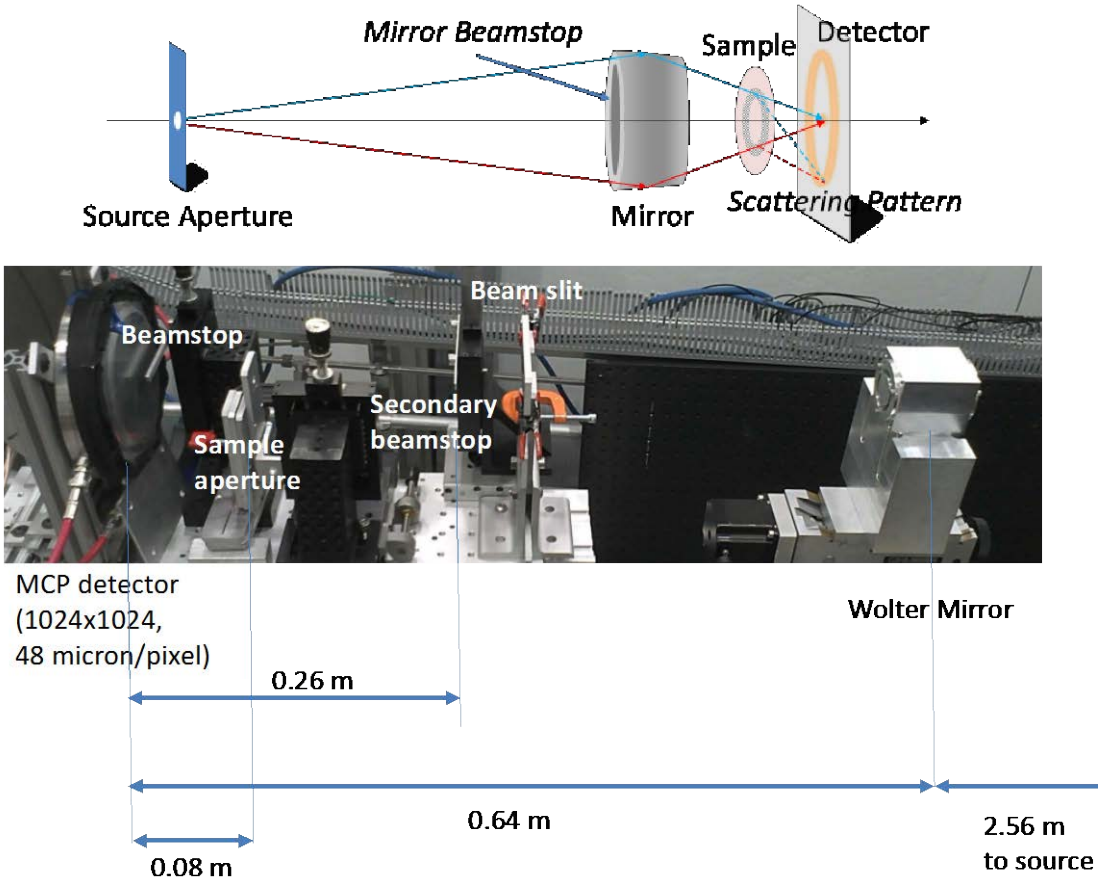

Figure 1. (Top) Schematic layout of the focusing-mirrors-based SANS instrument. The source aperture and the detector are located at two foci of the mirror. A sample is placed between the optics and the detector. Solid lines indicate trajectories of incident and reflected neutrons, focused at the detector. Dashed lines indicate trajectories of neutrons scattered by the sample. The shaded area of the sample indicates the area, which is illuminated by the beam. The drawing of the mirror is not to scale. **(Bottom)** Photograph of a section of the test SANS set-up. Only the part between the mirrors and the detector is shown, with corresponding distances marked. The detector, the beam stop, the sample aperture, and the mirrors are shown.

and the photograph of the experimental setup are shown in Figure 1. The mirrors create an image of the source aperture at the detector.

This demonstration experiment was done using small test optics with focal length of 3.2m. Standard SANS calibration samples were measured. Measurements of Silver behenate, a powder with the first Bragg peak at Q_0 = 0.1076 Å^{-1}, showed that the Q-resolution is approximately 14%. The Q-range was measured using the Debye-Bueche plot of the porous silica data, $I^{-1/2}$ vs Q^2, demonstrating that the instrument range extended down to $Q \cong 0.02$ Å^{-1}. Based on these results, we would expect fully optimized mirror-based SANS instruments to have a 50- to 100-fold combined improvement in signal rate and resolution [2].

Neutron imaging is a developing method, which is useful for many applications, such as multi-phase flow in porous media, water transport in fuel cells, degradation mechanisms in lithium batteries, texture propagation in crystalline materials, magnetic domains, etc. Traditional neutron-imaging instruments resemble pinhole cameras, as shown schematically in Figure 2(a). In order to achieve high resolution, the source aperture is often reduced to less than 10 mm, severely restricting the flux illuminating the sample. The goal of the imaging community is to

achieve the spatial resolution of ~1 μm, without reducing the signal rate to impractically low levels. Available neutron fluxes have so far prevented reaching this goal, but focusing optics can be used to overcome these limitations. In the neutron microscope shown in Figure 2(b), the resolution depends on the optics itself. Consequently, the source size, and thus the number of neutrons illuminating the sample increase substantially, leading to higher signal rates. In addition, optical magnification would result in better spatial resolution at the same detector pixel size. We demonstrated the achromatic neutron microscope at NIST using the same test mirrors as for SANS [3]. The spatial resolution and neutron flux were consistent with simulations. Subsequently, we tested larger mirrors at NIST and measured aberrations due to three contributions: gravity [4], figure errors of the mirrors and field curvature (the image is formed at the focal surface, which is not a plane).

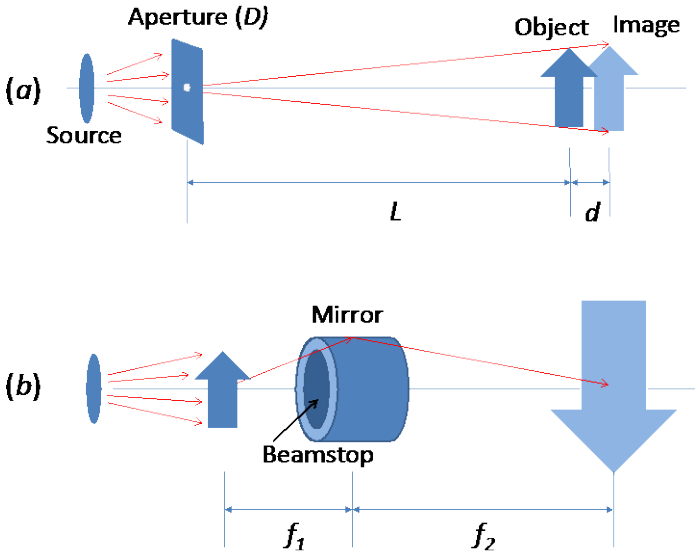

Figure 2. Schematic illustrations of neutron imaging instruments. A conventional pinhole-imaging system using a small aperture (a) and a microscope, equipped with axisymmetric grazing-incidence mirrors (b). The mirrors used in the test have diameters of approximately 30 mm and the total length of 60 mm. The focal distances are f_1 = 0.64 m and f_2 = 2.56 m, the source to detector distance is 3.2 m and the magnification is 4.

Axisymmetric supermirrors were prepared and tested at the Magnetism Reflectometer at SNS. The test sample was a surface of a conical frustum, shown in the inset of the Figure 3, with an opening angle of about 2°, a height of 45 mm, and a diameter of about 30 mm. The mandrel was coated with TiN separation layer, followed by NiC/Ti multilayer, followed by the Ni shell. The multilayer-coated Ni shell was then separated from the mandrel. Neutron reflectometry confirmed that the inner surface of the cone indeed formed an m=1.9 supermirror. The reflectivity is shown in Figure 3. For the tests, the cone was installed with its axis parallel to the neutron beam, while a very narrow beam was formed and reflected from a small section of the surface. Identical reflectivity was measured at different sections of the surface. (The paper describing the reflectivity in details is in preparation).

Future plans

While designing the optics for the neutron microscope, we must analyze in detail the three main contributions limiting the resolution of the image: field curvature, figure errors and gravity.

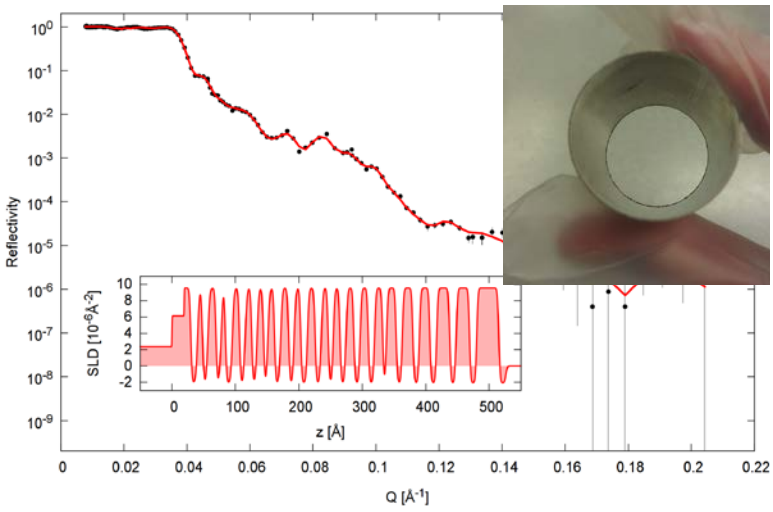

Figure 3. Reflectivity of an m-1.9 conic supermirror, as a function of the wave-vector transfer Q (Å^{-1}). Black circles with error bars are experimental points, while the red line is the fit. The lower insert shows the fit of the scattering-length density as a function of thickness. The upper insert shows the photograph of the cone held in the hand of an experimenter.

Field curvature means that the best image of an object is formed at a curved plane, as opposed to a flat detector. This is the leading aberration of Wolter optics. Figure errors are imperfections in the shape of the mirrors; these errors are measured figure errors of the mirrors, as an angular size of an image of a point source. Gravity changes the neutron trajectory between the sample and the detector, leading to image distortions, which become noticeable as the resolution approaches 10 μm. The correction is done by prisms, similar to SANS [4]. Aberrations are analyzed by ray-tracing simulations, which are compared with previous experimental results. Minimizing aberrations is the subject of the ongoing and future work.

Research supported by the U.S. Department of Energy, Office of Basic Energy Sciences, under Awards # DE-FG02-09ER46556 and DE-FG02-09ER46557.

Publication resulting from work supported by the DOE project over the last two years

[1] B. Khaykovich, M. Gubarev, D. Liu, B. D. Ramsey, D. E. Moncton, A new generation of neutron focusing optics, SPIE Newsroom (4 February 2014). http://spie.org/x106175.xml DOI: 10.1117/2.1201401.005243 (invited paper).

[2] D. Liu, B. Khaykovich, M.V. Gubarev, J.L. Robertson, L. Crow, B.D. Ramsey, and D.E. Moncton, Demonstration of a novel focusing small-angle neutron scattering instrument equipped with axisymmetric mirrors, Nature Communications **4**, 2556 (2013); doi: 10.1038/ncomms3556 (Highlighted by the Materials Research Society www.materials360online.com, MIT News http://www.mit.edu/, and other professional societies, such as AM&P e-news, Phys.org, etc.)

[3] D. Liu, D. Hussey, M. V. Gubarev, B. D. Ramsey, D. Jacobson, M. Arif, D. E. Moncton, and B. Khaykovich, Demonstration of achromatic cold-neutron microscope utilizing axisymmetric focusing mirrors. Applied Physics Letters **102**, 183508 (2013); doi: 10.1063/1.4804178

[4] B. Khaykovich, D. Hussey, D. Liu, M. V. Gubarev, B. D. Ramsey, D. Jacobson, M. Arif, and D. E. Moncton, Response to "Comment on 'Demonstration of achromatic cold-neutron microscope utilizing axisymmetric focusing mirrors'" Applied Physics Letters, **103**, 236102 (2013), doi:10.1063/1.4835175

Neutron Scattering Instrumentation Research and Development for High Spatial and Temporal Resolution Imaging at Oak Ridge National Laboratory

J.P. Hayward (jhayward@utk.edu), *University of Tennessee, Knoxville TN 37916*

I. Program Scope

Neutron scattering facilities like those available at Oak Ridge National Laboratory are enabling the discovery and development of advanced materials including those to be used for next generation energy storage systems. In spite of all the success that neutron imaging has enjoyed in recent years, even higher-impact research is limited by the current temporal and spatial resolution of neutron detection devices. In particular, the spatial resolution of all neutron imaging methods in use and under development is fundamentally limited by the variance introduced by the charged particles emitted from neutron absorption. Thus, we are investigating, designing and demonstrating an array of ~1 μm-sized glass scintillating fibers arranged via photonic-crystal-fiber patterning techniques— with particle tracking (a must) so that position resolution can be finer than that allowed by the charged particle ranges. The processes, knowledge and algorithms developed will allow for spatially (1 μm) and time resolved (<100 ns), high throughput neutron transmission imaging in large areas at reasonable costs in the near term.

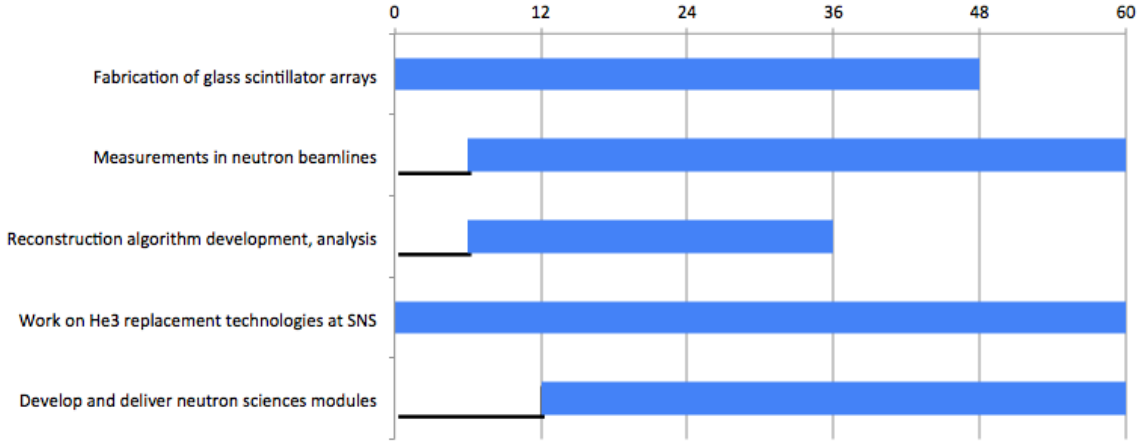

Figure 1. Project schedule with five tasks listed in rows at left and time given in months.

The planned project schedule is given in Figure 1, including the timeline for the first year of effort.

II. Recent Progress

Task 1 is the ***fabrication of glass scintillator microfiber arrays***, and it includes 6 subtasks over the first 4 years. In year 1, significant effort was spent on performing light transport simulations to support optical design of the microfiber array (Task 1.6). For a rapid, simple analysis to guide our starting design, simulations were first performed using available TRIM (the Transport of Ions in Matter) and ZEMAX codes. As illustrated in Figure 2, the former was used to transport the charged particle reaction products from neutron absorption, and the latter was used to propagate the generated optical light photons to the photosensor. This code was used to rapidly form expected images of charged particle tracks while varying fiber size, fiber spacing, bundle geometry, interaction depth, track orientation relative to the 2D photosensor, and scintillation brightness. From this initial modeling, it was known that fiber size should be ~1 μm and that the short arrays should be kept to a thickness of ~1 mm for light collection considerations. Subsequently, we completed a detailed model of the interaction and light

collection physics of our microfiber array design in a new Geant4.10.0p1 Monte Carlo workspace. One important role of this detailed model is to guide further iterations of the microfiber array optical design. It models the neutron interactions, scintillation light generation, light transport from the scintillator through a lens to the Image Intensifying CDD (ICCD), and the performance of the ICCD in recording the charged particle tracks. This model has been used to begin to examine the details of the scintillator array design, the effects of the ICCD design, neutron position reconstruction, and neutron gamma discrimination. We are now working on validating this model with a simple experiment, and a journal paper about this work is in the first stages of preparation.

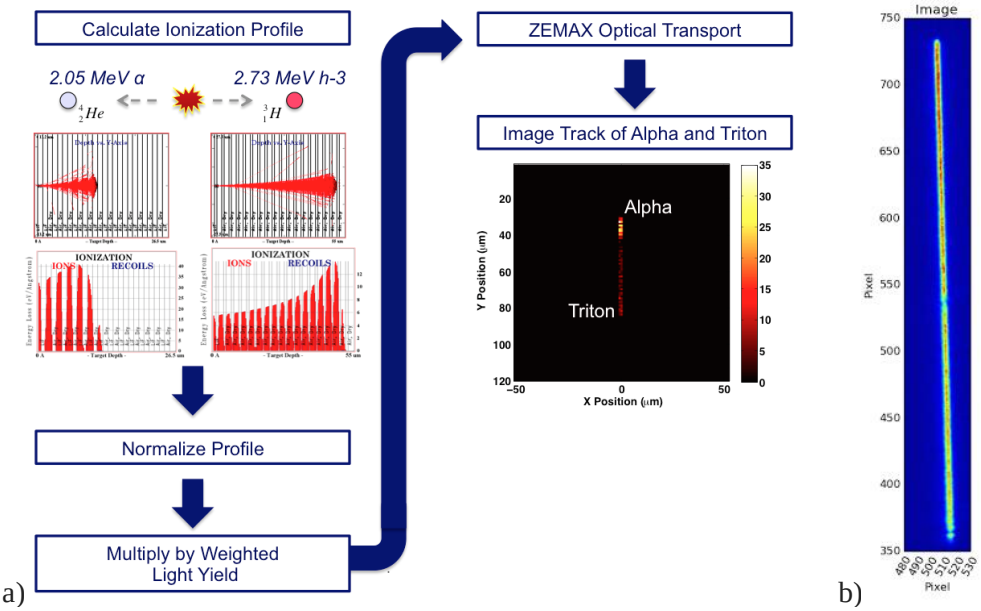

Figure 2. a) Illustration of Monte Carlo model output for a neutron interaction in scintillating microfiber array, shown along with simulated example image output from a neutron interaction. b) Measurement of a blue LED behind a 1 μm wide, 100 μm long slit in a photomask using our new ICCD camera.

As planned, work is also beginning on fabrication of a short glass scintillating glass fiber array using photonic crystal patterning techniques, starting with doped Li glass rods for the preform (Task 1.1). Our partner at the University of Southampton's Optoelectronics Research Centre is carrying out the fiber drawing work to our specifications. The initial design went through five design iterations, driven in part by the simulation output from Task 1.6. The selected first design for fabrication is shown in Figure 3. Each 1 μm diameter Li doped rod is surrounded by air-filled capillaries of the same diameter, and the doped rods are arranged in a 6 x 6 structure that is square in shape, surrounded by a soft glass jacket.

From our first experiments melting and drawing the Li glass fibers, we learned that: 1) a soft glass similar to fused silica must be used rather than fused silica, and 2) that the light output is improved when drawing fibers in a reducing atmosphere compared to the case where it is drawn in air. Specifically, the Li glass fiber light output is 6.9% higher when a set of 200 μm diameter Li glass fibers were redrawn in a reducing atmosphere at the University of Southampton compared to the case where they were drawn in air. Furthermore, our measurements and analysis suggest that those fibers redrawn in the reducing atmosphere scintillate only about 2% less brightly than the original monolithic Li glass rod from Nucsafe from which the fibers were redrawn. Altogether, these are encouraging first results, suggesting that we understand how to fabricate Li glass fibers for our microfiber array without reducing the scintillation light output compared to our monolithic starting material.

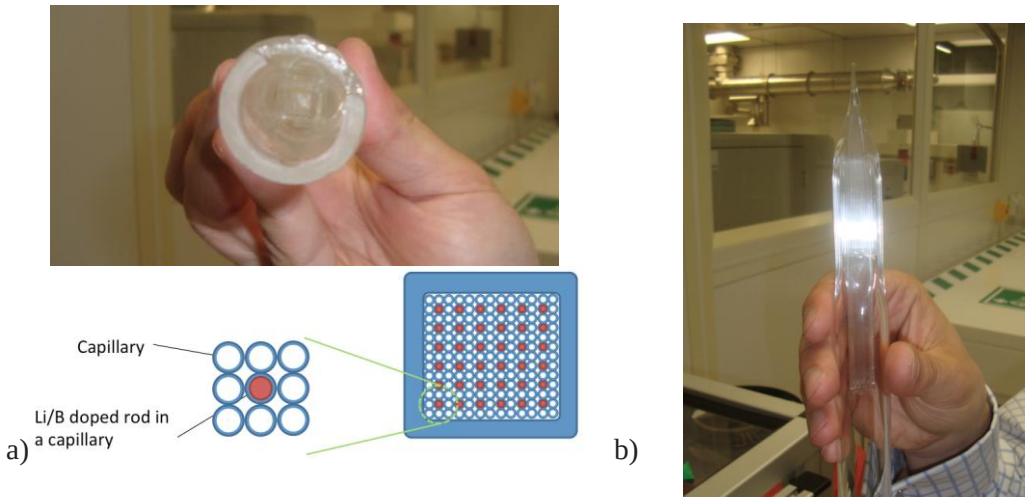

Figure 3. a) Illustration of the base structures in the first mircrofiber array being fabricated now at the University of Southampton. At left, a Li scintillating rod (red) is shown surrounded by a set of air capillaries. At right, a structure that holds 6 x 6 rods is shown surrounded by a glass jacket (not to scale). b) Photos are shown of our collaborator at Southampton holding a structured preform in his lab similar to the one that is about to be fabricated for the University of Tennessee according to the plan shown in (a). These photos were taken during the PI's visit to the UK.

Furthermore, we have prepared to begin our investigation of controlled thermal diffusion to drift ion dopants in undoped samples of Li glass (Task 1.2) this summer. We have procured samples of Li glass that do not scintillate because they are not doped with Ce^{3+}. These samples are being cut with a diamond saw to make more small samples for analysis. Furthermore, we have procured a Ce sputter target, and sputtering of samples will begin within the next few weeks. Following this step, the diffusion experiments will begin using an available tube furnace. We will first determine the diffusion coefficient of cerium in undoped lithium glass across a range of temperatures and drift times.

As an alternative approach to that described in our SOW, we are also investigating a different microstructured scintillator design in partnership with Radiation Monitoring Devices (RMD). Based upon our specifications, RMD proposes to make us a thin (~100 μm) layer of CsI:Tl pillars, each 1 μm wide, interlaced with LiF. The benefit of using CsI:Tl is that it is known to brightly scintillate at 65,000 photons/MeV. They would make this with available evaporators at RMD employing a structured substrate that would cause the CsI:Tl to nucleate and grow in the proper positions. The first version would be grown with natural Li for lower cost. Our Monte Carlo simulations have indicated that this design is worth pursuing in parallel with the described effort because the high light yield should allow us to achieve our target position resolution and neutron detection efficiency. Furthermore, to save cost, only a thin layer of LiF will be deposited in our first try, so it is not expected to penetrate deeply in between the CsI pillars. Yet, we expect that we will still be able to measure charged particle tracks, thereby demonstrating proof-of-concept of this alternative micro-fabrication method. Pursuit of two methods in parallel reduces the overall project risk, particularly the main risk of having 1 μm thin Li fibers not scintillate brightly enough to image charged particle tracks. We anticipate needing to use even more internal resources to fund this development work.

Referring back to Figure 1, **Task 2**, consisting of ***measurements at neutron beamlines***, also begins in Year 1, and this task continues until the end of Year 5. Tasks 2.1 and 2.2 require that the microfiber array be coupled to an ICCD device for readout. During the first part of the year, we were loaned an ICCD device for evaluation from ANDOR, and we subsequently purchased it

with cost sharing from the University of Tennessee. The ANDOR DH334T-18F-A3 ICCD is 18 mm in dimension and has 1024 x 1024 pixels with 13 x 13 μm pixel size, 40% peak QE, and contains a P43 phosphor with 5 ns gate width. It may be cooled to -40°C for low noise single photon sensitivity. We first evaluated the ICCD to demonstrate to ourselves that the more expensive, faster P46 phosphor was not required for our application, which it is not.

Figure 2a demonstrates that we were able to properly set up the optical imaging system to observe a 1 μm feature size in our university radiation instrumentation lab. In fact, this is an image of a slit in a custom photomask that is about the same size we expect our charge particle tracks to be in our scintillating microfiber array. The reader should note that this integrated image (Figure 2a) is brighter than we expect single charged particle tracks to be. The optical components that we procured for our measurements include a microscope objective lens to magnify the light emitted from the scintillator and a tube lens to properly focus that light onto the ICCD. The operation of the ICCD also required us to write software to control the ICCD, starting with the software development kits provided. Our application programming interface includes a python wrapper for C, multiprocessing capability, and remote monitoring functionality.

Furthermore, Task 2.4 specifies that we perform full system Monte Carlo simulations to support our understanding of the experimental results. As discussed already, our detailed simulation workspace in Geant4 includes the complete physics from neutron interaction to ICCD performance, so progress on this task is well underway.

Referring back to Figure 1, **Task 3**, titled ***reconstruction algorithm development and analysis***, begins in Year 1, and extends through Year 3. In Task 3.1, we are to research and develop algorithms for using measured charged particle track data from our glass fiber array to determine the interaction location of neutrons with resolution of 1 μm, first using simulated data for development and evaluation of the algorithm's sensitivity. The excellent progress on our detailed simulation workspace (Tasks 1.6 and 2.4) has already allowed us to get a significant start on Task 3.1. A few different reconstruction algorithms have been investigated. Our first results, which assume a conservative 6000 scintillation photons/n in Li glass, suggest that we can expect to achieve position resolution better than 2 μm using a design like that shown in Figure 3. Furthermore, first algorithm development results that consider the alternative CsI:Tl and LiF microstructured scintillator design described above show that expected position resolution for the alternative design is estimated to be ~ 1 μm using the first reconstruction algorithm investigated, which is based on a Hough transform.

III. Future Plans

We plan to follow the work plan detailed in the proposal according to the schedule shown in Figure 1. Fabrication and investigation of microfiber arrays will continue (Task 1), and testing of these arrays at ORNL beam lines will commence (Task 2). Algorithm development for reconstruction will continue, as planned (Task 3). Development and delivery of neutron science modules (Task 5) will commence during Year 2, as planned. Submission of peer-reviewed publications (Task 6) is also expected to accelerate in Year 2.

IV. Publications

Nothing to report. A journal paper is in the first stages of being prepared for submission to IEEE Transactions on Nuclear Science on the simulation work and supporting experimental validation.

National School on Neutron and X-ray Scattering

Suzanne G.E. te Velthuis (tevelthuis@anl.gov)
Materials Science Division, Argonne National Laboratory

Bryan C. Chakoumakos
Quantum Condensed Matter Division, Oak Ridge National Laboratory

Jonathan C. Lang, Esen E. Alp
Advanced Photon Source, Argonne National Laboratory

John D. Budai
Materials Science and Technology Division, Oak Ridge National Laboratory

Program Scope

Since 1999, the National School on Neutron and X-ray Scattering has provided a comprehensive introduction to the underlying theory of neutron and x-ray scattering and related experimental techniques that are available. The school plays an important strategic role in educating the United States scientific community in the capabilities of its national neutron and x-ray user facilities. While the two-week school was initially held at Argonne National Laboratory, in 2008 ANL partnered with Oak Ridge National Laboratory, and now participants spend equal time at both sites. The program includes both classroom lectures from experts in the field and hands-on experiments.

Recent Progress

The 14th, 15th and 16th National School on Neutron and X-ray Scattering were held August 12-25th, 2012, August 10th – 24th, 2013, and June 14th-28th, 2014, respectively. Interest from the scientific community in the school is strong as the school has been consistently oversubscribed, by over a factor of 3.6 in recent years. During the school, the participants (64 in 2012, 66 in 2013, 66 in 2014) each performed a total of four neutron scattering experiments using Oak Ridge National Laboratory's Spallation Neutron Source and High Flux Isotope Reactor beamlines. They also performed three to four x-ray

experiments at Argonne National Laboratory's Advanced Photon Source. On the last day of the school as small groups the students give a short presentation on one of the experiments they participated in. The feedback from the students is positive each year, and many of the students subsequently apply for postdoctoral positions at Argonne and other neutron and X-ray scattering facilities, or continue to use the facilities for their research.

To date, 961 participants have attended the school. The national character of the school is reflected in the wide geographic distribution of the participants that have attended as is shown in Fig. 1. Participating students have represented over 161 unique North American colleges and universities, spread over 48 different states, Washington DC, Puerto Rico, and Canada. About 18% of the participants attended schools in EPSCoR states. The distribution of the participants over the different states or territories generally tracks the distribution of the applicants.

Many of the participants continued to utilize these sources well past their graduate studies in their post-doctoral research positions and beyond. In fact, 70% of the participants who attended the school in the first year (1999) are currently active facility users, while averaged over 1999-2006 this percentage is at least 44% (see Figure 2). To date, three of the school's alumni have been invited to return to the school as lecturers, as they have become recognized experts in the field.

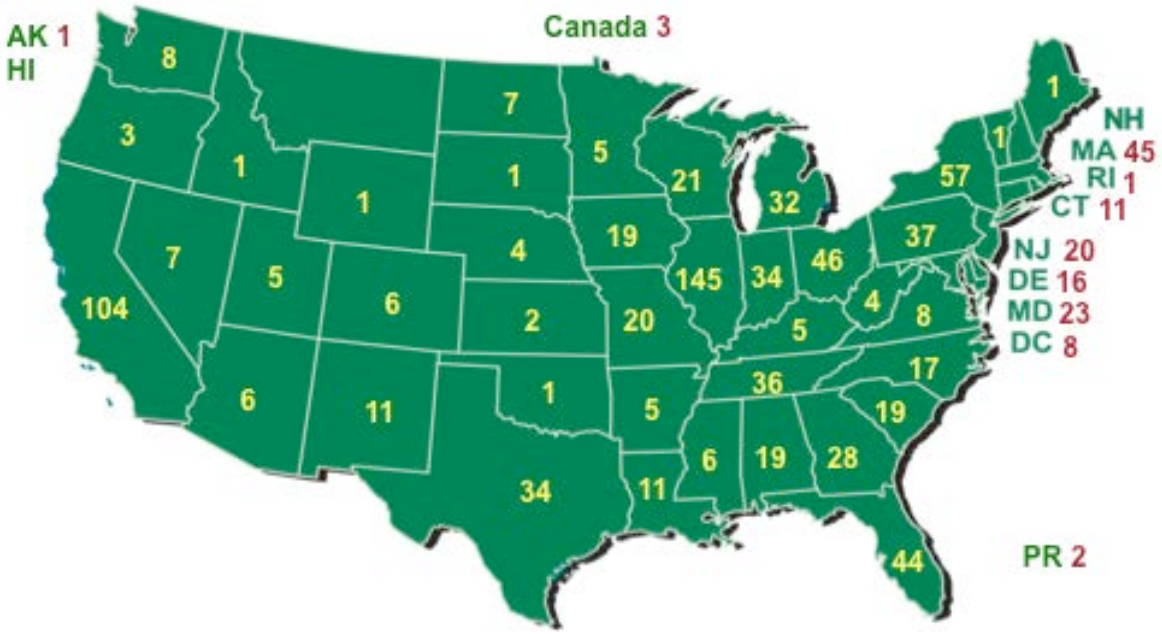

Figure 1: Geographic distribution of school participants from North America, 1999-2014.

Future Plans

The purpose of the school is to give the participants the opportunity to learn the fundamentals of the interaction of x-rays and neutrons with matter, as well as the

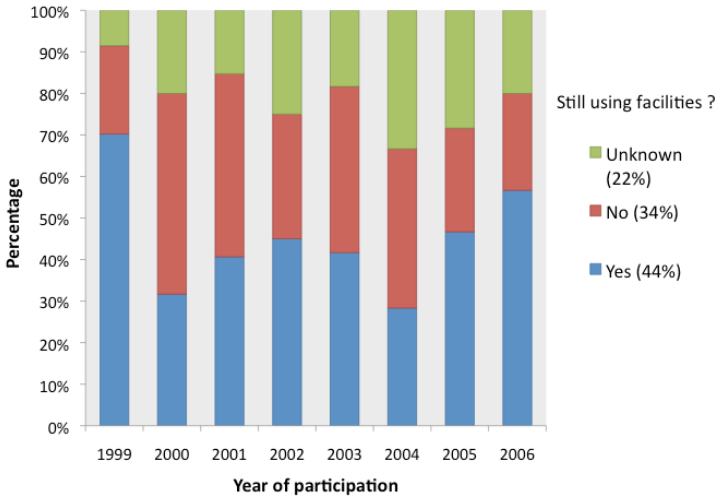

Figure 4: Percentages of 1999-2006 participants that are still using Neutron and or X-ray facilities[1].

methods of producing synchrotron radiation and neutrons. The school will dwell on the applications of these techniques to various scientific or technological areas, providing hands-on experience with instruments at neutron (HFIR, SNS) and x-ray (APS) facilities. The course, which will deal with all details of the interactions of x-rays and neutrons with matter, will be taught by leading experts in the field working at national facilities and universities and will represent a unique educational opportunity. The continuing participation of lecturers from outside the two organizing national laboratories is considered essential to preserving the national character of the school.

The school's directors will select at least 60 participants each year, consisting of graduate students from North American universities, postdoctoral researchers, investigators from U.S. universities, national laboratories and industries. The primary audience for the school is graduate students from U.S. institutions near the beginning of their thesis studies; therefore this group will make up at least 75% of each class. Due to capacity limitations, we expect no more than 70 students a year.

The National School on Neutron and X-ray Scattering will continue to be held for a period of two weeks, with dates chosen to minimize overlap with the academic year, other schools, and conferences, yet coinciding with the operation of the three facilities involved. The students will spend approximately one week at Argonne National Laboratory and one week at Oak Ridge National Laboratory, and if possible, the site at which the school starts is alternated each year.

Publications

Jonathan C. Lang, Suzanne te Velthuis, Bryan C. Chakoumakos, John D. Budai & Allen Ekkebus
National School on Neutron and X-ray Scattering
Synchrotron Radiation News, 26 (2013) 9-12.

[1]*As determined by searches of the internet and facility user records between 2009-2011.*

Neutron Scattering Study of Strongly Correlated Systems

T. Egami, ***Joint Institute for Neutron Sciences, University of Tennessee, Knoxville, TN 37996, Oak Ridge National Laboratory, Oak Ridge, TN 37831***

Program Scope

Neutron scattering study is an important component in two research projects supported by DOE-BES, *Atomistic and mesoscopic study of metallic glasses* (FWP-ERKCM40) and *Neutron Scattering Research Network for EPSCoR States* (DE-FG02-08ER46528). In the metallic glass FWP neutron scattering is used in the study of the atomic dynamics of metallic glasses and liquids in order to determine the mechanism of viscosity, atomic transport and glass transition in metallic glasses. In the EPSCoR project it is used in the study of spin dynamics and local lattice distortion in Fe-based superconductors. In both cases strong correlations, among atoms in the case of liquids and glass, and among electrons in the case of Fe superconductors, pose a major challenge in scientific efforts to understand these systems. We use a real-space approach to analyze the results of neutron scattering in order to determine these correlations directly. Neutron scattering research is closely coupled with the effort on simulation and theory, particularly in the case of research on metallic glasses.

Recent Progress

1. Atomic Dynamics in Metallic Liquids and Liquid He

Phonons are the vibrational elementary excitations in solids, but in liquids they are strongly scattered and overdamped. Instead, we discovered that the local topological excitations, the action of cutting or creating an atomic bond, are the elementary excitations in high-temperature liquids, by showing by molecular dynamics (MD) simulation that the Maxwell relaxation time, $\tau_M = \eta/G$, where η is viscosity and G is the high-frequency shear modulus, is equal to the time to lose or gain one nearest neighbor, τ_{LC}, as shown in Fig. 1 [P11]. This is an important discovery, because it relates a macroscopic quantity, τ_M, directly

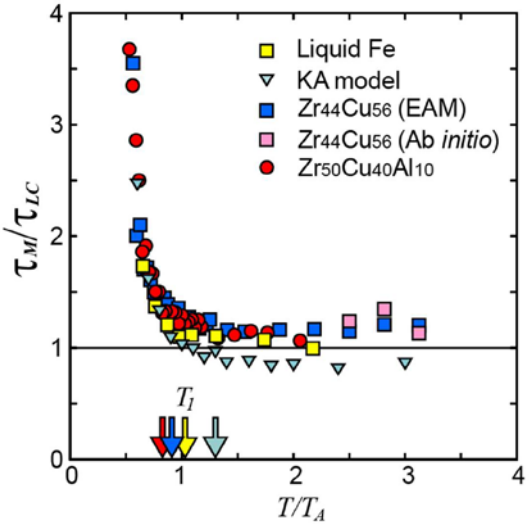

Fig. 1 The ratio of the Maxwell relaxation time, τ_M, to the time to lose or gain one nearest neighbor, τ_{LC}, obtained by molecular dynamics (MD) simulation with various classical potentials and by the *ab initio* MD [P11]. T_A is the crossover temperature.

to the microscopic quantity, τ_{LC}. To prove this by experiment we carried out neutron and *x*-ray inelastic scattering measurements on heavy and light waters, liquid aluminum and liquid helium. The measured dynamic structure factor, $S(Q,\omega)$, is Fourier-transformed into the dynamic pair-density function (DPDF), $\rho(r,\omega)$ [1]. Fig. 2 shows the difference in the DPDF of He^4 below (1.8 K) and above (2.85 K) the superfluid transition at T_{BE} = 2.17 K. The measurement of $S(Q,\omega)$ was carried out at the CNCS of the SNS. The intensity at 2 Å and $\omega \sim 0$ indicates the evidence of tunneling in the Bose-Einstein (BE) condensate. In the normal state He atoms are distinguishable, but in the BE condensate they are indistinguishable, resulting in tunneling between the closest neighbors at 2 Å. We also studied the dynamics of heavy and light waters and liquid aluminum. We plan to obtain the DPDF as well as the Van Hove function, $\rho(r,t)$ [2]. In particular by changing the amount of H_2O in D_2O we will determine the self-part of the Van Hove function. Then from the time evolution of the Van Hove function it will be possible to determine τ_{LC} directly by experiment.

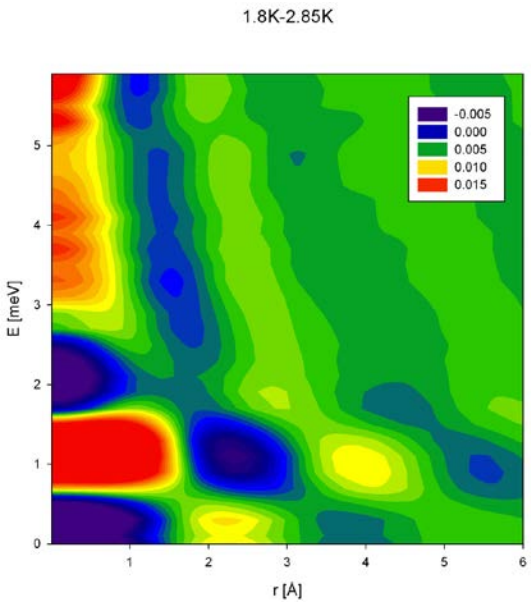

Fig. 2 Difference between the neutron DPDFs of liquid He^4 below (1.8 K) and above (2.85 K) the superfluid transition at 2.17 K.

2. Local Lattice Distortion and Spin Dynamics in Fe Based Superconductors

In Fe-pnictides we found strong local lattice distortion coupled to spin and superconductivity. By examining the neutron PDF of the parent (undoped) Fe-pnictides, we found that the local orthorhombic distortion is significantly larger than the average because of nano-scale twins [P6]. The formation of nano-scale twin must be the consequence of the phonon softening over a wide range of *Q* [3]. This partially explains the discrepancy between the AFM magnetization observed by neutron diffraction and the local spin polarization observed by spectroscopy [4]. We also found that local orthorhombic distortion persists even in doped superconductors which show no macroscopic orthorhombic distortion. It is most likely that the local orthorhombic distortion supports local AFM spin correlation, which is incoherent along the *c*-axis. We also continued the study of the spin dynamics in Fe-pnictides using inelastic neutron scattering [P8, P13, P16]. We established the presence of strong magnetic anisotropy, which can be understood only in terms of the orbital ordering and local lattice distortion.

Future Plans

We studied the atomic dynamics of heavy and light waters using inelastic x-ray scattering. The data will be combined with those of neutron scattering to separate H(D) dynamics from O

dynamics. We have recently built an electro-static liquid levitator for neutron scattering in collaboration with K. Kelton of Washington University. We will use the system with NOMAD (SNS) to study the structure, and with ARCS (SNS) to study the atomic dynamics. Our goal is to detect the local topological excitation which results in rapid increase in viscosity. With Fe superconductors we focus on establishing the ubiquitous nature of nano-twins observed earlier [P6], by examining a wide variety of compounds. We also plan to prove through the DPDF analysis that the loss of *c*-axis coherence due to random pinning of nano-twins by impurities cause the loss of long-range magnetic order, not the change in the Fermi surface.

References

1. W. Dmowski, S. B. Vakhrushev, I.-K. Jeong, M. P. Hehlen, F. Trouw and T. Egami, "Local Lattice Dynamics and the Origin of the Relaxor Ferroelectric Behavior", *Phys. Rev. Lett.*, **100,** 137602 (2008).
2. L. Van Hove, "Correlation in Space and Time and Born Approximation Scattering in Systems of Interacting Particles", *Phys. Rev.*, **95,** 249 (1954).
3. Jennifer Niedziela, D. Parshall, K. Lokshin, A. S. Sefat, A. Alatas and T. Egami, "Phonon Softening Near Structural Transition in $BaFe_2As_2$ Observed by Inelastic X-ray Scattering", *Phys. Rev. B*, **84,** 224305 (2011).
4. P. Vilmercati, A. Fedorov, F. Bondino, F. Offi, G. Panaccione, P. Lacovig,L. Simonelli, M. A. McGuire, A. S. M. Sefat, D. Mandrus,B. C. Sales, T. Egami, W. Ku and N. Mannella, "Itinerant Electrons, Local Moments, and Magnetic Correlations in the Pnictide Superconductors $CeFeAsO_{1-x}F_x$ and $Sr(Fe_{1-x}Co_x)_2As_2$", *Phys. Rev. B,* **85,** 220503 (2012).

Publications [FY12(July)-14 (June)]

P1. *Electron-Irradiation-Induced Structural Change in Zr-Hf-Nb Alloy*, T. Nagase, S. Anada, P. D. Rack, J. H. Noh, H. Yasuda, H. Mori and T. Egami, *Intermetallics,* **26,** 122 (2012).

P2. *The Use of Atomic Level Stress to Characterize the Structure of Irradiated Iron*, Madhusudan Ojha, D. M. Nicholson, Kh. Odbadrakh, Bala. Radhakrishnan, R. E. Stoller and T. Egami, *J. Phys.: Conf. Ser.* **402,** 012010 (2012).

P3. *Structured Water in Polyelectrolyte Dendrimers: Understanding Small Angle Neutron Scattering Results through Atomistic Simulation*, B. Wu, B. Kerkeni, T. Egami, C. Do, Y. Liu, Y. Wang, L. Porcar, K. Hong, S. C. Smith, E. L. Liu, G. S. Smith and W.-R. Chen, *J. Chem. Phys.,* **136,** 144901 (2012).

P4. *Glass Dynamics at High Strain Rates*, J. S. Langer and T. Egami, *Phys. Rev. E,* **86,** 011502 (2012).

P5. *Molecular Dynamics and Neutron Scattering Study of the Dependence of Polyelectrolyte Dendrimer Conformation on Counterion Behavior*, B. Wu, W.-R. Chen, T. Egami, X. Li,

Y. Liu, Y. Wang, C. Do, L. Porcar, K. Hong, L. Liu, G. Smith, and S. Smith, *J. Chem. Phys. B,* **137,** 064902 (2012).

P6. *Local Structural Variation as Source of Magnetic Moment Reduction in $BaFe_2As_2$,* J. L. Niedziela, M. A. McGuire and T. Egami, *Phys. Rev. B* **86**, 174113 (2012).

P7. *The Origin of Viscosity as seen through Atomic Level Stress Correlation Function,* V. A. Levashov, J. R. Morris and T. Egami, *J. Chem. Phys.* **138,** 044507 (2013).

P8. *Magnetic Anisotropy in Hole-doped Superconducting $Ba_{0.67}K_{0.33}Fe_2As_2$ Probed by Polarized Inelastic Neutron Scattering*, C. Zhang, M. Liu, Y. Su, L.-P. Regnault, M. Wang, G. Tan, T. BrÄuckel, T. Egami and P. Dai, *Phys. Rev. B*, **87,** 081101 (2013).

P9. *MeV Electron Iirradiation-Induced Structural Change in the bcc Phase of Zr-Hf-Nb Alloy with an Approximately Equiatomic Ratio,* T. Nagase, S. Anada, P. D. Rack, J. H. Noh, H. Yasuda, H. Mori and T. Egami, *Intermetallics,* **38,** 70 (2013).

P10. *Charge-Dependent Dynamics of a Polyelectrolyte Dendrimer and Its Correlation with Invasive Water,* B. Wu, Y. Liu, X. Li, E. Mamontov, A. I. Kolesnikov, S. O. Diallo, C. Do, L. Porcar, K. Hong, S. C. Smith, L. Liu, G. S. Smith, T. Egami and W.-R. Chen, *J. Amer. Chem. Soc.*, **135,** 5111 (2013).

P11. *Elementary Excitations and Crossover Phenomenon in Liquids,* T. Iwashita, D. M. Nicholson and T. Egami, *Phys. Rev. Lett.*, **110,** 205504 (2013).

P12. *First Principles Local Stress in Crystalline and Amorphous Metals,* D. M. Nicholson, Madhusudan Ojha and T. Egami, *J. Phys.: Condens. Matt.*, **25,** 435505 (2013).

P13. *Measurement of a Double Neutron Spin Resonance and an Anisotripic Energy Gap for Underdoped Superconducting $NaFe_{0.985}Co_{0.015}As$ Using Inelastic Neutron Scattering,* C. Zhang, R. Yu, Y. Su, Y. Song, M. Wang, G. Tan, T. Egami, J. A. Fernandez-Baca, E. Faulhaber, Q. Si and P. Dai, *Phys. Rev. Lett.,* **111,** 207002 (2013).

P14. *Structural Relaxation in $Pd_{42.5}Cu_{30}Ni_{7.5}P_{20}$ BMG below the Glass Transition,* O. Haruyama, T. Mottate, K. Morita, N. Yamamoto, H. Kato and T. Egami, *Mater. Trans. JIM*, **55,** 466 (2014).

P15. *Elementary Excitation and Energy Landscape in Simple Liquids*, T. Egami, *Mod. Phys. Lett. B,* **28,** 1430006 (2014).

P16. *The Effect of Pnictogen Height on Spin Waves in Iron Pnictides*, Chenglin Zhang, L. W. Harriger, Zhiping Yin, Weicheng Lv, Miaoyin Wang, Guotai Tan, Yu Song, D. L. Abernathy, Wei Tian, T. Egami, K. Haule, G. Kotliar and Pengcheng Dai, *Phys. Rev. Lett., in press*.

Session VIII

Panel Discussion

Discussion Leader:

Thomas Proffen

Session IX

Correlated Electron Materials

Institute for Quantum Matter

C. Broholm[1,2,3], N.P. Armitage[1], R.J. Cava[4], T.M. McQueen[1,5,6], O. Tchernyshyov[1] & A. Turner[1]

[1]Department of Physics and Astronomy, Johns Hopkins University, Baltimore, MD 21218
[2]NIST Center for Neutron Research, NIST, Gaithersburg, MD 20899
[3]Quantum Condensed Matter Division, ORNL, Oak Ridge, TN 37831
[4]Department of Chemistry, Princeton University, Princeton, NJ 08544
[5]Department of Chemistry, Johns Hopkins University, Baltimore, MD 21218
[6]Department of Materials Science, Johns Hopkins University, Baltimore, MD 21218

Program Scope

The Institute for Quantum Matter brings together expertise in materials synthesis, theory, and spectroscopy with neutrons and THz photons to discover, understand, and control materials dominated by collective quantum physics. Areas of interest include quantum spin liquids in frustrated magnets, superconductivity near magnetism, and topological insulators.

Recent Progress

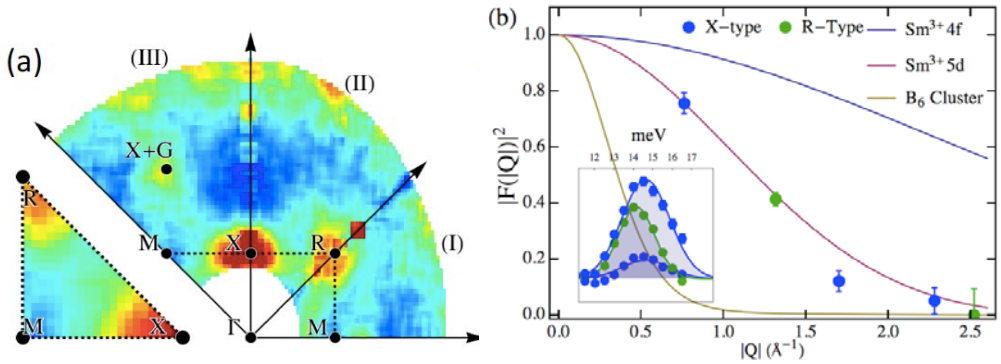

Fig. 1. Q-dependence within the 1st Brillouin zone of the integrated intensity of a spin resonance near 14 meV in the putative topological Kondo insulator SmB_6. (b) Q-dependence of the integrated intensity of the 14 meV resonance beyond the first Brillouin zone as a measure of the form factor, which resembles that of 5d electrons.

Following the recognition their band structures can be topologically non-trivial, there is renewed interest in Kondo insulators. For SmB_6 a mysterious surface conductivity might find explanation in topologically protected surface states. We show the surface conductivity of SmB_6 increases with carbon content. C is linked to more n-type carriers, larger low *T* specific heat, and a broader crossover to the insulator. XAS shows a change in Sm valence at the surface.

We present a full Q-space map of inelastic neutron scattering for the putative topological Kondo insulator SmB_6. The data reveal a collective exciton and we show the pseudo nesting conditions of a body diagonal dominated tight binding band structure accounts for the intensity pattern. The form factor indicates a prominent role for 5d electrons. The band structure is topologically non-trivial indicating a close connection between the pattern of inter-band neutron scattering and the topology of the band structure. Implementing strong f-electron repulsion through slave bosons, we show fluctuations within RPA can account for the exciton.

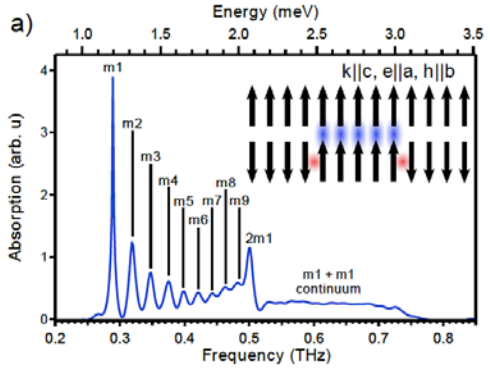

Figure. 2. THz absorption spectrum for $CoNb_2O_6$ at 1.6 K showing a hierarchy of excitations (m1-m9), the 2m1 excitation, and the continuum. The m1-m9 excitations can be modeled exceedingly well by a simple 1D Schrödinger equation in a linearly confining potential and its solutions based on Airy functions.

THz spectroscopy can probe low energy magnetic excitations of ferromagnetic and/or anisotropic spin systems that command intense interest due to unique collective properties. For quantum spin ice, THz photons provide access to the emergent electrodynamics of the U(1) spin liquid phase. At large B, both magnon and two-magnon excitations are observed in a <001> directed magnetic field and an unexpected left-hand polarized magnon. The g-factors are enhanced at low B indicating a crossover from magnons to the IQM proposed quantum string.

Using IQM crystals, we studied excitations in the 1D ferromagnetic Ising chain compound $CoNb_2O_6$ with THz spectroscopy. When antiferromagnetic (AFM) order develops at low *T*, nine spin flip bound states appear. Their energies are modeled by Airy function solutions to a 1D Schrodinger equation. The sequence of meson bound states terminates at a threshold near twice the lowest bound state energy. Above we see the two-particle continuum. At energies just below this threshold there is a prominent excitation from a bound state of bound states on neighboring chains. This assignment was corroborated by Tchernyshyov with theoretical evidence for a bound state below the 4-kink continuum.

As part of a larger study of cluster based inorganic magnetism, microwave and terahertz electron spin resonance, ^{7}Li nuclear magnetic resonance, muon spin rotation spectroscopies and neutron scattering was used to probe $LiZn_2Mo_3O_8$. The results show magnetism in $LiZn_2Mo_3O_8$ arises from a single isotropic S = 1/2 electron per Mo_3O_{13} cluster. The molecular spins form a triangular lattice with no magnetic ordering to *T*=0.07 K. Neutrons show this triangular-lattice AFM hosts collective magnetic excitations from spin ½ Mo_3O_{13} molecules. Apparently gapless (Δ< 0.2 meV) and extending at least up to 2.5 meV, this scattering involves 1/3 of the spins present above 100 K. The data are compatible with static or dynamic valence bonds.

The kagome spin-1/2 system is a central reference in frustrated magnetism. There is much progress in materials, experiments and theory and in the reporting period Tchernyshyov revisited the low-energy singlet sector of the model with an effective quantum dimer model. With exact diagonalizations we found embedding of a given process in its kagome environment leads to dramatic modifications of the amplitudes of the elementary loop processes. The resulting parameters are consistent with a Z2 spin liquid rather than with a valence-bond crystal, in agreement with the most recent density matrix renormalization group results.

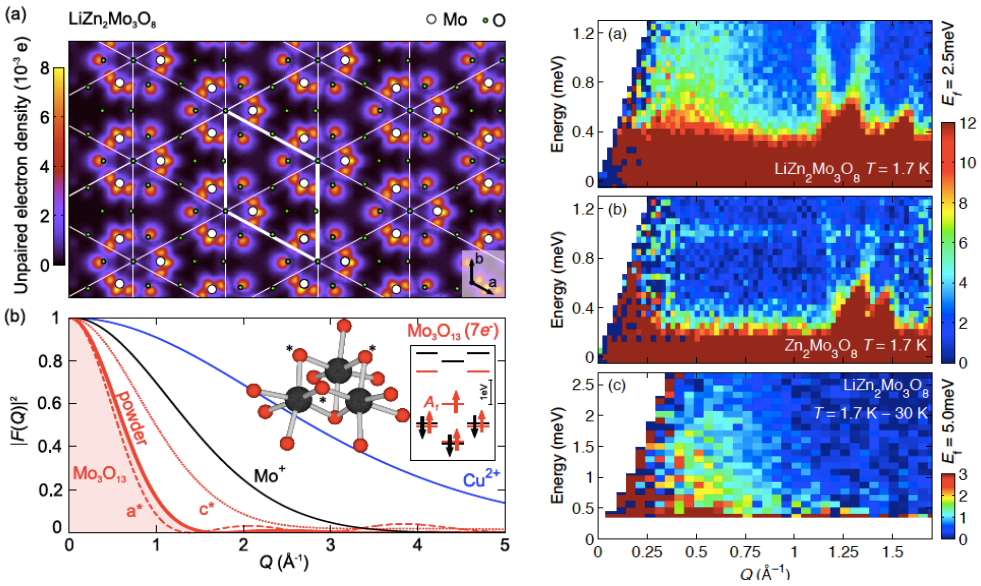

Fig. 3. Left: (a) spin distribution on Mo_3O_{13} clusters that form spin-1/2 degrees of freedom in $LiZn_2Mo_3O_8$. The corresponding form factor in (b) limits magnetic scattering to Q<1.3 $Å^{-1}$. Right: Inelastic magnetic scattering for (a) magnetic $LiZn_2Mo_3O_8$ and (b) non-magnetic $Zn_2Mo_3O_8$. (c) Shows the scattering for $LiZn_2Mo_3O_8$ is *T*-dependent.

The seminal theoretical work of Kitaev triggered interest in quantum magnets on honeycomb lattices. Spin-orbital models and anisotropic spin models are sought because they may display a spin-liquid state. Cava and his group commenced a search for interesting new physics and chemistry associated with the honeycomb lattice. We discovered two new delafossite honeycomb systems, $Cu_3Ni_2SbO_6$ and $Cu_3Co_2SbO_6$. Magnetic Ni^{2+} and Co^{2+} form a honeycomb lattice when Sb^{5+} orders on the triangular lattice. Non-magnetic Cu^{1+} sticks separate the planes. Inspired by the hydrated superconductor $Na_{1/3}CoO_2$:1.6H_2O, a similar hydration attempt was pursued here. The result was two new 2D materials $NaCo_2SbO_6$:2.3H_2O and $NaNi_2SbO_6$:2.3H_2O. There are two positive results: high oxidation states with improved M-O hybridization and enhanced 2D character. Clearly demonstrating the former effect, $NaCo_2SbO_6$:2.3H_2O is non-magnetic. However, $NaNi_2SbO_6$:2.3H_2O with Ni^{3+} realizes a honeycomb lattice magnet in the extreme spin-1/2 limit. Neutron scattering shows these compounds are quasi-2-D quantum magnets.

Future Plans

Informed by and coupled to theory, much synthesis work is ongoing to form materials with structures, quality, and energy scales for detailed neutron and THz experiments in quantum magnetism. Topological materials are playing an increasing role and THz photons and neutrons provide critical information. The high quality crystals from IQM are subjected to many measurements such as ARPES, XMCD, and STM through collaborations. We hope to probe quantum systems out of equilibrium with pulsed X-rays and pulsed neutrons in research linked to the theoretical work of Turner. There are continuing efforts to improve neutron methods to probe dynamic magnetic correlations in superconductors near magnetic instabilities.

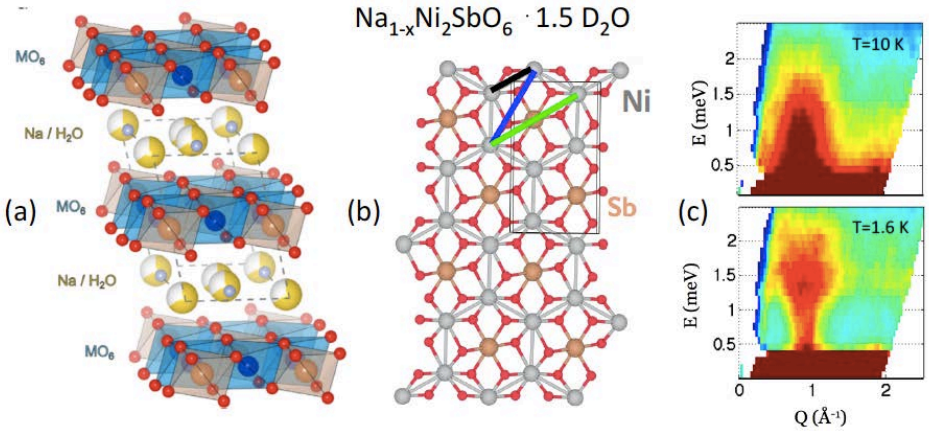

Fig. 4. Image of the new honeycomb S=1/2 quantum magnet $Na_{1-x}Ni_2SbO_6$:1.5D_2O discovered at IQM. (b) Image of three NN interactions. (c) neutron scattering from a powder sample showing strong inelastic scattering localized in Q-space though only extremely weak static short range spin order is detected.

Publications

1. "Direct link between bulk thermodynamic measurements and surface conduction in SmB_6," W. A. Phelan, S. M. Koohpayeh, P. Cottingham, J. W. Freeland, J. C. Leiner, C. L. Broholm, T. M. McQueen, arXiv:1403.1462, Phys. Rev. X **in press** (2014).
2. "Synthesis, floating zone crystal growth and characterization of the quantum spin ice $Pr_2Zr_2O_7$ pyrochlore," S.M. Koohpayeh, J.-J. Wen, B.A. Trump, C.L. Broholm, and T.M. McQueen, J. Cryst. Growth **402**, 291 (2014).
3. "The chemical instability of Na_2IrO_3 in the air," J.W. Krizan, J.H. Roudebush, G.M. Fox, and R.J. Cava, Mat. Res. Bull. **52**, 162-166 (2014).
4. "Strict limit on in-plane ordered magnetic dipole moment in URu_2Si_2," K. A. Ross, L.Harriger, Z. Yamani, W. J. L. Buyers, J. D. Garrett, A. A. Menovsky, J. A. Mydosh, and C. L. Broholm, arXiv:1402.2689, Phys. Rev. B **89**, 155122 (2014).
5. "Metallic state and charge order metal-insulator transition in a quasi-two-dimensional conductor κ-$(BEDT\text{-}TTF)_2Hg(SCN)_2Cl$," N. Drichko, R. Beyer, E. Rose, M. Dressel, J. A. Schlueter, S. A. Turunova, E. I. Zhilyaeva, and R. N. Lyubovskaya, Phys. Rev. B. **89** 075133 (2014).
6. "Local magnetism and spin correlations in the geometrically frustrated cluster magnet $LiZn_2Mo_3O_8$," J. P. Sheckelton, F. R. Foronda, LiDong Pan, C. Moir, R. D. McDonald, T. Lancaster, P. J. Baker, N. P. Armitage, T. Imai, S. J. Blundell, and T. M. McQueen, Phys. Rev. B **89**, 064407 (2014).
7. "Large-amplitude spin dynamics driven by a THz pulse in resonance with an electromagnon," T. Kubacka, J. A. Johnson, M. C. Hoffmann, C. Vicario, S. de Jong, P. Beaud, S. Grübel, S.-W. Huang, L. Huber, L. Patthey, Y.-D. Chuang, J. J. Turner, G. L. Dakovski, W.-S. Lee, M. P. Minitti, W. Schlotter, R. G. Moore, C. P. Hauri, S. M. Koohpayeh, V. Scagnoli, G. Ingold, S. L. Johnson, and U. Staub, Science **343**, 1333 (2014).

8. "A hierarchy of bound states in the 1D ferromagnetic Ising chain $CoNb_2O_6$ investigated by high resolution time-domain terahertz spectroscopy," C. M. Morris, R. Valdés Aguilar, A. Ghosh, S. M. Koohpayeh, J. Krizan, R. J. Cava, O. Tchernyshyov, T. M. McQueen, and N. P. Armitage, Phys. Rev. Lett. **112**, 137403 (2014).
9. "Ghost modes and continuum scattering in the dimerized kagome lattice antiferromagnet $Rb_2Cu_3SnF_{12}$," K. Matan, Y. Nambu, Y. Zhao, T. J. Sato, Y. Fukumoto, T. Ono, H. Tanaka, C. Broholm, A. Podlesnyak, and G. Ehlers, Phys. Rev. B **89**, 024414 (2014).
10. "Evidence for topologically protected surface states and a superconducting phase in $[Tl_4](Tl_{1-x}Sn_x)Te_3$ using photoemission, specific heat, magnetization measurements, and density functional theory," K.E. Arpino, D. C. Wallace, Y.F. Nie, T. Birol, P.D.C King, S. Chatterjee, M. Uchida, S. M. Koohpayeh, J.-J. Wen, K. Page, C. J. Fennie, K. M. Shen, T. M. McQueen, Phys. Rev. Lett. **112**, 017002 (2014).
11. "Molecular quantum magnetism in $LiZn_2Mo_3O_8$," M. Mourigal, W. T. Fuhrman, J. P. Sheckelton, A. Wartelle, J. A. Rodriguez-Rivera, D. L. Abernathy, T. M. McQueen, C. Broholm, Phys. Rev. Lett. **112**, 027202 (2014).
12. "Thermally driven ratchet motion of skyrmion microcrystal and topological magnon Hall effect," M. Mochizuki, X. Z. Yu, S. Seki, N. Kanazawa, W. Koshibae, J. Zang, M. Mostovoy, Y. Tokura, and N. Nagaosa, Nat. Mater. **13**, 241 (2014).
13. "Aging and reduced bulk conductance in thin films of the topological insulator Bi_2Se_3," R. Valdés Aguilar, L. Wu, A. V. Stier, L. S. Bilbro, M. Brahlek, N. Bansal, S. Oh, and N. P. Armitage, J. Appl. Phys. **113**, 153702 (2013).
14. "Optical floating zone crystal growth and magnetic properties of $MgCr_2O_4$," S. M. Koohpayeh, J. J. Wen, M. Mourigal, S. E. Dutton, R. J. Cava, C. Broholm, and T. M. McQueen, J. Cryst. Growth **384**, 39 (2013).
15. "Fractional topological insulators of Cooper pairs induced by proximity effect," P. Nikolic, T. Duric, and Z. Tesanovic, Phys. Rev. Lett. **110**, 176804 (2013).
16. Multiferroicity in the generic easy-plane triangular lattice antiferromagnet $RbFe(MoO_4)_2$, J.S. White, Ch. Niedermeyer, G. Gasparovic, C. Broholm, J.M.S Park, A. Shapiro, L. Demianets, M. Kenzelmann, Phys. Rev. B **88**, 060409(R) (2013).
17. "Unpaired Majorana modes in the gapped phase of Kitaev's honeycomb model," O. Petrova, P. Mellado, O. Tchernyshyov, Phys. Rev. B **88**, 140405 (2013).
18. "Localized states in the Mott insulator κ-$(BEDT\text{-}TTF)_2Cu[N(CN)_2]Cl$ as probed by photoluminescence," N. Drichko, R. Hackl, and J. Schlueter, Phys. Rev. B **88**, 115109 (2013).
19. "Dynamical structure factor of the triangular-lattice antiferromagnet," M. Mourigal, W. T. Fuhrman, A. L. Chernyshev, and M.E. Zhitomirsky, Phys. Rev. B **88**, 094407 (2013).
20. "Dynamics of an insulating skyrmion under a temperature gradient," Lingyao Kong and Jiadong Zang, Phys. Rev. Lett. **111**, 067203 (2013).
21. "Structure and properties of $Na_xM_2SbO_6 \cdot yH_2O$, M=Co(III), Ni(III) honeycomb oxyhydrates," J. H. Roudebush and R. J. Cava, J. Solid State Chemistry **204**, 178 (2013).

22. "Melting chiral order in terbium manganate ($TbMnO_3$) observed with resonant X-ray diffraction," S. W. Lovesey, V. Scagnoli, M. Garganourakis, S. M. Koohpayeh, C. Detlefs, U. Staub, J. Phys.: Condens. Matter **25**, 362202 (2013).
23. "Crystal structure and magnetic properties of the $Ba_3TeCo_3P_2O_{14}$, $Pb_3TeCo_3P_2O_{14}$, and $Pb_3TeCo_3V_2O_{14}$ langasites," J. Sol. Stat. Chem. **203**, 310 (2013).
24. "A sudden collapse in the transport lifetime across the topological phase transition in $(Bi_{1-x}In_x)_2Se_3$," L. Wu, M. Brahlek, R. V. Aguilar, A. V. Stier, C. M. Morris, Y. Lubashevsky, L. S. Bilbro, N. Bansal, S. Oh, and N. P. Armitage, Nat. Phys. **9**, 410 (2013)
25. "Fractional spinon excitations in The quantum Heisenberg antiferromagnetic chain," M. Mourigal, M. Enderle, A. Klopperpieper, J. S. Caux, A. Stunalt, and H. M. Rønnow, Nat. Phys. **9**, 435 (2013).
26. "Effective theory of fractional topological insulators in two spatial dimensions," P. Nikolic, Phys. Rev. B **87**, 245120 (2013).
27. "Universal features of counting statistics of thermal and quantum phase slips in nanosize superconducting circuits," A. Murphy, P. Weinberg, T. Aref, U.C. Coskun, V. Vakaryuk, A. Levchenko, A. Bezryadin, Phys. Rev. Lett. **110**, 247001 (2013)
28. "Quantum fluctuations in spin-ice-like $Pr_2Zr_2O_7$," K. Kimura, S. Nakatsuji, J.-J. Wen, C. Broholm, M. B. Stone, E. Nishibori, H. Sawa, Nat. Comm. **4**, 1934 (2013)
29. "Structure and magnetic properties of $Cu_3Ni_2SbO_6$ and $Cu_3Co_2SbO_6$ delafossites with honeycomb lattices," J. H. Roudebush, N. H. Andersen, R. Ramlau, V. O. Garlea, R. Toft-Petersen, P. Norby, R. Schneider, J. N. Hay, and R. J. Cava, Inorg. Chem. **52**, 6083 (2013)
30. "Stacking variants and superconductivity in the Bi-O-S system," W. A. Phelan, D. C. Wallace, K. E. Arpino, J. R. Neilson, K. J. Livi, C. R. Seabourne, A. J. Scott, and T. M. McQueen, J. Amer. Chem. Soc. **135**, 5372 (2013)
31. "Interaction proximity effect at the interface between a superconductor and a topological insulator quantum well," P. Nikolic and Z. Tesanovic, Phys. Rev. B **87**, 134511 (2013)
32. "A phenomenological Z2 lattice gauge theory of the spin-liquid state of the kagome Heisenberg antiferromagnet," Y. Wan and O. Tchernyshyov, Phys. Rev. B **87**, 104408 (2013).
33. "Theory of charge order and heavy-electron formation in the mixed-valence compound KNi_2Se_2," J.M. Murray and Z. Tesanovic, Phys. Rev. B **87**, 081103 (2013).
34. "Charge density wave fluctuations, heavy electrons, and superconductivity in KNi_2S_2," J. R .Neilson, A. Llobet, J.-J. Wen, M. R. Suchomel, and T. M. McQueen, Phys. Rev. B **87**, 045124 (2013).
35. "Charge and spin fractionalization in strongly correlated topological insulators," P. Nikolic, J. Phys: Condens. Matter **25**, 025602 (2013).
36. "Quasi-two-dimensional noncollinear magnetism in the Mott insulator $Sr_2F_2Fe_2OS_2$," L. L. Zhao, S. Wu, J. Wang, J. P. Hodges, C. Broholm, and E. Morosan, Phys. Rev. B **87**, 020406(R) (2013).

37. “Pairing instabilities in topological insulator quantum wells,” P. Nikolic and Z. Tesanovic, Phys. Rev. B **87**, 104514 (2013).
38. “Spin-1/2 Heisenberg antiferromagnet on kagome: a Z2 spin liquid with fermionic spinons,” Z.H. Hao and O. Tchernyshyov, Phys. Rev. B **87**, 214404 (2013).
39. “Fractionalized excitations in the spin-liquid state of a kagome-lattice antiferromagnet,” T.-H. Han, J. S. Helton, S. Chu, D. G. Nocera, J. A. Rodriguez-Rivera, C. Broholm, and Y. S. Lee, Nature **492**, 406 (2012).
40. “Unified formalism of Andreev reflection at a ferromagnet/superconductor interface,” T. Y. Chen, Z. Tesanovic, and C.L. Chien, Phys. Rev. Lett. **109**, 146602 (2012).
41. “Magnetic charge and ordering in kagome spin ice,” G.-W. Chern and O. Tchernyshyov, Phil. Trans. Roy. Soc. **A 370**, 5718 (2012).
42. “Magnetic field splitting of the spin-resonance in $CeCoIn_5$“, C. Stock, C. Broholm, Y. Zhao, F. Demmel, H.J. Kang, K.C. Rule, and C. Petrovic, Phys. Rev. Lett. **109**, 167207 (2012).
43. “From incommensurate correlations to mesoscopic spin resonance in $YbRh_2Si_2$,” C. Stock, C. Broholm, F. Demmel, J. Van Duijn, J. W. Taylor, H. J. Kang, R. Hu, and C. Petrovic, Phys. Rev. Lett. **109**, 127201 (2012).
44. “Evidence of a bond-nematic phase in $LiCuVO_4$,” M. Mourigal, M. Enderle, B. Fåk, R. K. Kremer, J. M. Law, A. Schneidewind, A. Hiess, and A. Prokofiev, Phys. Rev. Lett. **109**, 027203, (2012).
45. “Mixed-valence-driven heavy-fermion behavior and superconductivity in KNi_2Se_2“, J. R. Neilson, A. Llobet, A. V. Stier, L. Wu, J.-J. Wen, J. Tao, Y. Zhu, Z. B. Tesanovic, N. P. Armitage, and T. M. McQueen, Phys. Rev. B **86**, 054512 (2012) (Editors choice).
46. “Dimer impurity scattering, “reconstructed” nesting, and density-wave diagnostics in iron-pnictides,” J. Kang and Z. Tesanovic, Phys. Rev. B **87**, 220507(R) (2012).
47. “Quantum strings in quantum spin ice,” Y. Wan and O. Tchernyshyov, Phys. Rev. Lett. **108**, 247210 (2012).
48. “Low-energy electrodynamics of the Kondo-lattice antiferromagnet $CeCu_2Ge_2$,” G. Bossé, L. S. Bilbro, R. Valdés Aguilar, LiDong Pan, Wei Liu, A. V. Stier, Y. Li, L. H. Greene, J. Eckstein, and N. P. Armitage, Phys. Rev. B **85**, 155105 (2012).
49. “Terahertz response and colossal Kerr rotation from the surface states of the topological insulator Bi_2Se_3“, R. Valdes Aguilar, A.V. Stier, W. Liu, L.S. Bilbro, D.K. George, N. Bansal, J. Cerne, A.G. Markelz, S. Oh, and N.P. Armitage, Phys. Rev. Lett. **108**, 087403 (2012).
50. “Detecting non-magnetic excitations in quantum magnets,” Z. H. Hao, Phys. Rev. B **85**, 174432 (2012).
51. “Low temperature synthesis of LnOF rare-earth oxyfluorides through reaction of the oxides with PTFE,” S. E. Dutton, D. Hirai, R. J. Cava, Mat. Res. Bull. **47**, 714-718 (2012).
52. “Spin 1/2 delafossite honeycomb compound Cu_5SbO_6,” E. Climent-Pascual, P. Norby, N. H. Andersen, P. W. Stephens, H. W. Zandbergen, J. Larsen, and R. J. Cava, Inorg. Chem. **51**, 557 (2012).

Complex Electronic Materials

J. D. Thompson, F. Ronning, E. D. Bauer, T. Durakiewicz, M. Janoschek, J. J. Joyce, R. Movshovich, and H. Yasuoka*

Los Alamos National Laboratory, Los Alamos, NM 87545
***** Visiting Scientist, Japan Atomic Energy Agency, Tokai, Japan**

Program Scope

Complex electronic behaviors are most pronounced near magnetic/non-magnetic and metal/insulator boundaries in correlated materials and become particularly poorly understood as these boundaries are tuned to absolute zero temperature, i.e., to a quantum-critical point. With typically small characteristic energy scales, states of strongly correlated intermetallic compounds based principally on Ce, Yb, U and Pu can be tuned to these interesting boundaries with rather modest changes in a control parameter. The goal of this project is to develop an understanding of complex electronic materials and phenomena by discovering new examples of these and related materials that reveal both new states of electronic matter and the essential physics underlying their complex and collective states. Knowledge gained from studying correlated f-electron materials in parallel with technologically important d-electron materials provides a broad perspective necessary to guide the development of a microscopic theory of complex electronic materials. Success in this project of discovering new physics through new materials requires integration of materials preparation, in single crystal form where possible, with a necessarily broad suite of materials characterization techniques that probe static and dynamic degrees-of-freedom and their interactions on multiple length and time scales. Our approach is two-fold: one of initial exploratory research on new materials and phenomena and a second of in-depth investigations. At the exploratory stage, structure, transport, magnetic and thermodynamic measurements, often at very low temperatures, high pressures and high magnetic fields, are sufficient to identify new states that deserve more detailed study by various spin and charge spectroscopies, particularly neutron scattering, nuclear quadrupole/magnetic resonance and photoemission. DOE neutron and photon facilities, the Los Alamos NHMFL Pulsed Field Facility and Center for Integrated Nanotechnologies as well as an extensive network of experimental and theoretical collaborators substantially leverage in-house capabilities and are important to success of this project.

Recent Progress

Unconventional superconductivity in heavy-fermion $CeCoIn_5$ is ‘born’ out of strange normal state characterized by a linear-in-temperature resistivity and diverging specific heat divided by temperature. Just above a T_c of 2.3 K, the pressure-dependent resistivity deviates

slightly from its T-linear dependence, and long ago we had attributed this to the emergence of a pseudogap at $T_{PG}(P)$.[1] That speculation has been confirmed by tunneling conductance measurements carried out in collaboration with Yazdani's group at Princeton [2] and with Steffen Wirth [3] at the Max Planck Institute for Chemical Physics of Solids. As shown in Fig. 1a, the pseudogap persists even above the zero-temperature $H_{c2}^{[001]}$ =5T, and in Fig.1b, the temperature dependence of the pseudogap qualitatively follows the temperature dependence of a d-wave gap. The origin of this pseudogap remains to be determined, but its relationship to superconductivity (Fig. 1c) is reminiscent of the cuprate phase diagram.

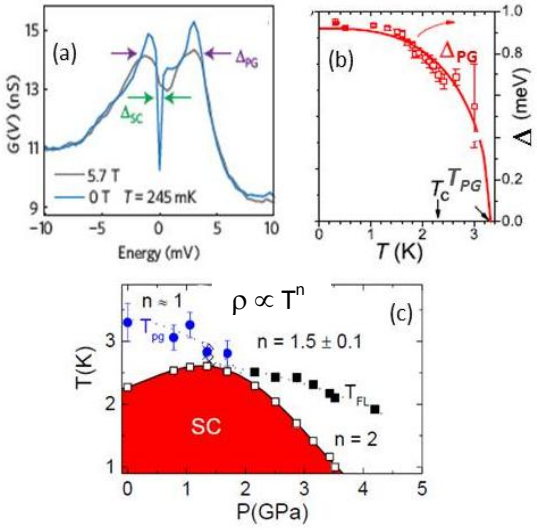

Fig. 1 Determination of the field [2] (a), temperature [3] (b) and pressure [3] (c) dependence of the pseudogap in $CeCoIn_5$. The solid cure in (b) is $\Delta(T) = \Delta_0[1-(T/T_{PG})^3]^{1/2}$.

We do not know if this pseudogap might influence the so-called Q-phase found just inside the low-temperature, high-field superconducting phase when H ⊥ [001], but coexistence of antiferromagnetic order and d-wave superconductivity in the Q-phase is even more interesting than previously thought. Careful neutron-diffraction measurements of the Q-phase find that the population of antiferromagnetic domains with orthogonal propagation wavevector changes abruptly as the field is rotated by only 0.2^0 away from the [100] direction.[4] This extreme sensitivity to field direction appears to be a consequence of the emergence of a Cooper-pair density wave (PDW) of mixed L=2,S=0/L=1,S=1nature that is predicted [5] when antiferromagnetic order and d-wave superconductivity are coupled. In this model, the magnetic field couples to the S=1 component of the PDW and controls the line node of the p-wavefunction, in turn determining the direction of the antiferromagnetic magnetic wavevector. A schematic illustration of the proposed PDW is shown in Fig. 2.

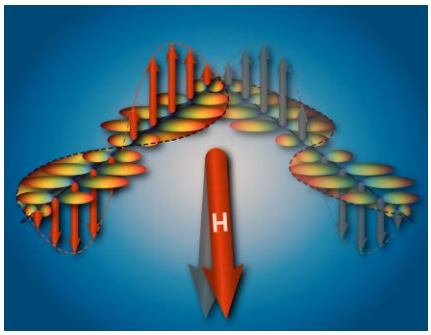

Fig. 2 Schematic illustration of a PDW inferred to exist in the Q-phase of $CeCoIn_5$.

The 'hidden order' (HO) phase that develops below 17.5 K in URu_2Si_2 continues to be mysterious and the subject of multiple theoretical proposals. Two recent proposals argue that the HO arises from hastatic order or a rank-5 superspin density wave. Both predict a small in-plane static magnetic moment of ≈ 0.015 μ_B/U. Our neutron-diffraction measurements on a 7-gm crystal of URu_2S_2 give a conservative upper limit of ≤ $1x10^{-3}\mu_B$/U on the in-plane moment, placing severe constraints on these interpretations. [6] Other theories associate HO with properties of a $5f^2$ localized configuration. Our high resolution ARPES measurements rule out

this possibility and further show that the HO produces a strongly momentum-dependent reconstruction of the Fermi surface.[7] Finally, our very high field NMR studies find that itinerant 5f electrons in the HO state undergo a first-order transition at a critical field of 35.6 T to phase II (Fig. 3), characterized by ordered Ising-like chains along the a-axis with ordered moments $\mu_0 \sim 0.6\mu_B$.[8]

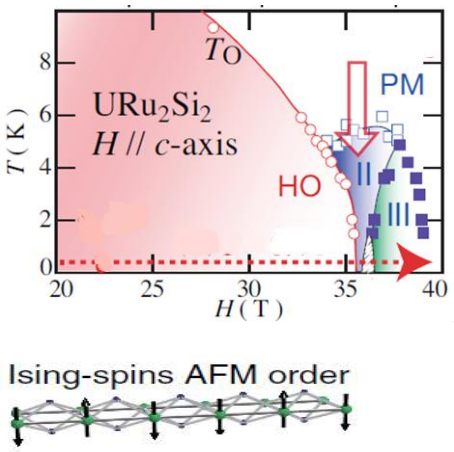

Fig. 3 Temperature-field phase diagram of URu_2Si_2 indicating phase II studied by NMR and proposed magnetic structure.

Future Plans

Initial exploratory and preliminary in-depth studies during the past few months suggest promising directions for research. In the area of new materials, we have started to explore a family of tetragonal materials $CeM_nAl_{2+2n}Si_2$ (M=Au, Rh, Ir, Pt). Several of these are magnetic and might become superconducting with applied pressure. Though not a new material, modestly heavy-fermion U_2PtC_2 has been explored very little, and our preliminary measurements suggest that its superconductivity may be quite unusual. We will continue these studies as well as search for Kondo-impurity responses in d-electron intermetallics. $CeRhIn_5$ is, in a sense, the 'mother' of Ce115 materials. We will determine the magnon spectrum in it (as well as in the heavy-fermion ferromagnet UGe_2) by neutron scattering, and explore the possibility of new quantum states that might emerge near $CeRhIn_5$'s field-tuned quantum-critical point at 50 T. The possibility of a topologically protected metallic surface state in Kondo insulators has become an interesting topic. We have begun preliminary studies of some candidate materials and will continue to pursue that subject using new techniques and approaches that we are developing.

References

[1] V. A. Sidorov *et al*., Phys. Rev. Lett. **89,** 157004 (2002). [2] B. Zhou *et al*., Nature Phys. **9**, 474 (2013). [3] S. Wirth *et al*., J. Phys. Soc. Jpn. **83**, 061009 (2014). [4] S. Gerber *et al*., Nature Phys. **10**,126 (2014). [5] A. Aperis *et al*., Phys. Rev. Lett. **104**, 216403 (2010). [6] P. Das *et al*., New J. Phys. **15**, 053031 (2013). [7] J-Q. Meng *et al*., Phys. Rev. Lett. **111**, 127002 (2013). [8] H. Sakai *et al*., Phys. Rev. Lett. **112**, 236401 (2014).

Publications

Only more significant publications supported by BES are listed from among approximately 65 since the beginning of FY13.

"Visualizing Nodal Heavy Fermion Superconductivity in $CeCoIn_5$," B. Zhou, S. Misra, E. H. daSilva Neto, P. Aynajian, R. E. Baumbach, J. D. Thompson, E. D. Bauer and A. Yazdani, Nature Phys. **9**, 474 (2013). (plus News and Views and cover)

"Surface Electronic Structure of the Topological Kondo-Insulator Candidate Correlated Electron System SmB_6," M. Neupane, N. Alidoust, S.-Y. Xu, T. Kondo, Y. Ishida, D.J. Kim, C. Liu, I. Belopolski, Y.J. Jo, T.-R. Chang, H.-T. Jeng, T. Durakiewicz, L. Balicas, H. Lin, A. Bansil, S. Shin, Z. Fisk and M.Z. Hasan, Nature Comm. **4**, 3991 (2013).

"Disorder in a Quantum Critical Superconductor," S. Seo, X. Lu, J.-X. Zhu, R. R. Urbano, N. Curro, E. D. Bauer, V. A. Sidorov, L. D. Pham, T. Park, Z. Fisk and J. D. Thompson, Nature Phys. **10**, 120 (2014). (plus News and Views and cover)

"Switching of Magnetic Domains Reveals Spatially Inhomogeneous Superconductivity," S. Gerber, M. Bartkowiak, J. L. Gavilano, E. Ressouche, N. Egetenmeyer, C. Niedermayer, A. D. Bianchi, R. Movshovich, E. D. Bauer, J. D. Thompson and M. Kenzelmann, Nature Phys. **10**,126 (2014).

"Persistent Optically Induced Magnetism in Oxygen-Deficient Strontium Titanate," W. D. Rice, P. Ambwani, M. Bombeck, J. D. Thompson, G. Haugstadt, C. Leighton and S. A. Crooker, Nature Mater. **13**, 481 (2014).

"Momentum-Resolved Evolution of the Kondo Lattice into 'Hidden Order' in URu_2Si_2," F. L. Boariu, C. Bareille, H. Schwab, A. Nuber, P. Lejay, T. Durakiewicz, F. Reinert, and A. F. Santander-Syro, Phys. Rev. Lett. **110**, 156404 (2013).

"Materials Prediction Scores a Hit," F. Ronning and J. L. Sarrao, Physics **6**, 109 (2013).

"Measurement of Two Low-Temperature Energy Gaps in the Electronic Structure of Antiferromagnetic USb_2 Using Ultrafast Optical Spectroscopy," J. Qi, T. Durakiewicz, S.A. Trugman, J.-X. Zhu, P.S. Riseborough, R. Baumbach, E.D. Bauer, K. Gofryk, J.-Q. Meng, J.J. Joyce, A.J. Taylor, and R.P. Prasankumar, Phys. Rev. Lett. **111**, 057402 (2013).

"Zero-Field Quantum Critical Point in $CeCoIn_5$," Y. Tokiwa, E. D. Bauer, and P. Gegenwart, Phys. Rev. Lett. **111**, 107003 (2013).

"Imaging the Three-Dimensional Fermi-Surface Pairing near the Hidden-Order Transition in URu_2Si_2 Using Angle-Resolved Photoemission Spectroscopy," J.-Q. Meng, P.M. Oppeneer, J.A. Mydosh, P.S. Riseborough, K. Gofryk, J.J. Joyce, E.D. Bauer, Y. Li, and T. Durakiewicz, Phys. Rev. Lett. **111**, 127002 (2013).

"Coexistence of Antiferromagnetism with Superconductivity in $CePt_2In_7$: Microscopic Phase Diagram Determined by ^{115}In NMR/NQR," H. Sakai, Y. Tokunaga, S. Kambe, F. Ronning, E. D. Bauer and J. D. Thompson, Phys. Rev. Lett. **112**, 206401 (2014).

"Emergent Antiferromagnetism out of the 'Hidden-Order' State in URu_2Si_2: High Magnetic Field Nuclear Magnetic Resonance to 40T," H. Sakai, Y. Tokunaga, S. Kambe, R. R. Urbano, M.-T. Suzuki, P. L. Kuhns, A. P. Reyes, P. H. Tobash, F. Ronning, E. D. Bauer and J. D. Thompson, Phys. Rev. Lett. **112**, 236401 (2014).

"Absence of a Static In-plane Magnetic Moment in the 'Hidden-Order' Phase of URu_2Si_2," P. Das, R.E. Baumbach, K. Huang, M.B. Maple, Y. Zhao, J.S. Helton, J.W. Lynn, E.D. Bauer, and M. Janoschek, New J. Phys. **15**, 053031 (2013).

"Microscopic Properties of the Heavy-Fermion Superconductor $PuCoIn_5$ Explored by Nuclear Quadrupole Resonance," G. Koutroulakis, H. Yasuoka, H. Chudo, P. Tobash, J. Mitchell, E. D. Bauer, and J. D. Thompson, New J. Phys. **16** 053019 (2014).

Additional publications since July 2012 follow:

H. Yasuoka, G. Koutrolakis, H. Chudo, S. Richmond, D. K. Veirs, A. I. Smith, E. D. Bauer, J. D. Thompson, G. D. Jarvinen and D. L. Clark, "Observation of ^{239}Pu nuclear magnetic resonance," *Science* **336**, 901 (2012).

P. Aynajian, E. H. da Silva Neto, A. Gyenis, R. E. Baumbach, J. D. Thompson, Z. Fisk, E. D. Bauer and A. Yazdani, "Visualizing the emergence of heavy fermions in a Kondo lattice," *Nature* **486**, 201 (2012).

X. Lu, H.-O. Lee, T. Park, F. Ronning, E. D. Bauer and J. D. Thompson, "Heat-capacity measurements of energy-gap nodes of the heavy-fermion superconductor $CeIrIn_5$ deep inside the pressure-dependent superconducting dome structure of its superconducting phase diagram," *Phys. Rev. Lett.* **108**, 027001 (2012).

W. K. Park, P. H. Tobash, F. Ronning, E. D. Bauer, J. L. Sarrao, J. D. Thompson, and L. H. Greene, "Observation of the hybridization gap and Fano resonance in the Kondo lattice URu_2Si_2," *Phys. Rev. Lett.* **108**, 246403 (2012).

M.M. Altarawneh, N. Harrison, G. Li, L. Balicas, P. H. Tobash, F. Ronning and E. D. Bauer, "Superconducting pairs with extreme uniaxial anisotropy in URu_2Si_2," *Phys. Rev. Lett.* **108,** 066407 (2012).

T. Park, H. O. Lee, I. Martin, X. Lu, V. A. Sidorov, K. Gofryk, F. Ronning, E. D. Bauer and J. D. Thompson, "Textured superconducting phase in the heavy fermion $CeRhIn_5$," *Phys. Rev. Lett.* **108**, 077003 (2012).

J.-X. Zhu, P. H. Tobash, E. D. Bauer, F. Ronning, B. L. Scott, K. Haule, G. Kotliar, R. C. Albers, and J. M. Wills, "Electronic structure and correlation effects in $PuCoIn_5$ as compared to $PuCoGa_5$," *Euro. Phys. Lett.* **95,** 57001 (2012)

H. B. Rhee, F. Ronning, J. X. Zhu, E. D. Bauer, J. N. Mitchell, P. H. Tobash, B. L. Scott, J. D. Thompson, Y. Jiang, C. H. Booth and W. E. Pickett, "$PuPt_2In_7$: A computational and experimental investigation," *Phys. Rev. B* **86**, 115137 (2012).

X. Lu, F. Ronning, P. H. Tobash, K. Gofryk, E. D. Bauer and J. D. Thompson, "Pressure-tuned point-contact spectroscopy of URu_2Si_2 from hidden order to antiferromagnetic states: similarity of the Fermi surface gapping," *Phys. Rev. B* **85**, 020402(R) (2012).

K. Gofryk, J.C. Lashley, F. Ronning, D. Safarik, F. Weickert, J.L. Smith, A. Leithe-Jasper, W. Schnelle, M. Nicklas, and H. Rosner, "Fully-gapped superconductivity in $Ba_{0.55}K_{0.45}Fe_{1.95}Co_{0.05}As_2$: a low-temperature specific heat study," *Phys. Rev. B* **85**, 224504 (2012).

T. Willers, D. T. Adroja, B. D. Rainford, Z. Hu, N. Hollmann, P. O. Koerner, Y. Y. Chin, D. Schmitz, H. H. Hsieh, H. J. Lin, C. T. Chen, E. D. Bauer, J. L. Sarrao, K. J. McClellan, D. Byler, C. Geibel, F. Steglich, H. Aoki, P. Lejay, A. Tanaka, L. H. Tjeng and A. Severing, "Spectroscopic determination of crystal-field levels in $CeRh_2Si_2$ and $CeRu_2Si_2$ and of the 4f(0) contributions in CeM_2Si_2 (M=Cu, Ru, Rh, Pd, and Au)," *Phys. Rev. B* **85**, 035117 (2012).

X. Gratens, L. Mendonca Ferreira, Y. Kopelevich, N. F. Oliveira, R. R. Urbano, R. A. Ribeiro, R. Movshovich, J. L. Sarrao, J. D. Thompson, Z. Fisk and P. G. Pagliuso, "Complex mixed state of the Pauli-limited superconductor $CeCoIn_5$," *Phys. Rev. B* **85**, 054502 (2012).

R. E. Baumbach, H. Chudo, Y. Yasuoka, F. Ronning, E. D. Bauer and J. D. Thompson, "$CeRu_2Al_2B$: A local moment 4f magnet with a complex T-H phase diagram," *Phys. Rev. B* **85**, 094422 (2012).

J. Kim, F. Ronning, N. Haberkorn, L. Civale, E. Nazaretski, Ni Ni, R. J. Cava, J. D. Thompson, and R. Movshovich, "Large magnetic penetration depth and thermal fluctuations in a $Ca_{10}(Pt_3As_8)[(Fe_{1-x}Pt_x)_2As_2]_5$ (x=0.097) single crystal," *Phys. Rev. B* **85**, 180504 (2012).

T. Klimczuk, C. H. Wang, K. Gofryk, F. Ronning, J. Winterlink, G. H. Fecher, J.-C. Griveau, E. Colineau, C. Felser, J. D. Thompson, D. J. Safarik and R. J. Cava, "Superconductivity in the Heusler family of intermetallics," *Phys. Rev. B* **85**, 174505 (2012).

D-J. Jang, J. B. Hong, Y. S. Kwon, T. Park, K. Gofryk, F. Ronning, J. D. Thompson and Y. Bang, "Evidence for ±s-wave pairing symmetry in LiFeAs: Specific heat study," *Phys. Rev. B* **85**, 180505 (2012).

S. Seo, D. Jang, T. Park, V. A. Sidorov, H. Lee, J. D. Thompson and Z. Fisk, "Pressure effects on the heavy-fermion antiferromagnet $CeAuSb_2$," *Phys. Rev. B* **85**, 205145 (2012).

P. H. Tobash, F. Ronning, J. D. Thompson, B. L. Scott, P. J. W. Moll, B. Batlogg and E. D. Bauer, "Single crystal study of the heavy-fermion antiferromagnet $CePt_2In_7$," *J. Phys.: Condens. Matter* **24**, 015601 (2012).

E. D. Bauer, M. M. Altarawneh, P. H. Tobash, K. Gofryk, J. N. Mitchell, R. D. McDonald, C. H. Mielke, F. Ronning, J.-C. Griveau, E. Colineau, R. Eloirdi, R. Caciuffo, B. L. Scott, O. Janka, S. M. Kauzlarich and J. D. Thompson, "Localized 5f electrons in superconducting $PuCoIn_5$: Consequences for superconductivity in $PuCoGa_5$," *J. Phys.: Condens. Matter* **24**, 052206 (2012).

R. E. Baumbach, T. Shang, M. Torrez, F. Ronning, J. D. Thompson and E. D. Bauer, "Local moment ferromagnetism in $CeRu_2Ga_2B$," *J. Phys.: Condens. Matter* **24**, 185702 (2012).

J. D. Thompson and Z. Fisk, "Progress in heavy-fermion superconductivity: Ce115 and related materials," *J. Phys. Soc. Jpn*. **81**, 011002 (2012). (Invited)

R. Slater, H. Bie, S. S. Stoyko, E. D. Bauer, J. D. Thompson and A. Mar, "Rare-earth chromium gallides RE_4CrGa_{12} (*RE* = Tb–Tm)," *J. Solid State Chem.* **196**, 409 (2012).

T. Park, X. Lu, H. O. Lee and J. D. Thompson, "Textured superconductivity in the presence of a coexisting order: Ce115s and other heavy-fermion compounds," *Physica C* **481**, 223 (2012). (Invited)

C. H. Booth, Y. Jiang, D. L. Wang, J. N. Mitchell, P. H. Tobash, E. D. Bauer, M. A. Wall, P. G. Allen, D. Sokaras, D. Nordlund, T. C. Weng, M. A. Torrez and J. L. Sarrao, "Multiconfigurational nature of 5f orbitals in uranium and plutonium intermetallics," *Proc. Nat. Acad. Sci.* **109,** 10205 (2012).

B.G. Ueland, C. F. Miclea, Y. Kato, O. Ayala-Valenzuelu, R. D. McDonald, R. Okazaki, P. H. Tobash, M. A. Torrez, F. Ronning, R. Movshovich, Z. Fisk, E. D. Bauer, I. Martin and J. D. Thompson "Controllable chirality-induced geometrical Hall effect in a frustrated highly-correlated metal," *Nature Commun*. **3**, 1067 (2012).

N. Harrison, P.J.W. Moll, S.E. Sebastian, L. Balicas, M.M. Altarawneh, J.-X. Zhu, P.H. Tobash, F. Ronning, E.D. Bauer and B. Batlogg, "Drastic change in the Fermi surface topology of URu_2Si_2 at high magnetic fields," *Phys. Rev. B* **88**, 180404 (R) (2013).

Y. Tokiwa, E. D. Bauer and P. Gegenwart, "Quasiparticle entropy in the high-field superconducting phase of $CeCoIn_5$," *Phys. Rev. Lett.* **109,** 116402 (2012).

K. Gofryk, F. Ronning, J.-X. Zhu, M. N. Ou, P. H. Tobash, S. S. Stoyko, X. Lu, A. Mar, T. Park, E. D. Bauer, J. D. Thompson and Z. Fisk, "Electronic tuning and uniform superconductivity in $CeCoIn_5$," *Phys. Rev. Lett.* **109**, 186402 (2012).

P. Das, J. S. White, A. T. Holmes, S. Gerber, E. M. Forgan, A. D. Bianchi, M. Kenzelmann, M. Zolliker, J. L. Gavilano, E. D. Bauer, J. L. Sarrao, C. Petrovic and M. R. Eskildsen, "Vortex lattice studies in $CeCoIn_5$ with H perpendicular to c," *Phys. Rev. Lett.* **108**, 087002 (2012).

V. A. Sidorov, X. Lu, T. Park, H. Lee, P. H. Tobash, R. E. Baumbach, F. Ronning, E. D. Bauer and J. D. Thompson, "Pressure phase diagram and quantum criticality of $CePt_2In_7$ single crystals," *Phys. Rev. B* **88**, 020503(R) (2013).Rapid Commun.

G. Li, Q. Zhang, D. Rhodes, B. Zeng, P. Goswami, R. E. Baumbach, P. H. Tobash, F. Ronning, J. D. Thompson, E. D. Bauer, and L. Balicas, "Bulk evidence for a time-reversal symmetry broken superconducting state in URu_2Si_2," *Phys. Rev. B* **88**, 134517 (2013).

V. R. Fanelli, J. M. Lawrence, E. D. Bauer, K. J. McClellan, J. D. Thompson, E. A. Goremychkin, R. Osborn, C. H. Booth, A. D. Christianson, and P. S. Riseborough, "Q-dependence of the spin fluctuations in the intermediate valence compound $CePd_3$," *J. Phys.: Condens. Matter **26**, 225602 (2014).*

F. L. Boariu, C. Bareille, H. Schwab, A. Nuber, P. Lejay, T. Durakiewicz, F. Reinert, and A. F. Santander-Syro, "Momentum-resolved evolution of the Kondo lattice into `hidden-order' in URu_2Si_2", *Phys. Rev. Lett.* **110,** 156404 (2013).

K. Huang, J.J. Hamlin, R.E. Baumbach, M. Janoschek, N. Kanchanavatee, D.A. Zocco, F. Ronning, and M.B. Maple, "Ferromagnetic quantum critical point in $UCo_{1-x}Fe_xGe$," *Phys. Rev. B* **87**, 054513 (2013).

B Woo, S. Seo, E. Park, J. H. Kim, D. Jang, T. Park, H. Lee, F. Ronning, J. D. Thompson, V. A. Sidorov and Y. S. Kwon, "Effects of pressure on the ferromagnetic state of the CDW compound $SmNiC_2$," *Phys. Rev. B* **87**, 125121 (2013).

R. E. Baumbach, V. A. Sidorov, Xin Lu, N. J. Ghimire, F. Ronning, B. L. Scott, D. J. Williams, E. D. Bauer, and J. D. Thompson, "Suppression of antiferromagnetism by pressure in $CaCo_2P_2$," *Phys. Rev. B* **89**, 094408 (2014).

N. Ni, W. E. Straszheim, D. J. Williams, M. A. Tanatar, R. Prozorov, E. D. Bauer, F. Ronning, J. D. Thompson and R. J. Cava, "Transport and thermodynamic properties of $(Ca_{1-x}La_x)_{10}(Pt_3As_8)(Fe_2As_2)_5$ superconductors," *Phys. Rev. B* **87**, 060507 (2013).

T. Shang, L. Yang, Y. Chen, N. Cornell, F. Ronning, J. L. Zhang, L. Jiao, Y. H. Chen, Y. Chen, A. Howard, J. Dai, J. D. Thompson, A. Zakhidov, M. B. Salamon and H. Q. Yuan, "Tunable interplay between 3d and 4f electrons in Co-doped iron pnictides," *Phys. Rev. B* **87**, 075148 (2013).

J. S. Kim, B.D. Faeth, Y. Wang, P.J. Hirschfeld, G. R. Stewart, K. Gofryk, F. Ronning, A. S. Sefat, K.Y. Choi, and K.H. Kim, "Specific heat to H_{c2}: evidence for nodes or deep minima in the superconducting gap of underdoped and overdoped $Ba(Fe_{1-x}Co_x)_2As_2$," *Phys. Rev. B* **86**, 014513 (2012).

H. Sakai, Y. Tokunaga, S. Kambe, R. E. Baumbach, F. Ronning, E. D. Nauer and J. D. Thompson, "NMR study for 4f-localized ferromagnet $CeRu_2Ga_2B$," *Phys. Rev. B* **86**, 094402 (2012).

B Woo, S. Seo, E. Park, J. H. Kim, D. Jang, T. Park, H. Lee, F. Ronning, J. D. Thompson, V. A. Sidorov and Y. S. Kwon, "Effects of pressure on the ferromagnetic state of the CDW compound $SmNiC_2$," *Phys. Rev. B* **87**, 125121 (2013).

J. Kim, N. Haberkorn, M. J. Graf, I. Usov, F. Ronning, L. Civale, E. Nazaretski, G. F. Chen, W. Yu, J. D. Thompson and R. Movshovich, "Magnetic penetration-depth measurement of a suppressed superfluid density of superconducting $Ca_{0.5}Na_{0.5}Fe_2As_2$ single crystals by proton irradiation," *Phys. Rev. B **86**,* 144509 (2012).

T. Zhou, G. Koutroulakis, J. Lodico, Ni Ni, J. D. Thompson, R. J. Cava and S. E. Brown, "Antiferromagnetic order in $Ca_{10}(Pt_3As_8)(Fe_2As_2)_5$ observed by ^{75}As NMR," *J. Phys.: Condens. Matter* **25**, 122201 (2013).

T. Klimczuk, V. Sidorov, A. Szajek, M. Werwinski, S. A. J. Kimber, A. L. Kozub, D. Safarik, J. D. Thompson and R. J. Cava, "Structure and paramagnetism in weakly correlated Y_8Co_5," *J. Phys.: Condens. Matter* **25**, 125701 (2013).

F. Ronning, J.-X. Zhu, T. Das, M.J. Graf, R.C. Albers, H.B. Rhee, and W.E. Pickett, "Superconducting gap structure of the 115s revisited," *J. Phys.: Condens. Matter* **24**, 294206 (2012).

O. Janka, R. E. Baumbach, J. D. Thompson, E. D. Bauer and S. M. Kauzlarich, "Crystal structure, magnetism and transport properties of $Ce_3Ni_{25.75}Ru_{3.16}Al_{4.1}B_{10}$," *J. Solid. State Chem*. **205**, 154 (2013).

R. E. Baumbach, X. Lu, F. Ronning, J. D. Thompson and E. D. Bauer, "Pressure tuned ferromagnetism in $CeRu_2M_2X$ (M=Al, Ga; X=B,C)," *J. Phys. Condens. Matter* **24**, 325601 (2012).

E. D. Bauer, P. H. Tobash, J. N. Mitchell and J. L. Sarrao, "Single crystal growth of plutonium compounds from molten metal fluxes," *Phil. Mag.*, **92**, 2466 (2012).

C. H. Booth, Y. Jiang, S. A. Medling, D. L. Wang, A. L. Costello, D. S. Schwartz, J. N. Mitchell, P. H. Tobash, E. D. Bauer, S. K. McCall, M. A. Wall and P. G. Allen, Self-irradiation damage to the local structure of plutonium and plutonium intermetallics. *J. Appl. Phys.*, **113** 093502 (2013).

T. Shang, R. E. Baumbach, K. Gofryk, F. Ronning, Z. F. Weng, J. L. Shang, X. Lu, E. D. Bauer, J. D. Thompson and H. Q. Yuan, "$CeIrIn_5$: Superconductivity on a magnetic instability," *Phys. Rev. B* **89**, 041101 (2014).

M. N. Ou, K. Gofryk, R. E. Baumabch, S. S. Stoyko, J. D. Thompson, J. M. Lawrence, E. D. Bauer, F. Ronning, A. Mar and Y. Y. Chen, "Hole doping effect on superconductivity in $Ce(Co_{1-x}Ru_x)In_5$," *Phys. Rev. B* **88**, 195134 (2013).

P. Aynajian, E. H. da Silva Neto, B. Zhou, S. Misra, R. E. Baumbach, Z. Fisk, J. Mydosh, J. D. Thompson, E. D. Bauer and A. Yazdani, "Visualizing heavy fermion formation and their unconventional superconductivity in f-electron materials," *J. Phys. Soc. Jpn*. **83**, 061008 (2014). (invited)

S. Wirth, Y. Prots, M. Wedel, S. Ernst, S. Kirchner, Z. Fisk, J. D. Thompson, F. Steglich and Y. Grin, "Structural investigations of $CeIrIn_5$ and $CeCoIn_5$ on macroscopic and atomic length scales," J. *Phys. Soc. Jpn.* **83**, 061009 (2014). (invited)

R. E. Baumbach, B. L. Scott, F. Ronning, J. D. Thompson and E. D. Bauer, "Single crystal study of antiferromagnetic $CePd_3Al_9$," *J. Phys.: Condens. Matter* **26**, 025601 (2014).

H. Chudo, G. Koutroulakis, H. Yasuoka, E. D. Bauer, P. H. Tobash, J. N. Mitchell and J. D. Thompson, "Weak itinerant antiferromagnetism in $PuIn_3$ explored using ^{115}In nuclear quadrupole resonance," *J. Phys.: Condens. Matter* **26,** 036001 (2014).

T. Zhou, G. Koutroulakis, J. Lodico, Ni Ni, J. D. Thompson, R. J. Cava and S. E. Brown, Antiferromagnetic order in $Ca_{10}(Pt_3As_8)(Fe_2As_2)_5$ observed by ^{75}As NMR," *J. Phys.: Condensed Matter* **25**, 122201 (2013).

Collaborator-driven publications

R. Yu, C. F. Miclea, F. Weickert, R. Movshovich, A. Paduan-Filho, V. S. Zapf and T. Roscilde, "Quantum critical scaling at a Bose-glass/superfluid transition: theory and experiment on a model quantum magnet," *Phys. Rev. B* **86**, 134421 (2012). [FWP contribution: participation in dilution fridge measurments and pawer writing]

J. Kim, N. Haberkorn, S-Z. Lin, L. Civale, E. Nazaretski, B. H. Moeckly, C. S. Yung, J. D. Thompson and R. Movshovich, "Superconducting properties of a MgB_2 thin film with large intraband diffusivity," *Phys. Rev. B* **85**, 180504 (2012). [FWP contribution: susceptibility measurement and assistance with technique development and paper writing]

J. Kim, N. Haberkorn, L. Civale, P. Dowden, A. Saxena, J. D. Thompson and R. Movshovich, "Direct observation of magnetic phase coexistence and magnetization reversal in a $Gd_{0.67}Ca_{0.33}MnO_3$ thin film," *Appl. Phys. Lett.* **100**, 022407 (2012). [FWP contribution: susceptibility measurement and assistance with technique development and paper writing]

R. Yu, L. Yin, N. S. Sullivan, J. S. Xia, C. Huan, A. Paduan-Filho, N. F. Oliveira, S. Haas, A. Steppke , C. F. Miclea , F. Weickert , R. Movshovich , E.-D. Mun , B. L. Scott ,V. S. Zapf and T. Roscilde, "Bose glass and Mott glass of quasiparticles in a doped quantum magnet," *Nature* **489**, 379 (2012). [FWP contribution: participation in dilution refrigerator measurments and paper writing]

J. Kim, N. Haberkorn, L. Civale, P. Dowden, and R. Movshovich, "Ferromagnetic bubble clusters in magnetic phase separated $Y_{0.67}Ca_{0.33}MnO_3$ thin films", *Appl. Phys. Lett.*(in press). [FWP contribution: assistance with technique development and paper writing]

J. Kim, L. Civale, E. Nazaretski, N. Haberkorn, F. Ronning, A. S. Sefat, Y. Tajima, B. H. Moeckley, J. D. Thompson and R. Movshovich, "Direct measurement of the magnetic penetration depth by magnetic force microscopy," *Supercond. Sci. Technol.* **25**, 112001 (2012). (Rapid Commun.) [FWP contribution: assistance with sample characterization, technique development and paper writing]

A. V. Tsvyashchenko, V. A. Sidorov, L. N. Fomichea, K. Gofryk, R. A. Sadykov and J. D. Thompson, "Magnetism and superconductivity in $EuFe_2As_2$ synthesized under high pressure," *Phys. Status Solidi B* **250**, 589 (2013). [FWP contribution: susceptibility measurement and assistance with pressure measurement and paper writing]

J. Zhang, P. H. Tobash, W. D. Pryz, D. J. Buttey, N. Hur, J. D. Thompson, J. L. Sarrao and S. Bobev, "Synthesis, structural characterization and physical properties of the early rare-earth metal digermanides $REGe_{2-x}$ ($x\approx1/4$) [RE=La-Nd, Sm]. A case study of commensurately and incommensurately modulated structures," *Inorganic Chem.* **52**, 953 (2013). [FWP contribution: susceptibility measurement and assistance with sample preparation]

F. S. Elkin, I. P. Zibrov, A. P. Novikov, S. S. Khasanov, V. A. Sidorov, A. E. Petrova, T. A. Lograsso, J. D. Thompson and S. M. Stishov, "Thermodynamics of the ferromagnetic phase transition in nearly half metallic CoS_2 at high pressures," *Solid State Commun.* **181**, 41 (2014). [FWP contribution: susceptibility/magnetization and high pressure measurements and help writing manuscript]

Local complexity and the mechanics of phase transitions in novel materials

Despina Louca, University of Virginia

Program scope

Novel materials of interest today provide unique opportunities through which emergent exotic states of matter that arise from the intricate coupling of the electronic and lattice degrees of freedom, and of their implications in the mechanics of phase transitions can be explored. Central to our subject of study is the evaluation of distinct structural features that arise from circumstances relating to the coexistence of two (or more) order parameters, the nucleation of different phases in the parent matrix, spin/charge density waves, the formation of structural patterns that break the global symmetry and are present even at equilibrium conditions. Such features have proven to be key components to our understanding of the evolution across phase boundaries. However, they cannot be readily characterized with traditional means used for probing single electron behavior. This is because their behavior is a collective effect, in response to strong interactions.

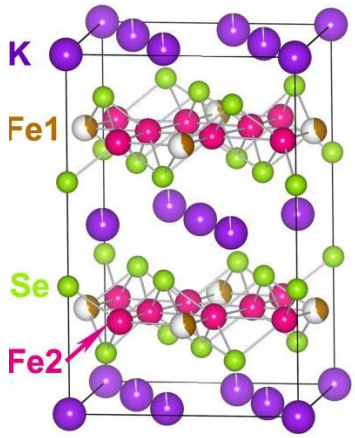

Fig. 1: The crystal structure of $K_xFe_{2-y}Se_2$ in the I4/m symmetry with Fe vacancies at the Fe1 site. The Fe2 site is always full.

The impact of the crystal structure permeates deep into the structure-property relationships. Many representative systems, old and new, provide a venue to explore unconventional behaviors, potentially leading to new physics. The tremendous interest stirred up from the discoveries of new topological insulators in two and three dimensions [1], graphene-type physics [2], the Fe-based superconductors [3] and the superconducting topological insulators [4], has led experimentalists and theorists alike to new quests in this ever-evolving field. Understanding the underlying mechanisms will most likely lead to discoveries of new emergent phenomena that may be better controlled. An important aspect of the underlying physics is that these systems display inhomogeneities at different length- and time-scales [5]. How does one cope with such complexity arising from this collective behavior? Nowadays, it is possible to tackle these problems because of unique experimental techniques, such as the pair density function analysis technique.

Recent progress

In this talk, the local structure of the Fe-based superconductors will be discussed. These systems provide an unprecedented possibility for manipulating their transition temperatures, T_C, by changing the chemistry of their structures, and exploring fluctuations in the magnetic, charge and orbital competing mechanisms. While the parent compound's ground state can either be insulating or metallic, magnetic or non-magnetic, superconductivity can be brought about by inducing disorder, by intercalation between the superconducting planes, and by spin wave fluctuations.

In the Fe-based superconductors [6], the close proximity of magnetism to superconductivity is as important as in the cuprates [7]. However, the ground state properties of the Fe-based system are quite and uniquely different from those of the cuprates, creating a fertile ground for substantial work. For example, magnetic fluctuations or even a magnetically ordered state can be present in

the superconducting phase, Fermi surface nesting leading to a spin density wave is important to some systems, while the phonon contribution to the superconducting mechanism is not negligible. If an electron-phonon coupling mechanism is assumed, the value of T_C obtained from the calculation is not high enough which suggests that they are not of the BCS type. The Fe-based crystal system consists of Fe tetrahedra coordinated by As/P or Se/Te. The calculations of electronic structures and magnetic properties point to an unusual sensitivity of the bond lengths between ions as well as the bond angles [8], and their precise nature has been determined via the local atomic structure [9].

From the analysis of the local structure, the Fe ligand environment is revealed which is a key component to determining the degree of hybridization of the Fe orbitals with their surrounding ligand ions that in turn affects electron itinerancy, the magnitude of the local moment as well as superconductivity. For instance, in $FeSe_{1-x}Te_x$, we observed that the local symmetry is lower than the average tetragonal *P*4/*nmm* crystal symmetry because the Se and Te ions do not share the same site, leading to two distinct *z* coordinates that exhibit two types of bond angles and two types of bond lengths with Fe. Such modulations of the ionic lattice can change the distribution of valence electrons. At the same time, in $Ba(Fe_{1-x}Co_x)_2As_2$, we studied how the structure distorts by overdoping that may in turn be related to the disappearance of superconductivity.

While suppression of long-range magnetic ordering occurs with the onset of superconductivity in the above systems, this is not the case in $K_xFe_{2-y}Se_2$ with a T_C of the order of 30 K or so [10]. The intercalated FeSe has a very complex phase diagram where the superconducting phase coexists with large magnetic moments and a high antiferromagnetic transition, T_N, close to 560 K and is sandwiched between semi-metallic (x < ~0.7) and insulating (x > ~0.8) antiferromagnetic states [11]. The crystal system shown in Fig. 1 consists of iron vacancies at one of the two possible crystal sites and of their ordering that gives rise to the $\sqrt{5} \times \sqrt{5} \times 1$ type unit cell with the I*4/m* crystal symmetry. The vacancies go through an order-disorder transition at T_S ~ 500 K, while in the high temperature disordered state, the symmetry is *I4/mmm*. This system presents an opportunity to investigate the interplay of magnetism, superconductivity and vacancies. It is currently debated whether this system is phase separated or not.

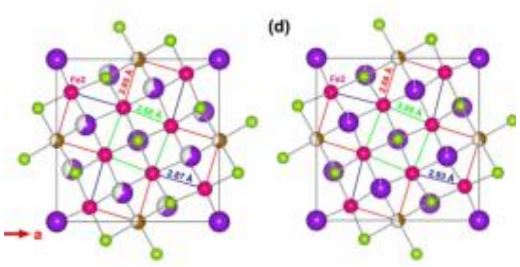

Fig. 2: The crystal structure of $K_xFe_{2-y}Se_2$ in the I4/m symmetry with vacancies. The crystal structure of $K_xFe_{2-y}Se_2$ in the I4/m symmetry with vacancies.

In a series of $K_xFe_{2-y}Se_2$ we investigated the local lattice via neutron scattering [12]. The local structure present in the superconducting state (with x ~ 0.8) can be described quite well using a superstructure consisting of equal ratios of the experimentally determined local structures corresponding to the x = 0.6 and 1.0 as shown in Fig. 2. This suggests that atomically, the x = 0.8 superconductor is not a different phase but evolves continuously by doping K into the vacancy ordered $\sqrt{5} \times \sqrt{5} \times 1$ structure. To reproduce the local configuration observed in the x ~ 0.8 composition, it is necessary to expand the inner square Fe2 plaquette (drawn in green) from the short Fe-Fe (shown on the left and corresponding to the x = 0.6 composition) to the long Fe-Fe bonds (shown on the right and corresponding to the x = 1.0 composition).

Future plans

This is indeed a very peculiar system partly because of the presence of vacancies both at the K and Fe sites and partly because magnetic order coexists with superconductivity. The true nature of the superconducting state has been hotly debated with many different scenarios put forth. With the debate centered on the crystal structure, it has been proposed that the superconducting state is stoichiometric and phase separates from the parent matrix. In another scenario, the superconducting state is not necessarily stoichiometric, and depending on the preparation conditions, different phases can be achieved. However, in yet another scenario, the vacancy ordered state is presumed to be the superconducting state with no phase separation.

Given that the answers appear to be sample dependent, a more systematic approach is necessary to address this issue. Thus we propose to continue exploring the sample growth conditions and studying the local symmetry.

References

1. "*Topological Insulators: Star Material*", G. Brunfiel, Nature **466**, 310 (2010).
2. "*Two-dimensional gas of massless Dirac fermions in graphene*", K. S. Novoselov, A. K. Geim, S. V. Morozov, D. Jiang, M. I. Katsnelson, I. V. Grigorieva, S. V. Dubonos and A. A. Firsov, Nature **438**, 192 (2005).
3. "*Iron-Based Layered Superconductor La[$O_{1-x}F_x$]FeAs (x = 0.05−0.12) with T_c = 26 K*", Y. Kamihara, T. Watanabe, M. Hirano and H. Hosono, J. Am. Chem. Soc. **130**, 3296 (2008).
4. "*Majorana Fermions and Exotic Surface Andreev Bound States in Topological Superconductors: Application to $Cu_xBi_2Se_3$*", T. H. Hsieh and L. Fu, Phys. Rev. Lett. **108**, 107005 (2012).
5. "*Why stripes? Spontaneous formation of inhomogeneous structures due to elastic interactions*", D. I. Khomskii and K. I. Kugel, Europhys. Lett. **55**, 208 (2001).
6. "*A novel large moment antiferromagnetic order in $K_{0.8}Fe_{1.6}Se_2$ superconductor*", W. Bao, Q. Huang, G. F. Chen, M. A. Green, D. M. Wang, J. B. He, X. Q. Wang, and Y. Qiu, *Chin. Phys. Lett.* **28**, 086104 (2011).
7. "*Evidence for Stripe Correlations of Spins and Holes in Copper-Oxide Superconductors",* J. M. Tranquada, B. J. Sternlieb, J. D. Axe, Y. Nakamura, and S. Uchida, Nature **375**, 561 (1995).
8. "*Effect of Structural Parameters on Superconductivity in Fluorine-Free $LnFeAsO_{1-y}$ (Ln = La, Nd)*", C.-H. Lee, A. Iyo, H. Eisaki, H. Kito, M. T. Fernandez-Diaz, T. Ito, K. Kihou, H. Matsuhata, M. Braden, and K. Yamada, J. Phys. Soc. Jpn. **77**, 083704 (2008).
9. "*The local atomic structure of superconducting Fe-Se-Te*", D. Louca, K. Horigane, A. Llobet, P. Tong, K. Yamada, Phys. Rev. B **81**, 134524 (2010).
10. "*Superconductivity in the iron selenide $K_xFe_2Se_2$ ($0 \leq x \leq 1.0$)*", J. Guo, S. Jin, G. Wang, S. Wang, K. Zhu, T. Zhou, M. He, and X. Chen, Phys. Rev. B **82**, 180520(R) (2010).
11. "*Electronic and magnetic phase diagram in $K_xFe_{2-y}Se_2$ superconductors*", Y. J. Yan, M. Zhang, A. F. Wang, J. J. Ying, Z. Y. Li, W. Qin, X. G. Luo, J. Q. Li, J. P. Hu and X. H. Chen, Sci. Rep. **2**, 00212 (2012).
12. *"The hybrid lattice of $K_xFe_{2-y}Se_2$: why superconductivity and magnetism can coexist"*,D. Louca, K. Park, B. Li, J. Neuefeind, J. Yan, Sci. Rep. **3**, doi:10.1038/srep02047 (2013).

Two year publication list

1. "Suppression of magnetic coupling by in-plane buckling in $SrFeO_2$", K. Horigane, A. Llobet, and D. Louca, Phys. Rev. Lett. **112**, 097001 (2014).
2. "Intertwining of frustration with magneto-elastic coupling in the multiferroic $LuMnO_3$", S. Yano, D. Louca, S. Chi, M. Matsuda, Y. Qiu, J. R. D. Copley, S. W. Cheong, J. Phys. Soc. JPN **83**, 024601 (2014).
3. "Structure and composition of the superconducting phase in alkali iron selenide $KyFe_{1.6+x}Se_2$", S. V. Carr, D. Louca, J. Siewenie, Q. Huang, A. Wang, X. Chen, P. Dai, Phys. Rev. B **89**, 134509 (2014).
4. "Dynamics of the local pair correlations in $FeSe_xTe_{1-x}$ determined by inelastic neutron scattering", K. Park, Y.-Q. Yan, and D. Louca, accepted in J. Supercond. Novel Magn. (2014).
5. "Dynamic octahedral fluctuations and the effects on orbital ordering in $YTiO_3$", B. Li, D. Louca, B. Hu, J. Zhou, N. A. Benedek, J. B. Goodenough, accepted J. Phys. Soc. JPN (2014).
6. "Local strain and anharmonicity in the bonding of $Bi_2Se_{3-x}Te_x$ topological insulators", K. Park, Y. Nomura, R. Arita, A. Llobet, D. Louca, Phys. Rev. B **88**, 224108 (2013).
7. "The hybrid lattice of $K_xFe_{2-y}Se_2$: why superconductivity and magnetism can coexist", D. Louca, K. Park, B. Li, J. Neuefeind, J. Yan, Scientific Reports **3**, doi:10.1038/srep02047 (2013).
8. "Magnetic transition broadening and local lattice distortion in the negative thermal expansion antiperovskites $Cu_{1-x}Sn_xNMn_3$", P. Tong, D. Louca, G. King, A. Llobet, J. C. Lin and Y. P. Sun, Appl. Phys. Lett. **102**, 041908 (2013).
9. "Dilute magnetism and magnetopolaron melting in $LaCo_{1-y}Ni_yO_3$", J. Yu, D. Phelan, J. A. Rodriguez-Rivera, D. Louca, J. Supercond. Novel Magn. **26**, 2627-2632 (2013).
10. "Oxygen mediated magneto-electric coupling in $LuMnO_3$", P. Tong, D. Louca, N. Lee, and S.-W. Cheong, Phys. Rev. B **86**, 094419 (2012).

A hierarchy of "meson" bound states in the 1D ferromagnetic Ising chain $CoNb_2O_6$ investigated by high resolution time-domain terahertz spectroscopy

C. M. Morris[1], R. Valdés Aguilar[1], A. Ghosh[1], S. M. Koohpayeh[1], J. Krizan[2], R. J. Cava[2], O. Tchernyshyov[1], T. M. McQueen[1], N. P. Armitage[1]*

[1]Institute for Quantum Matter, Johns Hopkins University
[2]Department of Chemistry, Princeton University

The Ising spin chain is one of the most paradigmatic examples of quantum complex material system. In this work, "kink" bound excited states have been studied in perhaps the most ideal realization of a one dimensional ferromagnetic Ising chain compound -- $CoNb_2O_6$ -- using high resolution time-domain terahertz spectroscopy. When magnetic order develops at low temperature, nine bound states of kinks become visible. Their energies can be modeled exceedingly well by the Airy function solutions to a 1D Schrodinger equation with a linear confining potential. This sequence of "meson" bound states terminates at a threshold energy near two times the energy of the lowest bound state. Above this energy scale we observe a broad feature consistent with the onset of the two particle continuum. At energies just below this threshold we observe a prominent excitation that we interpret as a novel bound state of bound states -- two pairs of kinks on neighboring chains. I will also discuss our preliminary work on this compound tuning with transverse magnetic field through the quantum critical point that is putatively described by an emergent E8 symmetry group.

* This research was conducted under the auspices of the Institute for Quantum Matter (IQM) at Johns Hopkins University, and supported by the U. S. Department of Energy, office of Basic Energy Sciences, Division of Materials Sciences and Engineering under grant DE-FG02-08ER46544.

Neutron Scattering Studies of Magnetism, Orbital Hybridization and Electron Itinerancy in Fe-based Superconductors

I. A. Zaliznyak (zaliznyak@bnl.gov), D. Fobes, M. Hücker, G. D. Gu, G. Y. Xu, and J. M. Tranquada
Condensed Matter Physics & Materials Science Department
Brookhaven National Laboratory, Upton, NY 11973-5000
A. Savici, B. Winn, O. Garlea and M. Lumsden
Neutron Sciences Directorate, Oak Ridge National Laboratory, Oak Ridge, TN 37831-6477

Program Scope

The physical mechanisms underlying the unconventional high-temperature superconductivity (HTSC) both in cupric oxides and in more recently discovered iron pnictide and chalcogenide materials remain poorly understood. Such understanding is needed because HTSC provides attractive technological opportunities and because it is now widely recognized that fundamental physical phenomena involved in HTSC are also common to many other material functionalities. Namely, a competition between strong correlation, which favors local-moment magnetism and kinetic energy of electron hopping (itinerancy), which depends on orbital hybridization and often involves low-energy orbital degrees of freedom, leads to the formation of new electronic and structural phases, and often to nano-scale phase separation. In addition to HTSC, these phases exhibit thermoelectric, multiferroic and magnetoresistive responses, all with potential technological functionalities. Their electronic nature is revealed by static and dynamical magnetism measured by neutron scattering and its correlation with the structure and the bulk transport properties.

In this project, we apply neutron scattering to investigate the nature of the magnetism and the character of magnetic correlations, focusing primarily on the $Fe_{1+y}Te_{1-x}(Se,S)_x$ system. In particular, we address the relative role of magnetic moments from localized electrons (meaning electrons at energies much greater than *kT* away from the Fermi energy, which do not participate in charge transport) and the conduction electrons. We consider the interaction between these two species and the role of degenerate 3*d* orbitals and orbital ordering in Fe-based materials, where the orbital-selective Mott transition is possible. We also investigate competing magnetic interactions and frustration and the role of hybridization of the electronic Wannier functions revealed by magnetic form factor.

Recent Progress

Orbital order and phase diagram of $Fe_{1+y}Te$. Recent studies by our group and others have established that electronic properties of the 11 iron chalcogenides are very sensitive to non-stoichiometric iron at interstitial sites. In particular, $Fe_{1+y}Te_{1-x}Se_x$ samples with same Se doping can be either superconducting or non-superconducting, depending on y. It was further established that the antiferromagnetic end member $Fe_{1+y}Te$ has a complex magneto-structural (y, T) phase diagram. At low concentrations, $y < 0.05$, there is a first-order magnetostructural transition from the paramagnetic tetragonal P4/nmm phase to monoclinic P21/m with bicollinear AFM order with propagation vector q = (0.5, 0, 0.5) and metallic resistivity, $dR/dT > 0$ [8]. At high $y > 0.12$,

the low-T phase is orthorhombic Pnmm, with an incommensurate helimagnetic spin order and the resistivity remains semiconducting. At intermediate y, the frustration effects of the interstitial Fe decouple different orders, leading to a sequence of transitions. In our recent work we have established that the development of bicollinear antiferromagnetic order and metallic electronic coherence at y ≈ 0.1 is uniquely associated with a hysteretic first-order transition to the bond-order wave (BOW) phase, which follows the monoclinic lattice distortion and the incommensurate magnetic order, but at a markedly lower temperature. The BOW state, Fig. 1, suggests ferro-orbital ordering, where electronic delocalization in ferromagnetic zigzag chains leads to metallic transport. This picture is also corroborated by our earlier study, where it was established that the total amount of magnetic scattering in $Fe_{1.1}Te$ decreases significantly, by about a factor 2, upon cooling from 100 K to 10 K, corresponding to change in the local-spin value from S = 3/2 to S = 1.

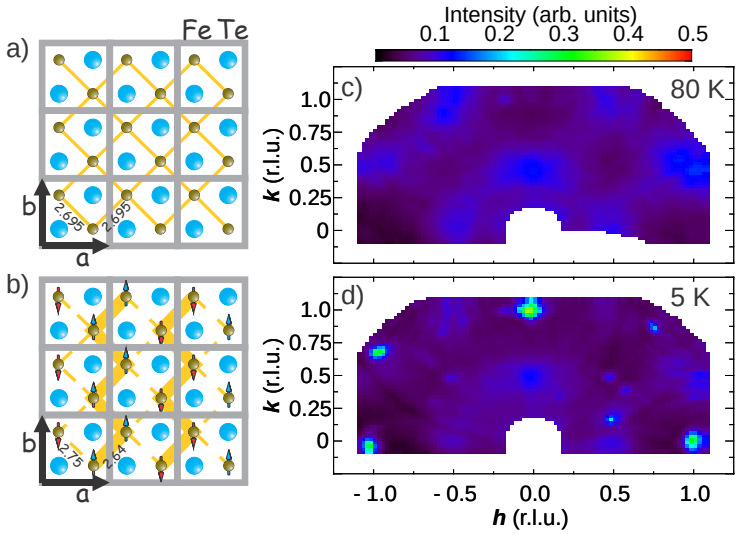

Figure 1. FeTe unit cell in the a-b plane, (a), and formation of zigzag chains with the bicollinear magnetic structure, (b). (c), (d) show elastic neutron scattering from $Fe_{1.09(1)}Te$ measured on HYSPEC (E_i = 7.75 meV). (1,0,0) and (0,1,0) Bragg peaks, which measure the zigzag order are seen at 5 K (d) but not at 80 K (c).

Plaquette liquid correlations in $Fe_{1+y}Te_{1-x}(Se,S)_x$. Our analysis of inelastic and quasielastic scattering in poorly-metallic magnetic state of Fe_{1+y} Te reveals short-range spin correlations where four-iron square plaquettes align ferromagnetically, with antiferromagnetic correlations between the neighboring plaquettes. When this material is doped, with Se or S, and begins to develop superconductivity, the structure of magnetic diffuse scattering changes. Here, we observe a different liquid-like magnetic response, which can be described by the newly emergent local structure of slanted four-iron antiferromagnetic plaquettes. These new local correlations break the C_4 symmetry of the underlying square lattice and can therefore be related to "nematicity" observed by other techniques. The competition between the two types of dynamical local magnetic structures is suggestive of liquid-liquid phase transition in the electronic spin system of FeTe when it is doped, with Se or S, to become a superconductor. It is revealed by the change in the relative population of the two phases with temperature, where the C_4 square plaquettes present in Fe_{1+y} Te become dominant at high T. The newly emerging slanted plaquettes perhaps reflect new electronic hybridization pattern, which is favored by the shift of atomic energy levels that results from doping and which facilitates electron pairing. The structure of a plaquette is probably reflective of particular electronic Wannier functions, which define the orbital content of electronic bands in the tight binding view. The experimentally observed extent of magnetic scattering in the wave vector space suggests strong covalent reduction of magnetic form factor, supporting strong hybridization of the 3*d* magnetic electrons of iron.

Future Plans

Temperature dependence of magnetic inelastic and quasielastic diffuse scattering in $Fe_{1+y}Te_{1-x}(Se,S)_x$ samples where the superconductivity is present reveals competition of two types of short-range plaquette correlations. We plan to further investigate the temperature and compositional dependence of these plaquette liquid phases and their relationship with transport and structural properties.

The BOW transition, which likely results from orbital ordering and electron delocalization, is observed in $Fe_{1.1}Te$. While orbital degrees of freedom are universally considered important in iron-based superconductors, they are still poorly understood and deserve further studies. In particular, we plan to search for specific excitations, perhaps of magneto-structural character, which are associated with the orbital order. These are expected near the corresponding (1, 0, 0) and (0, 1, 0) Bragg peaks, where we have previously observed unusually strong phonon intensity. Polarized neutron studies will be performed to identify magnetic component of these excitations. We also plan to investigate whether the decrease of the inelastic magnetic scattering intensity, which occurs in the same temperature range as BOW transition, is indeed associated with BOW formation, as it has been speculated. There have also been recent reports that an irreversible change in magnetic susceptibility of $Fe_{1+y}Te$ can be induced by applying high magnetic field. In our view, this change can be explained as a magnetic breakdown of the orbital-ordered, metallic state, resulting in electron localization. We plan to investigate this idea by performing quasi-Laue diffraction experiment on SEQUOIA and using pulsed magnetic fields up to 30 T.

Publications (past two years)

1. I. A. Zaliznyak, Z. J. Xu, J. S. Wen, J. M. Tranquada, G. D. Gu, V. Solovyov, V. N. Glazkov, A. I. Zheludev, V. O. Garlea, and M. B. Stone.
   Continuous magnetic and structural phase transitions in $Fe_{1+y}Te$.
   Phys. Rev. B **85**, 085105 (2012).
2. Qing Jie, Rongwei Hu, Emil Bozin, A. Llobet, I. Zaliznyak, C. Petrovic, and Q. Li.
   Electronic thermoelectric power factor and metal-insulator transition in $FeSb_2$.
   Phys. Rev. B **86**, 115121 (2012).
3. G. Simutis, S. Gvasaliya, M. Månsson, A. L. Chernyshev, A. Mohan, S. Singh, C. Hess, A. T. Savici, A. I. Kolesnikov, A. Piovano, T. Perring, I. Zaliznyak, B. Büchner, A. Zheludev.
   Spin Pseudogap in Ni-Doped $SrCuO_2$.
   Phys. Rev. Lett. **111**, 067204 (2013).
4. Igor A. Zaliznyak, John M. Tranquada.
   Neutron Scattering and Its Application to Strongly Correlated Systems.
   arXiv:1304.4214 (2013); in Strongly Correlated Systems: Experimental Techniques.
   Edited by A. Avella and F. Mancini (2014).
5. Daixiang Mou, R. M. Konik, A. M. Tsvelik, I. Zaliznyak, Xingjiang Zhou.
   Charge-density wave and one-dimensional electronic spectra in blue Bronze: Incoherent solitons and spin-charge separation.
   Phys. Rev. B **89**, 201116 (2014).
6. John M. Tranquada, Guangyong Xu, Igor A. Zaliznyak.
   Superconductivity, Antiferromagnetism, and Neutron Scattering.

J. Magn. Magn. Mater. **350**, 148-160 (2014).
7. David Fobes, Igor A. Zaliznyak, Zhijun Xu, Ruidan Zhong, Genda Gu, John M. Tranquada, Leland Harriger, Deepak Singh, V. Ovidiu Garlea, Mark Lumsden, Barry Winn.
Ferro-orbital ordering transition in iron telluride $Fe_{1+y}Te$.
Phys. Rev. Lett. **112**, 187202 (2014).

Other Poster Abstracts

Exploring exotic states in URu_2Si_2 and U_2PtC_2

E. D. Bauer[1], A. M. Mounce[1], H. Sakai[2], N. Wakeham[1], G. Koutrolakis[1], H. Sakai[2], Y. Tokunaga[2], S. Kambe[2], R. R. Urbano[3], M.-T. Suzuki[2], P. L. Kuhns[4], A. P. Reyes[4], P. H. Tobash[1], F. Ronning[1], H. Yasuoka[2], N. Ni[1], and J. D. Thompson[1]

[1]Los Alamos National Laboratory, Los Alamos, New Mexico 87545, USA
[2]Advanced Science Research Center, Japan Atomic Energy Agency, Tokai, Ibaraki 319-1195, Japan
[3]Instituto de Física "Gleb Wataghin", Universidade Estadual de Campinas, 13083-859 Campinas, SP, Brazil
[4]National High Magnetic Field Laboratory, Florida State University, Tallahassee, Florida 32310, USA

Program Scope

A component of our project on 'Complex Electronic Materials' is to discover and understand new states of matter that emerge from strong electronic correlations, particularly in f-electron systems. Unconventional forms of superconductivity are an example of new states that are of particular interest, and to understand the origin of unconventional superconductivity, it is necessary to explore both the nature of that superconductivity and the, often unusual, normal state out of which it develops.

Recent Progress

Novel states of matter arise from coupled spin, charge and lattice degrees of freedom in strongly correlated electron materials. In URu_2Si_2, a transition into a "hidden" order state occurs at T_{HO}=17.5 K, whose origin is not known despite 30 years of intense research. At much lower temperatures, superconductivity develops out of this hidden order. In part, progress on this problem has been impeded by spurious responses due to less than perfect samples. To minimize these complications, we have grown high quality single crystals of URu_2Si_2 prepared from our electro-refined elemental uranium. These new crystals permit more definitive tests of theoretical predictions.

A recent theory of "hastatic" order has been proposed to describe the order parameter of this novel state, involving two sets of U 5f electrons hybridized with a conduction electron bath.[1] Our recent neutron diffraction measurements[2] of URu_2Si_2 reveal that there is no induced magnetic moment within the ab-plane, as predicted by this hastatic order model. Nuclear magnetic resonance measurements have been performed in high magnetic fields up to 40 T to further investigate the hidden order state and adjacent magnetic phases.[3] We find evidence for a magnetic structure above H_c=35 T caused by an Ising-type anisotropy of the uranium magnetic

moments, providing a testable prediction for future theoretical models of the hidden order state in URu_2Si_2.

Superconductivity at T_c=1.5 K in U_2PtC_2 was discovered in 1969 but has remained largely unexplored.[4] We have performed nuclear magnetic resonance measurements[5] on aligned powders of this U-based tetragonal superconductor down to 100 mK and in magnetic fields up to 12 T. These measurements indicate the presence of ferromagnetic correlations in the normal state above T_c and a Knight shift that remains constant in both field orientations in the superconducting state. Along with a powerlaw behavior of the spin-lattice relaxation rate $1/T_1 \sim T^2$ below T_c, the experiments are consistent with an unconventional, spin-triplet superconducting order parameter. Thus, U_2PtC_2 may be a rare example of a spin-triplet superconductor in close proximity to ferromagnetism, as is likely the case in Sr_2RuO_4.

Future Plans

In URu_2Si_2, there are indications that additional symmetries are broken upon entering the hidden order state. In collaboration with Prof. Ian Fisher (Stanford Univ.), we will investigate the possibility that the hidden order is an electronic nematic phase, in which the rotational symmetry of the lattice is broken, but the translational invariance remains. Such nematic states have been observed in other correlated electron materials including the high-T_c cuprates, iron-pnictide superconductors and $Sr_3Ru_2O_7$. In addition, certain symmetries of the hidden order can be probed directly by Raman scattering techniques, which we will pursue in collaboration with Prof. Girsh Blumberg (Rutgers). Determining these symmetries will allow additional tests of theoretical proposals for the nature of the hidden order broken symmetries.

As these novel states of matter have appeared in the layered U-based materials URu_2Si_2 and U_2PtC_2, we will search for new physics in other layered materials. One promising family we will explore is the $CeT_nAl_{2n+2}Si_2$ (T=transition metal) tetragonal compounds, which are made of TAl_2 and $CeAl_2Si_2$ atomic building blocks.

References

(Bold references are attributed to our BES project)
[1] P. Chandra, P. Coleman, R. Flint, Nature **493**, 621 (2013).
[2] P. Das et al. New J. Phys. 15, 053031 (2013).
[3] H. Sakai et al. Phys. Rev. Lett. 112, 236401 (2014).
[4] B. T. Matthias et al. Proc. Nat. Acad. Sci. **64**, 459 (1969).
[5] A. M. Mounce et al. (submitted to Phys. Rev. Lett.).

Building Neutron Scattering Infrastructure in Louisiana for Advanced Materials

J. F. DiTusa[1] (ditusa@phys.lsu.edu), D. Zhang[2], J. Zhang[1], W. A. Shelton[3], J. C. Garno[2], R. Jin[1], V. T. John[4], R. Kumar[2], Y. M. Lvov[5], Z. Mao[6], E. Nesterov[2], E. W. Plummer[1], S. W. Rick[7], D. P. Young[1], M. Khonsari[8]

[1]Department of Physics and Astronomy, Louisiana State University, Baton Rouge, LA 70803
[2]Department of Chemistry, Louisiana State University, Baton Rouge, LA 70803
[3]Department of Chemical Engineering, Louisiana State University, Baton Rouge, LA 70803
[4]Department of Chemical and Biolmolecular Engineering, Tulane University, New Orleans, LA 70118
[5]Institute for Micromanufacturing, Louisiana Tech University, Ruston, LA 71272
[6]Department of Physics and Engineering Physics, Tulane University, New Orleans, LA 70118
[7]Department of Chemistry, University of New Orleans, New Orleans, LA 70148
[8]Louisiana Board of Regents, Baton Rouge, LA 70821

Program Scope: This recently awarded DOE EPSCoR / Louisiana Board of Regents program aims to build a major neutron scattering infrastructure capable of treating both soft and hard materials. The objectives of this initiative include: discovery of the role of coupling of degrees of freedom that determine the emergent properties of complex materials, training of highly talented students and postdocs in synthesis and neutron scattering techniques who will become the next generation of neutron users; and building a base of users of the Spallation Neutron Source (SNS) and the High Flux Isotope Reactor (HFIR) in the southern region of the USA;

The main scientific focus of this program is to understand the role of coupling in emergent complex materials and its impact on the structure/property relationship, and to explore how this information can be applied in the guided-design of materials with the desired properties. Our goal is to tune dominant couplings to enhance critical properties in order to derive new functionality. In particular, many of the most interesting materials display coupling both in their static and dynamical behavior, making neutron scattering the ideal tool to elucidate fundamental relationships. Understanding these relationships is key for the "directed design" of the next generation of materials for both fundamental research and technological applications.

Future Plans: Hard Materials. The exotic properties of many complex transition metal compounds are intimately related to nonlinear couplings between charge, spin, oribital, and lattice degrees of freedom. Emergent phenomena such as unconventional superconductivity, multiferroicity, colossal magnetoresistivity, metal-to-insulator transitions, and quantum phase transitions are the consequence of these couplings. The challenge to be addressed is to unravel these complex nonlinear couplings and to identify if a particular coupling gives rise to the observed behavior or if the interactions are more intimately coupled. Transition metal compounds offer exotic physical properties that are extremely susceptible to subtle changes with doping, magnetic field, and pressure. In particular, many of the most interesting materials display coupling between lattice and spin, both in their static and dynamical behavior so that neutron scattering measurements are often invaluable to elucidate the fundamental relationship

of this coupling to the observed phenomena. Our research will focus on the static and dynamic coupling in a carefully selected set of materials using elastic and inelastic neutron scattering as a function of uniaxial pressure and magnetic field.

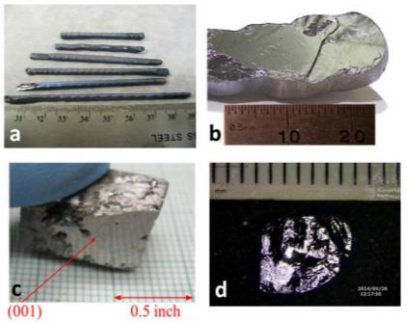

Fig. 1: Single Crystals grown in our laboratories a) Sr_2RuO_4 single crystals grown using the floating-zone method (Z. Mao) b) $Sr_3(Ru_{1-x}Mn_x)_2O_7$ crystal grown via floating-zone technique (R. Jin). c) Typical $Fe_{1.02}(Te_{0.6}Se_{0.4})$ single crystal (15g) grown using the self-flux method (Z. Mao). d) FeSi single crystal grown by flux method (D.

We plan to explore the transition metal ruthenate $Sr_3Ru_2O_7$, both in its nominally pure form and with Mn substitutions, $Sr_3(Ru_{1-x}Mn_x)_2O_7$, to search for evidence of coupling between phonon line width and dispersion and the magnetic excitation spectrum in single crystals (Fig. 1). We then will be able to compare with calculations to test our ability to simulate the dispersion and, possibly, the line width of phonons[1]. $Sr_3Ru_2O_7$ is a member of the Ruddlesden-Poper ruthenates $Sr_{n+1}Ru_nO_{3n-1}$ with n=2. It is an itinerant paramagnet but close to both an AFM and ferromagnetic (FM) instability[2], with an observation of quantum-critical behavior coupled with a metamagnetic transition[3]. In fact, FM fluctuations have been identified that may couple to the phonons[4,5]. Comparisons with calculations of electronic structure and phonons as a function of the magnetic states, induced by doping, magnetic field or uniaxial pressure, will allow us to identify potential mechanisms associated with these properties.

In the same vein, we will explore the single layer ruthenate, Sr_2RuO_4, with Co and Mn dopants to investigate whether disturbing the Ru sites causes a change in the *p*-wave superconducting state of the parent and/or stabilizes a magnetic ground state. We will use our STM to study the distribution of the dopants and how they perturb the electronic states nearby followed by systematic neutron scattering investigations in collaboration with ORNL. The goal is to reveal the evolution of magnetic excitation spectra and phonons with Co and Mn doping as well as the structural changes caused by doping, to establish a structure-property-magnetic field phase diagram. These proposed studies are expected to address the novel physics of orbital dependent magnetism and superconductivity observed in Sr_2RuO_4.

A second line of investigation involves the exploration of transition metal monosilicides and germanides that form in the cubic B20 crystal structure which is unusual in that it lacks a center of inversion symmetry[6]. As a result of this non-centrosymmetric structure, the Dzyaloshinskii-Moriya interaction is active and causes the itinerant magnetic phases that tend to form to be helimagnetic (HM) with wavelengths that vary from 3 to 90 nm[7]. This class of compounds includes MnSi, MnGe, $Fe_{1-x}Co_xSi$ and FeGe which have all received enormous recent attention because of the discovery of a novel topologically interesting magnetic phase[8]. In chiral magnets, solitons take the form of one-dimensional kinks or two-dimensional vortices called Skyrmionswhich are stabilized in a crystalline. They are extremely robust and can be manipulated by electric currents. This Skyrmion lattice phase consists of a hexagonal array of vortex-like swirls of spins with a 2-dimensional lattice constant set by the wavevector of the

zero-field HM phase. In this program, we will explore the effect of uniaxial pressure on the interesting magnetic states of B20 transition metal compounds.

Soft Materials: In the domain of soft matter, i.e. materials that include macromolecules, colloids, and surfactants, a recurring theme is the autonomous organization of molecular structures into mesoscale assemblies that give rise to a wide spectrum of properties. Understanding the interplay between molecular interactions, structure, and function is key for the "directed design" of next generation materials. Development of new strategies towards organic films with novel chemistry and controlled mesoscale structures is an important area of research. The main scope of our research is to investigate the growth and structure of optically or electrically active organic thin films that are prepared by novel chemistry, i.e. surface-confined controlled polymerization and layer-by-layer (LbL) deposition. These growth methods are expected to produce thin films with controlled and ordered structures that can deliver enhanced optical, electrical or mechanical properties relative to spin-coated films. The research will combine materials synthesis, neutron and X-ray scattering techniques, and multi-scale computational modeling to gain an understanding of the emergence and evolution of mesoscale structures and defects during the complex thin film growth processes.

The control of mesoscale organization and molecular structure of the polymers is particularly important in increasing the efficiency of organic polymer bulk heterojunction (BHJ) solar cells. Surface-confined polymerization of monomers ("grafting from" approach)[9] enables the in situ preparation of semiconducting polymer thin films (and devices based on them) directly from the small-molecule monomers, and affords greater control over mesoscale organization in the resulting films. Here, we will investigate the polythiophene (PT) thin film growth using a surface-confined improved Kumada catalyst transfer polymerization (KCTP) method recently developed by the Nesterov group (Fig. 2)[10]. We will probe the internal structure of these films via a combination of neutron reflectometry (NR) experiments and more traditional approaches available at LSU (GISAXS, atomic force microscopy (AFMi), etc.). In particular, surface-confined polymerization will be carried out via alternating exposure to solutions of the deuterated and non-deuterated monomer so that the resulting stratified structure can be probed in NR experiments. The unique ability of

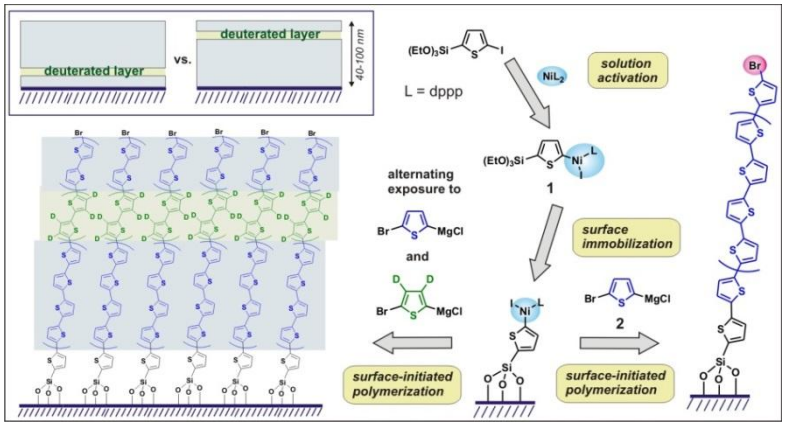

Fig. 2. Schematic outline of the preparation of surface-immobilized catalytic initiator **1**, and surface-confined *in situ* polymerization of monomer **2** to form PT thin film (on the right). Alternating exposure of surface-immobilized **1** to deuterated and non-deuterated monomer **2** to yield PT thin film deuterium-labeled in lateral layers (on the left). Insert shows the possibility to incorporate selectively deuterated layer at various positions to probe structural features across the film.

neutron reflectometry to provide the distribution of the deuterated material coupled with our ability to controllably obtain stratified deuteration will be used to probe polymer organization and alignment across the film.

Our team will also investigate the synthesis and structure of one-dimensional photonic crystals (1D-PCs) based on CP-dielectric polymer multilayered structures to explore the correlation of the magneto-optic effect with film structure via NR. We hypothesize that the 1D-PC will exhibit higher Faraday rotation than the pristine CP films at the photonic band edge due to the optical quantum confinement effect[11]. The mesoscale layers will be prepared using two approaches which deliver contrasting molecular orientation and alignment in the resulting thin films; surface –confined polymerization and layer-by-layer deposition. The multilayer structures will be studied in detail using NR to determine the layer thickness and film morphology, the quality of the interlayer phase separation (layer "intermixing"), and to optimize the experimental conditions to prepare the structures. Achieving enhanced contrast will require using selectively deuterated monomers, thus we will investigate layered thin films with deuterated PT or polystyrene layer.

We will also prepare laterally structured CP thin films using a combination of surface-confined polymerization and particle nanolithography. In addition to potential applications in thin-film electronic and optoelectronic devices, these films will be used as a testing ground to develop new capabilities for neutron scattering experiments, in particular, the possibility to probe working devices under operating conditions. To prepare the structured films, we will use particle lithography to create a hexagonally patterned array of catalytic initiator 1 on a solid substrate followed by surface-confined polymerization to prepare a patterned PT film as an array of hexagonally spaced mesoscale pillars covalently attached to the substrate. The understanding of molecular organization, polymer alignment, bulk morphology, and other important characteristics of the CP films will require the development and validation of neutron based methods in conjunction with computational simulations. The lateral periodicity of the films can be probed using GISAXS whereas in situ polymer growth and molecular organization within the mesoscale columns can be probed by NR and site selective deuterium labeling.

References

1. Qin, H. *et al. Phys. Rev. Lett*. 2010, **105**, 256402.
2. Ikeda, S.-I.; *et al. Phys. Rev. B* 2000, **62**, R6089-R6092.
3. Perry, R. S. *et al. Phys. Rev. Lett.* 2001, **86**, (12), 2661-2664.
4. Stone, M. B. *et al. Phys. Rev. B* 2006, **73**, (17).
5. Capogna, L. *et al. Phys. Rev. B* 2003, **67**, (1).
6. Wernick, J. H. *et al. Mater. Res. Bull.* 1972, **7**, 1431-1441.
7. Ishikawa, Y et al. *Solid State Commun.*1976, **19**, 525-528.
8. Muhlbauer, S. *et al. Science* 2009, 323, (5916), 915-919.
9. Marshall, N.; Sontag, S. K.; Locklin, *J. Chem. Commun.* 2011, **47**, 5681-5689.
10. Chavez, C. A.; Choi, J.; Nesterov, E. E. Macromolecules 2014, **47,** 506-516.
11. Fedyanin, A. A.; *et al. Magnetics, IEEE Transactions on* 2004, **40**, 2850-2852.

Impact of Local Structure on Functional Materials

E.D. Specht, J.D. Budai, O. Delaire, and M.E. Manley
Materials Science & Technology Division, Oak Ridge National Laboratory, Oak Ridge, TN

Program Scope

Nanoscale structure impacts the lattice dynamics of functional materials, more directly by scattering phonons and electrons to affect energy transport, and less directly by providing nuclei for phase transformations and as a factor in phase stability. Taking advantage of recent advances in neutron and x-ray diffuse scattering, local atomic arrangements in functional materials are measured, along with the changes in local order with composition, temperature, and other variables. Advanced computational methods are applied to understand how nanoscale order and lattice dynamics combine to control properties such as energy transport and mechanical behavior.

A complete description of the supporting FWP is provided in the accompanying abstract *Impact of Dynamic Lattice Instabilities and Microstructure on Functional Materials*.

Recent Progress

$AgCrSe_2$-type nanodomains in $AgSbTe_2$

The low thermal conductivity of single-crystal $AgSbTe_2$ with a simple (long-range) rock-salt structure has challenged the idea that low thermal conductivity is found in disordered materials with a complex crystal structure and loosely-packed atoms. Inelastic neutron scattering measurements imply that the low thermal conductivity derives from phonon scattering by nanoscale defects.[1] Diffuse neutron and electron scattering shows that the material contains defects with a size ~ 5 nm: various proposals have been made describing their atomic structure, including local ordering of Ag and Sb atoms on the NaCl lattice and nanoscale phase separation into coherent precipitates of Ag_2Te and Sb_2Te_3. [1-2] Our quantitative analysis of diffuse elastic x-ray and neutron scattering at APS 33-BM and SNS/ARCS rules out all previous proposed local atomic arrangements. The structure most consistent with observed scattering is the $AgCrSe_2$-type structure shown in Fig. 1. In the long-range NaCl-type $AgSbTe_2$ structure, atoms are distributed on a simple cubic lattice which has a close-packed (*ABC*) topology along the <111> directions. In $AgCrSe_2$ structure, the stacking is (*ABAABCBBCACC*), with some atoms

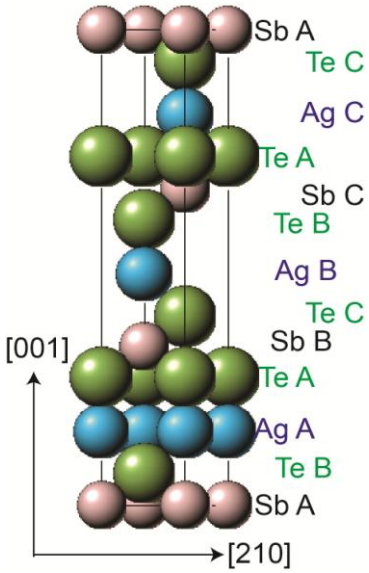

Figure 1. Local $AgCrSe_2$-type structure of nanoscale defects in $AgSbTe_2$

aligned in the [111] direction. This radical departure from the NaCl-type structure is made plausible by the chemical similarity between $AgCrSe_2$ and $AgSbTe_2$. While the actual structure is likely to preserve this precise structural stacking sequence only for short distances along the NaCl [111] direction, a robust result is that the structure consists of a mixture of fcc-type (*ABC*), hcp-type (*AB*), and Wurtzite-type (*AAB*) stacking.

Future Plans

Nanodomains in $AgBiSe_2$

We will investigate the influence of nanoscale atomic structure on energy transport in promising thermoelectric materials using neutron and x-ray scattering combined with theoretical modeling. $AgBiSe_2$ is chemically similar to $AgSbTe_2$, and similarly contains nanodomains.[1] By determining the local structure of defects in $AgBiSe_2$ related materials we will test whether the $AgCrSe_2$-type nanodomains found in $AgSbTe_2$ are a common feature chalcogenide rock-salt lattices.

Deformation mechanism of Ni-Co-Mn-In strain glass

We will initiate studies of the role of nanostructure in a related class of materials. Like $AgSbTe_2$ and related thermoelectrics, they have a simple long-range structure and a more complex nanostructure. While the nanostructure in thermoelectrics affects thermal transport, the nanostructure in *strain glasses* produces extraordinary mechanical properties. For ordered shape-memory materials, deformation phenomena such as shape memory and superelasticity originate from a martensitic structural transformation. Small changes in composition can change these to strain glasses, with similar deformation but no change in long-range structure.[3] Using diffuse elastic x-ray scattering, we will determine the changes in local structure which accommodate deformation. Working synergistically with studies of lattice dynamics using inelastic neutron scattering, we will determine how the development of long-range structural order is hindered, and how the absence of long-range order affects deformation.

References

1. J. Ma, O. Delaire, A. F. May, C. E. Carlton, M. A. McGuire, L. H. VanBebber, D. L. Abernathy, G. Ehlers, T. Hong, A. Huq, W. Tian, V. M. Keppens, Y. Shao-Horn and B. C. Sales, *Nature nanotechnology* 2013, vol. 8, pp. 445-51.
2. (a) Khang Hoang, S. Mahanti, James Salvador and Mercouri Kanatzidis, *Phys. Rev. Lett.* 2007, vol. 99, p. 156403. ; (b) E. Quarez, K. F. Hsu, R. Pcionek, N. Frangis, E. K. Polychroniadis and M. G. Kanatzidis, *J. Am. Chem. Soc.* 2005, vol. 127, pp. 9177-9190. ; (c) Christopher E. Carlton, Ricardo De Armas, Jie Ma, Andrew F. May, Olivier Delaire and Yang Shao-Horn, *J. Appl. Phys.* 2014, vol. 115, p. 144903. ; (d) Joshua D. Sugar and Douglas L. Medlin, *J. Alloys Compd.* 2009, vol. 478, pp. 75-82. ; (e) J. D. Sugar and D. L. Medlin, *J. Mater. Sci.* 2010, vol. 46, pp. 1668-1679.

3. (a) Shampa Sarkar, Xiaobing Ren and Kazuhiro Otsuka, *Phys. Rev. Lett.* 2005, vol. 95, p. 205702. ; (b) Yu Wang, Xiaobing Ren and Kazuhiro Otsuka, *Phys. Rev. Lett.* 2006, vol. 97, p. 225703.

Publications

1. M. E. Manley, J. W. Lynn, D. L. Abernathy, E. D. Specht, O. Delaire, A. R. Bishop, R. Sahul, and J. D. Budai, "Phonon localization drives polar nanoregions in a relaxor ferroelectric," *Nature Communications* 5, Article no. 3683 (2014).

2. C. E. Carlton, R. De Armas, J. Ma, A. F. May, O. Delaire, and Y. Shao-Horn, "Natural nanostructure and superlattice nanodomains in $AgSbTe_2$," *Jour. Appl. Phys.* **115**, 144903 (2014).

3. J. Ma, O. Delaire, A. F. May, C. E. Carlton, M. A. McGuire, L. H. VanBebber, D. L. Abernathy, G. Ehlers, T. Hong, A. Huq, W. Tian, V. M. Keppens, Y. Shao-Horn, and B. C. Sales, "Glass-like phonon scattering from spontaneous nanostructure in $AgSbTe_2$", *Nature Nanotechnology* **8**, 445-451 (2013).

4. R. I. Barabash, O. M. Barabash, E. A. Karapetrova, and M. E. Manley, "Structural and Dynamical Fluctuations in Off-Stoichiometric NiMnGa Shape-Memory Alloys," *Applied Physics Letters* **104**, 241905 (2014).

5. G. E. Ice and E. D. Specht, "Microbeam, timing and signal-resolved studies of nuclear materials with synchrotron X-ray sources," *Journal of Nuclear Materials* **425**, 233-237 (2012).

A complete list of publications for this FWP may be found in the abstract for *Impact of Dynamic Lattice Instabilities and Microstructure on Functional Materials*

Probing the complex temperature-pressure-magnetic field phase diagram of the heavy-fermion antiferromagnet $CeRhIn_5$ by means of neutron scattering

M. Janoschek[1], P. Das[1], S. Lin[1], F. Ronning[1], E. D. Bauer[1], C. D. Batista[1], C. Pfleiderer[2], T. Keller[3], G. Ehlers[4], J. D. Thompson[1]

[1] Los Alamos National Laboratory, Los Alamos, NM, USA
[2] Technische Universität München, Germany
[3] Max Planck Institut, Stuttgart, Germany
[4] Oak Ridge National Laboratory, USA

Program Scope

The heavy-fermion antiferromagnet $CeRhIn_5$ exhibits a particularly rich temperature-pressure-magnetic field phase diagram, in which several complex magnetic phases, unconventional superconductivity, and possibly charge degrees of freedom compete with each other. The ambient pressure, zero magnetic field ground state of $CeRhIn_5$ is antiferromagnetic with a propagation vector k = [0.5,0.5,0.297] below T_N = 3.8 K [1] and can be suppressed to zero temperature by application of pressure. This results in an antiferromagnetic quantum critical point at P_c = 2.3 GPa around which a broad superconducting dome emerges with a maximal T_c = 2.3 K [2]. This has led to the proposal that the unconventional superconductivity in the family of "115" compounds is mediated by quantum critical magnetic fluctuations [3]. On the other hand, isotropic scattering of charge carriers observed at P_c suggests that the unconventional superconductivity is mediated by multi-critical quantum fluctuations that occur in both spin and charge channels [2]. A crucial question thus is whether spin and charge fluctuations may arise from distinct quantum critical points at different pressures.

Here we report on recent high-resolution neutron spectroscopy at ambient pressure that probe the strength of magnetic interactions in $CeRhIn_5$ for the first time, and will allow us to determine whether magnetic interactions alone are strong enough to mediate the superconductivity in this compound. We have further used Larmor diffraction measurements carried out at ambient and high pressure in order to shed some light on the question of the existence of a second quantum critical point.

Recent Progress

We have recently carried out high-resolution neutron spectroscopy measurements on $CeRhIn_5$ using the Cold Neutron Chopper Spectrometer (CNCS) at the Spallation Neutron Source operated by the Oak Ridge National Laboratory [4]. Due to the highly absorbing sample (1/e length ≈ 0.5 mm for 3 meV neutrons) a flat plate sample was employed in combination with the new focusing guide recently installed at CNCS. As illustrated in Fig. 1 the measurements performed with incident energy E_i = 3.1 meV at 2 K allowed us to determine the full spin wave spectrum at ambient pressure. From fits to the spin wave dispersion the dominating nearest

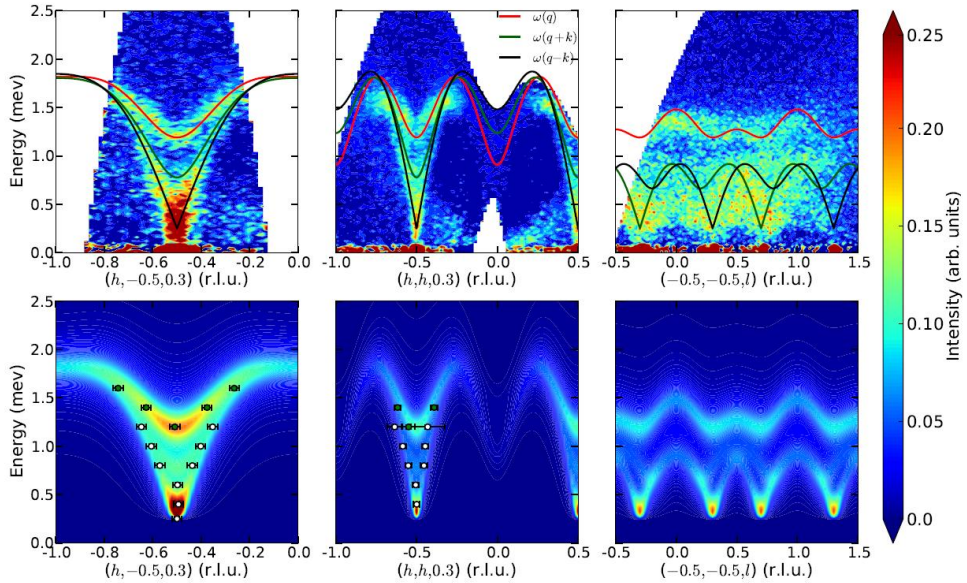

Fig. 1 Measured (top panels) and calculated (bottom panels) spin-wave dispersion for $CeRhIn_5$ [4] . The solid lines in the top panels are fits to the measured dispersion. The point in the bottom panels illustrate peak maxima extracted from momentum and energy cuts.

neighbor magnetic exchange constant was determined to be J_0 = 0.37 meV in very good agreement with T_N.

We have also performed Larmor diffraction measurements on $CeRhIn_5$ down to 500 mK and up to pressures of 1.9 GPa in a piston-cylinder pressure cell to investigate the question of an additional quantum critical point below P_c. At certain types of quantum critical points a divergence of the Grüneisen parameter (the ratio of the thermal expansion to the specific heat capacity) is predicted to occur [5]. At ambient pressure, highly accurate measurements of the thermal expansion coefficient are done best using capacitance dilatometry. Unfortunately, capacitance-based dilatometry is not possible under high pressure environments where quantum-phase transitions often occur, such as in $CeRhIn_5$. Larmor diffraction is not limited by Louiville's theorem as convention diffraction methods are, but instead encodes changes in the lattice parameters in the neutron polarization [6]. Our measurements on $CeRhIn_5$ have achieved a resolution of $\Delta a/a = 10^{-5}$, where suggested updates to the method may allow to reach an improved resolution of $\Delta a/a = 10^{-7}$. A distinct change of the thermal expansion between 1.5 and 1.9 GPa is observed suggesting that the Grüneisen parameter indeed diverges in this pressure regime. This pressure regime is in agreement with results of electrical transport and thermal measurements as function of pressure that suggest the existence of a distinct field-induced magnetic phase with a different propagation vector above 1.8 GPa. However, more detailed conventional and Larmor diffraction measurements with more pressure steps are required to conclude this study.

Future Plans

The exact knowledge of the spin wave dispersion of $CeRhIn_5$ will allow us to address the role of the magnetic interactions in the complex temperature-pressure-magnetic field phase diagram of this material in great detail. The theory developed to explain our measured spin-wave dispersions in $CeRhIn_5$ explains the general features of the known temperature-magnetic field

phase diagram [7], but we will investigate changes to spin wave spectrum as function of magnetic field to verify the predictions of this model. Moreover, we plan to investigate changes of the dynamical magnetic susceptibility between the normal and superconducting state in $CeRhIn_5$ (under pressure) or $CeRh_{1-x}Ir_xIn_5$. In combination with the already determined magnetic exchange constant J_0 this will allow us to calculate the change of the magnetic exchange interaction between the normal and superconducting state. This quantity is a critical input parameter for theories that propose that magnetic fluctuations mediate the unconventional superconductivity observed in heavy fermion materials. Finally, we will also extend our Larmor diffraction measurements to higher pressure above P_c to conclude our study.

References

[1] [1] W. Bao *et al.*, Phys. Rev. B **62**, R14621 (2000); [2] T. Park *et al.*, Nature **440**, 65 (2006); [3] C. Stock *et al.*, Phys. Rev. Lett. **100,** 087001 (2008). [4] P. Das *et al.*, (in preparation); [5] M. Garst *et al.*, Phys. Rev. B 72, 205129 (2005); [6] C. Pfleiderer *et al.*, Science **316**, 1871 (2007); [8] S. Raymond *et al.*, Jour. Condens. Matter Phys. **19**, 242204 (2007).

i-*R*-Cd and *R*Cd_6: A matched set of magnetic quasicrystals and approximants

A. I. Goldman, T. Kong, A. Kreyssig, A. Jesche, M. Ramazanoglu, K. S. Dennis, S. L. Bud'ko, and P. C. Canfield

Ames Laboratory, US DOE and Iowa State University

ABSTRACT

Since the initial discovery of quasicrystals, the search for new quasicrystalline systems, especially thermodynamically stable ones, as well as an understanding of their structural and physical properties has been of keen interest to the solid-state physics and chemistry communities. The discovery [1] of a new family of local-moment bearing binary quasicrystals, i-*R*-Cd (*R* = Gd through Tm + Y) is particularly exciting because they represent the compositionally simplest system for the study of the magnetic interactions in aperiodic systems. Examples of stable binary icosahedral quasicrystals are quite rare and, before the discovery of icosahedral quasicrystals in the R-Cd system, there were no known examples that featured localized magnetic moments. Furthermore, the existence of a corresponding set of cubic approximants, RCd_6, to i-*R*-Cd allows for direct comparisons between the low-temperature magnetic states of crystalline and quasicrystalline phases with fundamentally similar local structures, since RCd_6 may be described as a body-centered cubic packing of the same clusters of atoms as found in the newly discovered icosahedral phase. Interestingly, the RCd_6 approximants manifest long-range magnetic order at low temperatures [2,3], whereas the related icosahedral phase exhibits only spin-glass-like freezing at low temperatures [1,4]. These differences may be related directly to the effects of aperiodicity on magnetic interactions in the quasicrystal. In this poster, the magnetic properties of both the quasicrystalline and crystalline approximants via bulk susceptibility measurements, x-ray resonant magnetic scattering and magnetic neutron scattering will be presented.

[1] A. I. Goldman, T. Kong, A. Kreyssig, A. Jesche, M. Ramazanoglu, K. S. Dennis, S. L. Budʾko, and P. C. Canfield, Nature Mat. **12**, 715 (2013).
[2] M. G. Kim, G. Beutier, A. Kreyssig, T. Hiroto, T. Yamada, J. W. Kim, M. de Boissieu, R. Tamura, and A. I. Goldman, Phys. Rev. B **85**, 134442 (2012).
[3] A. Kreyssig, G. Beutier, T. Hiroto, M. G. Kim, G. S.Tucker, M. de Boissieu, R. Tamura, and A. I. Goldman, Phil. Mag. Lett. **93**, 512 (2013).
[4] Tai Kong, Sergey L. Bud'ko, Anton Jesche, John McArthur, Andreas Kreyssig, Alan I. Goldman and Paul C. Canfield, Phys. Rev. B **90**, 014424 (2014).

Complex Electronic Materials: Influences of quantum criticality on superconductivity in $CeCoIn_5$.

F. Ronning[1], R. Movshovich[1], X. Lu[1], R. Urbano[1], A. Mounce[1], E. D. Bauer[1], V. Sidorov[1], J.X. Zhu[1], S. Seo[2], T. Park[2], Z. Fisk[3], S. Gerber[4], M. Kenzelmann[4], J. D. Thompson[1]

[1] Los Alamos National Laboratory, Los Alamos, NM, USA
[2] Sung Kyun Kwan University, South Korea
[3] University of California. Irvine, CA, USA
[4] Paul Scherrer Institute, Switzerland

Program Scope

Complex electronic behaviors often appear at the boundary between magnetic and non-magnetic states. $CeCoIn_5$ is one such material which fortuitously lies precisely at that boundary in its virgin state. Consequently, its incredible high purity allows us to study many interesting consequences of such a non-Fermi liquid system. One consequence is the observation of a field induced phase transition to a magnetic state (the so-called Q phase) which lives strictly within the superconducting phase [1]. Studies of this phase allow for insight into the general competition between magnetism and superconductivity. In addition to novel phases, which appear as a consequence of the high purity and quantum fluctuations in $CeCoIn_5$, the high purity also allows us to better resolve the influence of intentionally adding impurities to a clean strongly correlated system [2].

Recent Progress

Our recent work on the Q-phase reveals that the magnetic order has an incredible sensitivity to the applied field direction. Careful neutron-diffraction measurements of the Q-phase find that the population of antiferromagnetic domains with orthogonal propagation wavevector changes abruptly as the field is rotated by only 0.2^0 away from the [100] direction.[3] This extreme sensitivity to field direction appears to be a consequence of the emergence of a Cooper-pair density wave (PDW) of mixed L=2,S=0/L=1,S=1nature that is predicted [4] when antiferromagnetic order and d-wave superconductivity are coupled. In this model, the magnetic field couples to the S=1 component of the PDW and controls the line node of the p-wavefunction, in turn determining the direction of the antiferromagnetic magnetic wavevector. A schematic illustration in real space of the proposed PDW is shown in Fig. 2.

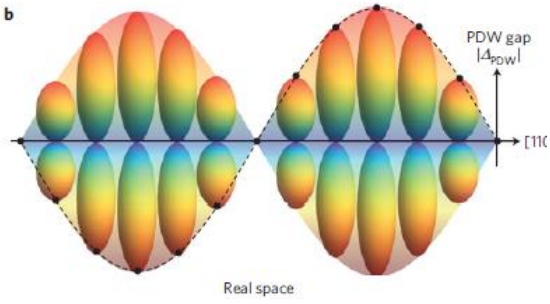

Fig. 2 Real space cartoon of Cooper pair density wave gap inferred to exist in the Q-phase of $CeCoIn_5$.

By doping the ultrapure $CeCoIn_5$ with as little as 1% Cd, one induces an antiferromagnet state [5]. This can be driven back to a quantum critical point with the application of pressure, and a robust superconducting state is found in the vicinity of the nominal quantum phase transition. We have shown that the critical magnetic fluctuations which one would anticipate in the presence of a quantum critical point have been quenched by the disorder in this system [6]. This indicates that the fluctuations responsible for the non-Fermi liquid behavior are part of a continuum of fluctuations that also induce the superconducting pairing.

Future Plans

Previous measurements of the phase diagram of $CeCoIn_5$ under pressure demonstrated a growth of the Q-phase with pressure, which is contrary to the typical observation of the suppression of magnetism with pressure in Ce-based compounds. We will conduct NMR measurements under pressure to investigate whether SDW state persists under pressure, a critical test for the PDW scenario. In addition, NMR is an excellent local probe which we will allow us to study the inhomogeneity of the spin fluctuations about impurity sites in $CeCoIn_5$. Finally, pressure has been used incredibly effectively to suppress magnetic order in $CeRhIn_5$ and reveal a quantum critical point similar to that observed in $CeCoIn_5$. We will exploit the use of high magnetic fields in conjunction with the BES 100 T science project, to explore the connection between field tuned and pressure tuned quantum criticality. Preliminary work reveals a Fermi surface transformation in applied magnetic field, as well as a sliding density wave of unknown character [7].

References

[1] A. Bianchi *et al*., Phys. Rev. Lett. **91**, 187004 (2003); R. Movshovich *et al*., Nature **427**, 802 (2004); B.-L. Young *et al*., Phys. Rev. Lett. **98**, 36402 (2007); M. Kenzelmann, *et al.* PRL **104**, 127001 (2010). [2] K. Gofryk *et al*., PRL **108**, 186402 (2012).
V. A. Sidorov *et al*., Phys. Rev. Lett. **89,** 157004 (2002). [2] B. Zhou *et al*., Nature Phys. **9**, 474 (2013). [3] S. Gerber *et al*., Nature Phys. **10**,126 (2014). [4] A. Aperis *et al*., Phys. Rev. Lett. **104**, 216403 (2010). [5] L.D. Pham, *et al.* PRL, **97**, 057404 (2006) [6] S. Seo, *et al*., Nature Phys. **10**,120 (2014). [7] L. Jiao, *et al.* ArXiv:1308.0294; P. Moll, *et al.* (unpublished)

Publications

Only more significant publications supported by BES and relevant to this specific poster are listed from among approximately 65 since the beginning of FY13.

"Disorder in a Quantum Critical Superconductor," S. Seo, X. Lu, J.-X. Zhu, R. R. Urbano, N. Curro, E. D. Bauer, V. A. Sidorov, L. D. Pham, T. Park, Z. Fisk and J. D. Thompson, Nature Phys. **10**, 120 (2014). (plus News and Views and cover)

"Switching of Magnetic Domains Reveals Spatially Inhomogeneous Superconductivity," S. Gerber, M. Bartkowiak, J. L. Gavilano, E. Ressouche, N. Egetenmeyer, C. Niedermayer, A. D. Bianchi, R. Movshovich, E. D. Bauer, J. D. Thompson and M. Kenzelmann, Nature Phys. **10**,126 (2014).

"Zero-Field Quantum Critical Point in $CeCoIn_5$," Y. Tokiwa, E. D. Bauer, and P. Gegenwart, Phys. Rev. Lett. **111**, 107003 (2013).

"Coexistence of Antiferromagnetism with Superconductivity in $CePt_2In_7$: Microscopic Phase Diagram Determined by ^{115}In NMR/NQR," H. Sakai, Y. Tokunaga, S. Kambe, F. Ronning, E. D. Bauer and J. D. Thompson, Phys. Rev. Lett. **112**, 206401 (2014).

A phenomenological theory for the Z_2 spin liquid phase of S=1/2 Heisenberg kagome Heisenberg antiferromagnet*

Yuan Wan and Oleg Tchernyshyov

Institute for Quantum Matter & Dept. of Physics & Astronomy, Johns Hopkins University

Quantum spin liquids are novel quantum phases of matter supporting fractionalized quasi-particles. Highly frustrated magnets provide a natural ground for the search for quantum spin liquids. The spin-1/2 kagome Heisenberg antiferromagnet (KHAF) stands out as one of the most promising candidate systems. However, the precise nature of its ground state is still under active debate. Recent numerical calculations based on density-matrix renormalization group (DMRG) show evidence for a possible Z_2 spin liquid phase, the effective description of which is a Z_2 gauge theory. Yet, the DMRG calculations alone cannot tell the explicit form of the effective theory. In this work, we construct a minimal Z_2 gauge Hamiltonian encapsulating the DMRG phenomenology in the S=0 sector. We generalize Misguich's Hamiltonian by including dimer density interactions. We show that our minimal model naturally produces the diamond resonance pattern observed in DMRG. Moreover, we show that the puzzling boundary effects arises naturally in our model. We also calculate the valence-bond pattern induced by a pinned singlet, which agrees well with the DMRG calculation.

*Phys. Rev. B **87**, 104408 (2013). This work was supported by the US Department of Energy, Office of Basic Energy Sciences, Division of Materials Sciences and Engineering, under grant DE-FG02-08ER46544.

Author Index

Author Index

Participant List

Participant List

Peter Armitage
Johns Hopkins University
npa@pha.jhu.edu

Alexander Balatsky
Los Alamos National Laboratory / Nordita
balatsky@hotmail.com

Eric Bauer
Los Alamos National Laboratory
edbauer@lanl.gov

Collin Broholm
Johns Hopkins University
broholm@jhu.edu

John Budai
Oak Ridge National Laboratory
budaijd@ornl.gov

Robert Cava
Princeton University
rcava@princeton.edu

Ravi Chandran
University of Utah
ravi.chandran@utah.edu

Sow-Hsin Chen
Massachusetts Institute of Technology
sowhsinl@mit.edu

Wei-Ren Chen
Oak Ridge National Laboratory
chenw@ornl.gov

Sang-Wook Cheong
Rutgers University
sangc@physics.rutgers.edu

Tammy Click
Oak Ridge Associated Universities
tammy.click@orau.org

Teresa Crockett
U.S. Department of Energy
Teresa.Crockett@science.doe.gov

Pengcheng Dai
Rice University
pdai@rice.edu

Olivier Delaire
Oak Ridge National Laboratory
delaireoa@ornl.gov

John DiTusa
Louisiana State University
ditusa@phys.lsu.edu

Takeshi Egami
University of Tennessee/ORNL
egami@utk.edu

Morten Eskildsen
University of Notre Dame
eskildsen@nd.edu

Eric Fullerton
University of California, San Diego
efullerton@ucsd.edu

Brent Fultz
California Institute of Technology
btf@caltech.edu

Henry Glyde
University of Delaware
glyde@udel.edu

Alan Goldman
Ames Laboratory/Iowa State University
goldman@ameslab.gov

Gary Grest
Sandia National Laboratories
gsgrest@sandia.gov

Martin Greven
University of Minnesota
greven@physics.umn.edu

Genda Gu
Brookhaven National Laboratory
ggu@bnl.gov

Jason Hayward
University of Tennessee
jhayward@utk.edu

Marc Janoschek
Los Alamos National Laboratory
mjanoschek@lanl.gov

Peter Johnson
Brookhaven National Laboratory
pdj@bnl.gov

Alamgir Karim
University of Akron
alamgir@uakron.edu

Boris Khaykovich
Massachusetts Institute of Technology
bkh@mit.edu

Arvind Kini
U.S. Department of Energy
A.Kini@science.doe.gov

Valery Kiryukhin
Rutgers University
vkir@physics.rutgers.edu

Andreas Kreyssig
Ames Laboratory
kreyssig@ameslab.gov

Connie Lansdon
Oak Ridge Associated Universities
connie.lansdon@orau.org

Chris Leighton
University of Minnesota
leighton@umn.edu

Eliane Lessner
U.S. Department of Energy
Eliane.Lessner@science.doe.gov

Despina Louca
University of Virginia
louca@virginia.edu

Mahesh Mahanthappa
University of Wisconsin-Madison
mahesh@chem.wisc.edu

Michael Manley
Oak Ridge National Laboratory
manleyme@ornl.gov

Michael Markowitz
U.S. Department of Energy
mike.markowitz@science.doe.gov

James Morris
Oak Ridge National Laboratory
morrisj@ornl.gov

Adam Moule
University of California, Davis
amoule@ucdavis.edu

Bradley Olsen
Massachusetts Institute of Technology
bdolsen@mit.edu

Dvora Perahia
Clemson University
dperahi@g.clemson.edu

Lilo Pozzo
University of Washington
dpozzo@uw.edu

Thomas Proffen
Oak Ridge National Laboratory
tproffen@ornl.gov

Roger Pynn
Indiana University
rpynn@indiana.edu

Dmitry Reznik
University of Colorado-Boulder
dmitry.reznik@colorado.edu

James Rhyne
U.S. Department of Energy
james.rhyne@science.doe.gov

Filip Ronning
Los Alamos National Laboratory
fronning@lanl.gov

Stephan Rosenkranz
Argonne National Laboratory
srosenkranz@anl.gov

Andrew Schwartz
U.S. Department of Energy
andrew.schwartz@science.doe.gov

David Singh
Oak Ridge National Laboratory
singhdj@ornl.gov

Sunil Sinha
University of California, San Diego
ssinha@physics.ucsd.edu

Andrei Sirenko
New Jersey Institute of Technology
sirenko@njit.edu

Eliot Specht
Oak Ridge National Laboratory
spechted@ornl.gov

Gregory Stephenson
Argonne National Laboratory
stephenson@anl.gov

Oleg Tchernyshyov
Johns Hopkins University
olegt@jhu.edu

Suzanne te Velthuis
Argonne National Laboratory
tevelthuis@anl.gov

Pappannan Thiyagarajan
U.S. Department of Energy
p.thiyagarajan@science.doe.gov

Joe Thompson
Los Alamos National Laboratory
jdt@lanl.gov

John Tranquada
Brookhaven National Laboratory
jtran@bnl.gov

David Vaknin
Ames Laboratory
vaknin@ameslab.gov

Philip Wilk
U.S. Department of Energy
philip.wilk@science.doe.gov

Lane Wilson
U.S. Department of Energy
lane.wilson@science.doe.gov

Guangyong Xu
Brookhaven National laboratory
gxu@bnl.gov

Arun Yethiraj
University of Wisconsin
yethiraj@chem.wisc.edu

Igor Zaliznyak
Brookhaven National Laboratory
zaliznyak@bnl.gov